The Dissertation Committee for Sheldon Myles Williams certifies that this is the approved version of the following dissertation:

Studies of Complexation and Properties of Metal Ion Guests with Macrocyclic Hosts using Electrospray Ionization Quadrupole Ion Trap Mass Spectrometry

Committee:

_____
Jennifer S. Brodbelt, Supervisor

_____
Jason A. Shear

_____
James Holcombe

_____
Eric Anslyn

_____
Christian Whitman

Studies of Complexation and Properties of Metal Ion Guests with Macrocyclic Hosts using Electrospray Ionization Quadrupole Ion Trap Mass Spectrometry

by

Sheldon Myles Williams, B.S., M.S.

Dissertation

Presented to the Faculty of the Graduate School of

The University of Texas at Austin

in Partial Fullfillment

of the Requirements

for the Degree of

Doctor Of Philosophy

The University of Texas at Austin

December 2003

Acknowledgements

I would like to express my deepest thanks to Dr. Jennifer S. Brodbelt and my family and friends for support, encouragement, advice, and instruction. I would also like to acknowledge Sheryl M. Blair for her work on the research presented in Chapter 3, and to Richard A. Bartsch and Xiaowu Huang for the synthesis and donation of the lariat ethers compounds studied in the research presented in Chapters 3 and 4, and to Alan P. Marchand, Dariusz Cal[‡], Zilin Huang, and Huiguo Lai for the synthesis and donation of the sulfur and nitrogen containing macrocycles studied in the research presented in Chapters 5 and 6. Finally, I would like to thank my mother, Judy Gilchrist, for her encouragement, support and, most of all, her love and acceptance.

Studies of Complexation and Properties of Metal Ion Guests with Macrocyclic Hosts using Electrospray Ionization Quadrupole Ion Trap Mass Spectrometry

Publication No. _____

Sheldon Myles Williams, Ph.D.

The University of Texas at Austin, 2003

Supervisor: Jennifer S. Brodbelt

This research is focused on the detection and analysis of host-guest chemistry involving primarily hosts that are novel organic compounds or cyclic peptides and guests that are metal ions. Detection and analysis are by electrospray ionization quadrupole ion trap mass spectrometry. The complexes studied are between organic host molecules such as (i) crown ethers and various analogs (modified lariat ethers, azacrown ethers, thiacrown ethers) or (ii) naturally occurring or synthetic cyclic peptides and metal ions, including alkali, alkaline

earth and heavy metal ions. The signals observed in the mass spectra are used to determine the effectiveness of the complexation, the entities involved in the complexes, and the stoichiometries of these entities that occur. The soft ionization nature of electrospray ionization allows many non-covalent complexes formed in solution to be viewed in the gas phase still intact. Various sample systems have been used to determine the selectivities of complexation for various ratios of miscible solvents, extractions of metals from aqueous solution phase to a non-miscible organic phase. Other experiments studied the effects of different metal ion guests on the fragmentation behavior of hosts. Evaluation of the results of these studies have implications for determining structural features of the host which can improve selectivities and avidities of hosts for particular guest species, detection of host compounds, and peptide residue sequencing, which have applications in fields of science such as chemical sensor development, biochemistry and environmental remediation.

Table of Contents

List of Figures

List of Tables

List of Schemes

CHAPTER 1

Introduction

1.1 General Introduction

This dissertation focuses on the development and application of electrospray ionization (ESI) mass spectrometry for problems related to molecular recognition, including the determination of relative selectivities of macrocycles for various metal ions, the relationship between complex structure and selectivities, and the development of methods to better identify macrocyclic analytes. The majority of this research involves (i) validating the quantification of selectivities of crown ethers with various metal ions, (ii) applying this methodology to the determination of selectivities of several classes of novel synthetic macrocyclic crown ether analogs, and (iii) using this information to determine selectivity trends and the structural features of the macrocycles and metal ions responsible for these trends. The host molecules used were macrocyclic compounds such as crown ethers, crown ether analogs, and cyclic peptides. In this introduction, the importance of the analysis of macrocycle complexes with metal ions is discussed along with a description of the theory of host-guest complexation and binding selectivity. This introduction ends with an overview of the chapters included in this dissertation.

1.1.1 Macrocyles

Generally speaking, macroycles are cyclic supramolecular assemblies composed of several moieties that could be described as subunits of a cyclic polymer. For instance, crown ethers [1-4], a well studied class of macrocycles, are composed of several alkoxy subunits. Macrocycles can contain a wide variety of subunits, including those where all the subunits are the same and those where different subunits make up the macrocycle. In addition, macrocycles can be modified with other functional groups covalently bonded to the cyclic portion of the molecule. Macrocycles have found several important and widespread applications to science and society. They have been used to selectively detect ions via impregnation of polymeric membranes of ion selective electrodes with macrocycles which, due to their structure, selectively bind one of several similar ions [5-10]. For example, macrocycles are being developed to distinguish increasingly between ions such as Li^+, Na^+, and K^+ ions, which tend to be major impurities in the presence of one another [7-10]. Macrocycles can be used for remediation of waters contaminated with toxic metal ions, such as heavy metals, by binding selectively to these metals in the presence of other common, non-toxic metal ions present in far larger concentrations, such as common alkali and alkaline earth metal ions [11-23]. Macrocycles may also be used to remove metal ions from water without being dissolved themselves via attachment to a stationary phase and support material through which the contaminated water is passed. Important

structural features of such remediation agents are discussed more in Chapters 6 and 7. Other applications include, but are not limited to, more efficient, environmentally beneficial mining of precious metals, enhanced detection methods for metal ion binding analytes, and understanding interactions of natural products and biomolecules with metal ions. Important examples of bioactive macrocycles are the cyclic polypeptides that function as antibiotics and drugs in applications such as antibacterial agents, and immunosuppresion and anti-cancer medications [24-26].

1.2 Binding Selectivity Measurements

1.2.1 Theory of Binding Selectivities

The affinity of a guest species, G, for a host molecule, H, can be described by the equilibrium reaction equation

$$\mathbf{G + H} \overset{\mathbf{K}}{\rightleftharpoons} \mathbf{GH}$$

and the equation

$$K = \frac{[GH]}{[G][H]}$$

where K is the association constant. For two guests with one host, the following equations apply:

$$K_1 = \frac{[G_1H]}{[G_1][H]} \qquad K_2 = \frac{[G_2H]}{[G_2][H]} \qquad \frac{[G_1H]}{[G_2H]} = \frac{K_1}{K_2} \bullet \frac{[G_1]}{[G_2]} = R$$

where *R* is the concentration ratio of the two host-guest complexes in solution. The R value can be estimated based on the intensities of two different host-guest complexes in the mass spectra, a method used extensively in this dissertation work.

1.2.2 Current Methods for the Determination of Binding Selectivities

In the case of small atomic or molecular species such as metals or alkyl amines complexed with macrocyclic ligands, the small species are referred to as 'guests' and the macrocycles as 'hosts' as depicted in Figure 1.1. The study of this class of complexes is thus referred to as 'host-guest chemistry.' Several methods have been historically used to determine the binding selectivities of guests for hosts in condensed phase solutions. These methods include potentiometry, conductivity, microcalorimetry, and NMR [2]. Most of these methods determine selectivities indirectly by evaluating the association constant (K) of one host with one guest or by measuring the relative selectivity value of one guest for a host relative to another guest with a known association constant with the host in the same solution. Then, by comparing the K values for different guests with a host, the relative selectivities for several guests for the host can be determined.

Figure 1.1 Host-guest complex structure.

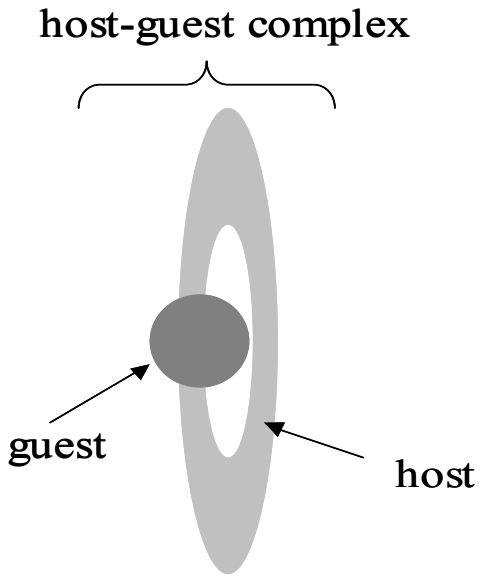

The NMR method involves the titration of a solution containing the host compound with the guest, usually in which the concentration of the host is fixed while the concentration of the guest is varied, as the NMR experiment normally monitors the shift of hydrogen-1 or carbon-13. The chemical shift of the host-guest complex is monitored, and a non-linear regression method is used to extrapolate the binding constant of the host guest complex. Many repetitive measurements are involved, which may require one hundred to one thousand times more sample than the ESI-MS methods described in this work. Potentiometric methods are similar to NMR methods in that repetitive titrations must be performed. During the titration, the changes in the concentration of the free guest ion are monitored with ion

selective electrodes. The solvent system chosen must be compatible with the ion selective electrode. Many electrodes are designed for aqueous solutions, making analysis in organic solvents problematic. Also, the choice of different electrodes available is limited, creating restrictions on the guest ions which can be studied. Calorimetric methods estimate binding constants by measuring the heat produced or consumed due to the occurrence of the binding reaction. A titration is usually performed where a fixed quantity of either the host or guest in solution is kept in a constant temperature vessel and this solution is titrated with small aliquots (10 to 20 μL) of the other complexation reagent. The heat flow required for the solution to return to the equilibrium temperature is then monitored for each injection. Titrations can be performed using several constant temperature values and the enthalpy of reaction and association constant can be determined by non-linear curve fitting. Microcalorimetry usually requires 10 to 100 μmol of host, while the ESI-MS method requires only 1 to 10 nmol of host. Also, only one complex can usually be analyzed in a solution at a time with microcalorimetry. Conductivity methods measure the decreases in conductance caused by the addition of a host molecule to solutions of constant ionic strength followed by analysis by nonlinear least squares to give association constants of the host-guest complexes. First the equivalent conductivity of the guest ion alone in solution at various concentrations is measured. Then the equivalent conductivity of solutions containing the guest ion and the host at the same concentration are measured at several concentrations.

Finally, the equivalent conductivity of solutions where the host is kept constant and that of the guest ion is varied are measured. The selectivity observed for complexing is a function not only of ionic size but also solvent [28-29].

The advantage of using such techniques for host-guest selectivity determinations is that the association constants for individual complexes are also determined in the process, which provides the affinity of the guest for the host in addition to the relative selectivities of several guests for the same host, or vice versa. The disadvantages of these methods are that they can often be very time consuming, involve volumes of at least 100 μl, and concentrations of at least 100 μM, and some are limited in the range of solvent systems that can be used. The time and sample volumes used can increase tremendously if titrations are necessary for the experiments, as is the case with NMR, calorimetry and potentiometric analyses.

Johnstone and coworkers began studying the relationship between solution-phase and gas-phase host-guest complex equilibria with mass spectrometry in 1983 with crown ethers and alkali metal cations using fast atom bombardment mass spectrometry (FAB-MS) and an aqueous glycerol matrix [30-32]. They found that the signal intensities for complexes of the host and guest ions reflected closely the calculated concentrations of these complexes in solution. In 1995, Langley et al. evaluated the use of FAB-MS for studying solution equilibrium concentrations of host-guest complexes of crown ethers and alkali metal cations [33]. They found

that certain experimental variables should be addressed. First, the FABMS matrix can have a dramatic effect on the signal ratios and second, protonated and metallated complexes have very different relative intensities when their concentrations are similar. However, for a series of alkali metal ions with the same host, the same matrix, and similar conditions for other experimental variables, the relationship was acceptable. In 1988, Bonas et al. determined the solution-phase equilibrium constants for 18-crown-6 with Na^+, K^+, Rb^+, and Cs^+ [34]. A study published by Abdoul-Carime in 1998 with electrospray ESI-MS determined that for alkali metal ions in competition with the same crown ether (12-crown-4, 15-crown-5, and 18-crown-6 were tested) the relative abundances of different complexes correlated well with their relative solution-phase concentrations [35]. He also determined that for different crown ethers in competition with the same metal ion, the largest crown ether always showed the highest affinity, in contradiction to the solution-phase results. This result indicated that the uncorrected ratio of signal intensities between different complexes is accurate for competition of several metal ions for the same host, but not for several hosts with the same metal ion. Young et al. published two papers in 1997 that demonstrated (i) that with the use of correction factors for the relative electrospray efficiencies of different compounds accurate determination of selectivities of several alkali metal ions toward the same dibenzo-crown ether could be simultaneously determined and (ii) the solution equilibrium constant for one host with one metal ion could be accurately

determined using competitive complexation of two hosts for the metal ion [36,37]. These methods by Young et al. were verified for several dibenzo-crown ethers.

Van Dorsselaer and co-workers established that the electrospray efficiency of an ion is related to its solvation energy [38], and showed that complexes that contain host molecules, such as crown ethers, with guest ions, such as metal ions of the same charge, have similar electrospray efficiencies when experimental conditions are kept constant, resulting in ESI-MS signals which correspond closely in relative intensity to the relative concentrations of the ions in the solution being analyzed. Van Dorssalaer's work also determined that roughly a ten-fold decrease in electrospray efficiency is predicted for a 70 kJ/mol increase in ion solvation energy [38].

The Brodbelt group has undertaken extensive investigations into solution phase selectivities, kinetics and thermodynamics of host-guest complexation by using mass spectrometry methods [42-60]. In 1998, Blair, Kempen, and Brodbelt reported the determination of binding selectivities in host-guest complexation by ESI-MS [42,43]. The first hosts studied were bis-crowned clefts (two 15-crown-5 moieties tethered together with quinoline group spacers) complexed with alkali metal ions and crown ethers and glymes with alkali metal, ammonium, and alkyl ammonium ions. The situations where correction factors are needed and the magnitude of these corrections were determined. For alkali metal ions competing with the same host, relatively small corrections in the ratios of ten to twenty percent

were necessary. Since then, work in the Brodbelt group has progressed from the study of simple crown ethers with alkali metals to the study of diaza crown ethers [44], lariat ethers [45,50,54,58], cage annulated crown ethers with nitrogen and sulfur heteroatoms [48,49,53,55,56,59,60], and calixerenes with alkali [42-47,49-55,57,58], alkaline earth [58], and transition metal ions [48,56,59,60]. Also, solvent systems besides pure methanol were investigated, including acetonitrile [44,54], chloroform [44,46,47,54-56,59,60], and water [42,58]. A new direction in research in the Brodbelt group involved a more comprehensive accounting of the variables which affect spray efficiencies in order to better understand the influence of the electrospray ionization process on competing complexation reactions [57].

It should be emphasized that all of the work reported in this dissertation, as well as the literature summarized above, focuses on the evaluation of binding selectivities in solution based on ESI-MS results, in contrast to binding properties in the gas phase as studied extensively by Armentrout [39] and Dearden [40-41]. In a gas-phase environment the relative binding affinities of macrocycles are largely dictated by the charge densities of the metal ions [39-41], whereas in the condensed phase, solvation effects increase the importance of "best fit" considerations, as well as hydrogen bonding and hydrophobic interactions [27].

For studies of host-guest complexation, ESI-MS has the advantages that it can analyze many complexes simultaneously (up to five complexes in the research discussed in this dissertation), complete analysis of these complexes in a few

minutes, and use less than 50 μl of solution at concentrations of analyte less than 1 μM. In addition, ESI-MS gives useful results for solvent systems from low polarity solvents such as chloroform to highly polar solvents such as methanol and water. ESI-MS is perhaps best for screening the binding properties of new hosts, and is somewhat less robust for quantitative measurements of binding constants.Though precise determinations of K values for host-guest complexes can be determined by ESI-MS, this usually involves the measurement of several samples obtained by titration. Generally, binding constants are determined by measuring the signal intensity of complex ions mass spectrometrically at many different guest-host ratios and a constant ionic strength. Next, a non-linear regression method is used to extrapolate the binding constant of the host guest complex. Several repetitions of the data must be collected and close control of instrumental conditions must be maintained in order to minimize errors and obtain a good association constant value.

The determination of relative selectivities of host-guest complexes by ESI-MS can be determined much more rapidly than single K values by ESI-MS or the other methods discussed, but has the current disadvantage that the solvation energies of the host-guest complexes being compared must be similar. This is because the quantity of desolvated ions of a given analyte that are formed by ESI is related to the solvation energy of the ions. For larger differences in solvation energies, correction factors called ‘spraying efficiencies’ can often be used to

obtain correct results. For some complexes the solvation energies are too different for their host-guest selectivities to be determined by ESI-MS, as is often the case for complexes formed for several hosts competing for one guest. However, in the cases of analyzing complexes formed with several guests competing with one host, the large size of the host common to all complexes compared to the small size of the guest ion usually results in similar solvation energies for the various complexes that result. The determinations of the relative selectivities in the research described in this dissertation are mostly for several guest ions towards the same host.

1.3 Overview of Dissertation Chapters

In Chapter 2, the instrumentation and experimental methods used in the research discussed in later chapters are introduced. Further details of the instrumentation and methods are discussed in the Experimental section of each chapter.

In Chapter 3, the evaluation of alkali metal cation selectivities of six lariat ethers with ether pendant groups by electrospray ionization-mass spectrometry in four methanolic solvent systems is described. The observed binding selectivities are affected by the number of oxygen atoms in the pendant ether group, the presence of a geminal propyl group, and to a lesser extent the polarity of the solvent environment. The results of *ab initio* calculations of several of the lariat ethers with alkali metal ions are also used to gain insight into the selectivity trends observed.

In Chapter 4, the alkali and alkaline earth metal binding selectivities of dibenzo-16-crown-5 and fifteen dibenzo-16-crown-5 lariat ether amides (LEAs), as determined by electrospray ionization mass spectrometry (ESI-MS), are studied. Additionally, the influence of the acid/base nature of the solution on metal cation selectivity is investigated. The validity of using ESI-MS for determination of selectivities is established by analogous experiments using hosts with known binding constants for the same metal cations and solvent systems. Collisionally activated dissociation (CAD) is used to evaluate the influence of the alkali metal cation binding on the fragmentation of the LEAs.

In Chapter 5, ESI-MS is used to evaluate the metal binding selectivities of an array of novel caged macrocycles for mercury(II), lead(II), cadmium(II), and zinc(II) ions. In homogenous methanol/chloroform solutions as well as extractions of metals from aqueous solution by macrocycles in chloroform, it is found that the type of heteroatom (S, O, N), cavity size, and presence of other substituents influence the metal selectivities. Several of the macrocycles in this study bind mercury very selectively and efficiently in the presence of many other metal ions and have an avidity towards mercury which was tunable by the size and combination of heteroatoms in the macrocycle ring and the number of cage groups attached. The extraction mechanism was further investigated by determining the variation in extraction selectivity as a function of the counter-ions of the mercury salts.

In Chapter 6, ESI-MS is used to evaluate the metal binding selectivities of an array of novel caged macrocycles for silver, gold, copper, nickel, zinc, iron, lead, manganese, and alkali metal ions. It is found that five of the new compounds display silver selectivity, and their relative affinities for various metals depends on the type, number, and arrangement of heteroatoms (N, O), the cavity size, and the presence of aromatic substituents. Alkali metal cation binding studies are used to evaluate the size-selectivities of the cavities of the macrocycles. Electronic structure calculation by B3LYP density function theory methods were used to model the metal complexes.

In Chapter 7, MS^n experiments with low energy CAD in a quadrupole ion trap are used to study the fragmentation of complexes of alkali, alkaline earth, and transition metal ions with naturally occurring and synthetic cyclic peptides is discussed and the results are compared with those obtained for protonated cyclic peptides. Complexes with metal ions were found to produce enhanced abundances of the most important fragments in identifying and characterizing cyclic peptides. For depsipeptides with alternating peptide and ester backbone bonds, sodium was found to be superior to protonated and other alkali metalated complexes for sequencing residues one at a time per MS^n cycle. Divalent metals, especially lead, were also found to be useful in the analysis of large cyclic depsipeptides with more than eight residues by preferentially cleaving off two residues at a time. For cyclic lipopeptides, cyclic peptides containing a fatty acid residue, complexes with silver

ion were found to provide enhanced abundances of important fragment ions. Complexes of nickel and silver ions with two cyclic peptides containing the physiologically important RGD motif were found to provide important complementary information to protonated peptide in MS^n analysis. For a more complete, updated version of Chapter 7, see Williams, et al. [61].

Chapter 8 briefly summarizes conclusions and future directions which can be deduced from Chapters 3-7.

1.4 References

1. Amabilino, D.B.; Preece, J.A.; Stoddart, J.F. Crown Ethers. *Macrocycle Synthesis*, Ed: Parker, D., Oxford University Press, Oxford, UK, **1996**, 71-91.

2. Bradshaw, J. S.; Izatt, R. M. Crown Ethers: The Search for Selective Ion Ligating Agents. *Acc. Chem. Res.*, **1997**, *30*, 338-345.

3. Arnaud-Neu, F.; Delgado, R.; Chaves, S.. Critical Evaluation of Stability Constants and Thermodynamic Functions of Metal Complexes of Crown Ethers (IUPAC Technical Report). *Pure Appl. Chem.*, **2003**, *75*, 71-102.

4. Bradshaw, J.S.; Izatt, R.M.; Bordunov, A.V.; Zhu, C.Y.; Hathaway, J.K. Crown Ethers. *Comprehensive Supramolecular Chemistry*, Ed.: Gokel, George W., **1996**, *1*, 35-95.

5. Fabre, B.; Simonet, J. Electroactive Polymers Containing Crown Ether or Polyether Ligands as Cation-Responsive Materials. *Coord. Chem. Rev.*, **1998**, *178-180(Pt. 2)*, 1211-1250.

6. Kimura, K.; Shono, T. Applications of Crown Compounds to Analytical and Separation Chemistry: Ion Sensor and Liquid Chromatography. *Studies Org. Chem.*,**1992**, *45*, 198-264.

7. Bartsch, R.A., Lu, J., Ohki, A., *J. Incl. Phenomena Mol. Recogn. In Chem*., **1998**, *32*, 133-150.

8. Ohki, A., Lu, J.-P., Hallman, J.L., Huang, X., Bartsch, J.A., *Anal. Chem*., **1995**, *67*, 2405-2408.

9. Ohki, A.; Lu, J.-P.; Bartsch, R.A.; *Anal. Chem.* **1994***, 66,* 651-654.

10. Ohki, A., Lu., J.-P., Huang, X., Bartsch, R.A., *Anal. Chem*., **1994**, *66*, 4332-4336.

11. Konyaeva, V. S.; Myshkin, A. E., *Russ. J. Gen. Chem.*, **1998**, *68*, 630-636.

12. Konyaeva, V. S.; Myshkin, A. E., *Russ. J. Gen. Chem.*, **1998**, 68, 637-642.

13. Konyaeva, V. S.; Myshkin, A. E., *Russ. J. Gen. Chem.*, **1998**, 68, 643-649.

14. Zalups, R. K., Molecular Interactions with Mercury in the Kidney. *Pharmacol. Rev*., **2000**, *52*, 113-143.

15. Wu, G., Jiang, W., Lamb, J. D., Bradshaw, J. S., Izatt, R. M., *J. Am. Chem. Soc.*, **1991**, *113*, 6538-6541.

16. Yamashita, K., Kurita, K., Ohara, K., Tamura, K., Nango, M., Tsuda, K., *React. Funct. Polym.*, **1996**, *31*, 47-55.

17. Zong, Z., Dong, S., Hu, Y., Xu, Y., Liu, W., *Eur. Polym. J.*, **1998**, *34*, 761-766.

18. Baumann, T. F., Reynolds, J. G., *Chem. Commun. (Cambridge)*, **1998**, *16*, 1637-1638.

19. Nelson, A. J., Reynolds, J. G., Baumann, T. F., Fox, G. A., *Appl. Surf. Sci.*, **2000**, *167*, 205-215.

20. Baumann, T. F.; Reynolds, J. G.; Fox, G. A., *React. Funct. Polym.*, **2000**, *44*, 111-120.

21. Saad, B., Sultan, S. M., Talanta, **1995**, *42*, 1349-1354.

22. Merrill, D. T., Van Maltby, C., Kahmark, K., Gerhardt, M., Melcer, H., *Tappi J.*, **2001**, 84, 63.

23. de Sousa, M., Bertazzoli, R., *Anal. Chem.*, **1996**, *68*, 1258-1261.

24. Davies, J.S. Cyclic Peptides. Cyclic Polymers (2nd Edition), Ed.: Semlyen, J.A., Kluwer Academic Publishers, Dordrecht, Netherlands, **2000**, 85-124.

25. Oberg K. Chemotherapy and Biotherapy in the Treatment Of Neuroendocrine Tumours. *Annals of Oncology*, **2001**, *12 Suppl. 2*, S111-4.

26. Fernandez-Lopez, S.; Kim, H.-S.; Choi, E.C.; Delgado, M.; Granja, J.R.; Khasanov, A.; Kraehenbuehl, K.; Long, G.; Weinberger, D.A.; Wilcoxen, K.M.; Ghadiri, M.R. Antibacterial Agents Based on the Cyclic D-L-Alpha-Peptide Architecture, *Nature*, **2001**, *412*, 452-455.

27. Martell, A.E., Hancock, R.D., Chapter 7: "Stability Constants and Their Measurement", *Metal Complexes in Aqueous Solutions,* Plenum Press: New York, **1996**.

28. Tusek-Bozic, L.; Danesi, P.R. Complexation Of Some Substituted Macrocyclic Polyethers With Alkali Metal Cations In Methanol, Dimethylsulfoxide And Acetonitrile. *J. Inorg. Nuc. Chem.*, **1979**, *41*, 833-7.

29. Evans, D. F.; Wellington, S. L.; Nadis, J. A.; Cussler, E. L. Conductance of Cyclic Polyether-Cation Complexes. *J. Solution Chem.*, **1972**, *1*, 499-506.

30. Johnstone, R. A. W.; Lewis, I. A. S. Crown Ether Complexes of Metallic Cations Investigated by Fast-Atom Bombardment. *Int. J. Mass Spectrom. Ion Phys.*, **1983**, *46*, 451-4.

31. Johnstone, R. A. W.; Rose, M. E., Macrocyclic Ligands Examined by Fast-Atom-Bombardment Mass Spectrometry: Direct Observation of Metal Cation Selectivity in Complexation. *J. Chem. Soc., Chem. Commun.*, **1983**, *21*, 1268-70.

32. Johnstone, R.A.; Lewis, I.A.S.; Rose, M.E. Fast Atom Bombardment Of Crown Ether/Cation Complexes In Solution. Inferences on Mechanisms of Energy Transfer. *Tetrahedron*, **1983**, *39*, 1597-603.

33. Langley, G.J.; Hamilton, D.G.; Grossel, M.C. Critical Re-Evaluation of FABMS Analysis Of Ligand-Cation Interactions. *J. Chem. Soc., Perkin Trans. 2,* **1995**, *5*, 929-33.

34. Bonas, Georges; Bosso, Claude; Vignon, Michel R. Fast Atom Bombardment Mass Spectrometry for Crown Ether-Alkali Cation Stability Constant Determination. *Rapid Commun. Mass Spectrom.*, **1988**, *2*, 88-9.

35. Abdoul-Carime, H. Chorand Crown Ether Macrocycle-Alkali Metal Cation 1:1 Complexes 'Host-Guest' Effect Investigated Directly by Mass Spectrometry. *J. Chem. Soc., Faraday Trans.*, **1998**, *94*, 2407-2410.

36. Young, D.-S.; Hung, H.-Y.; Liu, L.K. Estimation of Selectivities and Relative Cationization Efficiencies of Different [Crown + M]$^+$ By Electrospray Mass Spectrometry. *J. Mass Spectrom.*, **1997**, *32*, 432-437.

37. Young, D.-S.; Hung, H.-Y.; Liu, L.K. An Easy and Rapid Method for Determination of Stability Constants by Electrospray Ionization Mass Spectrometry. *Rapid Commun. Mass Spectrom.*, **1997**, *11*, 769-773.

38. Leize, E.; Jaffrezic, A.; Van Dorsselaer, A. Correlation between Solvation Energies and Electrospray Mass Spectrometric Response Factors. Study by Electrospray Mass Spectrometry of Supramolecular Complexes in Thermodynamic Equilibrium in Solution. *J. Mass. Spectrom.* **1996**, *31*, 537-544.

39. Armentrout, P.B. "Cation-Ether Complexes in the Gas Phase: Thermodynamic Insight into Molecular Recognition," *Int. J. Mass Spectrom*., **1999**, *193*, 227-240.

40. Nicoll, J.B.; Dearden, D.V. Reactions of Multidentate Ligands with Ligated Alkali Cation Complexes: Self-Exchange and 'Sandwich' Complex Formation Kinetics of Gas Phase Crown Ether-Alkali Cation Complexes. *Int. J. Mass Spectrom*., **2001**, *204*, 171-183.

41. Dearden, D.V.; Liang, Y.; Nicoll, J.B.; Kellersberger, K.A. Study of Gas-Phase Molecular Recognition using Fourier Transform Ion Cyclotron Resonance Mass Spectrometry (FTICR/MS). *J. Mass Spectrom.*, **2001**, *36*, 989-997.

42. Blair, S.M.; Kempen, E.C.; Brodbelt, J.S. Determination of Binding Selectivities in Host-Guest Complexation by Electrospray/Quadrupole Ion Trap Mass Spectrometry. *J. Am. Soc. Mass Spectrom.*, **1998**, *9*, 1049-1059.

43. Blair, S.M.; Brodbelt, J.S.; Madhusudhan, R.G.; Marchand, A.P. Evaluation of Binding Selectivities of Bis-Crowned Clefts by Electrospray

Ionization/Quadrupole Ion Trap Mass Spectrometry. *J. Mass Spectrom.*, **1998**, *33*, 721-728.

44. Brodbelt, J.S.; Kempen, E.; Reyzer, M.. Determination of Binding Selectivities by Electrospray Ionization Mass Spectrometry. *Struct. Chem.*, **1999**, *10*, 213-220.

45. Kempen, E.C.; Brodbelt, J.S.; Bartsch, R.A.; Jang, Y.; Kim, J.S.. Investigation of Alkali Metal Cation Selectivities of Lariat Ethers by Electrospray Ionization Mass Spectrometry. *Anal. Chem.*, **1999**, *71*, 5493-5500.

46. Goolsby, B.J.; Brodbelt, J.S.; Adou, E.; Blanda, M. Determination of Alkali Metal Ion Binding Selectivities of Calixarenes by Matrix-Assisted Laser Desorption Ionization and Electrospray Ionization in a Quadrupole Ion Trap. *Int. J. Mass Spectrom.*, **1999**, *193*, 197-204.

47. Blanda, M.T.; Farmer, D.B.; Brodbelt, J.S.; Goolsby, B.J. Synthesis and Alkali Metal Ion Binding Properties of Two Rigid Stereochemical Isomers of Calix[6]arene Bis-crown-4. *J. Am. Chem. Soc.*, **2000**, *122*, 1486-1491.

48. Blair, S.M.; Brodbelt, J.S.; Marchand, A.P.; Kumar, K.A.; Chong, H.-S. Evaluation of Binding Selectivities of Caged Crown Ligands toward Heavy Metals by Electrospray Ionization/Quadrupole Ion Trap Mass Spectrometry. *Anal. Chem.*, **2000**, *72*, 2433-2445.

49. Blair, S. M.; Brodbelt, J. S.; Marchand, A. P.; Chong, H.-S.; Alihodzic, S. Evaluation of Alkali Metal Binding Selectivities of Caged Aza-Crown Ether Ligands by Microelectrospray Ionization/Quadrupole Ion Trap Mass Spectrometry. *J. Am. Soc. Mass Spectrom.*, **2000**, *11*, 884-891.

50. Kempen, E.C.; Brodbelt, J.S. A Method for the Determination of Binding Constants by Electrospray Ionization Mass Spectrometry. *Anal. Chem.*, **2000**, *72*, 5411-5416.

51. Kempen, E.C.; Brodbelt, J.S.; Bartsch, R.A.; Blanda, M.T.; Farmer, D.B. Screening Metal Binding Selectivities of Macrocycle Mixtures by HPLC-ESI-MS and Postcolumn Reactions. *Anal. Chem.*, **2001**, *73*, 384-390.

52. Brodbelt, J.S. Probing Molecular Recognition by Mass Spectrometry. *Int. J.Mass Spectrom.*, **2000**, *200*, 57-69.

53. Reyzer, M. L.; Brodbelt, J. S.; Marchand, A. P.; Chen, Z.; Huang, Z.; Namboothiri, I. N. N. Determination Of Alkali Metal Binding Selectivities Of Caged Crown Ligands By Electrospray Ionization Quadrupole Ion Trap Mass Spectrometry. *Int. J. Mass Spectrom.*, **2001**, *204*, 133-142.

54. Williams, S.; Blair, S.M.; Brodbelt, J.S.; Huang, X.; Bartsch, R.A. Determination of Alkali Metal Cation Selectivities of Dibenzo-16-Crown-5 Lariat Ethers with Ether Pendant Groups by Using Electrospray Ionization Quadrupole Ion Trap Mass Spectrometry. *Int. J. Mass Spectrom.*, **2001**, *212*, 389-401.

55. Marchand, A.P.; Huang, Z.; Chen, Z.; Hariprakasha, H. K.; Namboothiri, I. N. N.; Brodbelt, J.S.; Reyzer, M.L. Synthesis, Alkali Metal Picrate Extraction, and Alkali Metal Cation Binding Selectivities of Some New Cage-Annulated Polyoxamacrocyclic Crown Ethers. *J. Heterocyc. Chem.*, **2001**, *38*, 1361-1368.

56. Williams, S.M.; Brodbelt, J.S.; Marchand, A.P.; Cal, D.; Mlinaric-Majerski, K. Metal Complexation of Thiacrown Ether Macrocycles by Electrospray Ionization Mass Spectrometry. *Anal. Chem.*, **2002**, *74*, 4423-4433.

57. Sherman, C.L.; Brodbelt, J.S. An Equilibrium Partitioning Model for Predicting Response to Host-Guest Complexation in Electrospray Ionization Mass Spectrometry. *Anal. Chem.*, **2003**, *75*, 1828-1836.

58. Williams, S.M.; Brodbelt, J.S.; Bartsch, R.A. Evaluation of Alkali and Alkaline Earth Metal Cation Selectivities of Lariat Ether Amides by Electrospray Ionization Mass Spectrometry. *J. Am. Soc. Mass Spectrom.*, **2003**, *14*, 1215-1228.

59. Williams, S.M., Brodbelt, J.S., Huang, Z, Lai, H., Marchand, A.P., Complexation of Silver and Co-recovered Metals with Novel Aza-Crown Ether Macrocycles by Electrospray Ionization Mass Spectrometry, *Analyst*, **2003**, *128*, 1352-1359.

60. Marchand, A. P.; Huang, Z.; Lai, H.; Brodbelt, J. S.; Williams, S. Synthesis and Electrospray Ionization Mass Spectrometric Evaluation of the Metal Cation Complexation Behavior of Cage-annulated Azacrown Ethers. *Heterocycles*, **2003**, accepted.

61. Williams, S.M.; Brodbelt, J.S. **2004**, manuscript in preparation.

CHAPTER 2

Experimental Techniques and Methods

2.1 Electrospray Ionization

Electrospray ionization (ESI) is a method of transferring analyte ions in a condensed phase solution to the gas-phase by applying a large electrical field of 1-5 kV between a needle from which the analyte solution is flowing, which serves as an electrode, and a counter-electrode [1-3]. As the charged droplets travel between the electrode and counter-electrode, they form what is known as a Taylor cone, within which the charged droplets are desolvated to become naked ions. In 2002, John Fenn was awarded a portion of the Nobel Prize in Chemistry for his contribution to the development of the ESI technique in mass spectrometry.

Of the several ionization methods used to ionize anaytes for mass spectrometric analysis, ESI is probably the gentlest technique currently available. Thus, covalent complexes survive the ionization and desolvation steps of ESI and can be studied in the gas-phase. This has made possible the mass spectrometric analysis of non-covalent ligand-substrate complexes involving protein complexes of subunits and co-factors, enzymes with inhibitors, polynucleic acids with drugs, macrocycles with guest ions, and metal ions with these compounds and many other

ligands. In many cases, when the solvation energies of different complexes are similar to each other, the ratios in which these complexes exist in solution are maintained in the gas-phase and the selectivities of a ligand for several substrates can be quantified using the intensities of signals for the complexes obtained mass spectrometric analysis. These studies have importance to many applications, some of which are mentioned in section 1.1 of this dissertation. The work in this dissertation is a continuation of work initiated in the Brodbelt group five years ago. Prior work by these investigators validated the quantitative analysis of complexes formed between alkali metal ions and crown ethers and cyclic and non-cyclic crown ether analogs, the semi-quantitative analysis of complexes containing several transition metal ions with these types of ligands and also explored the relationship between the structures of the complexes and selectivities of the hosts.

2.2 Quadrupole Ion Trap Mass Spectrometry

Qudrupole ion trap (QIT) mass spectrometers are recognized for their great sensitivity and ruggedness, as well as their simplicity of design, low cost and, consequently, their widespread availability [4-11]. In 1989 Hans Dehmelt and Wolfgang Paul shared half of the Nobel Prize in Physics for their development and study of the QIT, invented in 1953 [12], for this reason also referred to as the Paul trap. For the types of analysis described herein, the analyte ions in solution are transferred to the gas phase by ESI and guided into the QIT analyzer by a series of

electrical lenses. Although the ionization occurs at or near atmospheric pressure, the pressure in the QIT is maintained near one millitorr by high vacuum pumping to prevent loss of ions and their charge through collisions. A diagram of a cross sections of the QIT is shown in Figure 2.1. A radio frequency (RF) field emanating from the ring electrode of the QIT contains the ions within the trap and can trap and accumulate ions for several seconds or even minutes. By ramping the RF field voltage, ions can be ejected from the trap according to their mass-to-charge ratio to a detector, thus allowing separation and quantification of ions of different mass-to-charge ratios. Because the QIT can trap and accumulate ions simultaneously for several seconds, very low concentrations of analyte in the sample can often be detected by collecting the analyte ion for long periods of time before detection.

Figure 2.1 Quadrupole ion trap

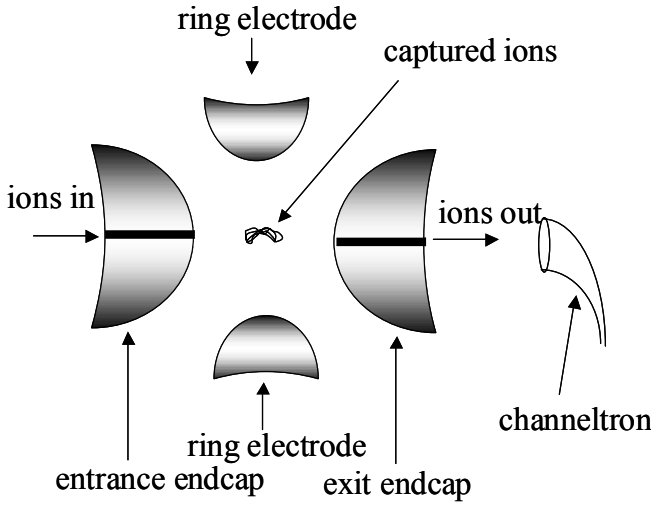

2.3 Isolation and Collision Activated Dissociation

By using scanning programs involving varying voltages on the end-cap and ring electrodes, ions of selected m/z values can be isolated in the QIT and other ions ejected, which can improve the sensitivity for this ion or allow one to perform gas phase reactions with it. To keep the ions in the QIT at a low enough kinetic energy to keep them trapped, a bath gas such as helium must be maintained in the QIT at about 1 mTorr. By applying a low AC voltage to the end-cap electrodes, the kinetic energy of the trapped ions can be increased such that the collisions of the ions with the bath gas result in fragmentation of the trapped ions. This will result in fragmentation of the precursor ions, forming product ions, which can then be further isolated or scanned out of the QIT to the detector to be used for structural analysis of the precursor ion. The necessary frequencies required to isolate the ion of interest and perform CAD on it are created using stored waveform inverse Fourier transform (SWIFT) calculations using LabView software. All of the research discussed in this dissertation involved the use of ESI-QIT mass spectrometry. Fragmentation reactions of precursor ions, referred to as collision activated dissociation (CAD) or collision induced dissociation (CID), are discussed in Chapters 5 and 8.

2.4 Electronic Structure Method Calculations

Theoretically determining the structures of host-guest complexes using electronic structure methods such as molecular mechanics, *ab initio* and density functional theory calculations can aid in understanding the results observed from mass spectrometry experiments. For the calculations described in Chapters 4 and 5, molecular mechanics conformational searches were performed using MMFF (Merck) force fields followed by *ab initio* calculations using a Restricted Hartree-Fock model at the 3-21G* level of theory. Calculations in Chapter 4 were performed with Spartan© software (Wavefunction Inc., Irvine, CA) operated on a Silicon Graphics O2 computer workstation with an IRIX 6.5 operating system and 300 MHz MIPS R5000 processor (Silicon Graphics Inc., Mountain View, CA). Calculations in Chapter 5 were performed with Spartan '02 PC© software [13] (Wavefunction Inc., Irvine, CA) operated on a Gateway PC with an Intel Pentium 4 processor. For the calculations described in Chapter 6, molecular mechanics conformational searches were performed using MMFF (Merck) force fields and the lowest energy conformer was then subjected to higher level methods. *Ab initio* calculations using a Restricted Hartree-Fock model at the 6-31G* level of theory were performed for all alkali metal complexes. B3LYP/6-31G* calculations were used for complexes containing copper, silver, or zinc ions. B3LYP/6-31G** calculations were used for complexes containing gold ions. Electronic structure

methods were calculated using Spartan '02 PC© software [13] (Wavefunction Inc., Irvine, CA) operated on a Gateway PC with an Intel Pentium 4 processor.

2.5 Additional Instrumental Design and Implementation

Mass spectrometry results in Chapters 4, 5, and 7 were obtained in whole or in part using a Finnigan ITMS mass spectrometer with a homebuilt ESI source and vacuum chamber based on a design from Oak Ridge National Laboratory. The mass spectrometry results in Chapter 4 used ITMS software modified by the Yost group at the University of Florida to perform SWIFT calculations. This software collected spectra by obtaining screen captures of them. Additional Ion Capture Mass Spectrometry (ICMS) software developed buy the Yost group which allowed for collection of a point-wise list of intensity versus m/z profile data of spectra from the mass spectrometer was installed. The ITMS SAP circuit board was modified according to the ICMS manual in order to implement the ICMS system.

For the mass spectrometry experiments in Chapter 7, a microspray ESI interface for the ITMS mass spectrometer which performed heated sheath gas assisted ESI was developed. This interface was found to be capable of suppressing protonated versus metalated ligand signal when using nitrogen gas and to greatly enhance signal intensities (approximately 10-fold) when using helium gas.

2.6 References

1. Loo, J.A.; Holsworth, D.D.; Root-Berstein, R.S. *Biol. Mass Spectrom.*, **1994**, *23*, 6-12.. Lamcharfi, E.; Chuilon, S.; Kerbal, A.; Kunesch, G.; Libot, F.; Virelizier, H. *J. Mass Spectrom.*, **1996**, *31*, 982-986. Robinson, C.V.; Chung, E.W.; Kragelund, B.B.; Knudsen, J.; Aplin, R.T.; Doulsen, F.M.; Dobson, C.M. *J. Am. Chem. Soc.*, **1996**, *118*, 8646-8653. Cheng, X.; Chen, R.; Bruce, J.E.; Schwartz, B.L.; Anderson, G.A.; Hofstadler, S.A.; Gale, D.C.; Smith, R.D. *J. Am. Chem. Soc.*, **1995**, *117*, 8859-8860.

2. Dole, M.; Mack, L.L.; Hines, R.L.; Mobley, R.C.; Ferguson, L.D.; Alice, M.B.; *J. Chem. Phys.*, **1968**, 49, 2240. Dole, M.; Mack, L.L.; Hines, R.L.; Mobley, R.C.; Ferguson, L.D.; Alice, M.B. *J. Chem. Phys*., **1979**, *71*, 4451.

3. Iribarne, J.V.; Thompson, B.A.; *J. Chem. Phys.*, *1976*, 64, 2287.

4. Stafford, G. Ion Trap Mass Spectrometry: A Personal Perspective. *J. Am. Soc. Mass Spectrom.*, **2002**, *13*, 589-596.

5. Hao, C.; March, R.E. A Survey of Recent Research Activity in Quadrupole Ion Trap Mass Spectrometry. *Int. J. Mass Spectrom.*, **2001**, *212*, 337-357.

6. March, R.E. Quadrupole Ion Trap Mass Spectrometry. A View at The Turn of The Century. *Int. J. Mass Spectrom.*, **2000**, *200*, 285-312.

7. Todd, J.F.J.; March, R.E. A Retrospective Review of the Development and Application of the Quadrupole Ion Trap Prior to the Appearance of Commercial Instruments. *Int. J. Mass Spectrom.*, **1999**, *190/191*, 9-35.

8. March, R.E. An Introduction to Quadrupole Ion Trap Mass Spectrometry. *J. Mass Spectrom.*, **1997**, *32*, 351-369.

9. March, R.E.; Todd, J.F. J. Eds. *Practical Aspects of Ion Trap Mass Spectrometry, Volume I: Fundamentals of Ion Trap Mass Spectrometr*y, CRC Press, New York, New York, **1995**, 430 pp.

10. March, R.E.; Todd, J.F. J. Eds. *Practical Aspects of Ion Trap Mass Spectrometry; Volume II: Ion Trap Instrumentation*, CRC Press, New York, New York, **1995**, 320 pp.

11. March, R.E.; Todd, J.F. J.; Eds. *Practical Aspects of Ion Trap Mass Spectrometry; Volume III: Chemical, Environmental and Biomedical Applications*, CRC Press, New York, New York, **1995**, 518 pp.

12. Paul, W.; Steinwedel, H.Z.; *Naturforsch.*, **1953**, *8a*, 448.

13. Kong, J.; White, C.A.; Krylov, A.I.; Sherill, C.D.; Adamson, R.D.; Furlani, T.R..; Lee, M.S.; Lee, A.M.; Gwaltney, S.R.; Adams, T.R.; Ochsenfeld, C.; Gilbert, A.T.B.; Kedziora, G.S.; Rassolov, V.A.; Maurice, D.R.; Nair, N.; Shao, Y., Bsley, N.A.; Maslen, P.E.; Dombroski, J.P.; Daschel, H.; Zhang, W.; Korambath, P.P.; Baker, J.; Byrd, E.F.C.; Van Voorhis, T.; Oumi, M.; Hirata, S.; Hsu, C.-P., Ishikawa, N.; Florian, J.; Warshel, A.; Johnson, B.G.; Gill, P.M.W.; Head-Gordon, M.; Pople, J.A. *J. Computational Chem.*, **2000**, *21*, 1532.

CHAPTER 3

Determination of Alkali Metal Cation Selectivities of Dibenzo-16-Crown-5 Lariat Ethers with Ether Pendant Groups Using Electrospray Ionization Quadrupole Ion Trap Mass Spectrometry

3.1 Introduction

The use of electrospray ionization – mass spectrometry (ESI-MS) [1-4] has proven to be successful for the analysis of a wide variety of non-covalently bound complexes. Moreover, numerous recent studies have shown that the equilibrium distribution of complexes in solution is reflected in the intensities of complexes observed in the mass spectra obtained upon ESI-MS of the solutions [5-35]. For determination of binding selectivities in host-guest chemistry, the intensities of complexes produced by ESI of solutions containing defined concentrations of one host and multiple guests are compared. ESI-MS analysis of binding selectivities has some advantages over the more conventional potentiometric, spectrophotometric and NMR titrimetric methods [36], such as reduced sample consumption, tolerance of a wide variety of solvent conditions and reduced analysis times.

This ESI-MS method for measuring selectivities has been investigated in great detail in our laboratory [21-29] for hosts such as crown ethers and other

macrocycles with guests like alkali metal, transition metal, heavy metal and ammonium ions. The ESI-MS method is most successful for analysis of host selectivities for a series of similar cations, resulting in the analysis of complexes with similar solvation energies. Thus, in these cases the resulting ESI mass spectral distributions of complexes generally agree well with the equilibrium distribution of complexes in solution, thus allowing the correlation of host structure/selectivity relationships. In the present work, ESI-MS is used to analyze the alkali metal binding selectivities of the six lariat ethers shown in Figure 3.1. All six of the lariat ethers have the same dibenzo-16-crown-5 skeleton, but they differ in the substituents attached to the center carbon of the three-carbon bridge. The first substituent consists of an ether of varied length and number of oxygen binding sites, and the second sidearm is either a hydrogen or a geminal propyl group.

The ability of lariat ethers to effectively complex metals has led to their development and optimization for use in ion selective electrode membranes [37–40]. Of these six lariat ethers, **1-4** have been investigated previously by conventional methods. Bartsch and co-workers incorporated each of these lariat ethers into PVC membranes and analyzed their alkali metal cation (Li^+, Na^+ and K^+) selectivities using a fixed interference method in aqueous solutions [39]. Based on the diameters of the metal ions (Li^+:1.36 Å, Na^+: 1.96 Å, K^+: 2.66 Å, Rb^+: 2.98 Å, Cs^+: 3.30 Å [41]), the cavity of unsubstituted dibenzo-15-crown-5 is expected to be optimal for complexation of Na^+ [39]. The potentiometric measurements

revealed that both **1** and **2** showed modest selectivity (i.e. less than half an order of magnitude difference in binding constants) for Na^+ over K^+ and pronounced selectivity for Na^+ over Li^+ (i.e., over three orders of magnitude difference in binding constants). Lariat ether **3** showed a comparable degree of selectivity for Na^+ over Li^+ and K^+ as **1** and **2**, but **4** exhibited substantially higher Na^+/K^+ selectivity than the other three, with a difference in Na^+ and K^+ binding constants of over an order of magnitude. The enhanced Na^+/K^+ selectivity on going from **2** to **4** was attributed to the ability of the second ether oxygen in the sidearm of **4** to coordinate the metal ion with optimization of the binding conformation provided by the presence of the propyl group. In general, the presence of a propyl group as the second pendant group assists in optimal pre-organization of the ether pendant group relative to the cavity, thus enhancing the overall Na^+/K^+ binding selectivity. In the present study, the alkali metal selectivities of **1 – 6** are examined by ESI-MS in several solvent systems.

3.2 Experimental Methods

3.2.1 Mass Spectrometry

All mass spectrometry experiments were performed with a Finnigan ion trap mass spectrometer (ThermoFinnigan, San Jose, CA) operating in the mass selective instability mode with modified electronics to allow axial modulation and

Figure 3.1 Lariat ethers.[a]

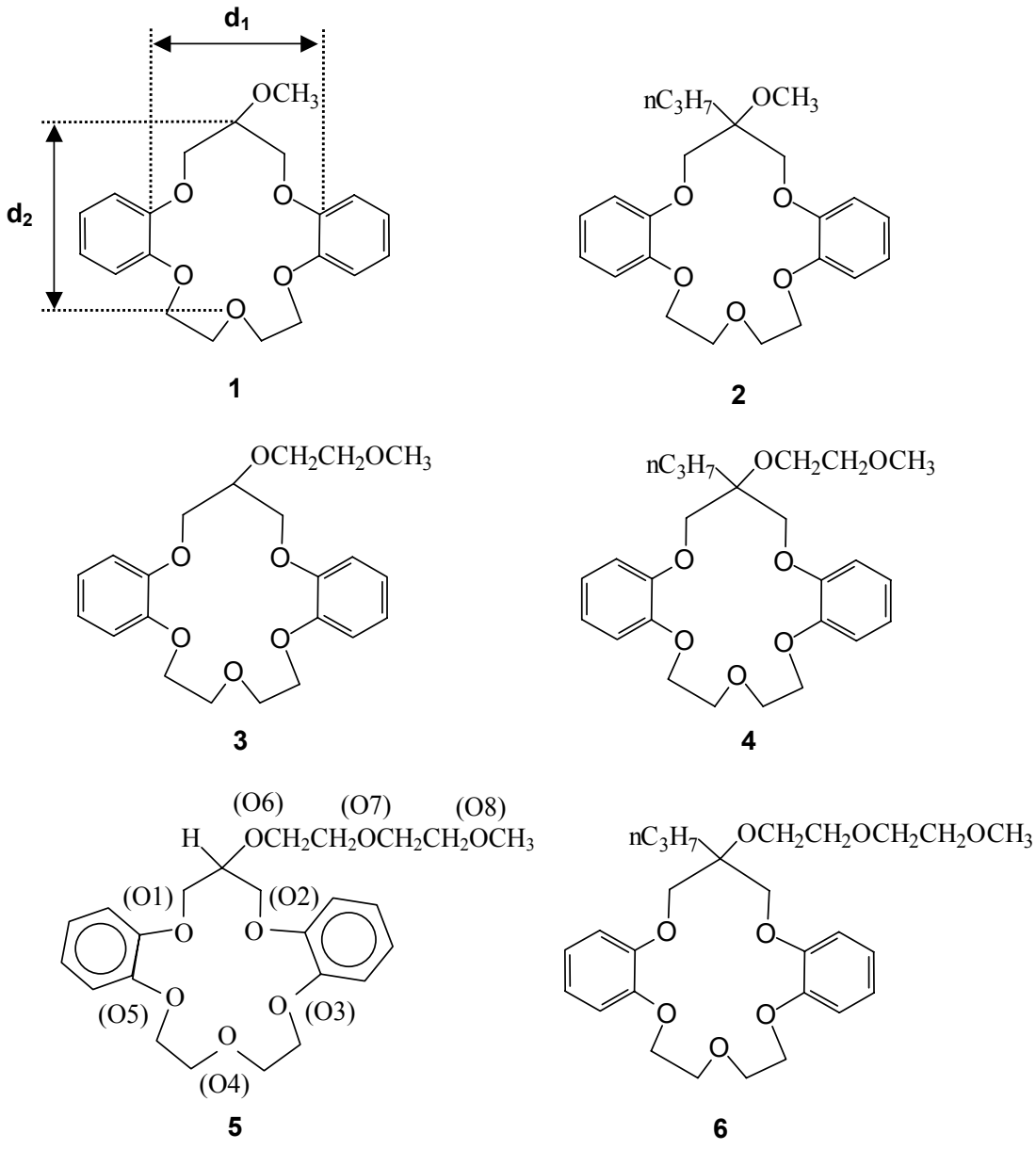

[a] d_1 and d_2, as defined with **1**, represent the center to center distances between the indicated atoms for **1** and for the analogs **2-6.** These distances are tabulated in Table 3.2. The numbering system of the oxygens for lariat ethers **1-6**, as it is used in this paper, is shown with **5**.

equipped with an in-house built electrospray source. The electrospray interface is based on a design developed by Oak Ridge National Laboratories (Oak Ridge, TN) involving a differentially pumped region containing ion focusing lenses [45]. The Harvard syringe pump system (Harvard Apparatus Inc., Holliston, MA) operated at a flow rate of 3.0 μl/min for all solutions. Neither a heated desolvation capillary nor a sheath flow gas was used. The ESI needle voltage was 3.0 kV. Each spectrum taken was an average of 30 scans. Reported values are the average of 120-240 scans.

For screening of the alkali metal cation selectivities of lariat ethers **1-6**, solutions containing a single host with multiple metal ions were analyzed. Previous studies have shown that only minimal correction factors, if any, are needed when using the ratio of the peak heights of two complexes (same host, different metal ions) to determine the alkali metal cation selectivities of each host [21-25], primarily because the host–metal complexes within a series have similar structures and solvation energies. Solutions containing one part of host and two parts of each metal ion were analyzed for each lariat ether in 99% methanol/1% chloroform, 75% methanol/25% chloroform, 50% methanol/50% chloroform, and 5% methanol/95% acetonitrile. The excess of metal ions relative to the lariat ether creates a more competitive binding environment for complexation with the host compound. Throughout the study, the minimum one part concentration of host was 5.0×10^{-5} M and concentrations of the metal ions were 1.0×10^{-4} M. The choices of 5.0×10^{-5}

M in lariat ether and 1.0 x 10^{-4} M in each alkali metal salt were used to ensure solubility of all salts in the solvent medium while maintaining conditions for increased selectivity over solutions containing one part host and one part of each guest metal ion. All metals salts used for these experiments were purchased from Aldrich Chemical Co. (Milwaukee, Wisconsin) and used without further purification. Theoretical values of solution equilibria conditions were obtained using MINEQL+ solution equilibria software, version 4.01 (Environmental Research Software, Hallowell, ME).

3.2.2 Ab initio Calculations

Molecular mechanics conformational searches were performed using MMFF (Merck) force fields followed by *ab initio* calculations using a Restricted Hartree-Fock model at the 3-21G* level of theory with Spartan© software (Wavefunction Inc., Irvine, CA) operated on a Silicon Graphics O2 computer workstation with an IRIX 6.5 operating system and 300 MHz MIPS R5000 processor (Silicon Graphics Inc., Mountain View, CA).

3.3 Results and Discussion

3.3.1 ESI-MS Strategy

Prior to mass spectrometric evaluation of the binding selectivities of lariat ethers **1-6**, studies of solutions containing dibenzo-18-crown-6, a model host, and alkali metal cations were undertaken to verify the correlation between ESI mass spectral intensities and the equilibrium distribution of complexes in solution. The known log K values for the dibenzo-18-crown-6/metal ion complexes in methanol are: 4.4 for Na^+, 4.8–5.0 for K^+, and 4.4-4.6 for Rb^+ [46]. For our calculations of the equilibrium distributions, the log K values of 4.4 for Na^+, 5.0 for K^+, and 4.6 for Rb^+ were utilized. From these log K values, the expected distribution of complexes in solution can be calculated for any initial concentrations of dibenzo-18-crown-6 and alkali metal cations, and then compared to the distribution of complexes detected in the mass spectra. Two sets of results are summarized in Table 3.1 for this type of experiment, involving either 1:1:1:1 or 1:5:5:5 methanolic solutions of dibenzo-18-crown-6 and three alkali metal cations, Na^+, K^+ and Rb^+. For both solutions, dibenzo-18-crown-6 preferentially binds K^+ over Rb^+ and Na^+, in good agreement with the calculated equilibrium preferences. Moving from a 1:1:1:1 host/metal ions mixture to a 1:5:5:5:5 host/metal ions mixture enhances the observed selectivity to a modest degree because the greater excess of metal

Table 3.1 Alkali metal cation selectivity of dibenzo-18-crown-6 in methanol.

	% $(DB18C6 + Na)^+$	% $(DB18C6 + K)^+$	% $(DB18C6 + Rb)^+$
1:1:1:1 in CH_3OH			
Theoretical equilibrium distribution[a,b]	20	52	28
Experimental ESI-MS distribution[b]	9	61	30
1:5:5:5 in CH_3OH			
Theoretical equilibrium distribution[c]	15	60	24
Experimental ESI-MS distribution[c]	7	68	25

[a]Theoretical values obtained using MINEQL+ solution equilibria software, version 4.01 (Environmental Research Software, Hallowell, ME), and the following log K values reported in the literature: $Na^+ = 4.4$, $K^+ = 5.0$, $Rb^+ = 4.6$ [46].
[b] The initial concentrations of DB18C6 and the three metal chlorides are each 2.0×10^{-4} M.
[c] The initial concentration of DB18C6 is 2.0×10^{-4} M and the three metal chlorides are each 1.0×10^{-3} M.

ions increases the competition between the various metal ions for the available host molecules. This trend in enhanced selectivity is reflected in both the calculated equilibrium distribution and the experimentally observed distribution of complexes.

Modest differences in the distribution of complexes and the degree of selectivity obtained for the ESI-MS results relative to the calculated equilibrium values are attributed to two factors. First, the range in the reported log K values for dibenzo-18-crown-6 [46] indicates a degree of variability that could alter the expected distribution of complexes by up to 10%. Second, formation of droplets in the electrospray process occurs in a partially humid laboratory atmosphere, thus meaning that the 100% methanolic environment is difficult to maintain. A small amount of water in the spray process may alter the observed alkali metal cation selectivity of dibenzo-18-crown-6 due to the modification of the polarity of the solvent.

3.3.2 Alkali Metal Cation Selectivities of Lariat Ethers

For evaluation of the alkali metal cation selectivities of lariat ethers **1-6**, each lariat ether was mixed with alkali metal salts in a 1:2:2:2:2 ratio (host : Li^+ : Na^+ : K^+ : Rb^+). Four different solvent environments were investigated for effects on binding selectivity: 99% methanol/1% chloroform (1% chloroform is required for solubilization of the lariat ethers), 75% methanol/25% chloroform, 50% methanol/50% chloroform, and 5% methanol/95% acetonitrile. Negligible differences in spray efficiencies are observed within each set of host/alkali metal

cation complexes, based on examination of the intensities of lariat ether/alkali metal cation complexes for solutions containing a single lariat ether in excess and only one metal ion (data not shown). Figures 3.2 and 3.3 illustrate examples of the mass spectra obtained in the four methanolic solvent systems for lariat ethers **1** and **4.** The spectra illustrate the 1:1 lariat ether/metal complexes are the dominant species and solvated adducts are not observed, so that only the ratio of the solvation energies of the former, which is nearly unity, needs to be considered. Moreover, it is evident that the solvent environment influences the selectivity of alkali metal cation complexation more significantly for lariat ether **1** than for **4**, as explained later.

Figure 3.4 summarizes the complete set of ESI-MS results obtained for the distributions of alkali metal cation complexes of the six lariat ethers, as measured by mass spectral peak intensities. Note that these experiments give a way of evaluating the selectivities, but not the absolute avidities, of the lariat ethers for the metal ions. Figure 3.4 illustrates that complexation of either Li^+ or Rb^+ is generally less favorable than complexation of Na^+ or K^+ for each of the lariat ethers, which is due to Na^+ and K^+ having ionic diameters closer to the diameter of the 16-Crown-5 ring of the lariat ethers so that Li^+ is too small and Cs^+ is too large to complex as effectively as Na^+ and K^+. Thus, the Na^+/ K^+ selectivities provide the most relevant comparisons, as highlighted in Figure 3.5.

Figure 3.2 ESI mass spectra of lariat ether 1 with LiCl, NaCl, KCl and RbCl (1:2:2:2:2).

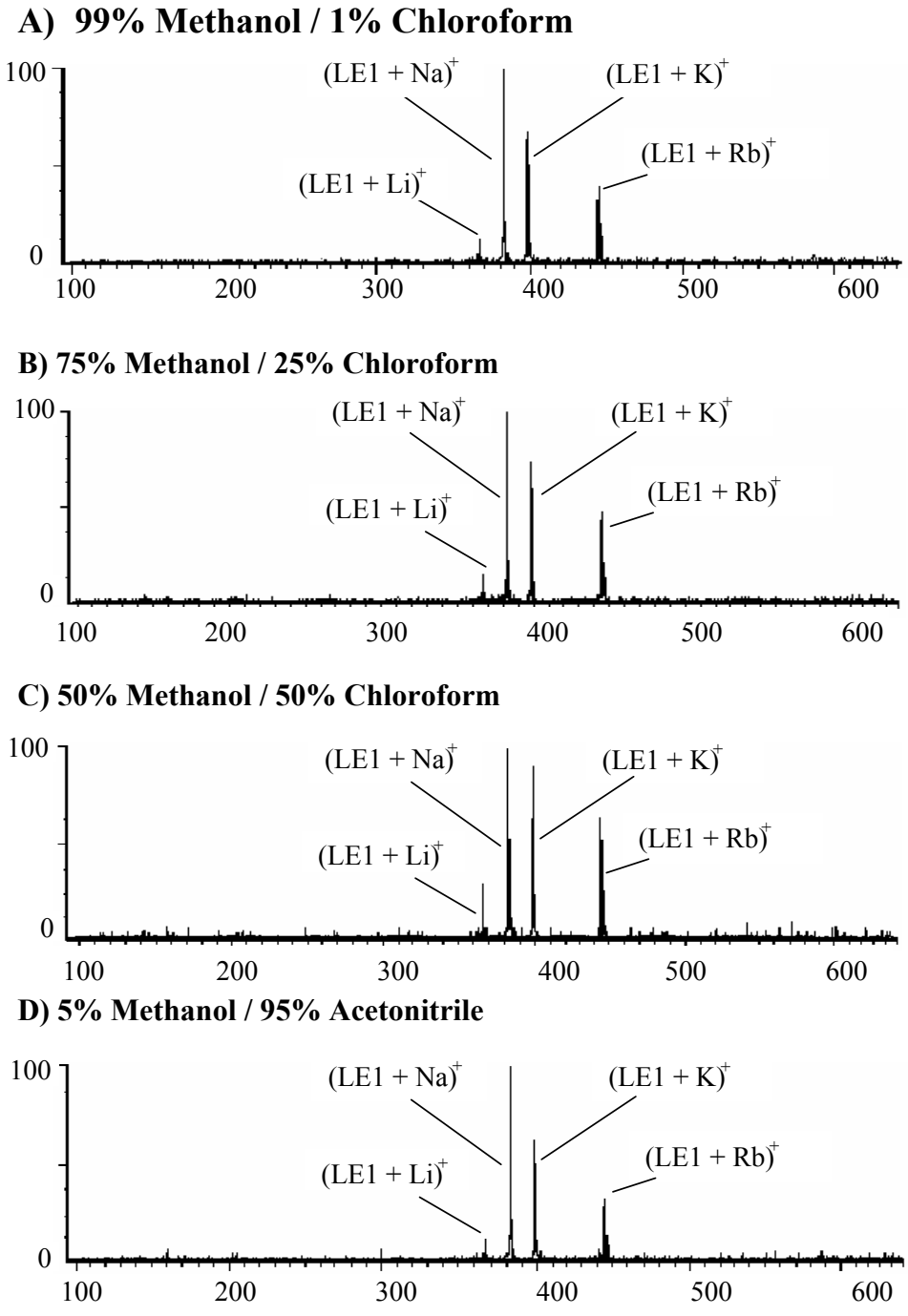

Figure 3.3. ESI mass spectra of lariat ether **4** with LiCl, NaCl, KCl and RbCl (1:2:2:2:2).

A) 99% Methanol / 1% Chloroform

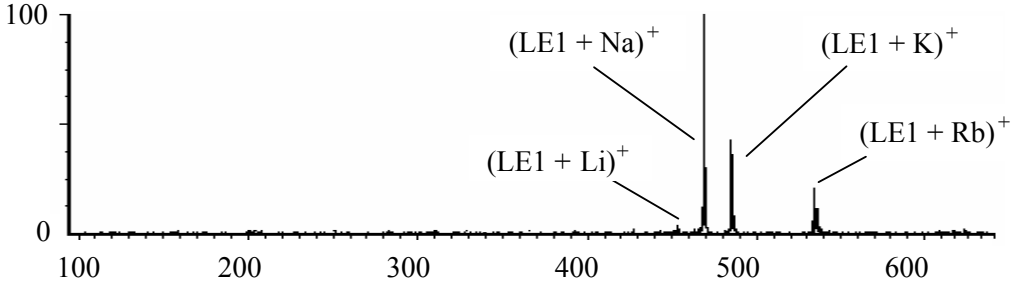

B) 75% Methanol / 25% Chloroform

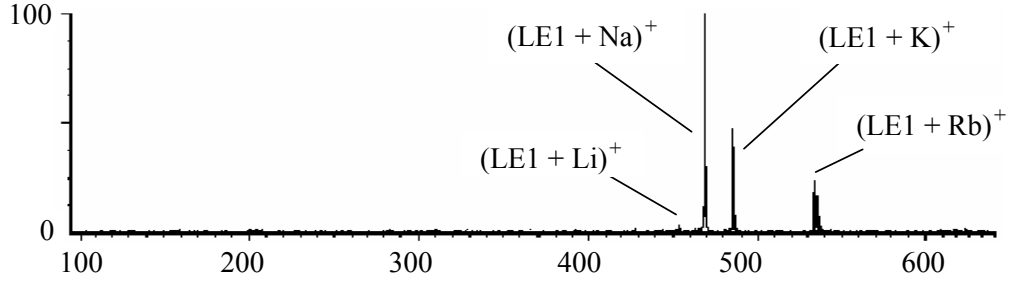

C) 50% Methanol / 50% Chloroform

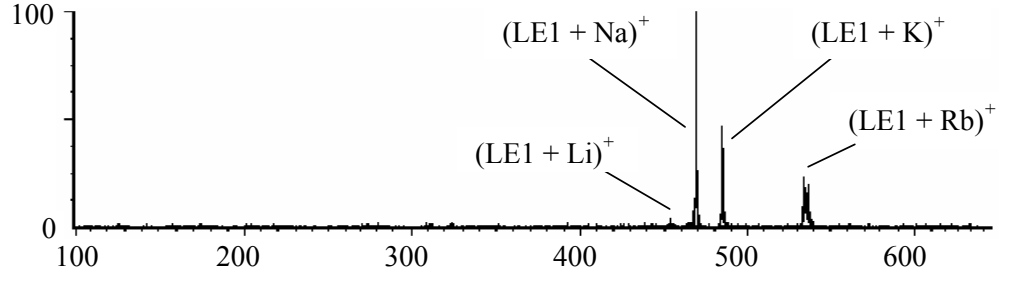

D) 5% Methanol / 95% Acetonitrile

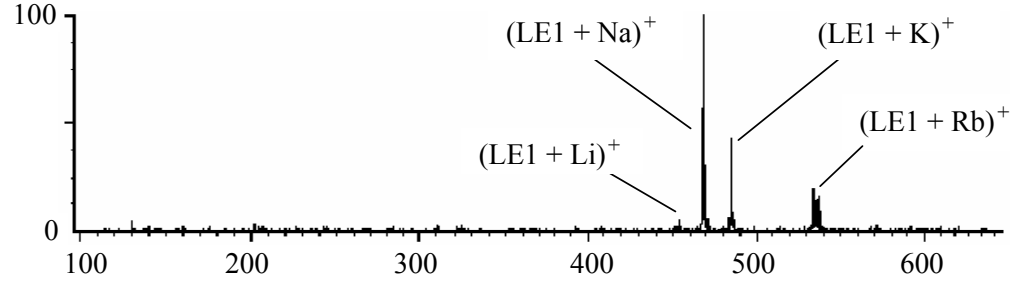

Figure 3.4 Variations in metal selectivity for lariat ethers.

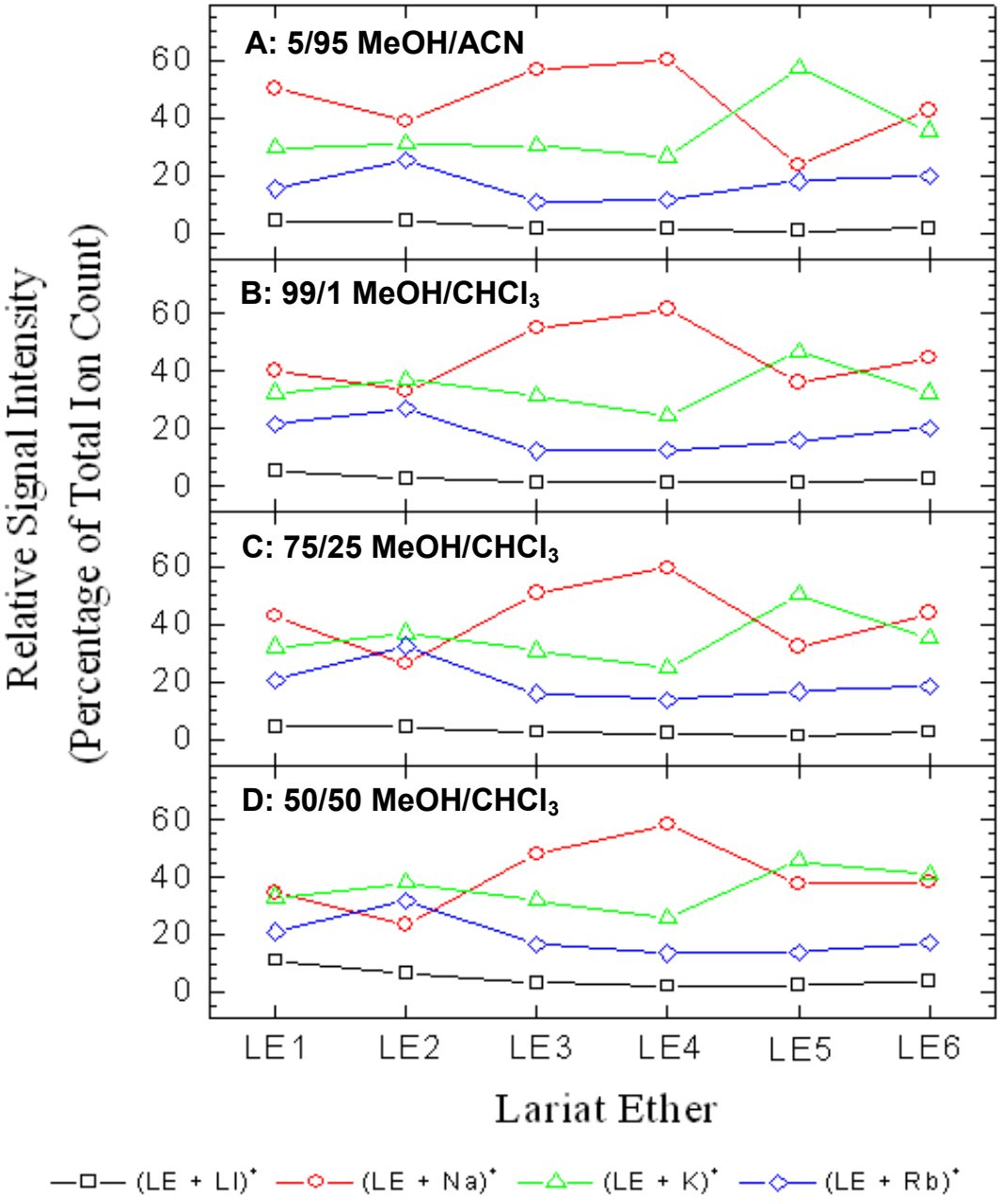

Figure 3.5 Variations in Na^+ versus K^+ selectivity in various solvent systems.

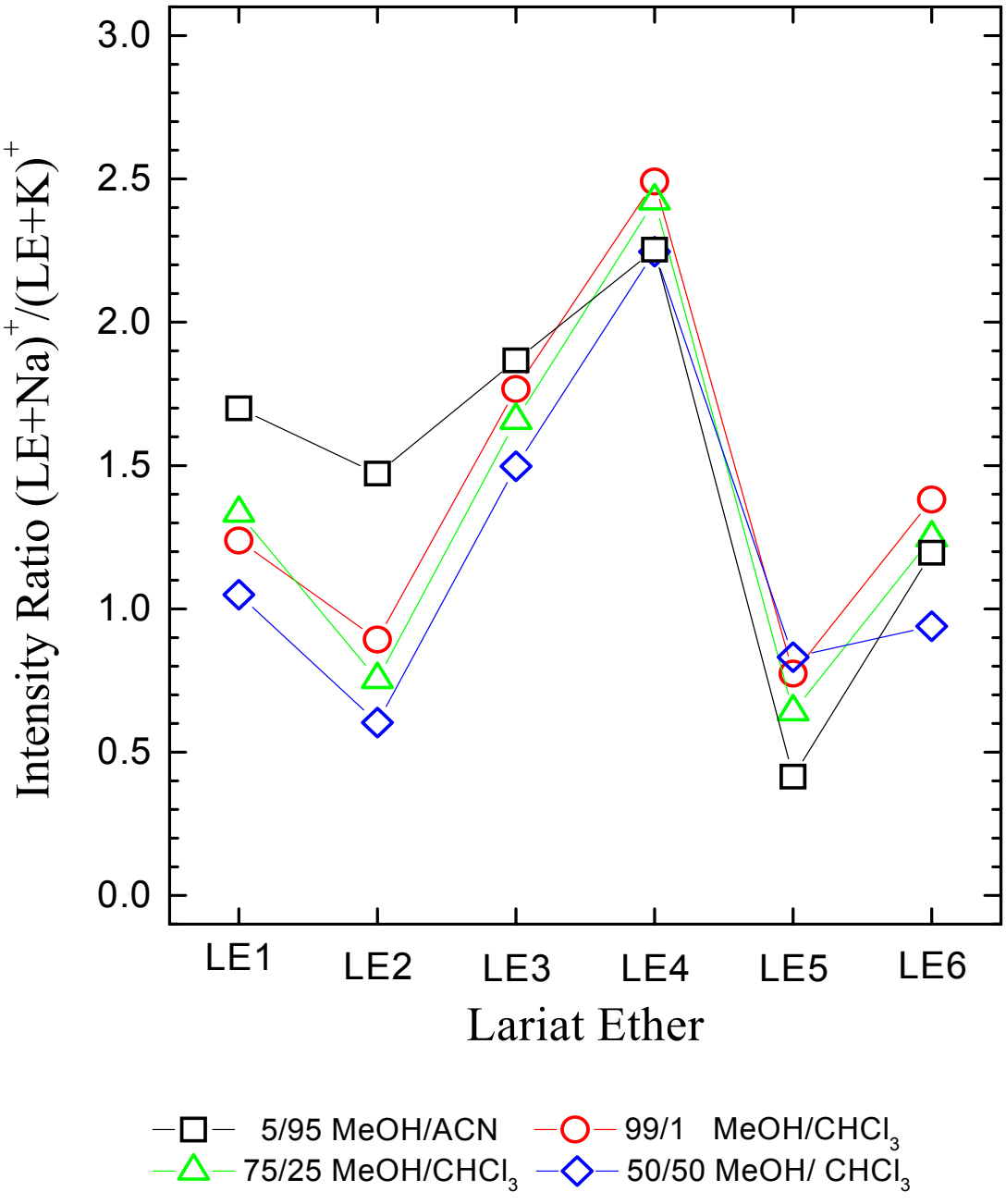

As seen in Figure 3.4, in a 99% methanol/1% chloroform solution, lariat ethers **1**, **3**, **4**, and **6** show the same selectivity trend: $Na^+ > K^+ > Rb^+ > Li^+$, while for **2** and **5** the order of Na^+ and K^+ is reversed. Addition of a geminal propyl group has been used in synthetic design strategies to assist in pre-organization of the lariat ether binding cavity and ether pendant group for enhanced Na^+ selectivity. However, this expected enhancement in selectivity was marginal in the potentiometric studies of the methoxy-substituted lariat ethers as well as in the present ESI-MS study [39], likely because the methoxy oxygen is not on a sufficiently long tether to allow it to optimally align its dipole with the alkali metal cation bound in the cavity. Addition of the geminal propyl group (i.e., in **2**) forces the methoxy group closer to the crown ether ring cavity through steric effects. Consequently, while the methoxy group in **1** was too short to interact well with either Na^+ or K^+ bound in the cavity, pushing the methoxy group closer to the cavity (i.e., in **2**) allows more optimal alignment of the dipole associated with the methoxy oxygen with the K^+ ion which is perched above the cavity of **2**, but does not enhance the interaction with the Na^+ ion which is nested within the cavity. A net decrease in Na^+/K^+ selectivity is thus observed for **2**. Lariat ether **3** exhibits a modest increase in Na^+/K^+ selectivity compared to **1** and **2**, presumably because the longer dioxapentyl ether pendant group can interact favorably to further stabilize the binding of Na^+ as it nests within the dibenzo-16-crown-5 cavity. Lariat ether **4** shows a further increase in Na^+/ K^+ selectivity and has the greatest Na^+ selectivity

of all of the six lariat ethers in this study. The Na^+ selectivity is enhanced for **4** because the propyl group enforces the conformation of the dioxapentyl group relative to the cavity, thus enhancing the exclusion of K^+. The alkali metal cation selectivities observed for **5** and **6** are particularly interesting because it was not intuitively obvious whether a longer ether pendant group (i.e. trioxaoctyl) would further anchor Na^+ in the cavity or enhance the stabilization of K^+ perching above the cavity. The ESI-mass spectrometric results confirm the latter for **5**, with a preference for complexation of K^+ over Na^+. Addition of a geminal propyl group reverses this selectivity, and thus lariat ether **6** shows a selectivity that is more similar to that of **1**. Apparently the propyl group in **6** does not assist the trioxaoctyl group in stabilizing the larger K^+ ion because pushing of the trioxaoctyl group further towards the 16-crown-5 cavity reduces the encapsulation volume to a size more amenable to Na^+ complexation.

As shown in Figure 3.5, in the less polar 75% methanol/25% chloroform, 50% methanol/50% chloroform, and more polar 5% methanol/95% acetonitrile solvent systems (electric dipole moments of solvents: μ_{CHCl3} = 1.01 D, μ_{MeOH} = 1.70 D, μ_{ACN} = 3.92 D [47]). A recurring loss in the Na^+/K^+ selectivity with decreasing solvent polarity is generally observed for **1**-**2**. Both **1** and **2** show more dramatic changes in Na^+/K^+ selectivity with solvent environment than are observed for **3** - **6**, confirming that the ether pendant group plays an important role in shielding the bound metal ion from external solvent changes, making the complexes with the

longer ether pendant group less susceptible to changes in stability with variation of the solvent polarity. Diminution of the Na^+/K^+ selectivity with reduced solvent polarity for **1** – **2** is due mainly to increases in complexation of both K^+ and Li^+ relative to Na^+ complexation (see Figure 3.4). The size of Na^+ is most similar to the cavity size of the 16-crown-5 ring, while the other ions have poorer fits which allow greater accessibility and potential for interaction with solvent molecules. Thus, there are greater enhancements in the interactions of the oxygen atoms of the 16-crown-5 cavity with Li^+ and K^+ in the less polar solvents, with the methoxy group having a minor influence on complexation. A large shift towards higher Na^+ selectivity is seen for **1** and **2** in the 5% methanol/ 95% acetonitrile solution as solvent molecules more polar than methanol interact with the more poorly fitting Li^+ and K^+. In addition, Na^+ has a larger decrease in solvation energy in acetonitrile vs. methanol compared to the change in solvation energy for K^+ [48], a factor which also may contribute to the enhancement in the formation of the lariat ether/Na^+ complexes for **1** and **2**. For **5** the reverse trend in selectivity is observed; in this case, K^+ possesses the best fit to the cavity formed by the 16-crown-5 ring and the trioxaoctyl pendant group. For lariat ether **4**, the small variation in selectivity with changes in solvent polarity is related to the presence of a pendant ether substituent which is long enough to anchor the nested Na^+ ion and whose conformation relative to the 16-crown-5 ring is stabilized by the geminal propyl

substituent, yet has sufficiently few oxygens to prohibit pulling the nested Na^+ ion out of the 16-crown-5 ring, as is apparently the case for **5** and **6**.

3.3.3 Molecular models and computational results

The results of molecular modeling and *ab initio* calculations for lariat ethers **1**, **3, 4**, and **5** with Na^+ and K^+ are presented in Table 3.2 together with plots of their cross-ring distances in Figure 3.6. As examples of the calculated structures, the Na^+ complexes of **1**, **3** and **5** (the three lariat ethers without the propyl groups) are illustrated in Figure 3.7. In these models the pendant ether group hovers above the metal ion, and the cavity adopts a rather concave shape. The methoxy pendant group is not positioned to strongly interact with the metal ion, unlike the longer dioxapentyl and trioxaoctyl groups. As shown in Figure 3.6, the distance between the inner carbons of the two opposing aryl rings (d_1 in Figure 3.1) as well as the cross-ring distance between the carbon to which the pendant groups are attached and the crown ether ring oxygen opposite it (d_2 in Figure 3.1) give an indication of the cavity sizes of the lariat ethers, as influenced by the associated pendant group(s). For instance, the distance between the aromatic rings (d_1) decreases slightly from 5.75 Å for $(\mathbf{1} + Na)^+$ to 5.63 Å for $(\mathbf{4} + Na)^+$, then drops dramatically from 5.63 Å to 4.33 Å from $(\mathbf{4} + Na)^+$ to $(\mathbf{5} + Na)^+$, respectively, indicating a compaction of the 16-crown-5 ring. For **4** and **5** in 99% methanol, the corresponding Na^+/K^+ selectivity

Table 3.2 RHF 3-21G* *Ab inito* calculations for lariat ethers **1-6** with Na^+ and K^+.

			Distances (Å)										
Complex		E (KJ/mol)	O1, M	O2, M	O3, M	O4, M	O5, M	O6, M	O7, M	O8, M	O,M ave.	d_1 (Å)[a]	d_2 (Å)[a]
1 + Na		361	2.31	2.27	2.33	2.25	2.22	2.28			2.28	5.75	5.00
1 + K		474	2.71	2.63	2.66	2.62	2.61	2.66			2.65	5.88	5.85
3 + Na		401	2.37	2.40	2.43	2.34	2.40	2.36	2.40		2.39	5.61	5.46
3 + K		515	2.73	2.65	2.69	2.69	2.66	2.64	2.70		2.68	5.83	5.88
4 + Na		431	2.36	2.41	2.43	2.34	2.38	2.41	2.36		2.38	5.63	5.52
4 + K		546	2.68	2.65	2.72	2.65	2.66	2.68	2.67		2.67	5.76	5.93
5 + Na		441	2.42	2.44	2.35	2.35	2.59	2.36	2.35	2.47	2.43	4.33	5.41
5 + K		555	2.72	2.70	2.81	2.73	2.70	2.67	2.75	2.73	2.73	5.80	5.91

Figure 3.6 Variations in size of lariat ether's 16-crown-5 ring.

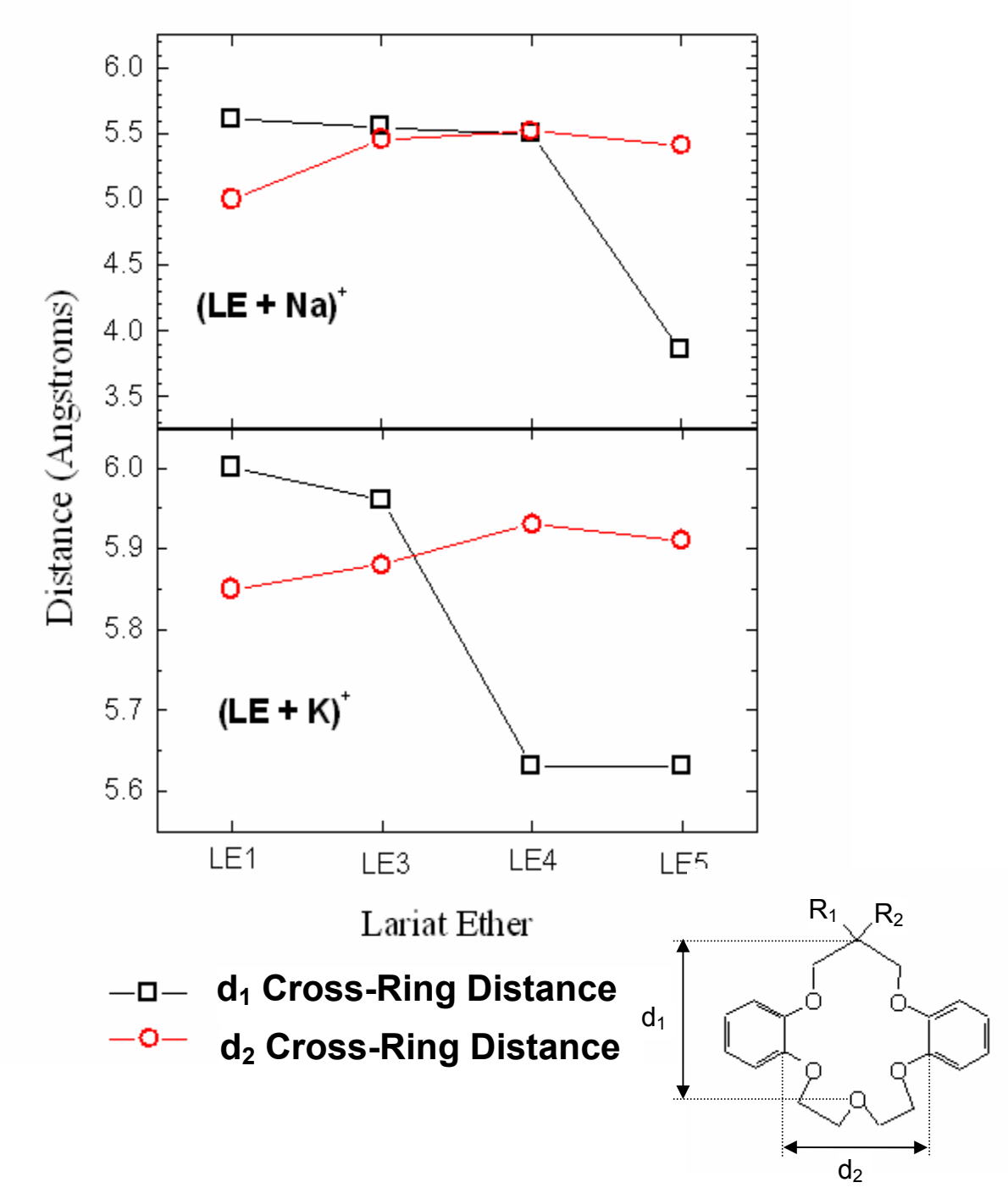

likewise drops significantly from about 2.5 to about 0.8. Simultaneously, the other cross-ring distance (d_2) increases for the Na^+ complexes from 5.00 to 5.52 Å from **1** to **4**, respectively, as the Na^+/K^+ selectivity correspondingly increases from about 1.3 to 2.5, then decreases to 5.41 Å for $(\mathbf{5} + Na)^+$ as the Na^+/K^+ selectivity drops. There is comparatively little change in the ring sizes of the K^+ complexes with variation in pendant groups (Figure 3.6). The compaction of the 16-crown–5 ring for the $(\mathbf{5} + Na)^+$ complexes that mirrors the drop in selectivity may occur because the pendant arm retains the ion above the ring and the oxygens crowd beneath it to maximize interactions.

From Table 3.2, the increase in average oxygen-metal ion distance on going from lariat ether **1** to **3** to **5** is due to the interactions of the longer ether group of **3** or **5** with Na^+ above the crown ether ring, thus effectively pulling Na^+ out of the cavity. The strengths of binding interactions involving the metal ion with the 16-crown-5 oxygens are reduced as the interactions with the longer ether pendant group are optimized.

The most important effect of the metal being pulled out of the crown ether cavity is to decrease the overall energy of binding to the crown ether ring while increasing the overall number of oxygen-metal ion bonds. This factor may contribute to the reduction in solvent effects on selectivities for **3**-**6** compared to **1** and **2**, along with the solvent shielding properties of the pendant ether substituent discussed above. The loss of fit of the 16-crown-5 cavity may result in increased

interactions of Na^+ with solvent molecules, such that ionic-polar interactions between Na^+ and the 16-crown-5 oxygens may consequently be more affected by solvent polarity. Such an effect occurs to a far lesser extent for K^+ which has a volume more similar to that of the enclosure formed between the pendant ether arm and crown ether ring, resulting in diminished solvent-dependent selectivity trends for **3** and **5**, and the absence of any clear solvent-dependent trends for **4** and **6**.

Models for both the Na^+ and K^+ complexes of **4**, the most selective lariat ether, are shown in Figure 3.7. These models demonstrate that although Na^+ can nest within the crown ether cavity, K^+ must perch above because its larger size prevents it from fitting into the ring. This ability of Na^+ to interact more effectively with the crown ether oxygens contributes to the selectivity for Na^+ over K^+ in the dibenzo-16-crown-5 lariat ethers. As shown in Table 3.2 and Figure 3.7, the propyl group of lariat ether **4** significantly enhances interaction of the terminal oxygen atom with the Na^+ ion.

From the *ab initio* models shown in Figures 3.7 and 3.8, in the Na^+ complexes of **1**-**4**, Na^+ is nested within the 16-crown-5 ring. However, for the Na^+ complex of **5**, Na^+ is suspended between the pendant arm and the 16-crown-5 ring, allowing it easier movement from the host to the solvent. As previously stated, for **6**, the added propyl geminal group pushes the trioxaoctyl group forward, thus forcing Na^+ further into the 16-crown-5 ring, resulting in its better encapsulation. From Figures 3.8 and 3.9, it can be seen that for K^+ complexes of **1**-**5**, K^+ remains

Figure 3.7 Complexation of Na^+ and K^+ by lariat ether **4**.[a]

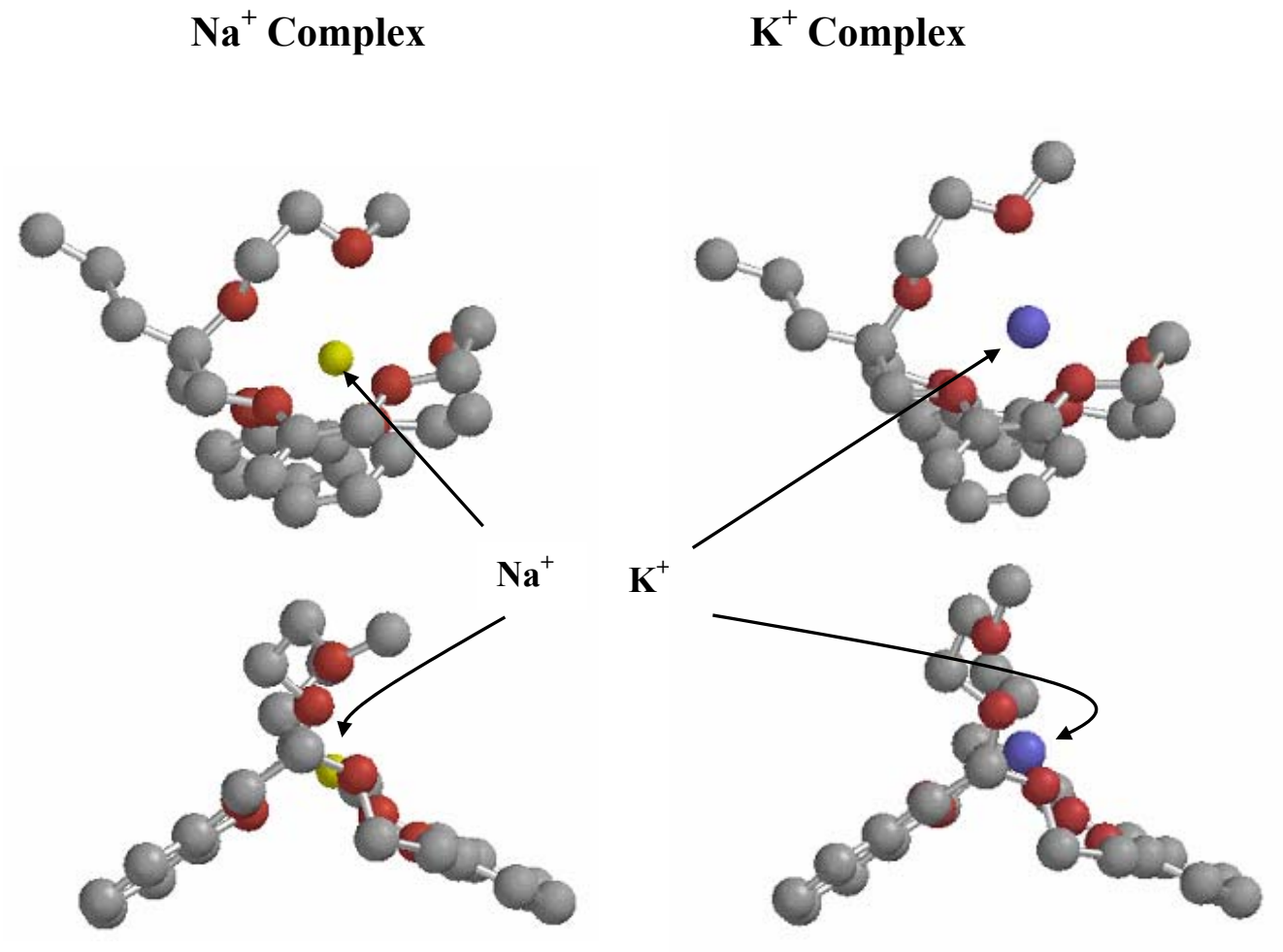

[a]Models in lower positions are rotated 90 degrees about the vertical axis with respect to the upper models. Oxygens are the darker atoms, carbons are the lighter atoms, and hydrogens are excluded for greater clarity.

Figure 3.8 Sodium complexation of lariat ethers **1**, **3**, and **5**.

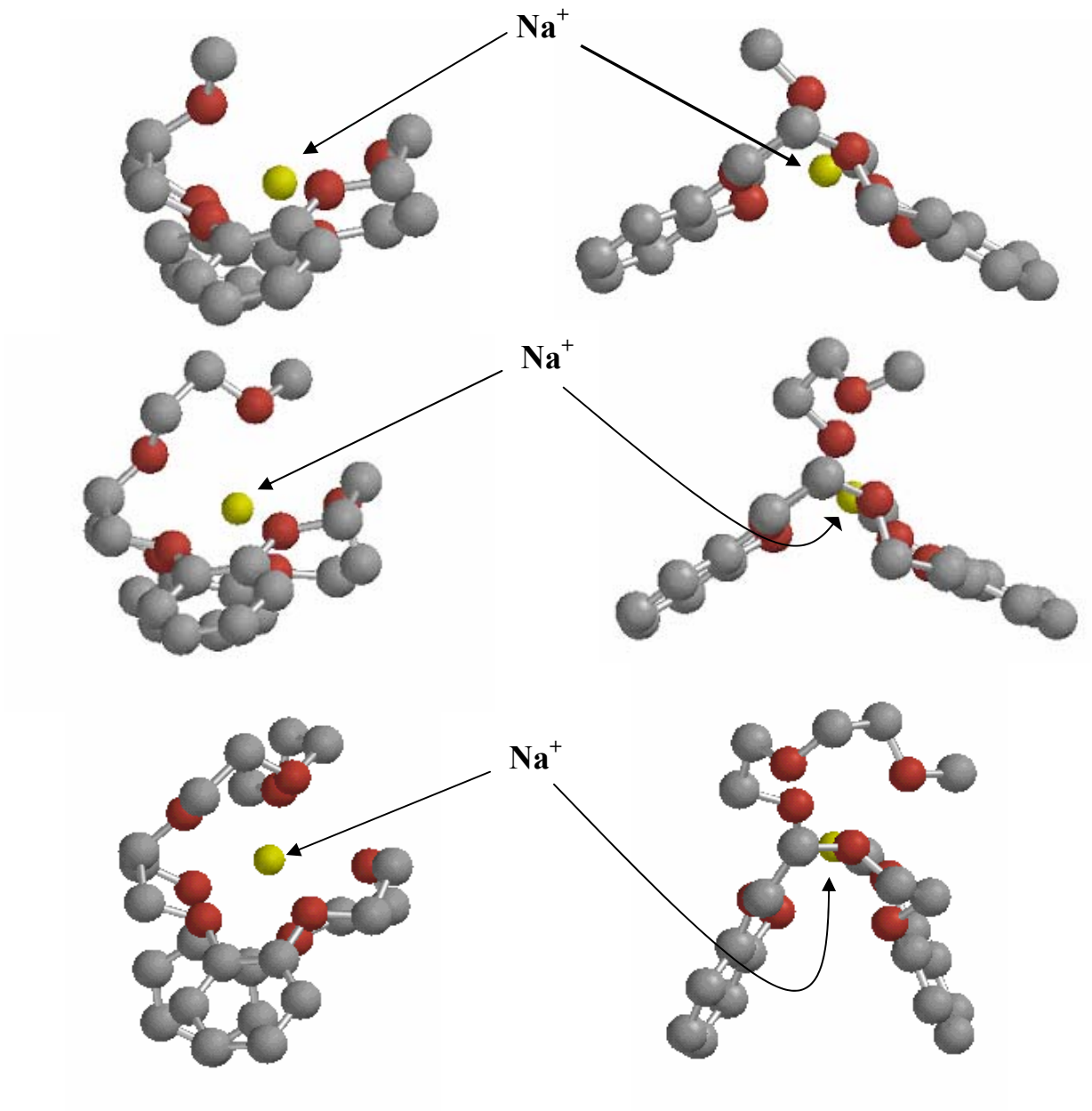

[a]Models in lower positions are rotated 90 degrees about the vertical axis with respect to the upper models. Oxygens are the darker atoms, carbons are the lighter atoms, and hydrogens are excluded for greater clarity.

Figure 3.9 Potassium complexation of Lariat Ethers 1, 3, and 5.[a]

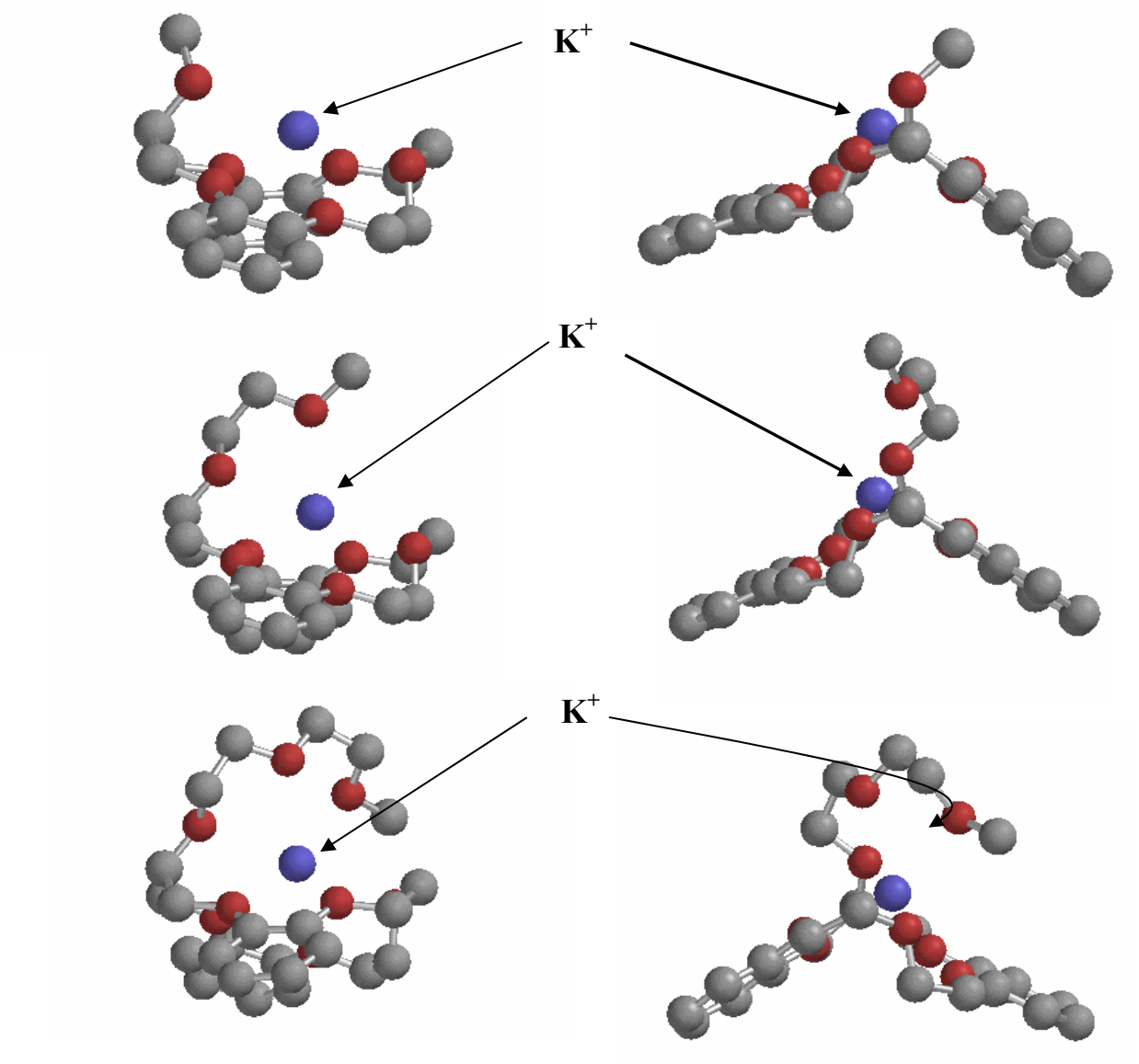

[a]Models in lower positions are rotated 90 degrees about the vertical axis with respect to the upper models. Oxygens are the darker atoms, carbons are the lighter atoms, and hydrogens are excluded for greater clarity.

virtually unchanged in its position perched above the 16-crown-5 ring. However, for the complex with **5**, the trioxaoctyl group is able to fully encapsulate K^+, thus restricting its access to the solvent compared to **1**-**4**. For **6**, the trioxaoctyl group is forced closer to the 16-crown-5 ring, thus creating an encapsulated area small enough to hinder entrance of K^+ into the crevice formed between the cyclic polyether cavity and pendant ether group.

3.4 Conclusions

The use of ESI-mass spectrometry allows rapid, efficient screening of binding selectivities in a variety of solvents. The preferences for binding different alkali metal cations can be monitored simultaneously, thus reducing the sample consumption and time for analysis. For the six lariat ethers studied in the present report, the presence of a dioxapentyl group in conjunction with a propyl sidearm (i.e., in **4**) creates the most Na^+ selective lariat ether. Addition of a longer trioxaoctyl pendant group results in a preference for complexation of K^+ over Na^+ because of optimization of interactions between the metal ion and the oxygen atoms of the trioxaoctyl group. Addition of a second sidearm, a propyl group, regenerates Na^+ selectivity because of a greater degree of pre-organization of the cavity in conjunction with optimization of the anchoring interaction with the metal ion provided by the ether pendant group. Decreases in polarity/dielectric constant of the solvent media generally lowers the Na^+/K^+ selectivity, possibly due to

favorably increasing the electrostatic interaction between K^+ and the 16-crown-5 ring while the Na^+ interactions with the ring are comparatively little affected. *Ab initio* calculations show that the addition of the dioxapentyl or trioxaoctyl group pulls Na^+ above the crown ether ring oxygens, increasing interaction with the former at the expense of interaction with the latter. The calculations also suggest that changes in pendant groups cause significant alterations in crown ether ring shape, which reveal a role of the pendant arm as the primary site of metal-oxygen interaction for ions with a poor fit to the encapsulated area of the lariat ether.

3.5 Acknowledgements

The National Science Foundation (CHE-9820755), the Welch Foundation (grants D-775 and F-1155) and the Texas Advanced Technology Program (003658-0206) are gratefully acknowledged.

3.6 References

1. Yamashita, M.; Fenn, J.B.; *J. Phys. Chem,* **1984**, *88*, 4451.

2. Fenn, J.B.; Mann, M.; Meng, C.K.; Wong, S.F.; Whitehouse, C.M.; *Mass Spectrom. Rev.,* **1990**, *9*, 37.

3. Smith, R.D.; Loo, J.A.; Edmonds, C.G., Barinaga, C.J.; Udseth, H.R.; *Anal. Chem.,* **1990**, *62*, 882.

4. Cole, R.B., Ed., *Electrospray Ionization Mass Spectrometry*, Wiley-Interscience, New York, 1997.

5. Loo, J.A.; Holsworth, D.D.; Root-Bernstein, R.S.; *Biol. Mass Spectrom.* **1994,** *23,* 6-12.

6. Lamcharfi, E.; Chuilon, S.; Kerbal, A.; Kunesch, G.; Libot, F.; Virelizier, H.; *J. Mass Spectrom.*, **1996**, *31*, 982-986.

7. Robinson, C.V.; Chung, E.W.; Kragelund, B.B.; Knudsen, J.; Aplin, R.T.; Doulsen, F.M.; Dobson, C.M.; *J. Am. Chem. Soc.* **1996**, *118*, 8646-8653.

8. Cheng, X.; Chen, R.; Bruce, J.E.; Schwartz, B.L.; Anderson, G.A.; Hofstadler, S.A.; Gale, D.C.; Smith, R.D.; *J. Am. Chem Soc.* **1995**, *117*, 8859-8860.

9. Cheng, Z.L.; Siu, K.W.M. ; Guevremont, R.; Berman, S.S.; *J. Am. Soc. Mass Spectrom.* **1992,** *3*, 281-288.

10. Chapeaurouge, A.; Bigler, L.; Shafer, A.; Bienz, S.; *J. Am. Soc. Mass Spectrom.* **1995,** *6*, 207.

11. Guevremont, R.; Siu, K.W.M.; Le Blanc, J.C.Y.; Berman, S.S.; *J. Am. Soc. Mass Spectrom.* **1992,** *3*, 216-224.

12. Wang, G.; Cole, R.B.; *Org. Mass Spectrom.* **1994,** *29,* 419-427.

13. Gokel, G.W.; Wang, K. *J. Org. Chem.* **1996,** *61*, 4693-4697.

14. Leize, E.; Jaffrezic, A.; Van Dorsselaer, A. *J. Mass. Spectrom.* **1996,** *31*, 537-544.

15. Young, D-S.; Hung, H-Y. Liu, L. K. *J. Mass. Spectrom.* **1997,** *32*, 432-437. Young, D-S.; Hung, H-Y. Liu, L. K. *Rapid Commun. Mass Spectrom.*, **1997**, *11*, 769-773.

16. Hsieh, Y.L.; Li, Y.-T.; Henion, J.D.; Ganem, B.; *Biol. Mass Spectrom.*, **1994**, 23*, 272.*

17. Cheng, X.; Chen, R.; Bruce, J.E.; Schwartz, B.L.; Anderson, G.A.; Hofstadler, S.A.; Gale, D.C.; Smith, R.D.; Gao, J.; Sigal, G.B.; Mammen, M.; Whitesides, G.M. *J. Am. Chem. Soc.* **1995**, *117*, 8859.

18. Sannes-Lowery, K.A.; Hu, P.; Mack, D.P.; Mei, H.-Y.; Loo, J.A., A*nal.Chem.*, **1997**, *69*, 5130.

19. Sannes-Lowery, K.A.; Mei, H.-Y.; Loo, J.A.; *Int. J. Mass Spectrom.,* **1999**, *193*, 115.

20. Wan, K.X.; Shibue, T.; Gross, M.L. *J. Am. Chem. Soc.* **2000**, *122*, 300.

21. Blair, S.M.; Kempen, E.C.; Brodbelt, J.S.; *J. Am. Soc. Mass Spectrom.*, **1998**, *9*, 1049-1059.

22. Blair, S.M.; Brodbelt, J.S.; Reddy, G.M.; Marchand, A.P.; *J. Mass Spectrom.*, **1998**, *33*, 721-728.

23. Kempen, E.C.; Brodbelt, J.S.; Bartsch, R.A.; Jang, Y.;Kim, J.S.; A*nal..Chem.*, **1999**, *71*, 5493-5500.

24. Brodbelt, J.; Kempen, E.; Reyzer, M.; *Struct. Chem.,***1999**, *10*, 213-220.

25. Blair, S.M.; Brodbelt, J.S.; Marchand, A.P.; Kumar, K.A.; Chong, H-S.; *Anal. Chem.*, **2000**, *72*, 2433-2445.

26. Goolsby, B.; Hall, B.J.; Brodbelt, J.S.; Adou, E.; Blanda, M.; *Int. J. Mass Spectrom.,* **1999**, *193*, 197.

27. Blanda, M.T.; Farmer, D.B.; Brodbelt, J.S.; Goolsby, B.; *J. Am. Chem. Soc.* **2000**, *122*, 1486.

28. M.L. Reyzer, J. S. Brodbelt, A.P. Marchand, Z. Chen, Z. Huang, I.N. N. Namboothiri, *Int. J. Mass Spectrom*., **2001**, *200*, 57-69.

29. S. Blair, J. Brodbelt, A. Marchand, H.-S. Chong, S. Alidhodzic, *J. Am. Soc. Mass Spectrom*., **2000**, *11*, 884-891.

30. E. Kempen, J. Brodbelt, *Anal. Chem*., **2000**, *72*, 5411-5416.

31. Lim, H.-K.; Hsieh, Y.L.; Ganem, B.; Henion, J.; *J Mass Spectrom*, **1995**, *30*, 708.

32. Loo, J.A.; Hu, P.; McConnell, P.; Mueller, W.T.; Sawyer, T.K.; Thanabal, V.; *J Am Soc Mass Spectrom*, **1997**, *8*, 234.

33. Young, D.-S.; Hung, H.-Y.; Liu, L.K.; *Rapid Commun. Mass Spectrom.*, **1997**, *11*, 769.

34. Jorgenson, T.J.D.; Roepstorff, P.; Heck, A.J.R.; A*nal.Chem.*, **1998**, *70*, 4427.

35. Griffey, R.H.; Hofstadler, S.A.; Sannes-Lowery, K.A.; Ecker, D.J.; Crooke, S.T.; *Proc. Natl. Acad. Sci. USA*, **1999***, 96*, 10129.

36. Martell, A.E., Hancock, R.D., Chapter 7: "Stability Constants and Their Measurement", *Metal Complexes in Aqueous Solutions,* Plenum Press: New York, **1996**.

37. Ohki, A.; Lu, J.-P.; Bartsch, R.A.; *Anal. Chem.* **1994***, 66,* 651-654.

38. Ohki, A., Lu., J.-P., Huang, X., Bartsch, R.A., *Anal. Chem*., **1994**, 66, 4332-4336.

39. Bartsch, R.A., Lu, J., Ohki, A., *J. Incl. Phenomena Mol. Recogn. In Chem*., **1998**, 32, 133-150.

40. Ohki, A., Lu, J.-P., Hallman, J.L., Huang, X., Bartsch, J.A., *Anal. Chem*., **1995**, 67, 2405-2408.

41. Shannon, R.D., *Acta Crystallogr., Sect. A: Found. Crystallogr*. **1976**, 32, 751-767.

42. Bartsch, R.A., Heo, G.S., Kang, S.I., Liu, Y., Strzelbicki, J.; *J. Org. Chem*., **1982**, 47, 457.

43. Hayashita, T., Goo, M.-J., Lee, J.C., Kim, J.-S., Krzykawski, J., Bartsch, R.A., *Anal. Chem*., **1990**, 62, 2283.

44. Bartsch, R.A., Bitalac, L.P., Cowey, C.L., Elshani, S., Goo, M.J., Huber, V.J., Ivy, S.N., Jang, Y., Johnson, R.J., Kim, J.S., Luboch, E., McDonough, J.A., Pugia, M.J., Son, B., Zhao, Q.*, J. Heterocyclic Chem*., **2000**, 37, 1337.

45. Van Berkel, G.J.; Glish, G.L.; McLuckey, S.A.; *Anal. Chem.* **1991***, 62,* 1281-1289.

46. Izatt, R.M.; Pawlak, K.; Bradshaw, J.S.; Bruening, R.L.; *Chem. Rev.*, **1991**, *91*, 1721-2085.

47. Weast, R.C., Ed., *CRC Handbook of Chemistry and Physics*, 68th Edition, CRC Press: **1987**, p. E-59.

48. Abraham, M.H., Liszi, J., *J. Chem. Soc., Faraday Trans. 1*, **1978**, 74, 1604.

CHAPTER 4

Evaluation of Alkali and Alkaline Earth Metal Cation Selectivities of Lariat Ether Amides by Electrospray Ionization Mass Spectrometry

4.1 Introduction

Electrospray ionization mass spectrometry (ESI-MS) [1-4] has been utilized successfully to analyze of a wide variety of non-covalent complexes [5-7], such as those formed in host-guest chemistry. Numerous recent studies have established that the equilibrium distribution of complexes in solution is reflected in the intensities of host-guest complexes observed in the ESI mass spectra [8-40]. To determine binding selectivities in host-guest chemistry, the intensities of complexes produced by ESI of solutions containing known concentrations of one host and multiple guests are compared. ESI-MS analysis of binding selectivities has several advantages over the more conventional potentiometric, spectrophotometric and NMR titrimetric methods [41], such as reduced sample consumption, tolerance of a wide variety of solvent conditions, and reduced analysis times.

An ESI-MS method for measuring condensed-phase selectivities has been extensively investigated in our laboratory for hosts, such as crown ethers and other

macrocycles, with guests like alkali metal, transition metal, heavy metal and ammonium cations [24-35]. The ESI-MS method is most successful for comparison of host selectivities for a series of similar cations, resulting in the analysis of complexes with similar solvation energies. In these cases, the resulting ESI mass spectral distributions of complexes generally agree well with the equilibrium distribution of complexes in solution, allowing the correlation between host structure and selectivity to be investigated. The electrospray efficiencies of ions in ESI-MS, are directly related to signal intensities:

$$I_i = k_i C_i \quad (1)$$

where I_i is the signal intensity for an ion, k_i is the electrospray efficiency, and C_i is the concentration of the ion in solution. Van Dorsselaer and co-workers established that the electrospray efficiency of an ion is related to its solvation energy,[17] and showed that complexes that contain host molecules, such as crown ethers, with guest ions, such as metal ions of the same charge, have similar electrospray efficiencies when experimental conditions are kept constant, resulting in ESI-MS signals which correspond closely in relative intensity to the relative concentrations of the ions in the solution being analyzed. Where solvation energies are significantly different, correction factors can often be determined and applied to achieve a quantitative or semi-quantitative relationship between peak intensities and ion concentrations in solution, as shown in this study. Van Dorssalaer's work

also determined that roughly a ten-fold decrease in electrospray efficiency is predicted for a 70 kJ/mol increase in ion solvation energy.[17] However, even in a highly polar solvent such as water the solvation energies for 222 cryptate with alkali metal ions varied by only 26 kJ/mol throughout the series of complexes (Li^+ through Cs^+).[17] As the average polarity of the solvent system decreases, one would expect the range of solvation energies to decrease as well. The measurement of gas-phase and solution selectivities by mass spectrometry has been reviewed by Schalley et al.[42,43]

In the present work, ESI-MS is used to analyze the alkali metal binding selectivities of dibenzo-16-crown-5 (**1**) and the fifteen lariat ether amides (LEAs) **2-16** shown in Figure 4.1 with several aims. The sensitivity of the ESI-MS method to subtle differences in binding properties of macrocycles that have similar substituents is examined, as well as assessing the ability of ESI-MS to determine pH dependence on binding selectivities of macrocycles with basic substituents. All fifteen of the LEAs have the same dibenzo-16-crown-5 skeleton, but the substituents attached to the center carbon of the propylene bridge of the crown ether ring differ. One sidearm is an oxyacetamide with substituents (R and R' groups) on the amide nitrogen of varying length and number of oxygen binding sites. The second substituent is either hydrogen or a geminal propyl group. Based on the diameters of the metal cations (Li^+ =136 pm, Na^+ = 196 pm, K^+ = 266 pm,

Figure 4.1 Dibenzo-16-crown-5 and lariat ethers amides (mol.wght. in Da).

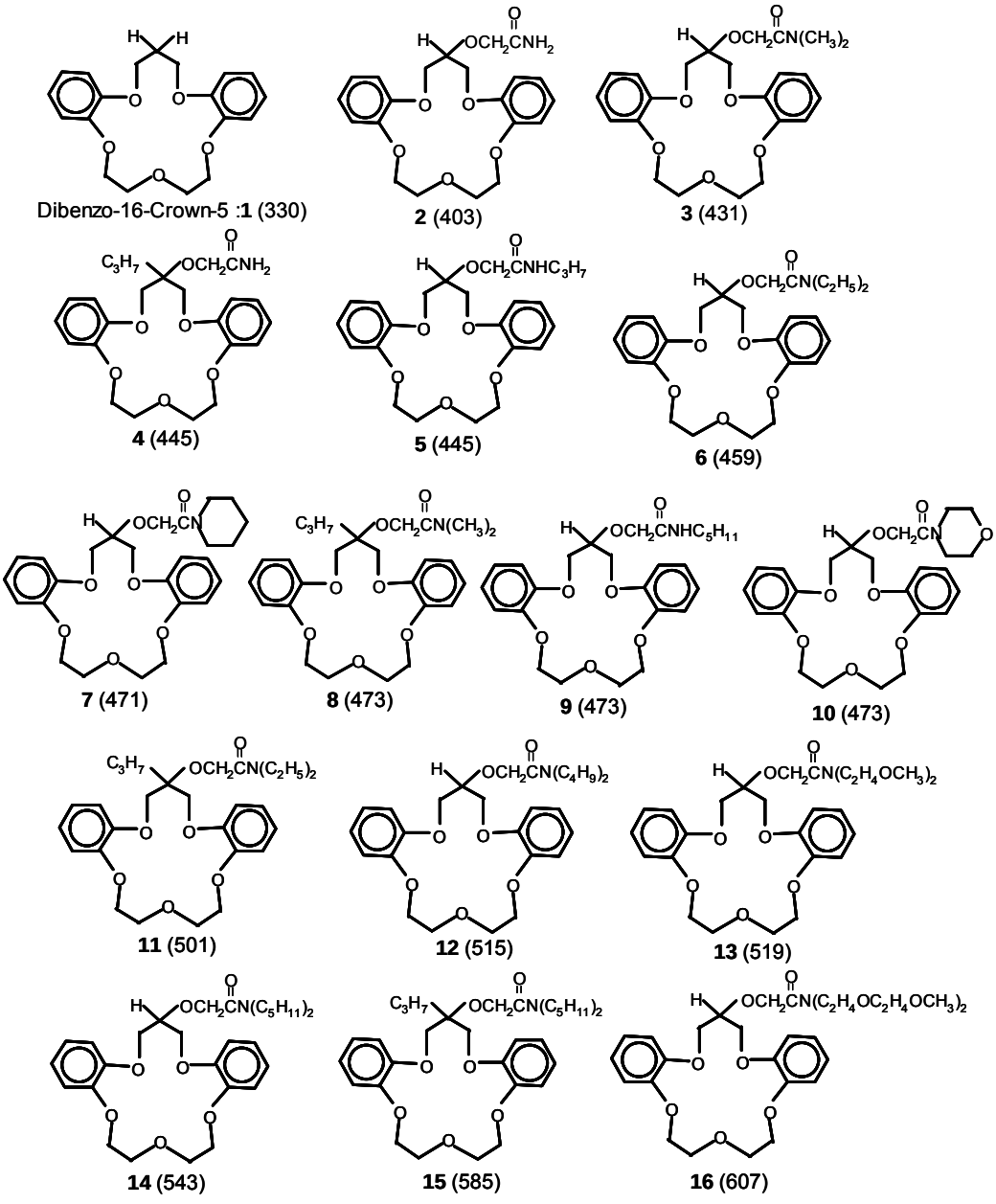

Rb^+ = 298 pm, and Cs^+ = 330 pm [44]), the cavity diameter of unsubstituted dibenzo-15-crown-5 (200 to 240 pm [45]) is expected to be optimal for Na^+ complexation (Figure 4.2). The present work focuses on the evaluation of binding selectivities in solution based on ESI-MS results, in contrast to binding properties in the gas phase as studied extensively by Armentrout [46] and Dearden.[47-48] In a gas-phase environment the relative binding affinities of macrocycles are largely dictated by the charge densities of the metal ions, [46-48] whereas in the condensed phase, solvation effects increase the importance of "best fit" considerations, as well as hydrogen bonding and hydrophobic interactions.[41]

The ability of lariat ethers to effectively complex metals has led to their development and optimization for use in ion selective electrode membranes [45,49-54]. Of the fifteen LEAs shown in Figure 4.1, **6**, **9**, **11**, **14**, and **15** have been investigated previously by conventional methods [51-54]. Bartsch and co-workers incorporated each of these five LEAs into PVC membranes and analyzed their alkali metal cation (Li^+, Na^+ and K^+) selectivities using potentiometry with the fixed interference method in aqueous solutions [55]. Brodbelt and Bartsch previously investigated four additional LEAs (**2**, **3**, **4** and **8**) in methanol using ESI-MS to determine their alkali metal cation selectivities [26]. In the present study, all fifteen LEAs were evaluated in methanolic solutions with alkali metal cations, Mg^{2+}, and Ca^{2+}, and as a function of the acid/base nature of the solution, thus

Figure 4.2 Mass spectra of LEAs with alkali chlorides in methanol: **(a) 6 (b) 11**.

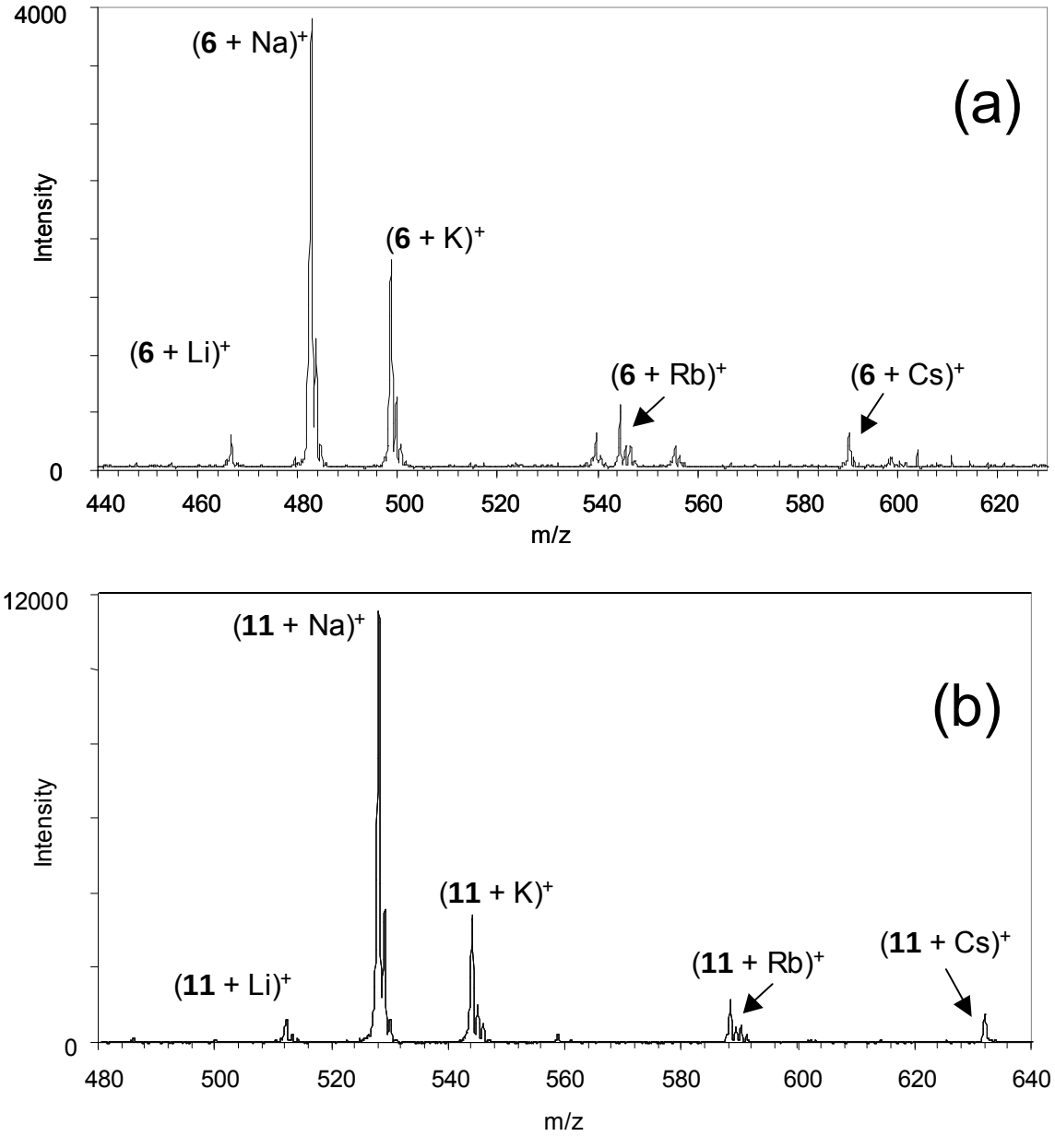

extending the study of lariat ether amide selectivities to solvent systems that are difficult to analyze by potentiometry, but well suited to ESI-MS analysis.

From the potentiometric measurements in aqueous solution by Bartsch and co-workers [51-54], the Na^+/K^+ selectivity of the LEAs increase in the order: **6** < **9** < **14** < **11** < **15**. The order of increasing Na^+/Li^+ selectivity was found to be: **11** < **15** < **6** < **14** < **9**. For all five LEAs, the order of binding constants was determined to be $Na^+ > K^+ > Li^+$. Among the conclusions drawn from these results was that the addition of the geminal propyl arm enhanced selectivity for Na^+ over K^+, but diminished the selectivity for Na^+ over Li^+. In general, the presence of a propyl group geminal to the oxyacetamide substituent encourages optimal pre-organization of the ether amide pendant group over the cavity, enhancing the overall Na^+/K^+ selectivity and reducing the Na^+/Li^+ selectivity. However, further lengthening or branching of the geminal arm does not significantly alter selectivity [43-49]. The changes in selectivity observed for geminal arm addition are short range in nature and do not extend significantly beyond the third methylene group. For the host molecules used in these previous studies by the Bartsch group, Na^+/Rb^+, Na^+/Cs^+, Na^+/Mg^{2+}, and Na^+/Ca^{2+} selectivities were determined only for LEAs **14** and **15** [53]. For Na^+/Rb^+, Na^+/Cs^+, and Na^+/Ca^{2+}, **15** always showed a greater selectivity for Na^+ than **14**, although the Na^+/Mg^{2+} selectivities of both macrocycles were the same, within experimental uncertainty. The binding constant

orderings for **14** and **15** were: **14**: $Na^+ > K^+ > Rb^+ > Cs^+ > Li^+ > Ca^{2+} > Mg^{2+}$ and **15**: $Na^+ > K^+ > Rb^+ > Li^+ > Cs^+ > Ca^{2+} > Mg^{2+}$, respectively.

4.2 Experimental

4.2.1 Mass Spectrometry

All mass spectrometric measurements except the collisionally activated dissociation (CAD) experiments were performed with a Finnigan ion trap mass spectrometer (ITMS) (ThermoFinnigan, San Jose, CA) operated in the mass selective instability mode with modified electronics to allow axial modulation and equipped with an in-house built electrospray source. The electrospray interface was based on a design developed by Oak Ridge National Laboratories (Oak Ridge, TN) with a differentially pumped region containing ion-focusing lenses [51]. Neither a heated desolvation capillary nor a sheath-flow gas were used on the ITMS. For solution deliveries, the syringe pump system (Harvard Apparatus Inc., Holliston, MA) was operated at a flow rate of 2.0 μl/min. The ESI needle voltage was 3.4 kV. Each spectrum was an average of data from 150 scans. Selectivity versus acidity data were from single experiments, while other mass spectrometry data were averages from three experiments on different days. The MS/MS experiments were performed on a ThermoFinnigan LCQ Duo mass spectrometer. The heated capillary was set at 125 ^oC and the sheath gas flow was 20 arbitrary units. The ESI

needle voltage was 5.0 kV on the LCQ Duo. Each spectrum was an average of data from 600 scans.

For screening of the alkali and alkaline earth metal cation selectivities of **1**-**16**, solutions containing a single host with multiple metal cations were analyzed. Solutions containing one part of host and two parts of each metal cation were analyzed for each LEA in methanol and methanol/water (3:1, v/v). The excess of metal cations relative to the LEA creates a more competitive binding environment for complexation with the host compound. Throughout the study, the concentration of each host was 5.0×10^{-5} M and concentrations of the metal cations were 1.0×10^{-4} M, except in the selectivity validation experiments (first section of Results and Discussion), where the concentrations are given. These concentrations were used to ensure solubility of all salts in the solvent while maintaining conditions for increased selectivity versus solutions containing one part of host and one part of each guest metal cation. Concentrations of H^+ and OH^- were set by addition of HCl or hydroxides of the alkali metal cations. Solutions had nominally neutral pH values unless otherwise indicated. Metal salts used for these experiments were purchased from Aldrich Chemical Co. (Milwaukee, Wisconsin) and used without further purification. The water used was 18 MO that was purified on site. Methanol was Certified A.C.S. Spectranalyzed® from Fisher. Ligands **1**-**16** were synthesized in the laboratories of Prof. Richard Bartsch by reported methods [57,58]. Other chemicals were 99%+ pure from Sigma-Aldrich and used as received. Theoretical

values of solution equilibria conditions were obtained using MINEQL+ solution equilibria software, version 4.01 (Environmental Research Software, Hallowell, ME).

4.2.2 Ab initio Calculations

Molecular mechanics conformational searches were performed using MMFF (Merck) force fields followed by *ab initio* calculations using a Restricted Hartree-Fock model at the 3-21G* level of theory with Spartan '02 PC© software (Wavefunction Inc., Irvine, CA) operated on a Gateway PC with an Intel Pentium 4 processor.

4.3 Results and Discussion

4.3.1 Validation of the ESI-MS Method for Determining Selectivities

Although the validity of determining host-guest selectivities by ESI-MS has been confirmed for macrocycles with alkali and various transition metal cations in numerous earlier studies by this group [24-35], new experiments were performed to assess differences in spray efficiencies for the LEA complexes and to validate this method for investigation of the alkaline earth metal cations, Mg^{2+} and Ca^{2+}. Since extensive host-guest binding constant data is available in the literature for 18-crown-6 [59], this macrocyclic polyether was used as the model host molecule. For

example, the intensities of (18-crown-6 + Mg^{2+}) and (18-crown-6 + Ca^{2+}) complexes were examined individually to estimate the ESI spray efficiencies, and then mixtures containing 18-crown-6 with both metal species were analyzed and corrected to reflect the solution equilibria. Table 4.1 compares the relative peak areas of the signals for the different complexes in the ESI mass spectra to the equilibrium distributions calculated in solution using literature binding constants for 18-crown-6 with Mg^{2+} and Ca^{2+} in methanol (log K for (18-crown-6 + Mg^{2+}) is 3.61 and log K for (18-crown-6 + Ca^{2+}) is 4.25 [59]). These results show that the relative signal intensities for complexes with these metal cations can be used to semi-quantitatively determine selectivities for solutions with the solvent systems tested. For complexes where relative abundances of the ESI-MS signals deviate from the relative abundances in solution by more than 10%, as is observed for the Mg^{2+} and Ca^{2+} complexes, the mass spectral signals must be multiplied by ESI response factors to correct for different electrospray efficiencies of the complexes.

For example, from the ESI-MS signal intensities of the (18-crown-6 + Mg^{2+}) and (18-crown-6 + Ca^{2+}) complexes for solutions containing just a single metal in excess, it is found that the (18-crown-6 + Mg^{2+}) complexes spray more efficiently than the (18-crown-6 + Ca^{2+}) complexes by a factor of nearly four. Thus, the difference in spray efficiencies must be calibrated and normalized by application of appropriate correction factors (i.e. such as dividing the apparent signal intensity of the Mg^{2+} complex by a factor of nearly four). After analyzing

Table 4.1 Distributions for (18-crown-6 + alkaline earth metal cation) complexes.

	Percentage (18-crown-6 + Mg^{2+})	Percentage (18-crown-6 + Ca^{2+})
Calculated distribution from log K values in solution[a]	20	80
Distribution from ESI-mass spectra[b]	46	54
Distribution from ESI-mass spectra with correction for spray efficiencies[c]	18	82

[a] Calculated using log K (18-crown-6 + Mg^{2+}) = 3.61 and log K (18-crown-6 + Ca^{2+}) = 4.25 in methanol [59].
[b]Concentrations were 3 x 10^{-4} M in $MgCl_2$, 3 x 10^{-4} M in $CaCl_2$, and 5 x 10^{-5} M in 18-crown-6. Standard deviations were $\pm$ 8%.
[c]Corrections were made by multiplying the uncorrected integrated intensities of (18-crown-6 + Mg^{2+}) and (18-crown-6 + Ca^{2+}) by the ratio of signals obtained for the same complexes in solutions of 6 x 10^{-4} M $MgCl_2$: 5 x 10^{-5} M 18-crown-6 (12:1), and 6 x 10^{-4} M $CaCl_2$: 5 x 10^{-5} M 18-crown-6 (12:1), respectively.

solutions containing 18-crown-6 and both metals and applying the appropriate correction factors, the distribution of Mg^{2+} and Ca^{2+} complexes shown in Table 4.1 agree well with the distribution predicted from the known log K values.

For the LEA complexes, the three-dimensional cavity effectively solvates the metal cations, thus reducing the variations in spray efficiencies of the different complexes (Table 4.2). Shown in Table 4.2 are the relative signal intensities obtained upon ESI-MS analysis of solutions containing one LEA and one metal in excess, with the final column showing the ratio of intensities obtained for the Mg^{2+} and Ca^{2+} complexes. This final column, in which the values are close to 1.0, suggests that the spray efficiencies for the LEA/alkaline earth metal complexes are similar, meaning that the correction factors when comparing the Mg^{2+}/Ca^{2+} selectivities of the LEAs are minimal. Estimated errors in both mass spectrometrically determined and theoretically calculated distributions in Tables 4.1 and 4.2 are similar, with peak area and literature binding constant uncertainties both at about ±8% relative error.

4.3.2 Alkali Metal Cation Selectivities

Examples of ESI-mass spectra obtained for solutions containing LEAs **6** and **11** with the five alkali metals in methanol are shown in Figure 4.2. The distributions of signal areas were obtained for the alkali metal complexes of **1**-**16** with two-fold excesses of LiCl, NaCl, KCl, RbCl, and CsCl in methanol. All of the

Table 4.2 Comparisons of distributions of metal cation complexes from mass spectral signal areas.

LEA	12:1 $MgCl_2$:Host[a] (LEA + Mg^{2+})	12:1 $CaCl_2$:Host[a] (LEA + Ca^{2+})	Signal Area Ratio (LEA + Mg^{2+})/(LEA + Ca^{2+})
4	33	38	0.88
6	38	39	0.98
11	40	44	0.90
14	41	34	1.2
15	31	26	1.17
Average signal area ratio (standard deviation)			**1.03 (0.15)**

[a] LEA concentration is 5 x 10^{-5} M in methanol; standard deviations of ±8%.

hosts shown in Figure 4.1 exhibited the same order of alkali metal cation selectivity: $Na^+ > K^+ > Rb^+ > Cs^+ \geq Li^+$. The relative percentage of lariat ether bound to Li^+, Rb^+, or Cs^+ showed little fluctuation throughout the series of macrocycles, with the intensities ranging from 7% to 14% for the Rb^+ complexes, 1% to 8% for the Cs^+ complexes, and 1% to 7% for the Li^+ complexes. This selectivity order follows the trend expected from the ionic diameters of the metal cations (diameters given in introduction) versus the inner diameter of the dibenzo-16-crown-5 ring (200 – 240 pm).[44, 45] Molecular models of LEA **2** with Na^+, K^+, and Rb^+ generated by *ab initio* calculations show that Na^+ nests within the plane of the ring, while K^+ and Rb^+ perch with their centers outside the plane of the ring (models not shown). Rb^+ is too large to fit within the three-dimensional cavity formed by the crown ether ring and the pendant oxyacetamide arm and must bind to the side of the polyether ring opposite to this pendant arm.

Since the LEAs show the greatest affinity for Na^+ and K^+, the Na^+/K^+ selectivity is plotted in Figure 4.3 to allow scrutiny of the degree of selectivity as a function of the pendant groups of the lariat ethers. A large degree of variation is seen for the LEAs, with Na^+/K^+ values that range from 1.8 to 6.1, although eleven of the lariat ethers have similar selectivities, in the range of 1.8 to 2.9. Variations in Na^+/K^+ selectivity are primarily due to the degree of interaction of the pendant arm with Na^+ and K^+ [48 - 54]. Enhancement in the Na^+/K^+ selectivity due to the presence of the geminal propyl arm is observed for **4** versus **2**, **8** versus **3**, **11** versus

Figure 4.3 Na^+/K^+ Selectivity ratio of macrocycles in methanol in order of increasing selectivity (L = lariat ether).

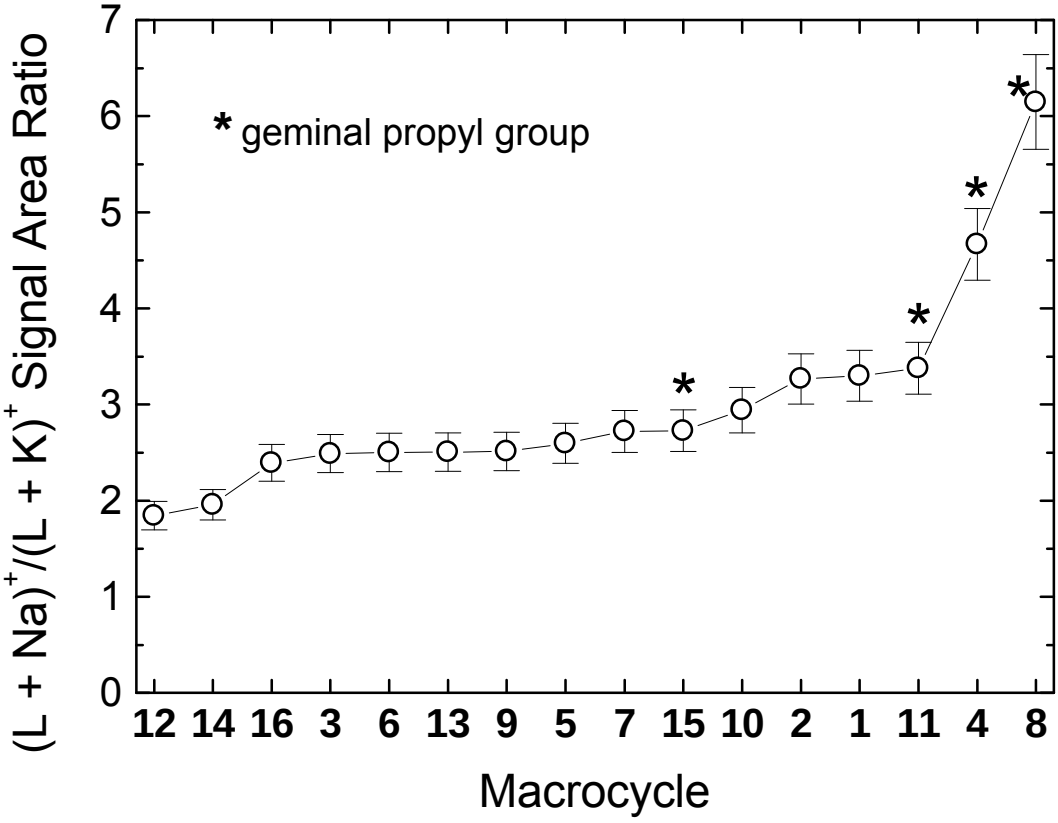

6, and **15** versus **14**. The propyl arm is thought to enhance Na^+ selectivity through steric effects that force the amide-containing pendant arm closer to the center of the cavity of the crown ether ring. The LEAs with the greatest Na^+/K^+ selectivities are those with hydrogens or methyl groups on the amide nitrogen and a geminal propyl arm, namely **4** and **8** with Na^+/K^+ selectivities of 4.7 and 6.1, respectively. The effects of geminal or *N*,*N*-di-substituted alkyl groups of the oxyacetamide pendant arm found in this study support the relative selectivities previously observed by the Bartsch group for LEAs in acidic aqueous solution with ion selective electrodes [52-54]. In methanol, the addition of an oxyacetamide pendant arm with one alkyl group slightly decreases the Na^+/K^+ selectivity versus that of **1** with no pendant arms. LEAs with *N*,*N*-di-substituted oxyacetamide pendant arms show Na^+/K^+ selectivities similar to those with oxyacetamide pendant arms containing one relatively short alkyl group and one hydrogen. When the alkyl groups on the *N*,*N*-di-substituted amide group reach four to five carbons in length, the Na^+/K^+ selectivity drops noticeably compared to LEAs with mono-substituted amide groups or those with di-substituted amide groups and shorter alkyl groups. It is surmised that the *N*,*N*-di-substituted amide decreases Na^+/K^+ selectivity through steric effects in which the bulky *N*,*N*-amide substituents force the amide-containing pendant arm farther from the center of the cavity of the crown ether ring, thus reducing the degree of interaction between the carbonyl oxygen and the metal cation. Substituting an ether oxygen for a methylene group in the *N*,*N*-di-

substituted amide (**13** versus **12** and **10** versus **6** and **16** versus **14)** regains some of the Na^+/K^+ selectivity lost by the purely hydrocarbon groups because of the nucleophilic attraction of the oxygens for the higher charge density of Na^+ versus K^+. Ultimately, whether the amide group is mono- or di-substituted does not seem to have a significant impact on Na^+/K^+ selectivity based on the similar selectivities determined for **9**, **5**, and **7** versus **3** and **6**. Rather, the total number of methylene groups (*i.e*. steric bulk) attached to the amide nitrogen is the more important factor.

In general, the presence of a geminal propyl group in the LEA significantly enhances the Na^+/K^+ selectivity, while increasing the number of methylene groups substituted on the amide nitrogen significantly decreases the Na^+/K^+ selectivity. Thus, the LEAs are versatile and highly "tunable" selectivity agents for Na^+ versus other alkali metal cations. The overall Na^+/K^+ selectivity of the LEAs in methanol is observed to be higher than for the lariat ethers with poly(oxa-alkyl) groups that were studied previously by the Brodbelt and Bartsch groups [33,35]. The latter were found to have Na^+/K^+ selectivity values from 0.8 to 4.0 versus 1.8 to 6.1 for the *N*,*N*-dialkyl LEAs.

4.3.3 Effect of Solution Acidity/Basicity on Metal Selectivities

Because the LEAs may be protonated, the acid/base nature of the solution could play a major role in their binding properties. ESI-MS was used to analyze solutions in which the hydrochloric acid and hydroxide content varied. The

Figure 4.4 ESI-mass spectra of LEA **6** with alkali metals at various acidities. **(a)** $p[H^+]_0 = 5.0$ **(b)** $p[H^+]_0 = 2.0$.

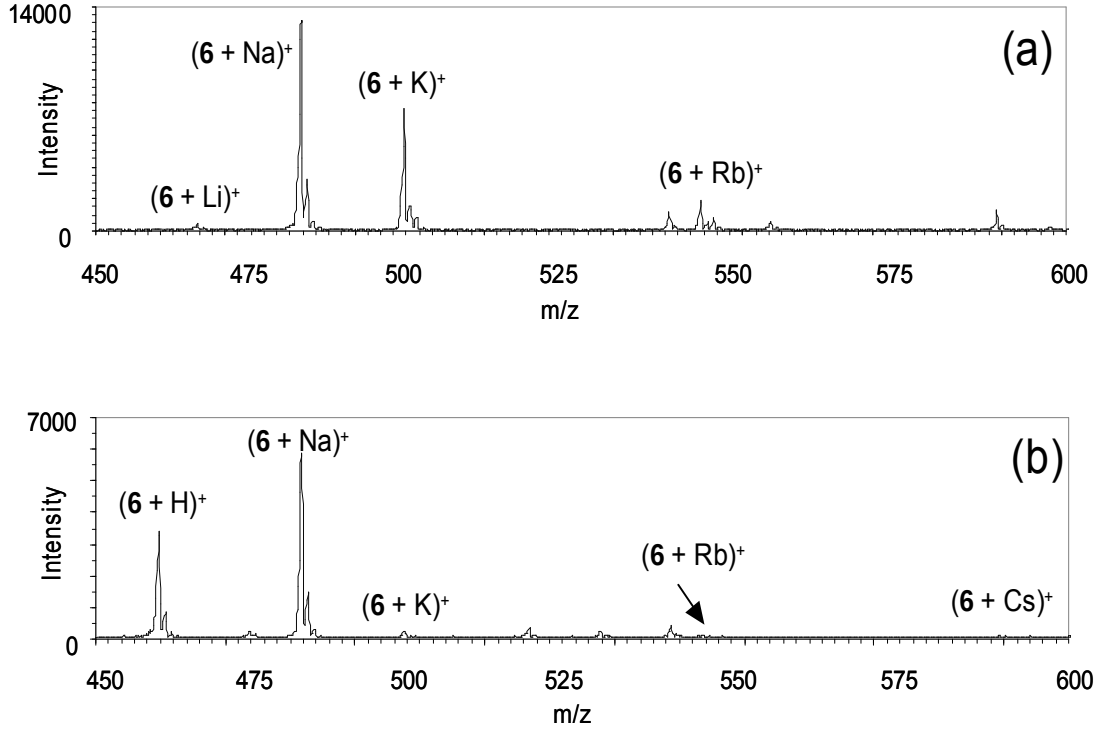

notations $p[H^+]_0$ and $p[OH^-]_0$ refer to the negative logarithm of the total concentration of HCl or hydroxide salt added, respectively. Figure 4.4 shows ESI-mass spectra for LEA **6** at two contrasting acid conditions. A significant shift in the distribution of complexes is observed in Figure 4.4A and 4.4B, with only the Na^+ complex surviving to a notable extent with the $p[H^+]_0 = 2.0$. The variation in Na^+/K^+ selectivity is summarized in more detail as a function of the $p[H^+]_0$ for LEA **6** and several other LEAs in Figure 4.5A. An alkali metal cation selectivity order of $Na^+ > K^+ > Rb^+ > Li^+$ with a Na^+/K^+ selectivity of approximately 2.5 persists in nominally basic ($p[OH^-]_0 = 3.4$) and neutral ($[H^+] = [OH^-] \approx 0$) solutions. However, in going from nominal $p[H^+]_0$ values of 5.0 to 3.0, the Na^+/K^+ selectivity increases to greater than 4.0, then increases to Na^+/K^+ selectivity values over twenty between $p[H^+]_0$ values of 2.5 to 2.0. We speculate that in basic and mildly acidic solutions, alkali metal complexation is able to effectively compete with protonation of the oxyacetamide nitrogen due to the conformational pre-organization that occurs because of the close proximity of the amide pendant arm to the metal cation binding macrocyclic cavity of the lariat ether amide, thus favoring metal complexes. As the $p[H^+]_0$ value progresses to less than 3.0, only Na^+, with a size best suited to both the polyether ring cavity diameter and coordination with the amide oxygen over the ring, is able to compete successfully with protonation of the amide nitrogen. Very similar results were obtained for the other LEAs tested (**5**, **9**, and **14)**. The Na^+/K^+ selectivity results obtained as a function of $p[H^+]_0$ for all four

Figure 4.5 Relative Na^+/K^+ selectivities of macrocycles versus acidity (L = macrocycle). (a) methanol (b) methanol/ water (3:1, v/v) (c) methanol with ionic strength maintained at 0.0104 M with $(CH_3)_4NCl$ (d) methanol with and without ionic strength maintained at 0.0104 M with $(CH_3)_4NCl$.

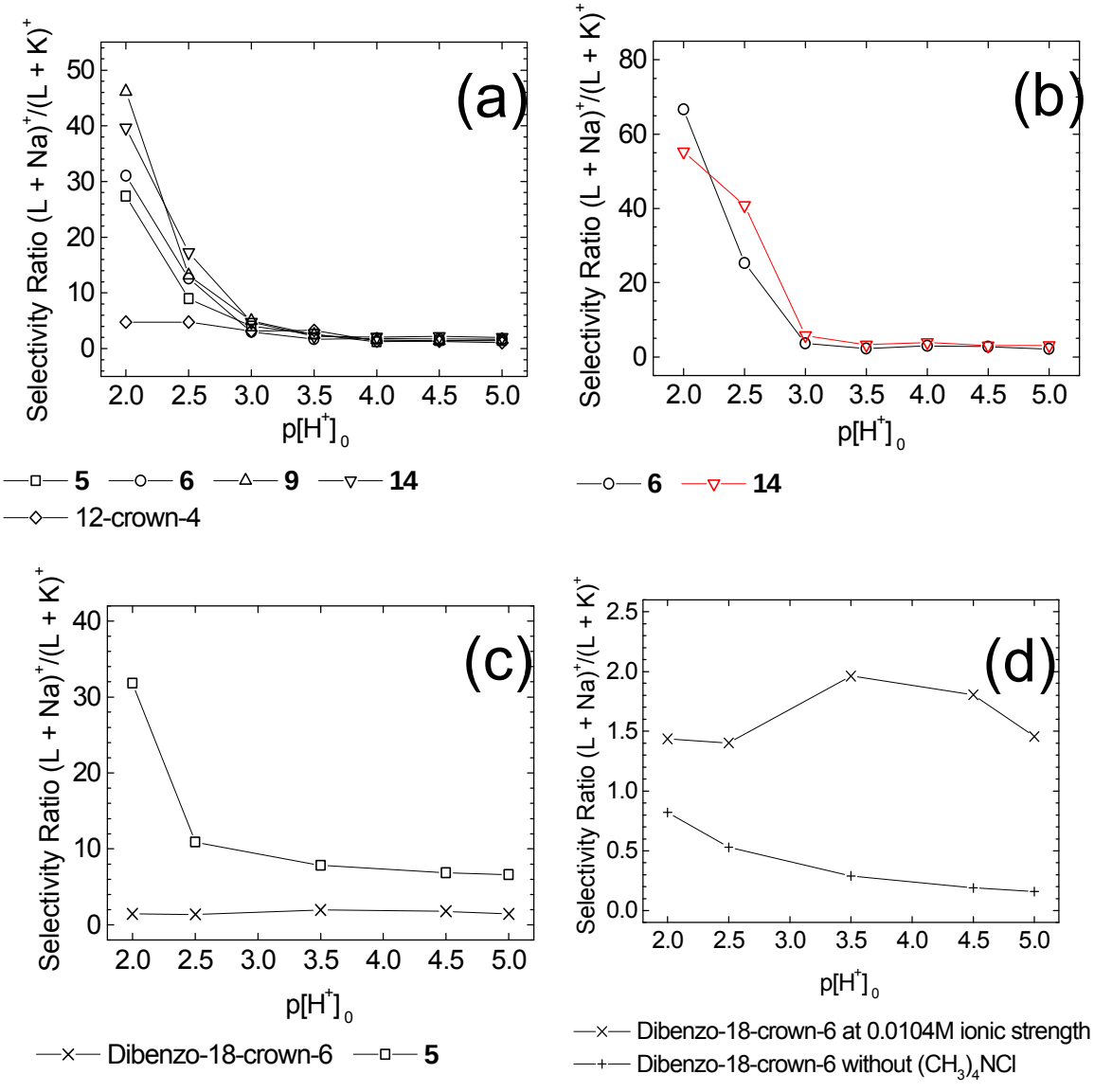

LEAs tested in methanol are shown in Figure 4.5A. Na^+/K^+ selectivities for **6** and **14** in methanol/water (3:1, v/v) are shown in Figure 4.5B.

To confirm that the large increase in Na^+/K^+ selectivity observed for solution acidities with $p[H^+]_0$ values less than 3.0 was indeed due to a change in binding selectivity rather than an effect of the acidic conditions on the electrospray process, the complexation of 12-crown-4 and dibenzo-18-crown-6 was analyzed as control systems under acidic conditions (Figures 4.6A and 4.5C). The degree of change in Na^+/K^+ selectivity for these two macrocycles from neutral conditions to $p[H^+]_0 = 2.0$ is very small, with the majority of 12-crown-4 and dibenzo-18-crown-6 molecules becoming protonated in solution and no major shift observed in the preference for complexation of Na^+ or K^+.

In addition, solutions in which the nominal $p[H^+]_0$ was varied while holding the ionic strength constant were analyzed to evaluate the impact of ionic strength on the Na^+/K^+ selectivities. The complexation of **5** and dibenzo-18-crown-6 were both tested at $p[H^+]_0$ values of 5.0, 4.0, 3.5, 2.5, and 2.0 with tetramethylammonium iodide present at concentrations necessary to maintain a constant ionic strength of 0.0104 M. As the acid content of the solution is increased, a large increase in Na^+/K^+ selectivity from six to greater than twenty still occurs for **5**, while the Na^+/K^+ selectivity of dibenzo-18-crown-6 remains constant at about 1.6 (Figure 4.5C). This is supporting evidence that the observed change in Na^+/K^+ selectivity of the LEAs results from a change in their chemical properties

Figure 4.6 Ca^{2+}/Mg^{2+} selectivity of macrocycles in methanol in order of increasing selectivity (L = macrocycle).

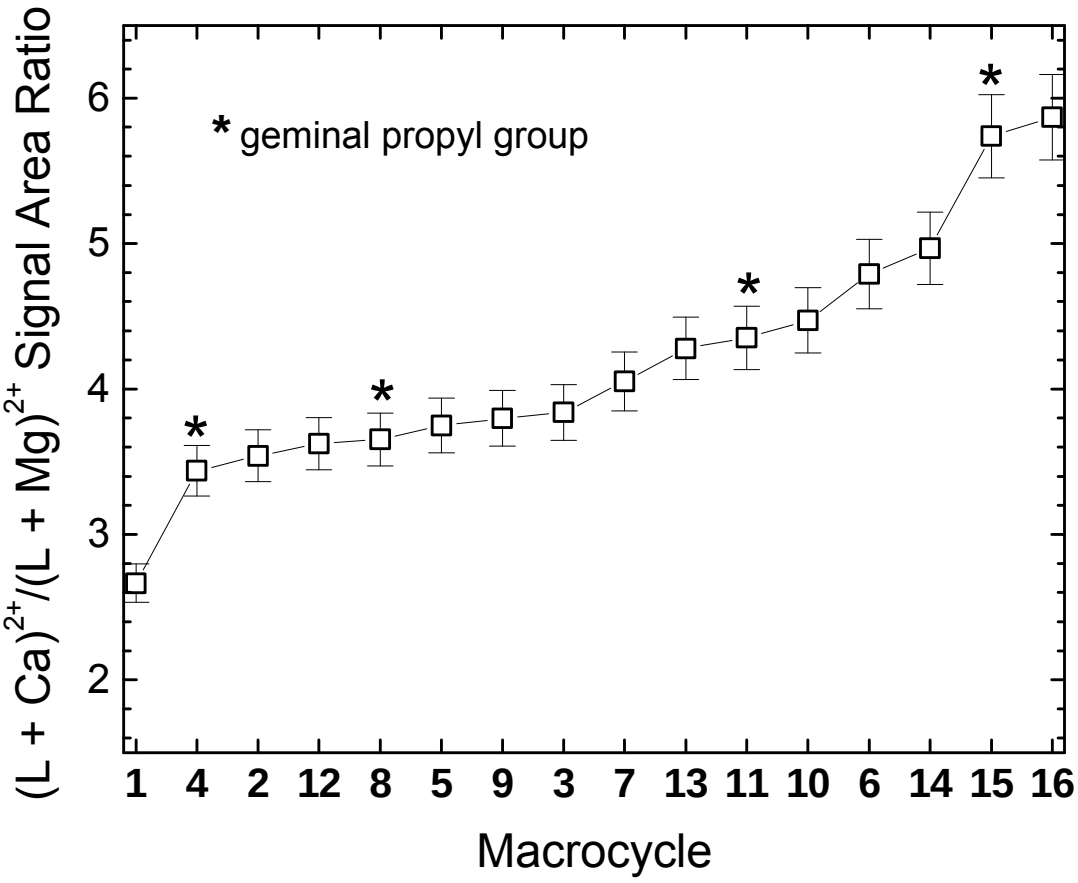

rather than an artifact of the electrospray process. The effect is presumably due to the preferential protonation of the amide nitrogen over complexation of Li^+, K^+ or Rb^+, with an effective competition between protonation and metal cation complexation only for Na^+, the metal cation that is most strongly bound. Note that artificially increasing the ionic strength, as done for the experiments whose results are illustrated in Figure 4.5C, also may cause an impact on the observed selectivities of the macrocycles. This effect is related to the mechanism of the ESI process and the suppression or enhancement of specific ions emerging from the spray due to their surface activities. For example, adding the trimethyl ammonium chloride to the solutions of the alkali metal chlorides with dibenzo-18-crown-6 causes a consistent increase in the Na^+/K^+ selectivities relative to those observed for solutions in which the auxiliary electrolyte was not added, as illustrated in Figure 4.5D.

It should be noted that during the electrospray process, the acidity of the emerging droplets will be altered relative to that of the bulk solution due to the evaporation of solvent and HCl from the electrospray droplets and proton generation due to electrochemical processes [60-66]. Faster evaporation of the solvent relative to that of HCl would mean that the total concentration of protonated species in the droplets would increase with time. According to Cook and co-workers, the decrease in the pH of aqueous solution droplets, initially at pH 6.89, at 2.0 mm from the ESI needle tip with a +3.5 kV needle voltage is about 0.60

pH units [60]. Similar results were reported by Agnes and co-workers in which the gas-phase concentrations of EDTA-metal ion complexes generated by ESI-MS from an aqueous solution at a needle voltage of –3.2 kV were found to exist at concentrations resembling those expected for solution acidities less than a pH unit higher than bulk solution from pH 5 to 8 [61]. However, at pH values lower than 5 and higher than 8, the EDTA-metal complexes in the gas-phase were present at concentrations nearly identical to the bulk solution, showing the ESI process had no significant influence on EDTA-metal concentrations [61]. Also, it should be considered that even though the ESI process may increase the acidity of the droplet environment, the metal ion concentration will also increase as the solvent evaporates from droplets. Taking all of these influences during the ESI process into consideration, the increase in proton concentration due to solvent evaporation should be balanced in part by a simultaneous increase in metal salt concentration and generation of protons in the methanolic solutions by the electrochemical reactions of ESI. The ESI-MS method seems to be an effective way to rapidly screen acid/base effects on the Na^+/K^+ selectivities of macrocycles, while conventional potentiometric methods can be reserved for more quantitative studies of the most relevant macrocycles as identified by the initial ESI-MS evaluation.

Based on the results shown in Figures 4.4 and 4.5, the LEAs are found to become highly Na^+ selective under moderately acidic solution conditions ($p[H^+]_0 <$ 3.0). Even in competition with proton binding, Na^+ is still able to maintain a stable

complex involving the lariat ether through interaction with the carbonyl oxygen of the amide and the oxygen atoms of the macrocyclic ring. K^+ is too large to interact well with the amide oxygen, and the protonation of the amide nitrogen is preferred over K^+ complexation. It appears that Na^+ is able to maintain interaction with the lariat ether to a greater degree than the other alkali metal cations in the presence of the amide nitrogen protonation equilibrium due to the higher association constant for Na^+. The LEAs have a small variation in Na^+/K^+ selectivity in solutions of low to moderate acidities, which is a valuable property in ion selective electrodes. They also show structural stability and a large shift to higher Na^+/K^+ selectivities at high acidities.

4.3.4 Alkaline Earth Metal Cation Selectivities

In a manner similar to that described for the experimental determination of the alkali metal cation selectivities, ESI-MS was used to evaluate the selectivities for the alkaline earth metal cations, Mg^{2+} and Ca^{2+}. The range in variation observed for the Ca^{2+}/Mg^{2+} selectivities (i.e. 3 to 6) of the LEAs is similar to the range observed for the Na^+/K^+ selectivities (2 to 6). Ca^{2+}/Mg^{2+} selectivity appears to be largely related to the overall size of the LEA. The general selectivity preference of the LEAs towards complexation with Ca^{2+} rather than Mg^{2+} can be understood in part due to the ionic radii of the cations. Figure 4.7 shows *ab initio* molecular

Figure 4.7 *Ab initio* molecular models of **2** with Mg^{2+} and Ca^{2+} ions. Black = oxygen, gray = carbon, light gray = nitrogen. Hydrogens not shown for clarity. Molecules on the left and right are rotated 90° around their vertical axis.

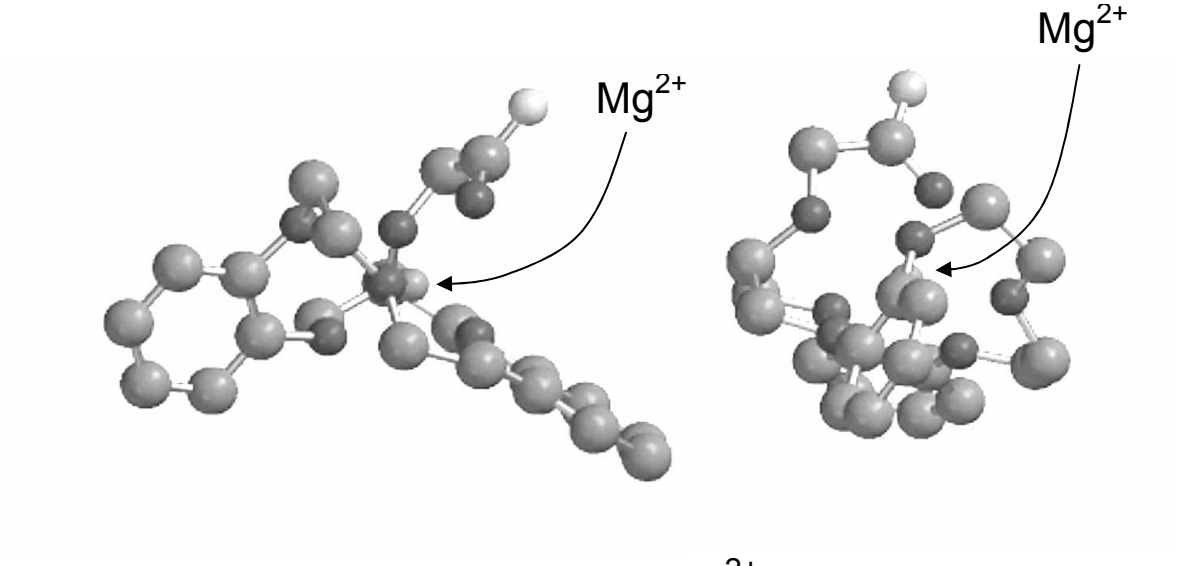

(**2** + Mg^{2+})

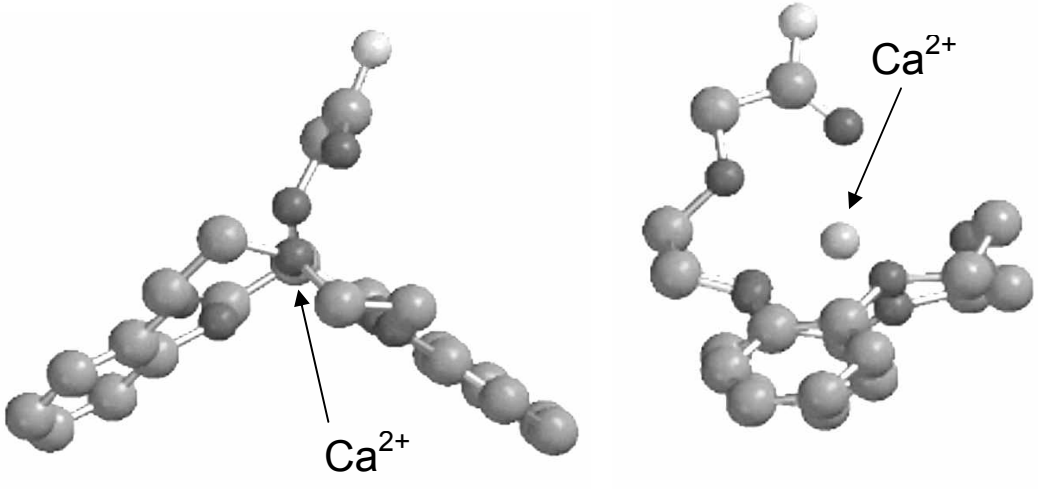

(**2** + Ca^{2+})

models of **2** complexed with Mg^{2+} and Ca^{2+}. The much smaller radius of Mg^{2+} compared to Ca^{2+} (78 pm and 106 pm, respectively [44]) requires significant distortion of the macrocyclic ring to attain a stable complex. However, the Ca^{2+} radius is only 6% larger than that of Na^{+}, so the size of Ca^{2+} is still quite a good fit for the three dimensional cavity of the LEA.

The geminal propyl arm present on **4**, **8**, **11**, and **15** has much less impact on selectivity with the alkaline earth metals than was observed with the alkali metals. The ionic radii of Na^{+}, Mg^{2+}, and Ca^{2+} are much smaller than the ionic radius of K^{+}. Thus, although the diameter of K^{+} is significantly larger than the diameter of the 16-crown-5 ring of the lariat ethers, the diameters of the other three ions are all small enough to nest within the lariat ether ring cavity. The geminal arm affects selectivity via steric effects which position and effectively decrease the distance between the amide containing pendant arm and the center of the crown ether ring cavity. Ions of ionic radii much larger than Ca^{2+} will be excluded to a significant extent because of a poorer fit in the resulting cavity of smaller volume. As a result, structural changes made directly to the amide containing pendant arm become more significant.

The increase in Ca^{2+}/Mg^{2+} selectivity with increasing size or mass of the lariat ether likely involves several factors. Because the alkaline earth dications have over twice the charge density of their corresponding alkali metal cations, polar solvent molecules with large dipole moments more readily displace the fairly non-

polar pendant groups from binding Mg^{2+}. Also, the different charge densities of the metal ions influence the degree to which the larger substituents on the amides interact with the relatively non-polar crown ether ring, the benzo-rings, and the solvent. When a LEA is complexed with Na^+ or K^+, the larger alkyl groups may have hydrophobic interactions with the less polar crown ether and benzo-rings in preference to the highly polar methanol solvent, and will do so more favorably with K^+ due to its lower charge density. Conversely, when the LEAs are complexed with Mg^{2+} or Ca^{2+}, the higher charge density of these dications may decrease this tendency for interaction of the alkyl amide substituent with the macrocycle, causing the alkyl groups to be preferentially solvated and pulling the oxyacetamide pendant arm away from the crown ether ring. Therefore, the LEAs with larger substituents will favor Ca^{2+} complexation over Mg^{2+}.

4.3.5 Collisionally Activated Dissociation of the Lariat Ether Complexes

Collisionally activated dissociation (CAD) experiments were undertaken for the alkali metal complexes with seven of the macrocycles to evaluate the fragmentation pathways as a function of the type of metal cation bound to the macrocycle, with comparison to the fragmentation patterns of the protonated macrocycles. Representative spectra are shown in Figures 4.8 – 4.10 for three protonated, Li^+-cationized, and K^+-cationized lariat ethers. CAD results for the

protonated LEAs are summarized in Table 4.3. Structures that fit many of the observed m/z values of the fragment ions are proposed in Scheme 4.1. Several common fragment ions are observed upon CAD of the protonated lariat ethers, including ions at m/z = 219 and 175 (structures A1 and A2 in Scheme 4.1) and ions at m/z = 181 and 137 (structures B1 and B2 in Scheme 4.1). Structures A1 and A2 and likewise B1 and B2 differ by a C_2H_4O unit, a common polyether sub-unit. These ions may cyclize and are characteristic of the benzo-crown ether skeletons of the lariat ethers. There are also common neutral losses for many of the protonated lariat ethers. Common losses include the elimination of 110 or 154 Da (C1 and C2, differing by a C_2H_4O unit) or loss of 136 or 180 Da (D1 and D2, differing by a C_2H_4O unit). These neutral products are illustrated in Scheme 4.1 and involve elimination of a phenyl ring from the protonated lariat ether. The other major dissociation pathways involve loss of the pendant arm (structure E in Scheme 4.1). Table 4.3 summarizes the occurrence of these various pathways for six of the protonated LEAs in addition to dibenzo-16-crown-5. It is clear that there is a distribution of fragments involving loss of half of the dibenzo-16-crown-5 macrocyclic skeleton in addition to those fragments that only involve loss of the pendant group or part of the pendant group.

The fragmentation patterns of both the Li^+ and Na^+ complexes are generally similar for each lariat ether, so these will be discussed together. There are four

Table 4.3 CAD results for protonated dibenzo-16-crown-5 and LEAs (mol. weight).

Fragment Ion	Relative Intensity [a]						
	1 (330)	**2** (403)	**5** (445)	**6** (459)	**9** (473)	**11** (501)	**14** (543)
P - H_2O[b]	+		+	+	+		
A1		++	++	++	++		++
A2		+++	+++	+++	+++		+++
B1	+++	++	+++	++	+++	+	++
B2	++						
P - C1	+++	+++	+++		++		++
P - C2		++	++		++		++
P - D1	+++	++	++	++	++		++
P - D2			++		++		++
E		+++	+++	++	+++	+++	++

[a] +++ = dominant products with intensities that are >50% of the base peak, ++ = products with intensities that are 10-50% of the base peak, + = low intensity products. [b] P = protonated molecule.

Scheme 4.1 Common product ions and neutral losses observed in CAD mass spectra of protonated LEAs.

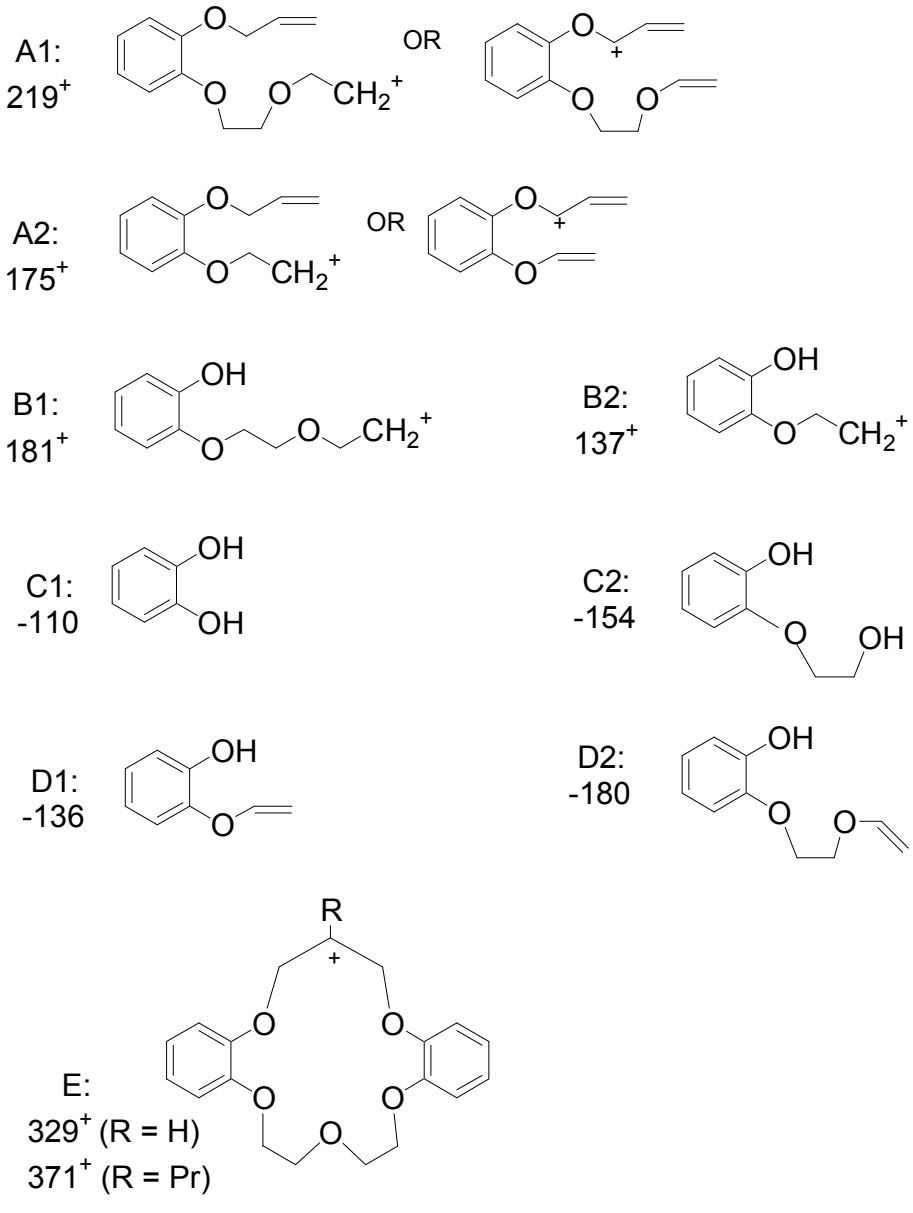

pathways observed for the Li^+ complexes. One dominant process involves loss of the pendant arm(s) with the propyl bridge of the crown ether ring, resulting in the intense product ion at m/z 296 for the Li^+ complexes in Figure 4.8B, 4.9B, and 4.10B (refer to Scheme 4.2). The second main process involves loss of just the amide pendant group, resulting in the product ion at m/z 335 in Figures 4.8B and 4.9B and the ion at m/z 377 in Figure 4.10B for the propyl substituted lariat ether (Scheme 4.2). The loss of 28 Da is also consistently observed for the Li^+ and Na^+ complexes (Figures 4.8B and 4.9B). Based on MS/MS/MS experiments, this loss of 28 Da was confirmed to be the elimination of C_2H_4, not the loss of CO. For example, if the primary fragment ion at m/z 438 in Figure 4.9B is isolated and activated, this ion dissociates by loss of the entire amide substituent, thus confirming that the carbonyl group is still retained in the ion at m/z 438. The fourth common dissociation pathway of the Li^+-cationized complexes involves the loss of 136 Da, which is attributed to the neutral loss D1 illustrated in Scheme 4.1. Most of the dominant fragmentation pathways for the Li^+ and Na^+ complexes involve loss of all or some portion of the pendant group, thus leading to product ions that are observed with significantly higher mass-to-charge ratios than those observed for the protonated lariat ethers. Pathways that involve cleavages of the macrocyclic skeleton (i.e. ones that produce fragment ions at lower mass-to-charge values) are far less favorable than observed for the protonated lariat ethers.

Figure 4.8 CAD of complexes of LEA **2**. (a) $(\mathbf{2} + H)^+$ (b) $(\mathbf{2} + Li)^+$ (c) $(\mathbf{2} + K)^+$.

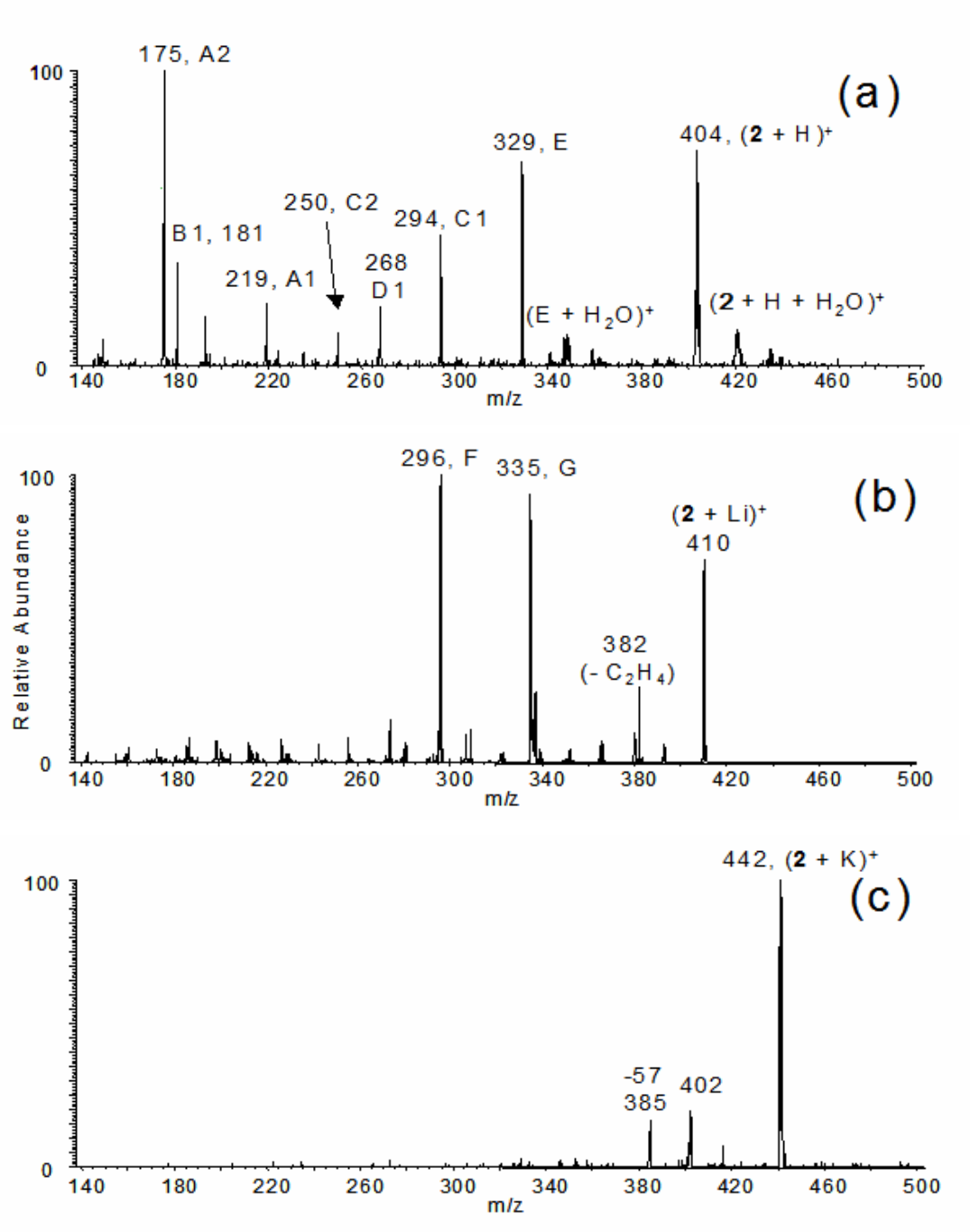

Figure 4.9 CAD of complexes of LEA **6**. (a) $(\mathbf{6} + H)^+$ (b) $(\mathbf{6} + Li)^+$ (c) $(\mathbf{6} + K)^+$.

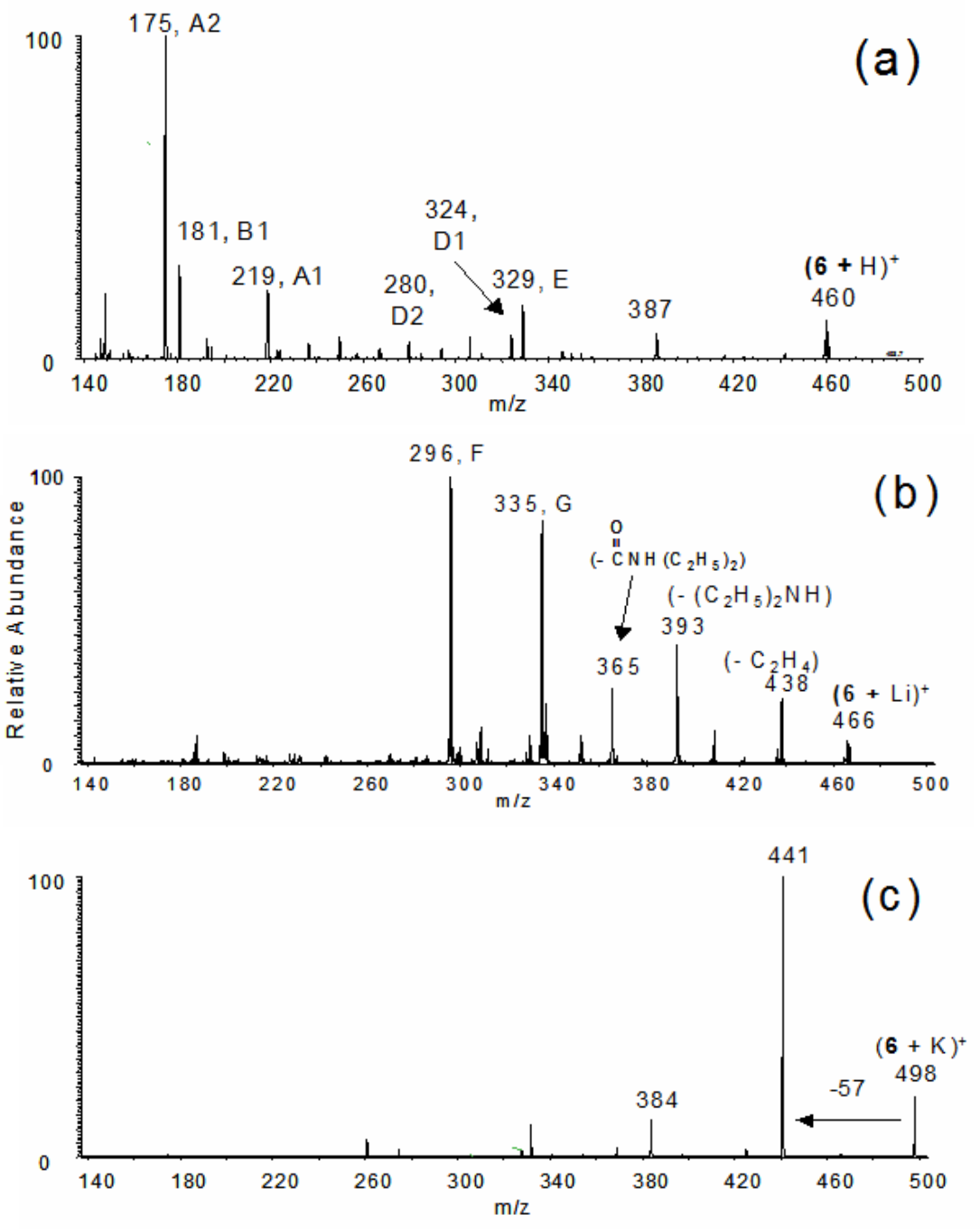

Figure 4.10 CAD of complexes of LEA **11**. **(a)** (**11** + H)$^+$ **(b)** (**11** + Li)$^+$ **(c)** (**11** + K)$^+$.

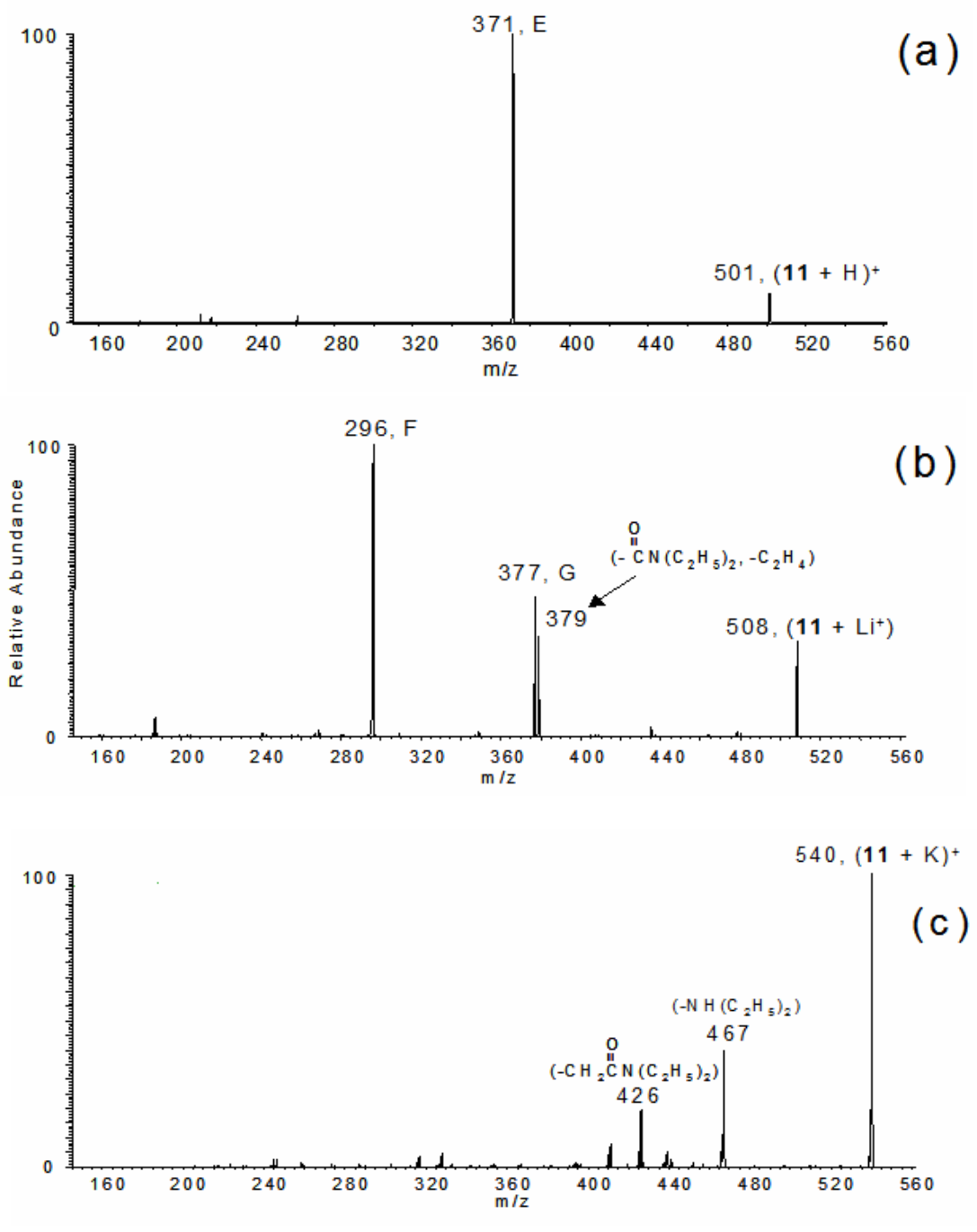

Scheme 4.2 Predominant product ions observed in the CAD mass spectra of alkali metal complexes.

F:

296^+ (Li^+)

312^+ (Na^+)

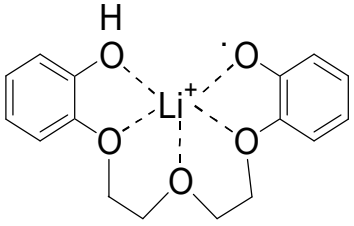

G:

335^+ (R = H)

377^+ (R = Pr)

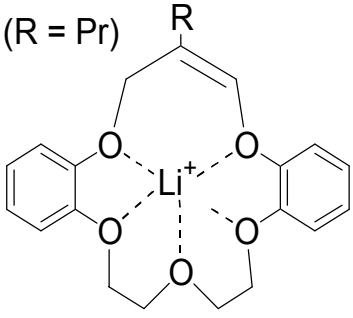

Loss of 57 Da for K^+ complexes

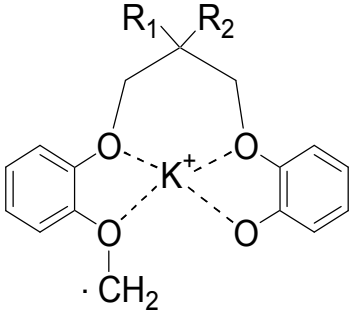

The K^+ complexes generally do not dissociate by the same pathways seen for the protonated, Li^+ or Na^+ complexes. In fact, the K^+ complexes for several of the LEAs and dibenzo-16-crown-5 dissociate predominantly by elimination of K^+, resulting in no structurally diagnostic ions nor involving covalent bond cleavages of the macrocycle. This type of disassembly is characteristic of loosely bound non-covalent complexes in which the total energy of the macrocycle/K^+ bonds is substantially lower than the energies of the covalent bonds of the macrocycle. For a few of the lariat ethers, namely **2, 6**, **9**, and **14**, a common dissociation pathway is loss of 57 Da, presumably due to elimination of $C_3H_5O^{\cdot}$ from the macrocyclic skeleton (Scheme 4.2). This pathway is unlike any of those observed for the Na^+ and Li^+ complexes and suggests that K^+, when bound more strongly to the LEA, may be anchored to a different site than that of the smaller, more charge dense metal cations. The Rb^+ and Cs^+ complexes generally dissociate solely by elimination of the metal cation. This fragmentation pathway is typical for weakly bound complexes.

In summary, the types of fragmentation patterns observed vary dramatically for the protonated lariat ethers relative to the metal-cationized complexes. Fragmentation involving cleavages of the covalent bonds in the macrocyclic skeleton is much more pronounced for the protonated lariat ethers. The diverse array of fragmentation pathways for the protonated lariat ether suggests that the proton is mobile upon activation of the complex or that the proton may initially be

localized at several different sites prior to activation. The Li^+ and Na^+ complexes dissociate preferentially by elimination of the pendant groups, suggesting that the metal cation is nested in the cavity of the macrocycle. The complexes involving the larger alkali metal cations typically disassemble upon activation, implying weakly bound complexes.

4.4 Conclusions

In summary, the ESI-MS method proves to be an efficient way to evaluate the acid/base dependence of metal binding and to screen the alkaline earth metal cation selectivities of novel macrocyclic hosts, thus further extending the range of applications of the ESI-MS method for problems related to host-guest complexation and ligand selectivity. Dibenzo-16-crown-5 lariat ethers with amide pendant arms show a selectivity order towards alkali metal cations of $Na^+ > K^+ > Rb^+ > Cs^+ > Li^+$, with relatively weak complexation of Rb^+, Cs^+, and Li^+. Addition of an oxyacetamide group and a propyl group as geminal side arms on the dibenzo-16-crown-5 lariat ether framework enhances the Na^+/K^+ selectivity in all cases, but the enhancement is greatest when the amide group is di-substituted with two methyl groups. Protonation of the amide nitrogen enhances the Na^+/K^+ selectivity of the LEAs by up to an order of magnitude. This enhancement results from protonation of the amide nitrogen which precludes Li^+, K^+, or Rb^+ cation binding by the amide pendant group. The protonation electrostatically repels metal cations

that do not nest as well as Na^+ in the dibenzo-16-crown-5 cavity, while only Na^+ can compete against protonation for complexation of the macrocycle.

Binding of Ca^{2+} over Mg^{2+} is favored by all the LEAs in methanol, as observed in the studies in aqueous solution conducted by Bartsch, *et. al.*, [48]. Ca^{2+}/Mg^{2+} selectivity generally increases with the increasing mass of the LEA, in contrast to the Na^+/K^+ selectivity. Also, Ca^{2+}/Mg^{2+} selectivity is unaffected by the presence of a geminal propyl group on the LEAs.

Li^+ and Na^+ remain bound to the macrocyclic cavity upon activation of the complexes, while K^+ and larger alkali metal cations are mainly ejected during CAD. The different fragmentation patterns observed for the protonated LEAs versus the Li^+- and Na^+-cationized LEAs supports different binding sites.

4.5 Acknowledgements

Funding for this work was provided by The Welch Foundation (Grants F-1155 to JSB and D-775 to RAB) and the National Science Foundation (CHE-9820755).

4.6 References

1. Yamashita, M.; Fenn, J.B. Electrospray Ion Source. Another Variation on the Free-Jet Theme. *J. Phys. Chem*,**1984**, *88*, 4451-4459.

2. Fenn, J.B.; Mann, M.; Meng, C.K.; Wong, S.F.; Whitehouse, C.M. Electrospray Ionization-Principles and Practice. *Mass Spectrom. Rev.*,**1990**, *9*, 37-70.

3. Smith, R.D.; Loo, J.A.; Edmonds, C.G., Barinaga, C.J.; Udseth, H.R. New Developments in Biochemical Mass Spectrometry: Electrospray Ionization. *Anal. Chem.*,**1990**, *62*, 882-899.

4. Cole, R.B., Ed., *Electrospray Ionization Mass Spectrometry*, Wiley-Interscience, New York, 1997.

5. Veenstra, T. D. Electrospray Ionization Mass Spectrometry in the Study of Biomolecular Non-Covalent Interactions. *Biophys. Chem.* **1999**, *79*, 63-79.

6. Loo, J. A. Electrospray Ionization Mass Spectrometry: A Technology for Studying Noncovalent Macromolecular Complexes. *Int. J. Mass Spectrom.* **2000**, *200*, 175-186.

7. Schalley, C. A. Supramolecular Chemistry goes Gas Phase: the Mass Spectrometric Examination of Noncovalent Interactions in Host-Guest Chemistry and Molecular Recognition. *Int. J. Mass Spectrom.* **2002**, *194*, 11-39.

8. Loo, J.A.; Holsworth, D.D.; Root-Bernstein, R.S. Use of Electrospray Ionization Mass Spectrometry to Probe Antisense Peptide Interactions. *Biol. Mass Spectrom.* **1994,** *23*, 6-12.

9. Lamcharfi, E.; Chuilon, S.; Kerbal, A.; Kunesch, G.; Libot, F.; Virelizier, H. Electrospray Ionization Mass Spectrometry In Supramolecular Chemistry: Characterization of Non-Covalent Cyclodextrin Complexes. *J. Mass Spectrom.*, **1996**, *31*, 982-986.

10. Robinson, C.V.; Chung, E.W.; Kragelund, B.B.; Knudsen, J.; Aplin, R.T.; Doulsen, F.M.; Dobson, C.M. Probing the Nature of Noncovalent Interactions by Mass Spectrometry. A Study of Protein-CoA Ligand Binding and Assembly. *J. Am. Chem. Soc.* **1996**, *118*, 8646-8653.

11. Cheng, X.; Chen, R.; Bruce, J.E.; Schwartz, B.L.; Anderson, G.A.; Hofstadler, S.A.; Gale, D.C.; Smith, R.D. Using Electrospray Ionization FTICR Mass

Spectrometry to Study Competitive Binding of Inhibitors to Carbonic Anhydrase. *J. Am. Chem. Soc.* **1995**, *117*, 8859-8860.

12. Cheng, Z.L.; Siu, K.W.M. ; Guevremont, R.; Berman, S.S. Electrospray Mass Spectrometry: A Study on Some Aqueous Solutions of Metal Salts. *J. Am. Soc. Mass Spectrom.* **1992,** *3*, 281-288.

13. Chapeaurouge, A.; Bigler, L.; Shafer, A.; Bienz, S. Correlation of Stereoselectivity and Ion Response in Electrospray Mass-Spectrometry. Electrospray Ionization-Mass Spectrometry as a Tool to Predict Chemical Behavior? *J. Am. Soc. Mass Spectrom.* **1995,** *6*, 207-211.

14. Guevremont, R.; Siu, K.W.M.; Le Blanc, J.C.Y.; Berman, S.S. Are the Electrospray Mass Spectra of Proteins Related to Their Aqueous Solution Chemistry? *J. Am. Soc. Mass Spectrom.* **1992,** *3*, 216-224.

15. Wang, G.; Cole, R.B. Disparity Between Solution-Phase Equilibria and Charge State Distributions in Positive-Ion Electrospray Mass Spectrometry. *Org. Mass Spectrom.* **1994,** *29*, 419-427.

16. Gokel, G.W.; Wang, K. Correlation of Solution and Gas Phase Complexation Assessed by Electrospray Ionization Mass Spectrometry: Application to One-, Two-, and Three-Ring Macrocycles. *J. Org. Chem.* **1996,** *61*, 4693-4697.

17. Leize, E.; Jaffrezic, A.; Van Dorsselaer, A. Correlation between Solvation Energies and Electrospray Mass Spectrometric Response Factors. Study by Electrospray Mass Spectrometry of Supramolecular Complexes in Thermodynamic Equilibrium in Solution. *J. Mass. Spectrom.* **1996,** *31*, 537-544.

18. Young, D-S.; Hung, H-Y. Liu, L. K. An Easy and Rapid Method for Determination of Stability Constants by Electrospray Ionization Mass Spectrometry. *J. Mass. Spectrom.* **1997,** *32*, 432-437.

19. Hsieh, Y.L.; Li, Y.-T.; Henion, J.D.; Ganem, B. Studies of Non-Covalent Interactions of Actinomycin D with Single-Stranded Oligodeoxynucleotides by Ion Spray Mass Spectrometry and Tandem Mass Spectrometry. *Biol. Mass Spectrom.*, **1994**, 23, *272-276.*

20. Cheng, X.; Chen, R.; Bruce, J.E.; Schwartz, B.L.; Anderson, G.A.; Hofstadler, S.A.; Gale, D.C.; Smith, R.D.; Gao, J.; Sigal, G.B.; Mammen, M.; Whitesides, G.M. Using Electrospray Ionization FTICR Mass Spectrometry to Study

Competitive Binding of Inhibitors to Carbonic Anhydrase. *J. Am. Chem. Soc.* **1995**, *117*, 8859-8860.

21. Sannes-Lowery, K.A.; Hu, P.; Mack, D.P.; Mei, H.-Y.; Loo, J.A. HIV-1 Tat Peptide Binding to TAR RNA by Electrospray Ionization Mass Spectrometry. A*nal.Chem.*, **1997**, *69*, 5130-5135.

22. Sannes-Lowery, K.A.; Mei, H.-Y.; Loo, J.A. Studying Aminoglycoside Antibiotic Binding to HIV-1 TAR RNA by Electrospray Ionization Mass Spectrometry. *Int. J. Mass Spectrom.*, **1999**, *193*, 115-122.

23. Wan, K.X.; Shibue, T.; Gross, M.L. Non-Covalent Complexes between DNA-Binding Drugs and Double-Stranded Oligodeoxynucleotides: A Study by ESI Ion-Trap Mass Spectrometry. *J. Am. Chem. Soc.* **2000**, *122*, 300-307.

24. Blair, S.M.; Kempen, E.C.; Brodbelt, J.S. Determination of Binding Selectivities by ESI/Quadrupole Ion Trap Mass Spectrometry. *J. Am. Soc. Mass Spectrom.*, **1998**, *9*, 1049-1059.

25. Blair, S.M.; Brodbelt, J.S.; Reddy, G.M.; Marchand, A.P. Evaluation of Binding Selectivities of Bis-Crowned Clefts by Electrospray Ionization/Quadrupole Ion Trap Mass Spectrometry. *J. Mass Spectrom.*, **1998**, *33*, 721-728.

26. Kempen, E.C.; Brodbelt, J.S.; Bartsch, R.A.; Jang, Y.;Kim, J.S. Investigation of Alkali Metal Cation Selectivities of Lariat Ethers by Electrospray Ionization Mass Spectrometry. A*nal..Chem.*, **1999**, *71*, 5493-5500.

27. Brodbelt, J.; Kempen, E.; Reyzer, M. Determination of Binding Selectivities by Electrospray Ionization Mass Spectrometry. *Struct. Chem.*,**1999**, *10*, 213-220.

28. Blair, S.M.; Brodbelt, J.S.; Marchand, A.P.; Kumar, K.A.; Chong, H-S. Evaluation of Binding Selectivities of Caged Crown Ligands towards Heavy Metals by Electrospray Ionization/Quadrupole Ion Trap Mass Spectrometry. *Anal. Chem.*, **2000**, *72*, 2433-2445.

29. Goolsby, B.; Hall, B.J.; Brodbelt, J.S.; Adou, E.; Blanda, M. Determination of Alkali Metal Ion Binding Selectivities of Calixerenes by MALDI and ESI in a Quadrupole Ion Trap. *Int. J. Mass Spectrom.*, **1999**, *193*, 197-204.

30. Blanda, M.T.; Farmer, D.B.; Brodbelt, J.S.; Goolsby, B. Synthesis and Alkali Metal Ion Binding Properties of Two Rigid Stereochemical Isomers of Calix[6]arene-Bis-Crown-4. *J. Am. Chem. Soc.* **2000**, *122*, 1486-1491.

31. Reyzer, M.L., Brodbelt, J. S., Marchand, A.P., Chen, Z., Huang, Z., Namboothiri, I.N. N. Determination of Alkali Metal Binding Selectivities of Caged Crown Ligands by Electrospray Ionization Quadrupole Ion Trap Mass Spectrometry. *Int. J. Mass Spectrom*., **2001**, *200*, 57-69.

32. Blair, S., Brodbelt, J., Marchand, A., Chong, H.-S., Alidhodzic, S. Evaluation of Alakli Metal Binding Selectivities of Caged Aza-Crown Ligands by Electrospray Ionization Quadrupole Ion Trap Mass Spectrometry. *J. Am. Soc. Mass Spectrom*., **2000**, *11*, 884-891.

33. Williams, S.; Blair, S. M.; Brodbelt, J. S.; Huang, X.; Bartsch, R. A. Determination of Alkali Metal Cation Selectivities of Dibenzo-16-Crown-5 Lariat Ethers with Ether Pendant Groups using Electrospray Ionization Quadrupole Ion Trap Mass Spectrometry. *Int. J. Mass Spectrom.*, **2001**, *212*, 389-401.

34. Williams, S. M.; Brodbelt, J. S.; Marchand, A. P.; Cal, D.; Mlinaric-Majerski, K. Metal Complexation of Novel Thia-Crown Ether Macrocycles by Electrospray Ionization Mass Spectrometry. *Anal. Chem.*, **2002**, *74(17)*, 4423-4433.

35. Kempen, E., Brodbelt, J. A Novel Method for the Determination of Binding Constants by Electrospray Ionization Mass Spectrometry. *Anal. Chem*., **2000**, *72*, 5411-5416.

36. Lim, H.-K.; Hsieh, Y.L.; Ganem, B.; Henion, J. Recognition of Cell-Wall Peptide Ligands by Vancomycin Group Antibiotics: Studies using Ion Spray Mass Spectrometry. *J. Mass Spectrom.*, **1995**, *30*, 708-714.

37. Loo, J.A.; Hu, P.; McConnell, P.; Mueller, W.T.; Sawyer, T.K.; Thanabal, V. A Study of Src SH2 Domain Protein-Phosphopeptide Binding Interactions by Electrospray Ionization Mass Spectrometry. *J. Am. So.c Mass Spectrom.*, **1997**, *8*, 234-243.

38. Young, D.-S.; Hung, H.-Y.; Liu, L.K. An Easy and Rapid Method for Determination of Stability Constants by Electrospray Ionization Mass Spectrometry. *Rapid Commun. Mass Spectrom.*, **1997**, *11*, 769-773.

39. Jorgensen, T.J.D.; Roepstorff, P.; Heck, A.J.R. Direct Determination of Solution Binding Constants for Noncovalent Complexes between Bacterial Cell Wall Peptide Analogs and Vancomycin Group Antibiotics by Electrospray Ionization Mass Spectrometry. A*nal.Chem.*, **1998**, *70*, 4427-4432.

40. Griffey, R.H.; Hofstadler, S.A.; Sannes-Lowery, K.A.; Ecker, D.J.; Crooke, S.T. Determinants of Aminoglycoside-binding Specificity for rRNA by using Mass Spectrometry. *Proc. Natl. Acad. Sci. USA*, **1999**, *96*, 10129-10133.

41. Martell, A.E., Hancock, R.D., Chapter 7: "Stability Constants and Their Measurement", *Metal Complexes in Aqueous Solutions,* Plenum Press: New York, **1996**.

42. Schalley, C.A. Supramolecular Chemistry Goes Gas Phase: The Mass Spectrometric Examination Of Non-Covalent Interactions In Host-Guest Chemistry And Molecular Recognition. *Int. J. Mass Spectrom.*, **2000**, *194*, 11-39.

43. Schalley, C.A. Molecular Recognition and Supramolecular Chemistry in the Gas Phase. *Mass Spectrom. Rev.*, **2001**, *20*, 253-309.

44. Shannon, R.D. Revised Effective Ionic Radii and Systematic Studies of Interatomic Distances in Halides and Chalcogenides. *Acta Crystallogr., Sect. A: Found. Crystallogr*. **1976**, 32, 751-767.

45. Bartsch, R.A.; Lu, J.; Ohki, A. Potentiometric Selectivities of Dibenzo-16-Crown-5 Compounds for Alkali and Alkaline Earth Metal Cations and Ammonium Ions. *J. Incl. Phenomena Mol. Recogn. In Chem.*, **1998**, 32, 133-150.

46. Armentrout, P.B. "Cation-Ether Complexes in the Gas Phase: Thermodynamic Insight into Molecular Recognition," *Int. J. Mass Spectrom.*, **1999**, *193*, 227-240.

47. Nicoll, J.B.; Dearden, D.V. Reactions of Multidentate Ligands with Ligated Alkali Cation Complexes: Self-Exchange and 'Sandwich' Complex Formation Kinetics of Gas Phase Crown Ether-Alkali Cation Complexes. *Int. J. Mass Spectrom.*, **2001**, *204*, 171-183.

48. Dearden, D.V.; Liang, Y.; Nicoll, J.B.; Kellersberger, K.A. Study of Gas-Phase Molecular Recognition using Fourier Transform Ion Cyclotron Resonance Mass Spectrometry (FTICR/MS). *J. Mass Spectrom.*, **2001**, *36*, 989-997.

49. Ohki, A.; Lu., J.-P.; Huang, X.; Bartsch, R.A. Alkali Metal, Alkaline Earth Metal, and Ammonium Ion Selectivities of Dibenzo-16-Crown-5 Compounds with Functional Side Arms in Ion-Selective Electrodes. *Anal. Chem.*, **1994**, 66, 4332-4336.

50. Ohki, A.; Lu, J.-P.; Hallman, J.L.; Huang, X.; Bartsch, J.A. Sodium Ion-Selective Electrodes Based on Dibenzo-16-crown-5 Compounds with Pendent Ester Groups. *Anal. Chem*., **1995**, 67, 2405-2408.

51. Ohki, A.; Lu, J.-P.; Bartsch, R.A. Effect of Side-Arm Variation in Dibenzo-16-crown-5 Compounds on the Potentiometric Selectivity for Sodium Ion. *Anal. Chem.*, **1994**, *66*, 651-654.

52. Ohki, A.; Lu., J.-P.; Maeda, S.; Bartsch, R.A. Sodium Ion-Selective Electrodes Based on Dibenzo-16-crown-5 Compounds with Pendent Amide Groups. *Anal. Chem.*, **1994**, *66*, 1743-1746.

53. Ohki, A.; Iwaki, K.; Naka, K.; Maeda, S.; Collier, J.J; Jang, Y.; Hwang, H-.S., Bartsch, R.A. Comparison Of Dibenzo-16-Crown-5 Compounds with Pendent Amide Groups as Sodium Ionophores in Ion-Selective Electrodes and in Solvent Extraction. *Electroanalysis.* **1996**, *8*, 615-618.

54. Ohki, A.; Iwaki, K.; Naka, K.; Kamata, S.; Maeda, S.; Lu, J.-P.; Bartsch, R.A. Sodium Ion Sensors Based on Dibenzo-16-Crown-5 Compounds with Amide Side Arms. *Supramol. Chem.* **1996**, *6*, 391-394.

55. Recommendations for Nomenclature of Ion-Selective Electrodes. *Pure Appl. Chem.*, **1976**, *48*, 127-132.

56. Van Berkel, G.J.; Glish, G.L.; McLuckey, S.A. Electrospray Ionization Combined with Ion Trap Mass Spectrometry. *Anal. Chem.* **1990**, *62*, 1284-1285.

57. Pederson, C.J., Cyclic Polyethers and Their Complexes with Metal Salts. *J. Am. Chem. Soc*., **1967**, 89, 7017-7036.

58. Kasprzyk, S.P., Bartsch, R.A., Synthesis of Dibenzocrown Ethers with Pendant Amide Groups. *J. Heterocyclic Chem*., **1993**, 30, 119-123.

59. Izatt, R.M.; Pawlak, K.; Bradshaw, J.S.; Bruening, R.L. Thermodynamic and Kinetic Data for Macrocycle Interactions with Cations and Anions. *Chem. Rev*., **1991**, *91*, 1721-2085.

60. Zhou, S.; Edwards, A.G.; Cook, K.D., Van Berkel, G.J. Investigation of the Electrospray Plume by Laser-Induced Fluorescence Spectroscopy. *Anal. Chem.*, **1999**, *71*, 769-776.

61. Wang, H.; Agnes, G.R. Kinetically Labile Equilibrium Shifts Induced by the Electrospray Process. *Anal. Chem.*, **1999**, *71*, 4166-4172.

62. Mansoori, B.A.; Volmer, D.A.; Boyd, R.K. Wrong-Way-Round Electrospray Ionization of Amino Acids. *Rapid Commun. Mass Spectrom.*, **1997**, *11*, 1120-1130.

63. Zhou, S.; Cook, K.D. Protonation in Electrospray Mass Spectrometry: Wrong-Way-Round or Right-Way-Round? *J. Am. Soc. Mass Spectrom.*, **2000**, *11*, 961-966.

64. Easterly, C.E.; Hercules, D.M.; Houalla, M. Electrospray-Ionization Time-of-Flight Mass Spectrometry: pH-Dependence of Phosphomolybdate Species. *Appl. Spectrosc.*, **2001**, *55*, 1671-1675.

65. Julian, R.R.; Beauchamp, J.L. Site Specific Sequestering and Stabilization of Charge in Peptides by Supramolecular Adduct Formation with 18-Crown-6 Ether by Way of Electrospray Ionization. *Int. J. Mass Spectrom.*, **2001**, *210/211*, 613–623.

66. Sutrisno; Baran, Y.; Lawrance, G.A.; von Nagy-Felsobuki, E. I. Determination of Acid Dissociation Constants of Neamine By Potentiometric and Electrospray Mass Spectral Techniques. *Struct. Chem.*, **2001**, *12(2)*, 189-195.

CHAPTER 5

Metal Complexation of Novel Thia-Crown Ether Macrocycles by Electrospray Ionization Mass Spectrometry

5.1 Introduction

Heavy metals, one of the most hazardous classes of pollutants in water sources due to their non-biodegradability, have caused widespread water endangerment, contamination of fish, and serious health problems.[1] Numerous remediation methods are currently under development [2-5], including e.g., (i) the use of electrolytic recovery of water to reduce metals to their elemental forms, (ii) the use of novel high capacity ion exchange resins or zeolites, and (iii) the extraction of metals by microorganisms or plants, such as fungal adsorption, bioleaching with bacteria or phytoremediation for soil sediment. Novel macrocycles are currently being developed and evaluated for use as selective, recyclable ligands for extraction of heavy metals from contaminated water [6-16]. Fast, efficient feedback about metal selectivities and avidities will aid the design and development process.

Electrospray ionization mass spectrometry (ESI-MS) shows promise for rapid screening of binding selectivities in host-guest chemistry [17-37], offering

versatility in a variety of solvent systems and requiring minimal sample consumption. In addition, ESI-MS allows for the analysis of low micromolar quantities of the macrocycles directly complexed with the metal ions of interest. ESI-MS provides complementary information not available with the purely elemental capabilities of (i) ICP-MS and ICP-AES, which are commonly used for heavy metal detection, (ii) NMR analysis, which often requires higher concentrations of analyte and cannot be used for analyzing several complexes simultaneously, and (iii) electrochemical analysis, which is limited to a smaller number of compatible solvents and higher ionic strengths than ESI-MS.

The use of macrocycles for metal binding has been recognized for some time [38-40]. Recently, there has been an increasing interest in using sulfur-containing compounds for complexation of heavy metals for potential applications in the biology of heavy metal complexation with sulfur containing biomolecules [41-45] and the removal of heavy metals such as silver [14,46], copper [13], and mercury [10-15,47,48] from wastewaters. Both acyclic sulfur-containing ligands [47,48] and cyclic thiacrown ethers [10-15] have been used in such applications.

Thiacrown ethers have been attached through covalent linkages to various linker groups which allow them to be incorporated into polymers. In these previous studies, macrocycles with sulfur heteroatoms were incorporated into a polymer by a lariat covalent linkage via an amine nitrogen or ether oxygen on the macrocycle.[10-14] Thiacrown ether macrocycle based agents have recently been patented for use in

extracting heavy metals for wastewater remediation [49-50]. Heavy metal extraction agents could be further improved by using structures which minimize the solubility in an aqueous environment and yet are able to efficiently extract the desired metal ion from the wastewater. For use in acidic, alkaline, and/or flowing systems, a rugged linkage to a stationary phase is desirable for the extracting agent. Some thiacrown ether structures have been shown to be resistant to the corrosive effects of acidic conditions [11,12,51,52]. The addition of an aliphatic cage structure to thiacrown ethers, such as with those in the present work, has resulted in several macrocycles that are insoluble in protic solvents such as water and methanol.

In the present study, ESI-MS is used to evaluate the metal binding selectivities of three commercially available thiacrown ethers (**1**-**3** in Figure 5.1) and an array of novel thiacrown ethers (**4**-**16** in Figure 5.1) for mercury(II), lead(II), cadmium(II), and zinc(II) ions. The depicted attachment of one or more cage groups to macrocycles of different ring sizes and various combinations of heteroatoms including sulfur, oxygen, and nitrogen, allows for versatile tuning of the macrocycle's metal binding cavity and extraction properties. The cage group also provides a remote site for covalent lariat group attachment, which minimizes the alteration of binding properties yet allows incorporation into a polymer for creating resins. It is, in fact, observed in this study that the type of heteroatom (S,

Figure 5.1 Thia-crown ether macrocycle structures.

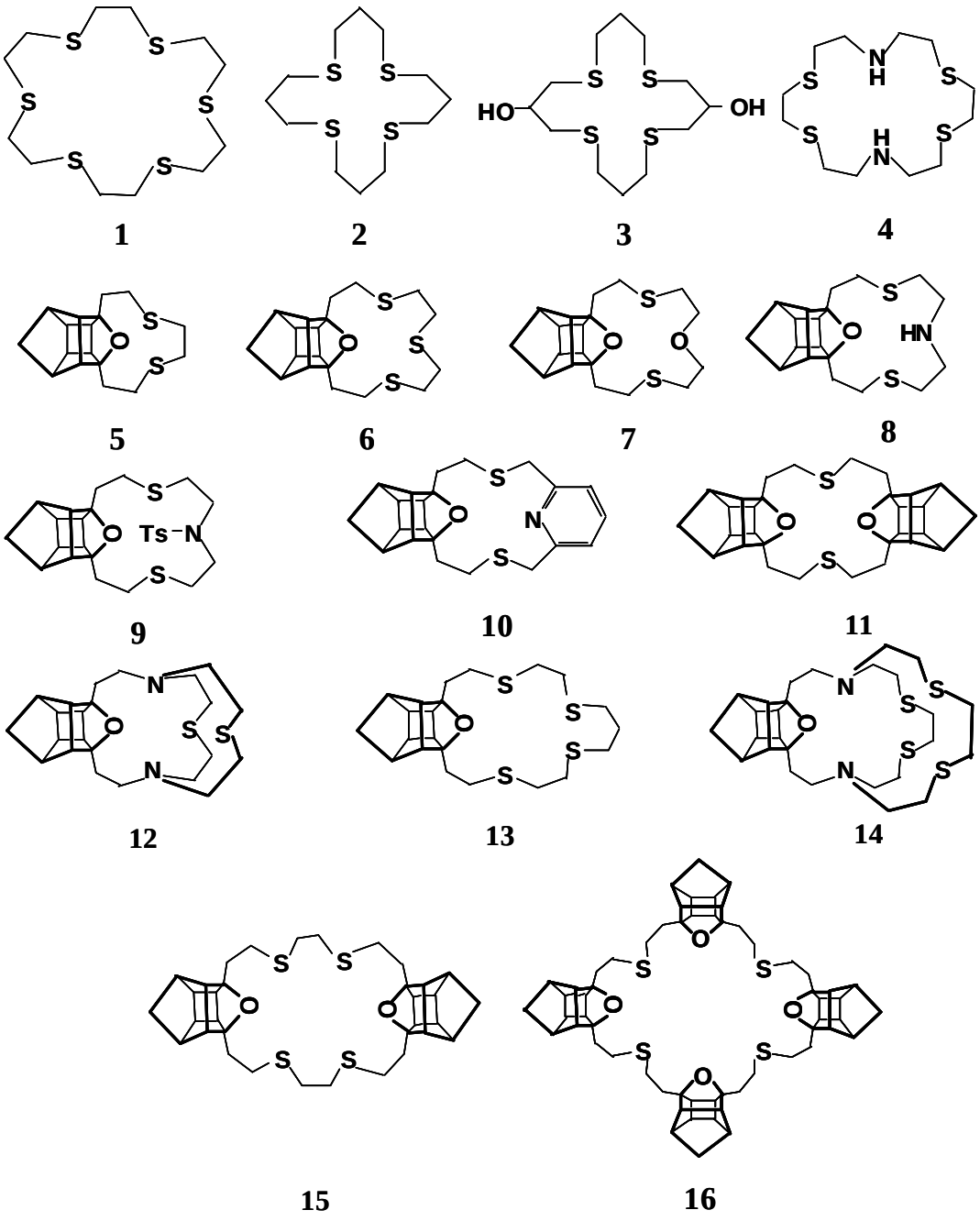

O, N), cavity size, and presence of other substituents influence the metal selectivities.

The dual site of carbon-carbon attachment to the thiacrown ether ring and the completely hydrocarbon nature of the cage provide for a rugged, hydrolysis-resistant linkage for potential incorporation into polymers. For this reason, several of these water-insoluble macrocycles that exhibited superior affinity for the heavy metal ions and a high selectivity for mercury in our initial binding assays have been tested for their ability to selectively extract mercury(II) in the presence of other metal ions including lead(II), cadmium(II), zinc(II), copper(II), alkali, and alkaline earth ions from an aqueous environment into an organic environment. These extraction experiments will serve as an initial evaluation of the capabilities of the thiacrown ethers studied herein for the removal of mercury ion from an aqueous environment. Variations in the size, combinations of heteroatoms, and number of attached cage groups resulted in large differences in the complexation measured by ESI-MS which can be semi-quantitatively correlated with the macrocycle's avidity for mercury(II) ion.

5.2 Experimental

All mass spectrometry experiments were performed on a ThermoQuest LCQ Duo quadrupole ion trap mass spectrometer (ThermoFinnigan, San Jose, CA) operated in the ESI mode with a needle voltage of 5.0 kV, a heated-capillary

temperature of 150°C, and sheath flow nitrogen gas set at 25 arbitrary units. The Harvard syringe pump system (Harvard Apparatus Inc., Holliston, MA) was operated at a flow rate of 10 μl/min for all experiments except the low metal ion concentration experiments where a flow rate of 60 μl/min was used. Lens voltages were set for all experiments by using a tune file created by auto-tuning the LCQ on the $[\mathbf{1} + Cd + ClO_4]^+$ signal with a solution containing 2.5 x 10^{-5} M of the macrocycle and each guest metal ion in 50% methanol/50% chloroform. Occasional retuning for other complexes showed little variation in spectral quality or intensity of any of the peaks compared to the aforementioned tuning method. The vacuum chamber was operated at a nominal pressure of 1 x 10^{-5} torr with He. Spectra used for this report are an average of 600 scans. All metals salts used for these experiments were purchased from Aldrich Chemical Co. (Milwaukee, Wisconsin) and used without further purification. HPLC-grade OmniSolv methanol and chloroform were purchased from EM Science (Gibbstown, NJ). The water used for these experiments was high purity (18MΩ) that had been purified on-site.

For the screening of metal cations binding to thia-crown ethers, solutions containing a single macrocycle with multiple metal ions in 50% methanol/50% chloroform were analyzed. Concentrations of macrocycle and each metal perchlorate were 2.5 x 10^{-5} M. Metal salts added to the solution were perchlorate salts of cadmium(II), lead(II), mercury(II), and zinc(II). For evaluation of spray efficiencies, the correlations between signal intensities of the complexes and their

concentrations were estimated using perchlorate salts of cadmium(II), lead(II), and zinc(II) at a five-fold excess, and of mercury(II) at five- and two-fold excesses and equivalent concentrations, relative to thiacrown ethers **7** and **13** . Each of the metal perchlorates were mixed individually with each of **7** and **13** (separately) in 50/50 chloroform/methanol solvent systems. Because the binding constants for similar macrocycles with heavy metals in methanol are greater than 10^3 and are likely an order of magnitude greater in 50/50 methanol/chloroform, over eighty percent of the thiacrown is assumed to be bound. In fact, ions due to complexes other than $(\text{macrocycle} + \text{Hg} + \text{ClO}_4)^+$ were minor or unobserved with the excesses of metal perchlorate versus macrocycle used for spray efficiency comparisons.

For initial extraction experiments, the aqueous phase contained 0.25 M cadmium(II) chloride, mercury(II) chloride, lead chloride, and zinc(II) chloride and the organic phase contained 2.0×10^{-4} M of one macrocycle in chloroform. For this type of experiment, 1.5 ml of the aqueous phase solution and 1.5 ml of the organic phase solution were combined in a vial, vortexed for 4 minutes, and allowed to settle for 5 minutes. A 1.0 ml portion of the organic phase was then aspirated into a separate vial with an autopipetter for ESI-MS analysis. In order to estimate the spray efficiencies of the different $(\text{macrocycle} + \text{Hg} + \text{Cl})^+$ complexes observed in the spectra for the extraction experiments, homogeneous solutions of mercury(II) chloride at various concentration ratios relative to each of several thiacrown ethers in solvent systems of 50/50, 80/20, and 90/10 chloroform/methanol were

investigated. (Since neither mercury chloride nor mercury perchlorate are soluble above very low micromolar concentrations in 99+% pure chloroform, the chloroform/methanol mixtures were used). Signal intensities for (macrocycle + Hg + Cl)$^{+}$ complexes were determined similar to those for the perchlorates with thiacrown ethers in 50/50 chloroform/ methanol solvent systems.

For all other extraction experiments the same method was used except for variations in the metal salts and macrocycles and their concentrations. For the competitive extraction assay for various macrocycles towards mercury(II) chloride, 1 x 10^{-4} M mercury(II) chloride in the aqueous phase and 2 x 10^{-4} M each of **6**, **7**, **13**, **15**, and **16** were used, and the mass spectra signals of each complex in the chloroform were compared. For experiments involving the effects of competing alkali and alkaline earth metal chlorides, compounds **6** or **16** were used for all experiments at a concentration of 1.0 x 10^{-4} M, the concentration of mercury(II) chloride was 0.010 M and 1.0 x 10^{-4} M for the 100:100:1 and 100:1:1 competing-ion:metal-ion:macrocycle concentration ratio, respectively, and the competing metal chloride was 0.010 M except in the set of experiments where sodium chloride concentration was varied. For the effects of copper salts on mercury ion extraction, compounds **7** and **16** were used at 1.0 x 10^{-4} M, the mercury(II) chloride concentration was 1.0 x 10^{-3} M, and the copper(II) chloride concentration was varied. For the counter-ion selectivity experiments, two solutions were used. For the first solution, 7 x 10^{-5} M of each mercury salt was mixed with 5 x 10^{-5} M of **16**.

For the second solution, 2.5 x 10^{-3} M of mercury(II) perchlorate and mercury(II) acetate were mixed with 1 x 10^{-4} M of **16**. Experiments conducted for the purpose of detecting the extraction of low metal ion concentrations used both a 1:1 **15**:mercury(II) chloride molar ratio with mercury ion concentration varying from 1.0 x 10^{-4} M to 1.0 x 10^{-5} M and a mixture with a fixed 2 x 10^{-4} M concentration of **16** in chloroform and an aqueous mercury(II) chloride concentration from 1 x 10^{-4} M to 3 x 10^{-6} M. Experiments performed to determine the effects of alkali and alkaline earth metal ions on mercury ion complexation with the thiacrown ether macrocycles in 50/50 methanol/chloroform solution used equimolar 2.5 x 10^{-5} M concentrations of one or more alkali or alkaline earth metal perchlorates, mercury perchlorate, and **6** or **16**.

.

5.3 Results and Discussion

In order to assess the metal selectivities of the macrocycles shown in Figure 5.1, a variety of ESI-MS experiments were undertaken. First, the approximate binding selectivities of the macrocycles were screened based on ESI-MS analysis of methanol/chloroform solutions containing each macrocycle and an array of metals. Then, an extensive series of extraction experiments was undertaken in which the ten most promising macrocycles were dissolved in chloroform and used to extract metals from an aqueous solution. For these experiments, the chloroform phase was analyzed by ESI-MS. Counter-ion effects and competitive binding from

non-heavy metals, including alkali, alkaline earth, and copper metal salts, were examined. In addition to these comparisons of binding selectivities involving different metals and ligands, the spray efficiencies for the various complexes were measured.

In order to estimate the spray efficiencies of complexes containing different ligands or different metals, the signal intensities of (macrocycle + metal(II) + anion)$^+$ complexes in solution were estimated by adding an excess of metal salt to solutions containing one of the thiacrown ether macrocycles. For each 50/50 methanol/chloroform solution containing one metal perchlorate and one thiacrown ether, the signal intensities of the complexes were tallied based on summing the isotopes of the expected complexes. An example is shown in Figure 5.2, in which the spray efficiencies for complexes containing **13** and different metals (Figure 5.2A) and for complexes containing Hg and different macrocycles (Figure 5.2B) are compared. For example, the relative intensities for the complexes involving **13** were (normalized to 100%) 49% for zinc, 73% for Cd, 100% for Pb, and 87% for Hg. The analogous values for the complexes involving **7** were 56% for zinc, 58% for Cd, 100% for Pb, and 40% for Hg. Thus, the [macrocycle + metal(II) ion + ClO_4]$^+$ signal intensities for each solution containing a different metal but the same macrocycle typically varied by up to a factor of two. This means that when comparing solutions containing the same ligand with different metals, the observed

Figure 5.2 Relative spray efficiencies for (A) (Macrocycle + metal + ClO_4)$^+$ in 50/50 chloroform/ methanol solutions containing 2.5 x 10^{-5} M macrocycle and 1.25 x 10^{-4} M $HgCl_2$, (B) (Macrocycle + Hg + Cl)$^+$ in 80/20 chloroform/ methanol solutions containing 2 x 10^{-5} M macrocycle and 2.25 x 10^{-5} M $HgCl_2$.

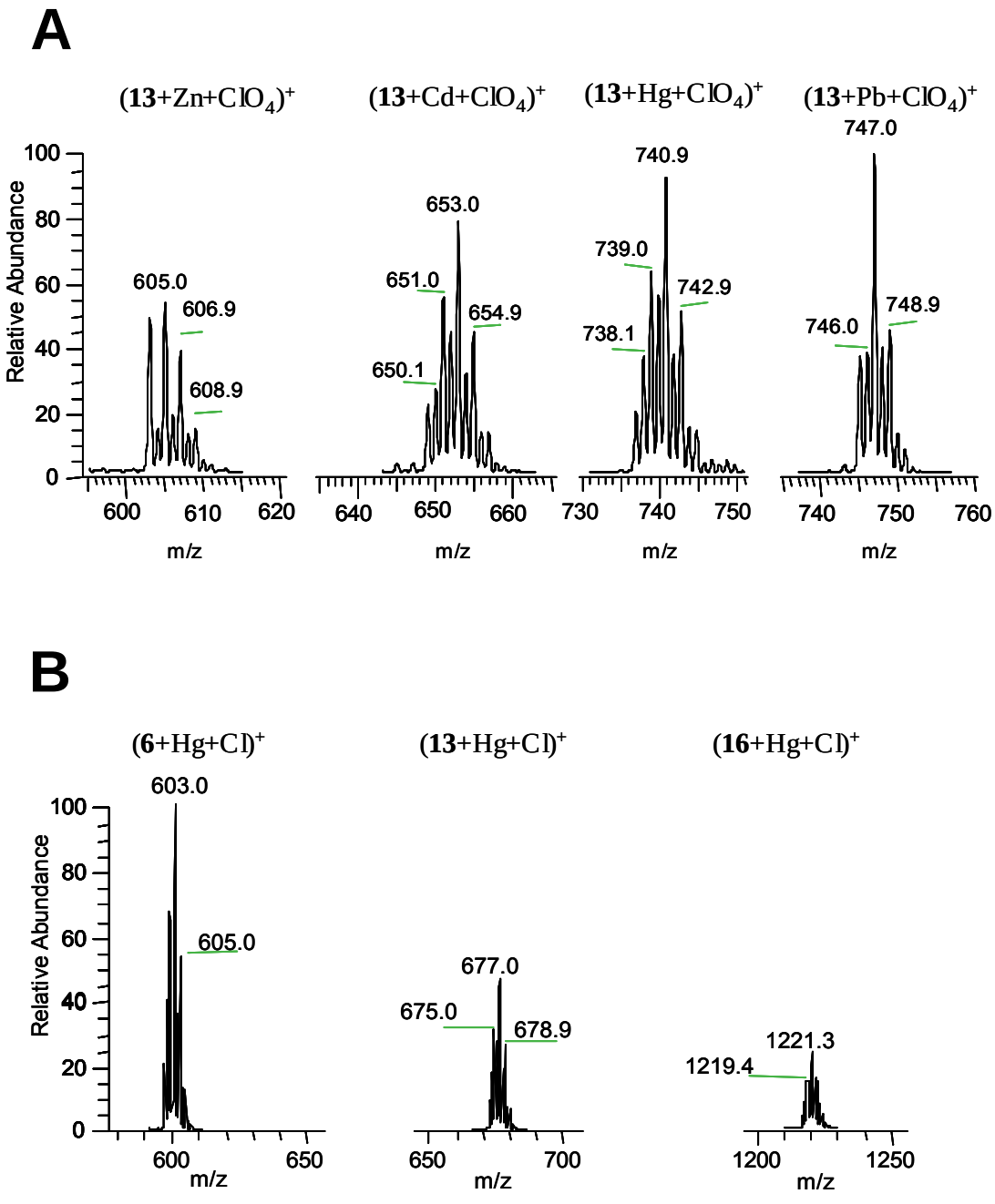

intensities for the complexes are influenced by the relative spray efficiencies; in this case resulting in a scaling factor of up to two. Similar measurements of ESI spray efficiencies were undertaken for the extraction experiments. To simulate the extraction experiments which involved analysis of only the chloroform phase after extraction of an aqueous solution with a macrcocycle-containing chloroform solution, a solvent system of 80/20 chloroform/methanol was chosen in order to approximate the chloroform phase while maintaining the solubility of mercury chloride concentrations in the tens of micromolar level. Again, one metal salt, mercury chloride, was added in excess to a solution of one thiacrown ether, and the intensities of all the isotope peaks for a given complex were tallied in the ESI mass spectra. $HgCl_2$:macrocycle concentration ratios of 9:1 for **6**, **7**, **13**, **15**, and **16**, and a series of $HgCl_2$:macrocycle concentration ratios from 4.5:1 to 1.13:1 for **6**, **13**, and **16** were used to survey the spray efficiencies. For example, the relative intensities for the complexes involving Hg were (normalized to 100%) 100% for **6**, 46% for **13**, and 26% for **16** (data shown in Figure 5.2B). Based on these experiments, the variation in spray efficiencies among the complexes differed by up to a factor of four. This means that when comparing solutions containing the same metal with different macrocycles, the observed intensities for the complexes are influenced by the relative spray efficiencies; in this case resulting in a scaling factor of up to four.

5.3.1 Macrocycle/Heavy Metal Complexation in 50/50 Methanol/ Chloroform

The thiacrown ether macrocycles were found to be insoluble in pure methanol or water at micromolar or higher concentrations, thus making them good candidates for water insoluble wastewater remediation agents. Micromolar levels of both the macrocycle and salts of cadmium, lead, mercury, and zinc (which are insoluble in chloroform) can be easily dissolved in a homogenous 50/50 methanol/chloroform solvent solution. This approach can be used to semi-quantitatively determine the relative affinities of these metals for the various macrocycles without the added complexities of extraction and proton donation from water. Solutions containing each macrocycle and equimolar concentrations of cadmium, lead, zinc, and with or without mercury were analyzed.

As presented in Figure 5.3, the ESI-mass spectra for the solutions containing a macrocycle and the metal perchlorates in 50/50 methanol/chloroform typically consist of dominant signals for singly charged tertiary complexes including a macrocycle, a metal ion and single counter-ion, (macrocycle + metal + $ClO_4)^+$, as well as complexes of a macrocycle and a doubly-charged metal ion, (macrocycle + metal)$^{2+}$, which are occasionally dominant. Lower intensity signals due to higher order complexes containing two macrocycles are often seen as well. The results for the spectra of each of the solutions containing one macrocycle with three metal salts (cadmium, lead and zinc) or four metal salts (cadmium, lead, zinc,

Figure 5.3 ESI-MS of **16** with metals in 50/50 methanol/chloroform solution (L = **16**). (A) **16** with $Cd(ClO_4)_2$, $Pb(ClO_4)_2$, and $Zn(ClO_4)_2$ (1:1:1:1). (B) **16** with $Cd(ClO_4)_2$, $Hg(ClO_4)_2$, and $Zn(ClO_4)_2$ (1:1:1:1).

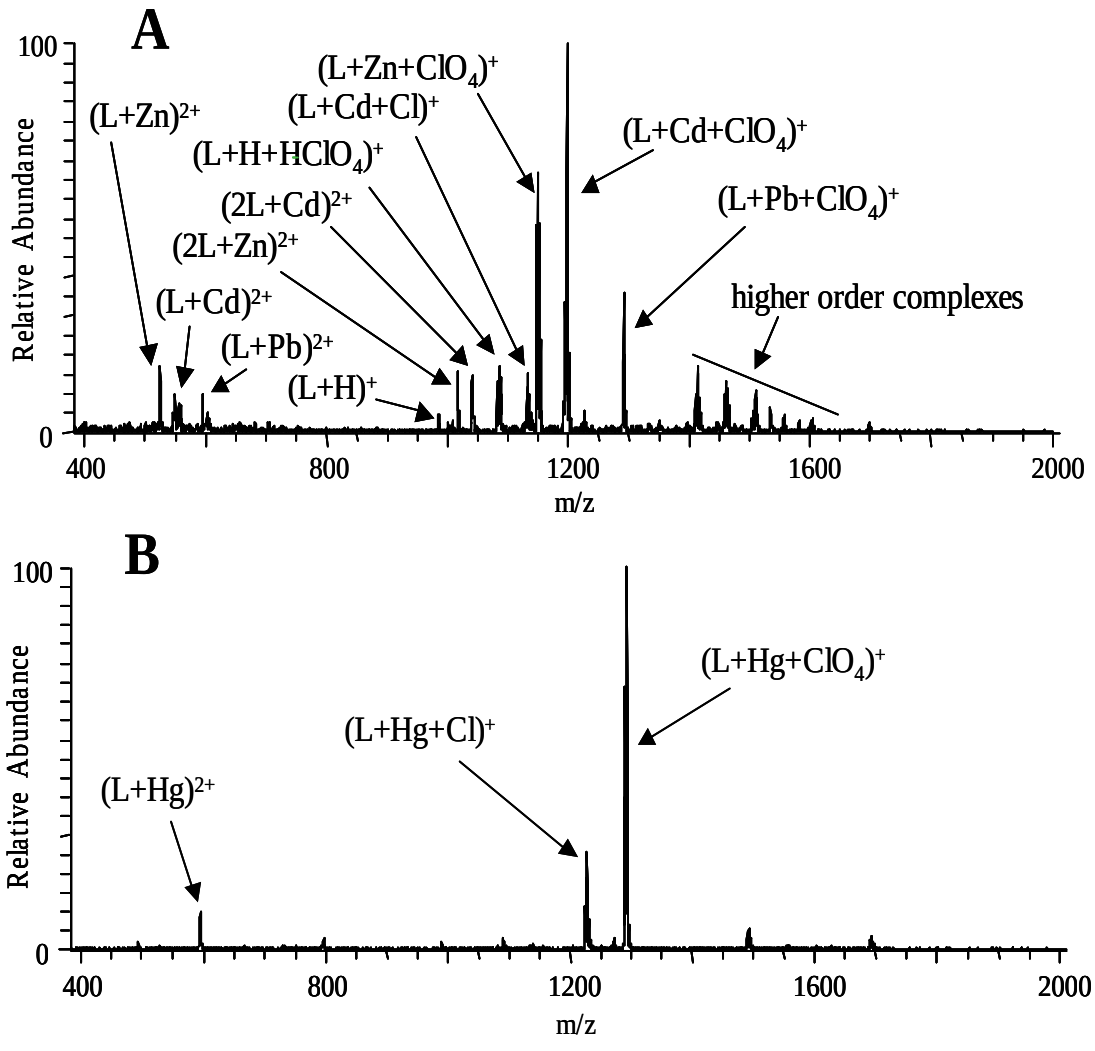

and mercury) are compared in Table 5.1. These selectivity comparisons are semi-quantitative, which is reasonable given the similarities of spray efficiencies for the thiacrown complexes with different heavy metals. With this understanding, the quality of the spectra was determined based on (i) the signal-to-noise of the dominant (macrocycle + metal + ClO_4)$^+$ complex using ionization times which optimize intensity without detrimental space charging effects and (ii) whether or not the noise and/or interference peaks present were large enough in intensity or m/z value to interfere with the detection and identification of species present. The spectrum quality is assessed in Table 5.1 to indicate the level of signal-to-noise of the complexes (i.e. excellent: S/N > 100, very good: S/N > 50 and few background ions, good: S/N > 50 with other background ions of significant intensity, fair: S/N up to 25, poor: low S/N and many background ions.)

Signal intensities in Table 5.1 were determined by summing all of the intensities of the isotope peaks for the (macrocycle + metal ion + ClO_4)$^+$ ions for each metal. Based on the relative spray efficiencies determined for the complexes of the different metal ions, the “greater than” symbol (>) indicates a signal intensity difference of greater than two-fold, and the “much greater than” symbol (>>) indicates a signal difference of greater than five-fold relative to the other ions in the series. The relative signal intensities for fortuitous species, such as cationic sodium, copper, and hydrogen ions, are included in Table 5.1 even though their

Table 5.1 Relative selectivities of sulfur containing macrocycles for metal ions in 50/50 methanol/chlororoform

Macrocycle	$Cd(ClO_4)_2$, $Pb(ClO_4)_2$, and $Zn(ClO_4)_2$ Added to Solution of Macrocycle			$Cd(ClO_4)_2$, $Hg(ClO_4)_2$, $Zn(ClO_4)_2$, and $Pb(ClO_4)_2$[a] Added to Solution of Macrocycle		
	Spectrum Quality	Dominant Complex Intensity[b]	Complexes Observed[c]	Spectrum Quality	Dominant Complex Intensity[b]	Complexes Observed[c]
1	fair	5.0E7	Cd,Pb,Zn>Cu>>Na^e,H^e	poor[f]	—	none
2	fair	1.0E8	Zn>Cd,Pb>Cu>>Na^e,H^e	good	6.4E7	Hg>Cd,Zn,Cu>>Na^e,H^e
3	fair	5.3E7	Cd,Pb,Zn>>Cu^e,Na^e,H^e	fair	3.9E7	Hg>>Zn,Cd>>Na^e,H^e
4	good	3.7E7	Cd>>Pb,Zn,H>>Cu^e,Na^e	good	3.0E7	Hg>>H>>Cd^e,Zn^e,Cu^e,Na^e
5	good	4.6E7	Na>>Cd,Pb,Zn,Cu>>H^e	fair	6.0E7	Hg>>Cd, Zn,Cu>>Na^e, H^e
6	very good	3.8E7	Zn>Cd>Pb>Cu>H>> Na^e	good	6.1E7	Hg>Cd,Zn>Cu>H>>Na^e
7	good	1.3E8	Cd,Pb,Zn>>Na>Cu,H	very good	3.9E8	Hg>> all others[e]
8	excellent	5.7E7	H>>all others	very good	1.9E7	H>Hg>>Cd^e,Zn^e,Cu^e,Na^e
9	very good	2.4E8	Cd,Pb,Zn>>Na,H>Cu	good	3.3E6	Hg>Cd,Zn>Cu,H>>Na^e
10	very good	1.2E8	H>Cd,Pb,Cu>>Zn^e,Na^e	good	4.5E8	Hg>>Cd^e,Zn^e,Cu^e,Na^e,H^e
11	good	2.0E8	Cd,Zn>Pb,H>Cu,Na	very good	5.9E8	Hg>>Cd,Zn,H>>Cu^e,Na^e
12	excellent	1.2E9	H>>all others[e]	excellent	1.1E9	H>>all others[e]
13	excellent	1.9E8	Pb>Cd>Zn>Cu,H>>Na^e	good	1.4E8	Hg>Cd,Cu>Zn^e,Na^e,H^e
14	excellent	1.2E9	H>Cd>>Cu>Pb>>Zn^e,Na^e	very good	2.5E8	Hg>>Cu>>Cd^e,Zn^e,Na^e,H^e
15	very good	9.3E7	Pb, Cd,Zn>Cu>>Na^e,H^e	very good	6.8E7	Hg>>Cd,Cu>>Zn^e, Na^e,H^e
16	good	9.0E7	Cd,Pb,Zn>H>Cu>>Na^e	good	1.4E9	Hg>Zn>Cd,Cu>>Na^e,H^e

concentrations are unknown, to show the degree to which these interferences compete with the intentionally added metal ions. The signal intensities of the singly charged metal complexes in the ESI-mass spectra were used to estimate the relative binding selectivities and avidities of the macrocycles for cadmium(II), lead(II), mercury(II), and zinc ions. The results in Table 5.1 were used for the purpose of acquiring a preliminary understanding of which thiacrown ethers possessed high avidity and/or selectivity for particular heavy metal ions.

When the selectivities of the various macrocycles towards zinc, cadmium, and lead ions are compared, it is observed that several of these macrocycles show similar avidities for all three metal ions (**1**, **3**, **7**, **9**, **15**, and **16**), as in Figure 5.3A, or only small differences in selectivity (**2**, **6**, **11**, and **13**). Only **4** shows a strong preference for one of the three metal ions, showing a "much greater" selectivity towards cadmium.

Mercury(II) complexes are usually the dominant species or only species observed for the solutions containing this mercury salt, even in the presence of cadmium, lead, and zinc, as exemplified in Figure 5.3B, a result which suggests that most of the thia-crown ethers have substantial mercury ion selectivities. One macrocycle, **5**, with only two sulfur atoms and a small cavity size, appears to prefer to bind to adventitious sodium ion impurity over the much greater quantity of heavy metal ions in solution. This result suggests that the cavity of **5** is too small to permit efficient binding of any of the heavy metals.

Macrocycles **8**, **10**, **12**, and **14** greatly prefer to bind to a proton over the metal ions present, except mercury, with **8** and **12** binding only a proton to the exclusion of metal ions present in the homogenous solutions, including mercury. Presumably, these results reflect the high basicity of these macrocycles due to the two nitrogen atoms and, for the highly proton specific **8** and **12**, the small cavity size.

These initial findings in homogenous methanol/chloroform solutions were used to select candidates for extraction of metal ions from an aqueous phase into a chloroform organic phase in order to further evaluate the ability of these macrocycles as agents for extracting heavy metals from an aqueous environment. The ones giving the most intense mercury complexes include **2**, **3**, **4**, **6**, **7**, **9**, **11**, **13**, **15**, and **16**. By using these ten selected compounds, the extraction process serves as a model for wastewater extraction and also can be used to determine the selectivities of macrocycles towards heavy metal cations.

5.3.2 Extraction Analysis

5.3.2.1 Selective Mercury Ion Extraction from Aqueous Solution.

Due to the exclusive mercury selectivity of most of the thia-crown ether macrocycles, the ten macrocycles that displayed the best combination of clean spectra and high signal-to-noise ratio for the corresponding mercury complexes

were used to study mercury(II) ion extraction from aqueous solutions. Extractions that employed mercury(II) perchlorate generally were unsuccessful. The observed spectra were similar to that shown for **15** in Figure 5.4A, with the macrocycle extracting mercury with adventitious chloride ion rather than with either abundant perchlorate ion or no counterion. The appearance of the copper complex for **15** in Figure 5.4A is related to the presence of adventitious copper and is discussed later.

Extraction of mercury(II) chloride was much more successful, as shown by the spectrum for **15** in Figure 5.4B and for all the macrocycles tested in Table 5.2. The data in Table 5.2 afford a semi-quantitative summary of the extraction efficiencies of the macrocycles based on the signal intensities (all isotopes summed) per unit of ionization time (last column in Table 5.2) of the mercury complexes obtained by using identical extraction conditions and the relative spray efficiencies estimated for the different (macrocycle + Hg + Cl)$^+$ complexes. Over the range of different ionization times used, the signal intensity obtained with the ion trap scales directly with time. This linear relationship of ionization time and signal intensity was mapped for times ranging from 2 ms to 1000 ms for solutions containing 2.0 x 10^{-5} M concentrations of one macrocycle and one metal salt, and correlation coefficients of 1.0 were routinely obtained. The reasons for the more effective extraction of the chloride containing complexes relative to the perchlorate

Figure 5.4 ESI-MS of macrocycle-containing chloroform phase after extraction of aqueous phase. (A) **15** with $Cd(ClO_4)_2$, $Pb(ClO_4)_2$, $Hg(ClO_4)_2$, and $Zn(ClO_4)_2$ (1:125:125:125:125). (B) ESI-MS of macrocycle-containing chloroform phase after extraction of aqueous phase. **16** with $CdCl_2$, $PbCl_2$, $HgCl_2$, and $ZnCl_2$ (1:125:125:125:125).

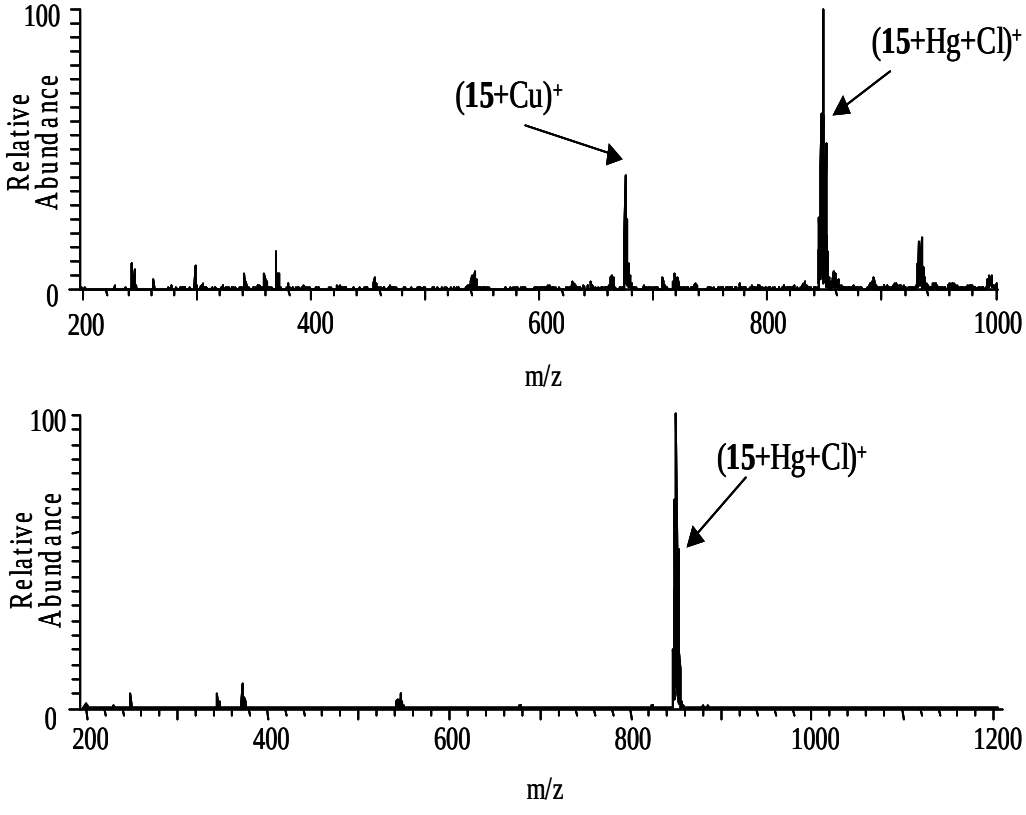

Table 5.2 Relative efficiencies of mercury(II) extraction by sulfur containing macrocycles.

Rank	Macrocycle	Identified Ions	Ionization Time (ms)	(Macrocycle + Hg + Cl)$^+$ Intensity x 1E7	Ion current per second of ionization time (IU/s) for (Macrocycle + Hg + Cl)$^+$ x 1E8
Best	**15**	$(L+Hg+Cl)^+$	0.5	9.0	1800
Good	**16**	$(L+Hg+Cl)^+$	5	18	360
	13	$(L+Hg+Cl)^+$ $(L+Cu)^+$	6	20	330
	7	$(L+Hg+Cl)^+$ $(L+Cu)^+$	10	14	140
	6	$(L+Hg+Cl)^+$	10	12	120
	2	$(L+Hg+Cl)^+$ $(L+Cu)^+$	10	5.0	50
Poor	**9**	$(L+Hg+Cl)^+$ $(L+Cu)^+$	300	7.0	2.3
	3	$(L+Hg+Cl)^+$ $(L+Cu)^+$	150	3.0	2.0
	11	$(L+Hg+Cl)^+$ $(L+Cu)^+$	300	3.0	1.0
Worst	**4**	Noise	-	-	-

$[Macrocycle]_{(o)}$:$[metal\ chlorides]_{(aq)}$ 1:125:125:125:125
Macrocycle:$CdCl_2$:$PbCl_2$:$ZnCl_2$:$HgCl_2$
Flow Rate = 10µl/min

containing complexes are discussed in detail below in the discussion of counter-ion influence on mercury extraction.

The extraction avidities of the macrocycles for mercury(II) ion appear to be a balance among the number of heteroatoms, the number of sulfur atoms, the size of the metal ion binding cavity, and the degree of flexibility of the cavity ring. Of the macrocycles tested, **15** gave the best extraction efficiency. Its superior performance is likely due to a combination of several factors. According to x-ray crystallography studies, the central cavity ring of the macrocycle must be a chain of greater than fourteen atoms for the mercury(II) ion to sit in the plane of the ring [53]. **13**, **15**, and **16** are the only macrocycles in Table 5.2 that have central cavity rings with chains of more than fourteen atoms. Since mercury (II) ion is known to form coordination numbers from 2 to 8 [54], it is likely that of these three compounds, **15** provides the best combination of interactions (four S, two O, and one Cl) and cavity fit. For **16**, the two additional oxygens may add more sites for interaction with the mercury ion, but the significantly larger cavity size and added distance between the sulfurs probably interferes with the ability of sulfurs to attain a geometry as favorable as that which can be achieved for **15**. In addition, **16** is more rigid than **15**, due to the presence of the two additional cages in **16**. **15** has a greater avidity for mercury ion than **16** does because the cavity in **16** is too large and too inflexible (due to the four cages) to permit its reduction to the more effective size of **15**.

The avidity of **13** toward mercury(II) ion is less than **15**, but not because **13** is too large or inflexible, but because it is too flexible and requires a greater loss of entropy to optimally coordinate to the mercury ion than **15**. Macrocycles **6** and **7** are very similar, and the difference in heteroatoms does not appear to make a substantial difference in their mercury ion avidities. Both **6** and **7** show a lower affinity for mercury ion than **13**, **15**, and **16** because their metal ion binding cavity is too small (fourteen atom cavity ring).

A competitive extraction assay with 1 x 10^{-4} M mercury(II) chloride in the aqueous phase and 2 x 10^{-4} M each of **6**, **7**, **13**, **15**, and **16** was used to further compare the mercury avidities of these five macrocycles which showed the greatest mercury affinities based on the previous experimental results. The mass spectral signals of each mercury complex obtained upon ESI-MS analysis of the chloroform phase were compared (data not shown). In this assay, **15** emerges as the macrocycle with the greatest mercury affinity, followed by **13** and **16**. This experiment showed a signal ratio for mercury complexes of **15** and **13** of 3:1, respectively. The competitive assay likewise indicated that **13** extracts mercury(II) chloride more competitively than **16** (signal ratio for complexes of **13** and **16** is 30:1, respectively). The signal-to-noise values for the signals of complexes of **6** and **7** in the competitive assay were too low to reasonably estimate signal ratios.

The importance of rigidity and entropy effects in the mercury ion affinities towards the macrocycles is demonstrated by the two commercial macrocycles, **2**

and **3**, which, due to the trimethylene groups between heteroatoms and the lack of any cage groups, have lower mercury ion avidities than **6**, **7**, **13**, **15**, and **16**. For **9**, the presence of the tosyl group results in steric hindrance to metal ion binding which reduces its affinity below that of other fourteen atom cavity ring macrocycles such as **6** and **7**. Too much rigidity in a macrocycle coupled with a small cavity size, such as **11**, which has a sixteen atom cavity ring and two cage groups, results in a cavity that is unable to effectively coordinate the mercury ion, unlike the less rigid **6**, **7**, and **9**. The poor performance of **4** is due to both the proton affinity of the two secondary amine groups in the ring, which allows protons to compete effectively with mercury ion for **4**, a lack of rigidity due to the absence of cage groups, and the relative lack of hydrophobic structure, which renders **4** water-soluble.

5.3.2.2 Extraction of Mercury at Micromolar Concentrations

To determine the extent to which the extraction of mercury can be monitored by mass spectrometry, the best performing macrocycles in this study, **15** and **16,** were used to determine the lower limit at which extraction of mercury from water into chloroform can be detected. In this part of the study, the two phases were vortexed for four minutes prior to ESI-MS analysis of the macrocycle-containing chloroform phase. For the (macrocycle + Hg + Cl)$^+$ ion with decreasing equimolar concentrations of mercury(II) chloride and **15** in the aqueous and organic phases,

respectively, a lower-limit-of-extraction (SNR = 3) of 1.1 x 10^{-5} M (2 ppm Hg) was determined, although efforts to optimize the limit-of-extraction were limited by the availability of the macrocycle. In an analogous experiment with **16** a fixed macrocycle concentration of 2 x 10^{-4} M was used for each extraction due to greater sample quantities. For this experiment with **16**, a lower-limit-of-extraction (SNR = 3) of 5 x 10^{-6} M (1 ppm mercury) was determined. The slopes of the log-log plots for these experiments with **15** and **16** are 2 and 1, respectively, which indicates that the extraction process is second order (the concentration of complex is proportional to the product of the mercury chloride and macrocycle concentrations) and is pseudo-first order when the macrocycle concentration is held constant. This result indicates that a significant improvement in the detection of the limit-of-extraction could be obtained by using a fixed concentration of **15** for extractions, as was done with **16**.

5.3.2.3 Counter-ion Influence on Mercury Extraction

In order to further understand the factors that influence the efficiency of mercury extraction, the effect of the counter-ion was examined. Figure 5.5A shows the ions observed from competitive complexation of **16** and mercury(II) ion with chloride, bromide, iodide, acetate, and perchlorate counter-ions after extraction of an aqueous phase containing the five mercury salts with chloroform containing **16**. Since neither the acetate not the perchlorate containing complexes could be

Figure 5.5 Competitive extraction from H_2O to $CHCl_3$ of mercury(II) ion with various counterions. (A) **16** with $Hg(ClO_4)_2$, $HgCl_2$, $HgBr_2$, HgI_2, and $Hg(CH_3COO)_2$ (1:1.4:1.4:1.4:1.4). (B) **16** with $Hg(ClO_4)_2$ and $Hg(CH_3COO)_2$ (1:25:25).

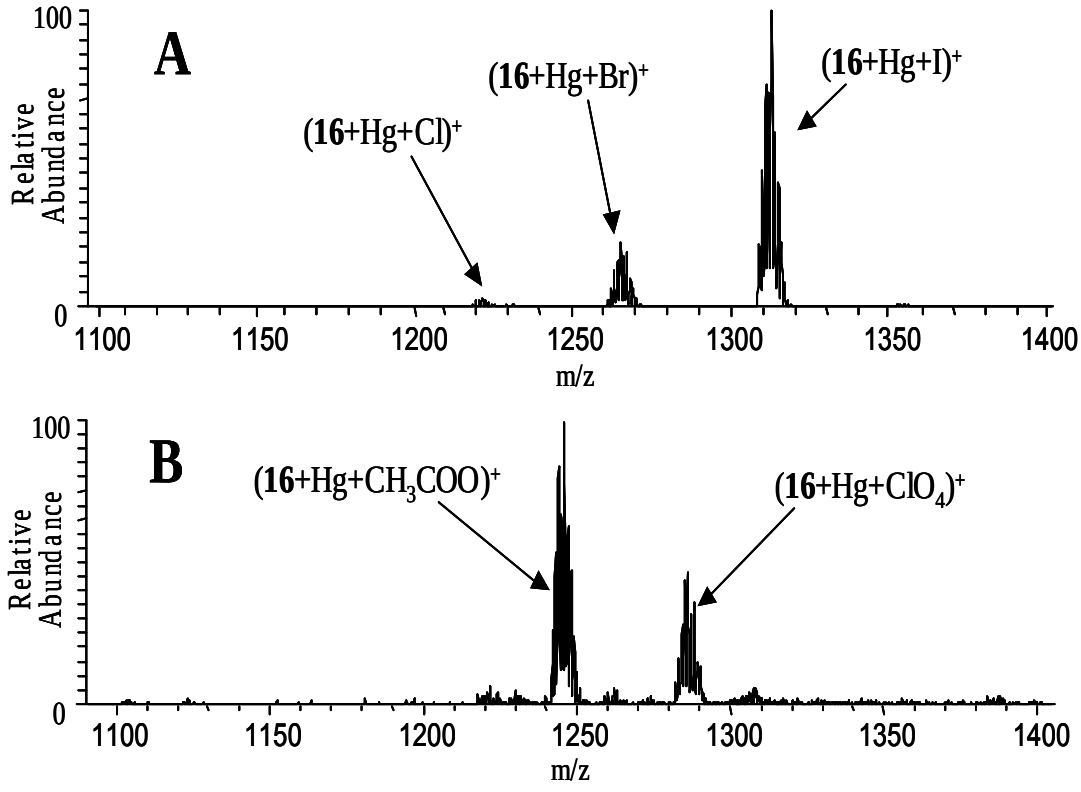

observed in Figure 5.5A, a second analogous experiment using a larger excess of only acetate and perchlorate salts was performed, with the results shown in Figure 5.5B. The observed order of counter-ion selectivity is iodide > bromide > chloride > acetate > perchlorate, most likely due to effects including counter-ion size and metal/counter-ion binding energy. The log K values for the reaction:

$$Hg^{2+}_{(aq)} + X^{-}_{(aq)} \leftrightarrow HgX^{+}_{(aq)}$$

(where X^- is the counter-ion), the solubilities of the five mercury salts tested, and the thermochemical radii of the five corresponding counter-ions are presented in Table 5.3.

With regard to counter-ion size, the polyatomic ions with branching carbon-oxygen and chloride-oxygen molecular bonds may hinder optimum interaction of mercury with the macrocycle binding cavity, accounting for the selectivity order: halides >> acetate > perchlorate. On the other hand, the larger the counter-ion, the lower its charge density, thereby rendering it more easily transferred from water to chloroform, which accounts for the selectivity order of the halides: iodide > bromide > chloride. However, the selectivity order can also be explained effectively in terms of the metal/counter-ion binding energy which affects the distribution of metal ions and metal-macrocycle complexes with two, one or no counter-ions attached, which may also influence the ability of the macrocycle to extract the metal ion into chloroform. In order to maintain charge balance, for every mercury(II) ion that is extracted into the chloroform phase by the thiacrown

Table 5.3 Solubility, association constant, and thermochemical radius data for various mercury(II) salts and their counter-ions.

Property	$Hg(ClO_4)_2$	$Hg(CH_3COO)_2$	$HgCl_2$	$HgBr_2$	HgI_2	
Solubility (g solute/100g solution)	>25[a]	20[b,e], 21[c,f], 25[d,g]	6.81[c,e], 7.30[c,e]	0.61[c,e]	0.0048[c,e], 0.0044[c,e], 0.0059[c,e], 0.01[d,e]	
log K_{rxn}[h]	<2[a,i]	5.89[j]	6.74[i]	9.00[i]	12.87[i]	
	Hg^{2+}	ClO_4^-	CH_3COO^-	Cl^-	Br^-	I^-
Thermochemical radius (pm)	112[k]	225[l]	194[l]	168[l]	190[l]	211[l]

[a] Predicted from solubility tests within our lab based and tabulated results for mercury(II) acetate and other perchlorate complexes
[b] From reference 55 [c] From reference 56 [d] From reference 57 [e] 25 °C [f] – 1.5 °C [g] 10 °C
[h] log K_{rxn} value is for the reaction: $Hg^{2+}_{(aq)} + X^-_{(aq)} \leftrightarrow HgX^+_{(aq)}$, where X^- is the counter-ion [i] 0.5 M, 25 °C, from reference 58
[j] 0.5 M, 25 °C, from reference 59 [k] From reference 60 [l] From references 61, provided uncertainty for radii of anions is $\pm$19 pm

ether, two chlorides must enter the chloroform phase as well (or, though not observed, some other negative species must be transferred to the chloroform phase or a positive species transported to the chloroform phase). Since the energy required to solvate a naked chloride anion by the chloroform would be prohibitive under the circumstances of the extraction, the chloride ions must transfer into the chloroform in very close proximity to the positive mercury ions. Therefore, it stands to reason that the counter-ions in mercury salts that have the largest mercury-anion binding energy and lowest solubilities in water will be associated with the mercury ions the most in the aqueous phase and therefore will facilitate the most mercury extraction. For the series of counter-ions: chloride, bromide, and iodide, the electronegativities decrease from chloride to iodide, resulting in differences of Pauling electronegativities of 1.16, 0.96, and 0.66, respectively, between mercury and the counter-ion. In addition, the "effective electronegativity" for the interacting oxygen in acetate ion would be expected to be greater than for chloride and the electronegativity of the interacting oxygen in perchlorate would be expected to be greater than for acetate. However, when mercury is bound to the sulfur atoms in the thiacrown ether cavities, where the mercury-sulfur electronegativity difference is about 0.58, these essentially covalent interactions will greatly decrease the covalent character of the mercury-anion bonding, making it more electrostatic in nature. Thus, in the extraction process and after the mercury-thiacrown complex is in the chloroform phase, the counter-ions will likely

maintain a weaker, more electrostatic interaction with the [macrocycle + Hg]$^{2+}$ complex as a whole, since the mercury will be well nested within the surrounding heteroatoms of the thaicrown ether cavity, especially for the larger thiacrown ethers **13**, **15**, and **16**. However, it will be much more likely for one chloride ion to maintain an inner- or outer-sphere interaction with the metal center of the thiacrown-mercury complex than for both chloride ions to participate, so that there will probably be one counter-ion with an inner- or outer- sphere interaction with the complexed mercury and another maintaining a much weaker electrostatic interaction with the [macrocycle + Hg + X]$^{+}$ complex as a whole.

The order of the solubilities and log K's for the aqueous association constants support this conclusion and, although no solubility or association constant data for mercury(II) perchlorate were found, it was determined in our laboratory that mercury(II) perchlorate is at least twice as soluble in water as mercury(II) acetate, strongly suggesting that the mercury(II) perchlorate has a significantly larger solubility and smaller association constant than mercury(II) acetate.

5.3.3.4 Interference of Group I, Group II, and Transition Metal Salts on Mercury Extraction

Competitive extraction experiments that involve group I and II metal chlorides at equimolar and 100-fold excess concentrations relative to mercury(II) chloride were undertaken with **6** and **16** in order to evaluate mercury extraction

selectivity in the presence of other common metals. For macrocycles **6** and **16**, only mercury was extracted for all of the experiments (data not shown). In order to determine whether the preference for mercury extraction stems from the larger binding constants for mercury or greater aqueous-chloroform transfer efficiency, solutions in 50/50 methanol/chloroform containing equimolar concentratons of **16,** several group I and II metal perchlorates and mercury(II) perchlorate were analyzed. Once again, the complexation of mercury(II) ion occurs to the exclusion of group I and group II metal ions (data not shown), demonstrating that binding to mercury(II) ion is greatly favored over binding to group I and II ions regardless of the solvent environment.

Although group I and II metals may not complex with the Table 5.2 macrocycles in the presence of mercury(II) chloride, it was possible that they could indirectly reduce the extraction efficiencies of the macrocycles or suppress the ESI signals when they are present in large excess relative to mercury. In order to determine if any observable interference with mercury extraction and/or detection occurs, the intensities of the (**16** + Hg +Cl)$^+$ and (**6** + Hg + Cl)$^+$ ions were monitored in separate experiments after extractions of aqueous phase containing with NaCl added at concentrations from 10- to 100-fold in excess of mercury(II) chloride. For the range 0.001 M ≤ [NaCl] ≤ 0.1 M, which includes the range of NaCl concentrations typically found in wastewater, no loss in signal is observed (data not shown). This result demonstrates that typically encountered salt

concentrations in wastewater should not significantly inhibit mercury extraction and ESI-MS detection. Similar experiments involving addition of other heavy metals instead of alkali metals showed that all of the macrocycles in Table 5.2 also show no detectable extraction avidity toward cadmium, lead, and zinc ions when these metal ions are added at the same concentration as mercury in the aqueous phase. These ions are present in much lower concentrations than group I and II metal ions in wastewater, but they have properties that are more similar to those of mercury ion. The lack of avidity shown by the macrocycles toward cadmium, lead and zinc ions further demonstrates their high level of extraction selectivity toward mercury ions.

The presence of copper complexes with some of the macrocycles in the ESI- mass spectra, due to the presence of copper impurity in the mercury(II) chloride salt or from surfaces of the ESI interface components in contact with the analyte solution, suggests that copper might interfere competitively in mercury extraction. An experiment was undertaken in order to determine the degree to which copper present in the extraction mixture interferes with mercury extraction and/or detection. The intensities of (i) (**7** + Hg + Cl)$^+$ ion, with **7** being one of the smallest macrocycles in Table 5.2 (fourteen atom ring), and (ii) (**16** + Hg +Cl)$^+$ complex, with **16** being the largest macrocycle in Table 5.2 (thirty-two atom ring), were monitored after extraction experiments that involved $HgCl_2$:$CuCl_2$ concentration ratios between 10:1 and 1:10 in the aqueous phase and **16** or **7** in

chloroform. The peak for the macrocycle/copper complex corresponds to complexation of a singly charged copper ion in which the ESI process reduces the copper from its +2 to +1 oxidation state, a phenomenon observed by other researchers in ESI experiments, and thought to occur by electron capture [62,63].

The results of these experiments are shown graphically in Figure 5.6. No appreciable change in the relative intensity of the copper complexes of either **7** or **16** with respect to the analogous (macrocycle + Hg + Cl)$^+$ complexes is seen until the $CuCl_2$:$HgCl_2$ concentration ratio exceeds 10:1. This result demonstrates that both of these macrocycles have a greater selectivity for mercury than copper. This result also indicates that when copper complexes are observed in the spectra for solutions where no copper was added, it is not due to trace copper in solution but more likely is due to contact with copper elements in the ESI interface during analysis.

5.4 Conclusions

Sulfur containing crown ether macrocycles have been shown to display potential as agents for selectively extracting and detecting aqueous mercury ion over a large concentration range. Many of the macrocycles in this study bind to mercury very selectively and efficiently in the presence of many other metal ions and have an avidity towards mercury which can be fine tuned by varying the size and combination of heteroatoms in the macrocycle ring and the number of cage

Figure 5.6 ESI-MS of macrocycle-containing chloroform phase after extraction from H_2O to $CHCl_3$. Selectivity for $CuCl_2$ versus $HgCl_2$. (A) Macrocycle **16**. (B) Macrocycle **7**.

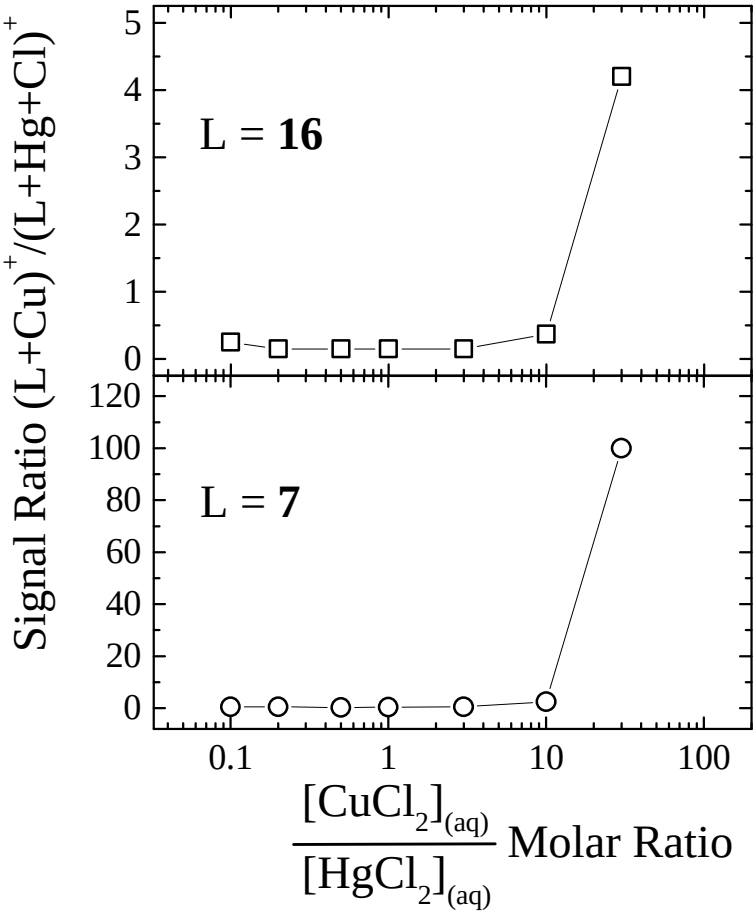

groups attached. Macrocycle cavities with several sulfurs and additional oxygens arranged to bind to mercury with a square-planar geometry appear to be most ideal. Mercury ion extraction is greatly enhanced as the hydrophilicity and the dissociation energy of the metal-anion ion pair in the aqueous medium is reduced. Lower charge density and more compact, monoatomic counter-ion structure can also reinforce extraction enhancement.

5.5 Acknowledgements

J. S. B. thanks the Welch Foundation (Grant F1155), the National Science Foundation (Grant 9820755), and the Texas Advanced Technology Program (Grant 003658-0206) for financial support of this work. A. P. M. thanks the Robert A. Welch Foundation (Grant B-0963), the Texas Advanced Technology Program (Grant 003658-0206), and the U. S. Department of Energy (Grant DE-FG07-98ER14936 for financial support in this study. Kata Mlinaric-Majerski thanks the Ministry of Science and Technology of the Republic of Croatia (Grant P-00980702) for support of this work.

5.6 References

1. Vernet, J-P., *Heavy Metals in the Environment*, Elsevier: New York, 1991.

2. Salomons, W., Forstner, U., Mader, P., Eds., *Heavy Metals: Problems and Solutions*, Springer-Verlag: New York, 1995.

3. *Innovations in Ground Water and Soil Cleanup: From Concept to Commercialization*, National Research Council, National Academy Press: Washington, DC, 1997.

4. Freeman, H. M., Ed., *Standard Handbook of Hazardous Waste Treatment and Disposal*, McGraw-Hill: New York, 1997.

5. Mogens, H., Harremoes, P., Jansen, J. L. C., Arvin, E., *Wastewater Treatment: Biological and Chemical Processes*, Springer-Verlag: New York, 1997.

6. Gros, C., Rabiet, F., Denat, F., Brandes, S., Chollet, H., Guilard, R., *J. Chem. Soc., Dalton Trans.*, **1996**, *7*, 1209-14.

7. Chollet, H., Babouhot, J-L., Barbette, F., Guilard, R., *Chelating Cation-Exchange Resins Containing Grafted Polyazacycloalkanes for Removal of Metals from Wastewater*, **2001**, Patent Appl.: PCT Int. Appl. WO 2001015806.

8. Vaidya, B., Porter, M. D., Utterback, M. D., Bartsch, R. A., *Anal. Chem.*, **1997**, *69*, 2688-2693.

9. Laney, E. E., Lee, J. H., Kim, J. S., Huang, X., Jang, Y., Hwang, H-S., Hayashita, T., Bartsch, R. A., *React. Funct. Polym.*, **1998**, *36*, 125-134.

10. Baumann, T. F., Reynolds, J. G., *Chem. Commun. (Cambridge)*, **1998**, *16*, 1637-1638.

11. Nelson, A. J., Reynolds, J. G., Baumann, T. F., Fox, G. A., *Appl. Surf. Sci.*, **2000**, *167*, 205-215.

12. Baumann, T. F.; Reynolds, J. G.; Fox, G. A., *React. Funct. Polym.*, **2000**, *44*, 111-120.

13. Zong, Z., Dong, S., Hu, Y., Xu, Y., Liu, W., *Eur. Polym. J.*, **1998**, *34*, 761-766.

14. Yamashita, K., Kurita, K., Ohara, K., Tamura, K., Nango, M., Tsuda, K., *React. Funct. Polym.*, **1996**, *31*, 47-55.

15. Saad, B., Sultan, S. M., Talanta, **1995**, *42*, 1349-1354.

16. Yordanov, A. T., Roundhill, D. M., *New J. Chem.*, **1996**, *20*, 447-451.

17. Blair, S., Kempen, E., Brodbelt, J. S., *J. Am. Soc. Mass Spectrom.*, **1998**, *9*,1049 - 1059.

18. Blair, S. M., Brodbelt, J. S., Reddy, G. M., Marchand, A. P, *J. Mass Spectrom.*, **1998**, *33*, 721 - 728.

19. Brodbelt, J. S., Kempen, E., Reyzer, M., *Structural Chemistry*, **1999**, *10*, 213-220.

20. Goolsby, B. J.; Brodbelt, J. S.; Adou, E.; Blanda, M., *Int. J. Mass Spectrom.*, **1999**, *193*, 197-204..

21. Kempen, E. C., Brodbelt, J. S., Bartsch, R. A., Jang, Y., Kim, J. S., *Anal. Chem.*, **1999**, *71*, 5493-5500.

22. Blanda, M. T., Farmer, D. B., Brodbelt, J. S., Goolsby, B., *J. Am. Chem. Soc.*, **2000**, *122*, 1486-1491.

23. Blair, S. M., Brodbelt, J. S., Marchand, A. P., Kumar, K. A., Chong, H-S., *Anal. Chem.*, **2000**, *72*, 2433-2445.

24. Kempen, E., Brodbelt, J., *Anal. Chem.*, **2000**, *72*, 5411-5416.

25. Blair, S., Brodbelt, J., Marchand, A., Chong, H-S., Alidhodzic, S., *J. Am. Soc. Mass Spectrom.*, **2000**, *11*, 884-891.

26. Reyzer, M. L., Brodbelt, J. S., Marchand, A. P., Chen, Z., Huang, Z., Namboothiri, I. N. N., *Int. J. Mass Spectrom.*, **2001**, *204*,133-142.

27. Kempen, E. C., Brodbelt, J. S., Bartsch, R., Blanda, M. T., Farmer, D. B., *Anal. Chem.*, **2001**, *73*, 384-390.

28. Marchand, A. P., Huang, Z., Chen, Z., Hariprakasha, H., Namboothiri, I. N. N., Brodbelt, J. S., and Reyzer, M. L., accepted to *J. Heterocyclic Chem.*, June 2001.

29. Williams, S., Blair, S.M., Brodbelt, J. S., Huang, X., Bartsch, R.A., accepted to *Int. J. Mass Spectrom.*, March 2001.

30. Cheng, Z. L.; Siu, K. W. M.; Guevremont, R.; Berman, S. S., *J. Am. Soc. Mass Spectrom.*, **1992**, *3*, 281-288.

31. Guevremont, R.; Siu, K. W. M.; Le Blanc, J. C. Y.; Berman, S. S., *J. Am. Soc. Mass Spectrom.*, **1992**, *3*, 216-224.

32. Wang, G.; Cole, R. B., *Org. Mass Spectrom.*, **1994**, *29*, 419-427.

33. Chapeaurouge, A.; Bigler, L.; Shafer, A.; Bienz, S., *J. Am. Soc. Mass Spectrom.*, **1995**, *6*, 207-211.

34. Gokel, G. W.; Wang, K., *J. Org. Chem.*, **1996**, *61*, 4693-4697.

35. Leize, E.; Jaffrezic, A.; Van Dorsselaer, A., *J. Mass. Spectrom.*, **1996**, *31*, 537-544.

36. Young, D-S.; Hung, H-Y. Liu, L. K., *J. Mass. Spectrom.*, **1997**, *32*, 432-437.

37. Young, D-S.; Hung, H-Y. Liu, L. K., *Rapid Commun. Mass Spectrom.*, **1997**, *11*, 769-773.

38. Izatt, R. M., Pawlak, K., Bradshaw, J. S., *Chem. Rev.*, **1991**, *91*, 1721-2085.

39. Rodriguez, L. J., Xu, M.; Eyring, E. M.; Petrucci, S., *Pure Appl. Chem.*, **1989**, *61*,1593-1596.

40. Busch, D. H., Cairns, C., *Prog. Macrocyclic Chem., 3,* **1987**, 1-51.

41. Chakrabarti, P., *Biochemistry*, **1989**,*28*, 6081-6085.

42. Konyaeva, V. S.; Myshkin, A. E., *Russ. J. Gen. Chem.*, **1998**, 68, 630-636.

43. Konyaeva, V. S.; Myshkin, A. E., *Russ. J. Gen. Chem.*, **1998**, *68*, 637-642.

44. Konyaeva, V. S.; Myshkin, A. E., *Russ. J. Gen. Chem.*, **1998**, *68*, 643-649.

45. Zalups, R. K., *Molecular Interactions With Mercury in the Kidney, Pharmacol. Rev.*, **2000**, *52,* 113-143.

46. Wu, G., Jiang, W., Lamb, J. D., Bradshaw, J. S., Izatt, R. M., *J. Am. Chem. Soc.*, **1991**, 113, 6538-6541.

47. Merrill, D. T., Van Maltby, C., Kahmark, K., Gerhardt, M., Melcer, H., *Tappi J.*, **2001**, 84, 63.

48. de Sousa, M., Bertazzoli, R., *Anal. Chem.*, **1996**, *68*, 1258-1261.

49. Mori, A.; Takeshita, H.; Kojima, T., *Preparation of Troponoid Thiacrown Ether as Sequestering Agents for Mercury Ions*, **1993**, Patent Appl.: Jpn. Kokai Tokkyo Koho, JP 05294958.

50. Baumann, T. F.; Reynolds, J. G.; Fox, G. A., *Thiacrown Polymers for Removal of Mercury From Waste Streams*, **2000**, Patent Appl.: PCT Int. Appl., WO 2000052004.

51. Baumann, T. F.; Reynolds, J. G.; Fox, G. A., *WM 99 Proc.*, **1999**, 2225-2230.

52. Reynolds, J.G.; Baumann, T. F.; Nelson, A. J.; Fox, G. A., *Abstr. Pap. - Am. Chem. Soc. (2000), 220th IEC-086*.

53. Alcock, N. W., Herron, N., Moore, P., *J. C. S. Dalton*, **1978**, *5*, 394-399.

54. Cotton, F. A., Wilkinson, G., *Advanced Inorganic Chemistry, 5th Ed.*, Wiley-Interscience: New York, 1988, pp. 597-622.

55. Stephen, H., Stephen, T., Eds., *Solubilities of Inorganic and Organic Compounds, Vol. 1: Binary Systems, Part 1*: Pergamon Press, The Macmillan Company, New York, 1963, pp. 37-38 and 816-821.

56. Linke, W. F., Ed., *Solubilities: Inorganic and Metal-Organic Compounds, Vol. 1, 4th ed.*: D.Van Nostrand Company, Inc., Princeton, NJ, 1958, pp. 1180-1232.

57. Weast, R. C., Ed., *Handbook of Chemistry and Physics, 68th Edition*, CRC Press: Boca Raton, FL, 1987, pp. B106-B107.

58. Smith, R. M., Martell, A. E., Eds., *Critical Stability Constants, Vol. 4: Inorganic Complexes*: Plenum Press, New York, 1976, pp. 104-126.

59. Martell, A. E., Smith, R. M., Eds., *Critical Stability Constants, Vol. 3: Other Organic Ligands*: Plenum Press, New York, 1977, p. 6.

60. Dasent, W. E., *Inorganic Energetics: An Introduction*: Cambridge University Press, New York, 1982, p. 76.

61. Roobottom, H. K., Jenkins, H. D. B., Passmore, J., Glasser, L., *J. Chem. Ed.*, **1999**, *76*, 1570-1573.

62. Ginanelli, L., Amendola, V., Fabbrizzi, L., Pallavicini, P., Mellerio, G. G., *Rapid Commun. Mass Spectrom.*, **2001**, *15*, 2347-2353.

63. Lavanant, H., Virelizier, H., Hoppilliard, Y., *J. Am. Soc. Mass Spectrom.*, **1998**, *9*, 1217-1221.

CHAPTER 6

Complexation of Silver and Co-recovered Metals with Novel Aza-Crown Ether Macrocycles by Electrospray Ionization Mass Spectrometry

6.1 Introduction

For applications involving the selective recognition, detection, extraction, or removal of specific metals in complex mixtures, the design and development of macrocyclic ligands continues to evolve [1-3]. Macrocycles have been used for selective metal detection with ion selective electrodes [4] and selective metal removal of heavy metals such as silver [5,6], copper [7], and mercury [8-14] from wastewaters. Also, macrocycles have been widely developed for ion exchange and affinity resins [15-16] and may have future applications in more efficient and environmentally beneficial mining of precious and semi-precious metals such as silver, gold, copper, and nickel.

The binding properties of the ligands play critical roles in the ability to target specific metals of interest, and thus there are many strategies for designing compounds with the appropriate selectivity, such as for silver, a metal that has numerous practical uses. Several ongoing studies are investigating the

complexation properties of silver with ligands containing nitrogen, sulfur, and oxygen heteroatoms such as heterocyclic amines [17,18], calixarene derivatives and other macrocycles [19-24], thiolates [25], and unsaturated polymers [26]. Also, new ligands are being developed for aqueous extraction [27] of silver and for speciation and removal of silver from natural waters [28]. For example, one recent study has demonstrated the high selectivity of nitrogen-containing crownophane macrocycles towards silver in the presence of iron, manganese, nickel, cobalt, copper and zinc ions [23]. Another study has shown the high silver selectivity of thiolariat ethers in the presence of lead, manganese, nickel, cadmium, cobalt, copper, zinc, and alkali metal ions [29].

The determination of binding selectivities is an important step in the optimization of new metal-selective ligands, and there continues to be development of improved analytical methods for addressing this problem. Electrospray ionization mass spectrometry (ESI-MS) has been widely used to estimate binding constants, assess binding selectivities, and to determine structure/binding relationships for both an array of biological systems and for host-guest complexes involving macrocycles and cationic guests [30-52]. Electrospray ionization-mass spectrometry has been especially useful for rapid screening of binding selectivities because of both its ease of coupling with HPLC and the structural information obtainable through MS^n techniques [53-56]. In the present study, ESI-MS is used to evaluate the metal binding properties of a series of novel azacrown ethers (**1 - 6**

in Figure 6.1), along with four commercially available macrocycles as reference compounds, (**7** - **10** in Figure 6.1). The selectivities for silver(I), copper(II), gold(III), nickel(II), iron(III), manganese(II), cobalt(II), lead(II), and zinc(II) ions are evaluated, along with a comparison of the alkali metal selectivities. Silver and gold, precious metals, are typically present in ores with the base metals, manganese, nickel, copper, and iron, which occur in significant quantities but are of much lower commercial worth [57]. The selectivities of the ligands in Figure 6.1 for the co-recovered metals and ore impurity metals are evaluated based on ESI-MS analysis of solutions containing mixtures of metals. The depicted attachment of cage groups and benzyl groups to macrocycles of different ring sizes and various combinations of oxygen and nitrogen heteroatoms allows for versatile tuning of the selectivities and solubilities of the macrocycles. The cage group also provides a remote site for potential lariat group attachment, which minimizes the alteration of binding properties of the macrocycle yet allows incorporation of the ligand into a polymer for creating resins. The hydrophobicity of the cage groups and aromatic groups may also aid in reducing the solubility of the macrocyclic complexes in polar solvents so that extraction from these solvents may be more efficiently accomplished. Based on the metal selectivity results obtained in this work, macrocycles **3** and **4**, which exhibit superior affinity and selectivity for Ag^+ versus other metals in our initial binding assays, have also been tested for their ability to

Figure 6.1 Structures of ligands (molecular weight in Da).

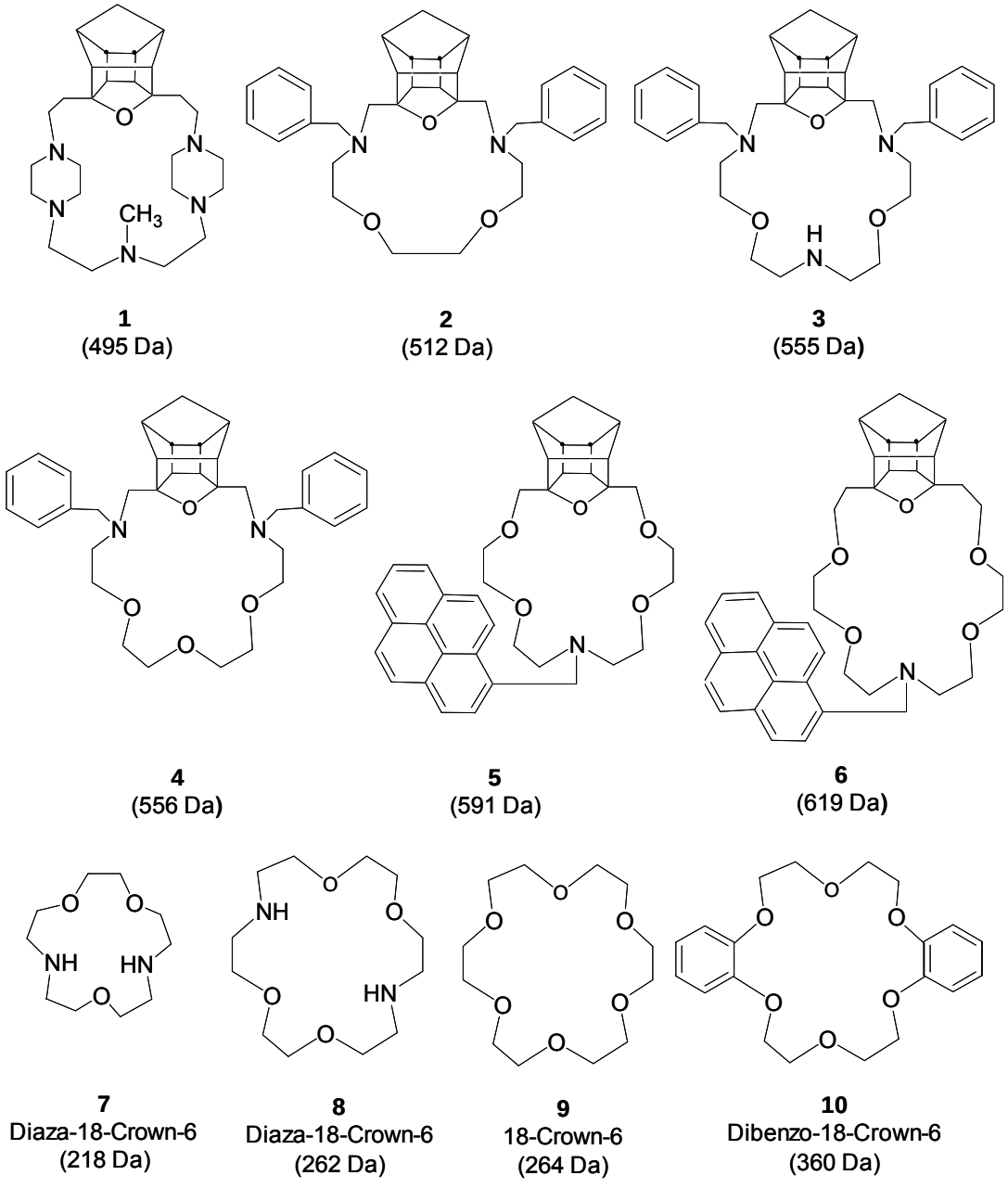

selectively extract Ag^+ from an aqueous solution into an organic phase as a model for possible future applications of the ligands in ion extraction columns.

6.2 Experimental

All experiments were performed with a Finnigan ITMS quadrupole ion trap mass spectrometer (ThermoFinnigan, San Jose, CA) equipped with an ESI source. The Harvard syringe pump (Harvard Apparatus Inc., Holliston, MA) was operated at a flow rate between 2 and 5 μl/min for all experiments, and the ESI needle voltage was 3.4 kV. A nitrogen sheath-flow gas at 5 psi was used for experiments involving multiple transition metal binding, and no sheath gas was used for the experiments involving solutions containing alkali metals ions with or without silver ions. Each spectrum was an average of 150 scans. For screening of the alkali and transition metal ion selectivities of macrocycles **1**-**10**, solutions containing a single macrocycle with multiple metal ions were analyzed. Solutions containing one part of macrocycle and three parts of each metal ion were analyzed for each ligand in pure methanol. The excess of metal ions relative to the ligands creates a more competitive binding environment for complexation with the macrocycle. Throughout the study, the concentration of each host was 5.0×10^{-5} M and concentrations of the metal ions were 1.5×10^{-4} M. These concentrations were used to ensure solubility of all salts in the solvent medium while maintaining conditions for increased selectivity. Metal salts used for these experiments were purchased

from Aldrich Chemical Co. (Milwaukee, Wisconsin), except the hydrogen tetranitratoaurate(III) which was purchased from J and J Materials Incorporated (Neptune City, New Jersey). All chemicals were used as received. The water used was 18 MO that was purified on site. Methanol was Certified A.C.S. Spectranalyzed® from Fisher. The syntheses of host molecules **1-6** have been reported elsewhere [58].

Extractions of aqueous metal ions by the host into chloroform were conducted with 5×10^{-3} M or 1×10^{-3} M of each metal salt in aqueous solution and 2×10^{-4} M macrocycle in chloroform. Approximately 1.5 mL of each of the two phases were combined in a vial, vortexed for two minutes, then allowed to equilibrate for five minutes. The organic phase was then separated from the aqueous phase by aspiration and analyzed by ESI-MS.

6.2.1 Electronic Structure Calculations

Molecular mechanics conformational searches were performed using MMFF (Merck) force fields and the lowest energy conformer was then subjected to higher level methods. *Ab initio* calculations using a Restricted Hartree-Fock model at the 6-31G* level of theory were performed for all alkali metal complexes. B3LYP/6-31G* calculations were used for complexes containing copper, silver, or zinc ions. B3LYP/6-31G** calculations were used for complexes containing gold ions. Electronic structure methods were calculated using Spartan '02 PC© software

(Wavefunction Inc., Irvine, CA) operated on a Gateway PC with an Intel Pentium 4 processor.

6.3 Results and Discussion

It was expected that the caged aza-crown ethers would show some selectivity for silver because of the known affinity of nitrogen for silver [59-60]. In addition to the six caged azacrown ethers shown in Figure 6.1, four reference compounds were chosen to assist in elucidating the importance of several factors on the metal selectivities: the nitrogen heteroatoms relative to oxygen heteroatoms, the size of the cavity, and the presence of the aromatic substituents. Diaza-15-crown-5 (**7**) is similar to **1** and **2** in cavity size and the presence of the nitrogen groups. Diaza-18-crown-6 (**8**) is similar to **3 - 6** in cavity size and presence of the nitrogen atoms. 18-Crown-6 (**9**) bears similarity to the caged aza-crown ethers in its cavity size and the presence of oxygens, yet allows the evaluation of the impact of the nitrogen atoms on the metal binding properties. Dibenzo-18-crown-6 (**10**) was selected as another reference host because it possessed two aromatic rings.

The following experimental strategy was undertaken. First, the size-selectivities of the macrocycles were estimated based on competitive complexation experiments involving alkali metal ions because the alkali metals lack d orbitals and thus represent simple charged spheres (the ionic radii for all the metal ions used in this study are tabulated in Table 6.1). Then the selectivities of the

Table 6.1 Ionic diameters.[62]

Ion	Ionic diameter (pm)
Li^+	156
Na^+	186
K^+	266
Rb^+	298
Cs^+	330
Cu^+	182
Ag^+	226
Mn^{2+}	182
Au^{3+}	182
Cu^{2+}	144
Zn^{2+}	166
Ni^{2+}	156
Pb^{2+}	264
Fe^{3+}	134
Co^{3+}/Co^{2+}	128/164

macrocycles for silver and other transition metals were evaluated, in addition to the selectivities for silver relative to alkali metals. The complexation of the transition metals were competitively tested as two separate groups to simplify analysis. Ag^{+}, Cu^{2+}, Au^{3+}, Mn^{2+}, Co^{2+}, and Zn^{2+} nitrates were mixed in one set of solutions with one macrocycle per solution, and Ag^{+}, Ni^{2+}, Fe^{3+}, and Pb^{2+} salts were mixed in a second set of solutions likewise with one macrocycle per solution. The solutions were analyzed by ESI-MS, and the intensities of the metal complexes were used to compare the relative metal binding selectivities of the ligands. Although an evaluation of the selectivities for just the various monopositive Group IB metals (Cu^{+}, Ag^{+}, Au^{+}) would be envisioned as an interesting comparative study to allow the assessment of size-dependent factors relative to electronic effects on selectivities, this was not possible due the very low solubility of Cu^{+} and Au^{+} in all but strong acid media.

When comparing intensities of ions observed in a mass spectrum, one must always consider the relative ionization efficiencies of the detected species, and this is of special concern for ESI methods where the "spray" efficiencies are known to depend on both the chemical and physical properties of the ions [61]. Thus, the relative spray efficiencies of different macrocycle/metal complexes were estimated based on spraying solutions containing a single macrocycle and a single metal and comparing the observed intensities for the different complexes. In the present study, macrocycles **3, 4** and **9** (18-crown-6) were selected as examples to illustrate

the range in spray efficiencies for the various macrocycle/transition metal complexes. Table 6.2 shows the relative signal intensities, reported as percentages based on peak areas, obtained for the metal complexes obtained from the ESI-MS analysis of 12:1 metal:macrocycle mixtures in methanol for **3, 4** and **9**. The spray efficiencies vary by ± 60% RSD from the mean of the percentages for the eight metals, excluding Co^{2+}, which showed no binding. For **3** and **4,** Cu^{2+}, Au^{3+} and Fe^{3+} showed little or no complexation, indicating that the nitrogen-containing caged macrocycles have very low affinities for these metals, and thus relative spray efficiencies could not be estimated. For the metals of greatest interest in this study (Ag^{+}, Zn^{2+}, Mn^{2+}, and Pb^{2+}), the spray efficiencies for complexes of **3** and **4** generally varied by a factor of two to six, with the Pb^{2+} complexes always having the largest spray efficiencies. In practical terms, this means that the Pb^{2+} complexes are more intense relative to the Ag^{+} complexes, all other factors being equal, and the observed intensities should be normalized by the appropriate correction factor in order to make direct quantitative comparisons of binding affinities for different metal ions.

6.3.1 Selectivity of Macrocycles towards Alkali Metals

In order to estimate the size-selectivities of the caged aza-crown ethers, ESI mass spectra were obtained for solutions containing lithium, sodium, potassium,

Table 6.2 Relative percent signal intensities[a] for transition metal complexes normalized to the most intense signal for a given macrocycle

Macrocycle	Cu^{2+}	Au^{3+}	Zn^{2+}	Ni^{2+}	Mn^{2+}	Fe^{3+}	Pb^{2+}	Ag^{+}	Co^{2+}
3	0	2	14	10	36	0	100	33	0
4	5	2	46	17	43	0	100	40	0
9	36	27	47	20	100	71	77	21	0

[a] Error is ± 30% RSD. All complexes described have a positive charge of one due to association with nitrate counter-ions.

rubidium, and cesium hydroxides with each of macrocycles **1** – **10**. Representative spectra are shown in Figure 6.2 for macrocycles **2**, **3** and **4**. The distributions of the alkali metal complexes, based on integration of the ion peak areas, for macrocycles **1** – **10** are summarized in Figure 6.3. Two of the caged macrocycles show notable alkali metal selectivities. Macrocycle **1** is strongly Li^+ selective, indicating a relatively small cavity diameter (perhaps around 160 ± 15 pm). Macrocycle **5** was found to be strongly K^+ selective, suggesting a cavity size in the range of 260 ± 20 pm. The other new macrocycles, **2, 3, 4,** and **6**, are relatively non-selective, and thus have cavities sufficiently large to accommodate K^+ or Rb^+ as well as other smaller ions. None of the macrocycles show much affinity for the large Cs^+ cation. By using the relative abundances of alkali metal complexes found in the ESI mass spectra to estimate the sizes of the cavities based on a "best fit" concept, macrocycles **2**, **3**, **4**, and **6** are suggested to have cavity diameters of about 220 ± 15 pm, 230 ± 15 pm, 240 ± 15 pm, and 290 ± 15 pm, respectively. Finally, considering the ionic diameter of the silver ion (226 pm) [62] and the concept of "best fit" based only on the ionic radii of the metals versus cavity size, silver ion would be predicted to be most suited to the cavity diameter of **2** or **3**, with a potential preference for **3** because of its slightly larger cavity. However, as will be discussed below, silver selectivity is greatest for macrocycles **4**, **5**, and **6**, presumably due to the importance of factors other than just the size-based fit of the metal with the cavity.

Figure 6.2 Alkali metal complexation of macrocycle (A) **2**, (B) **3**, and (C) **4**. Macrocycle: metal ratio is 1:3:3:3:3.

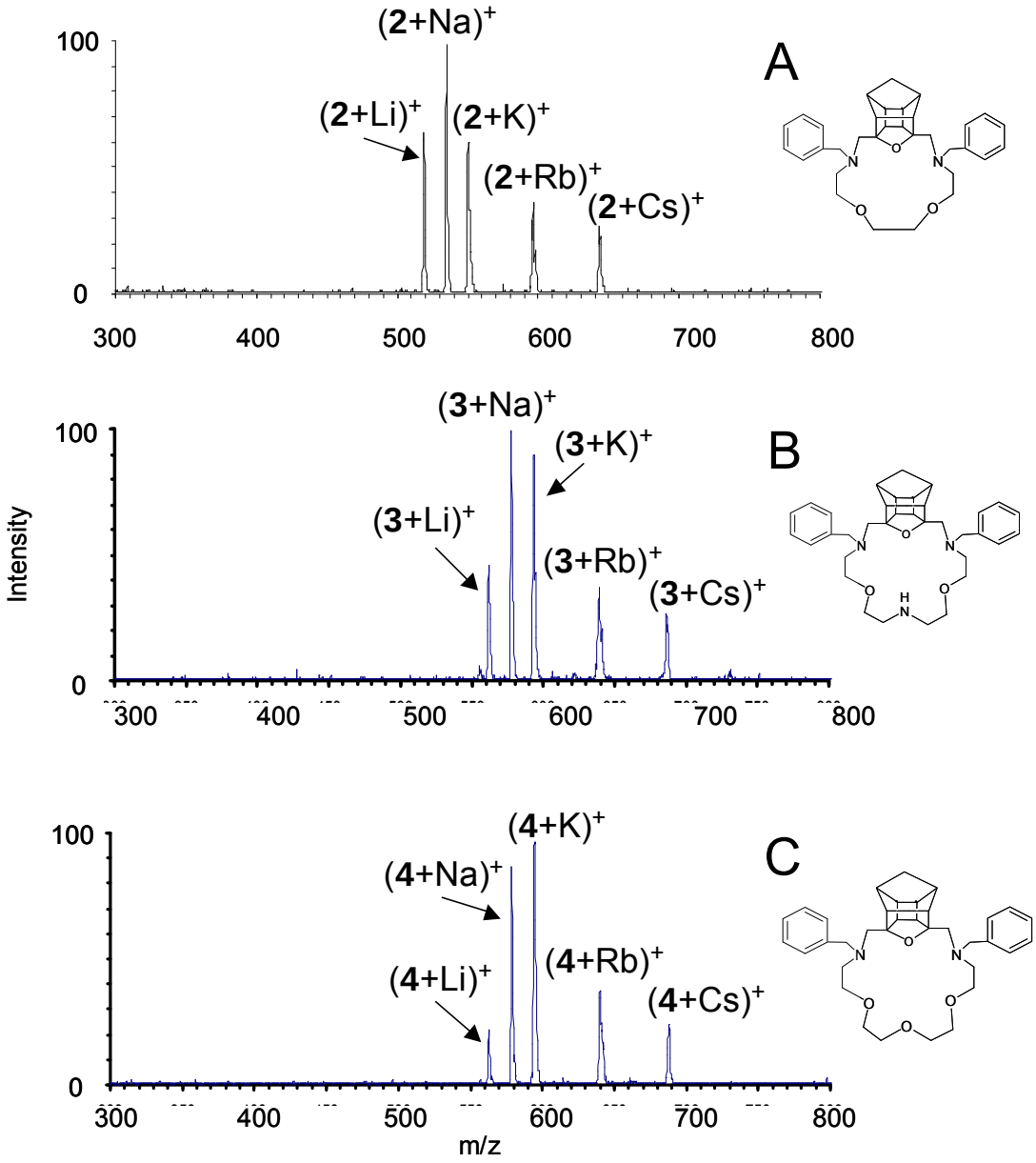

Figure 6.3 Relative distribution of alkali metal complexes for solutions containing 1:3:3:3:3:3:3 macrocycle:LiOH:NaOH:KOH:RbOH:CsOH.

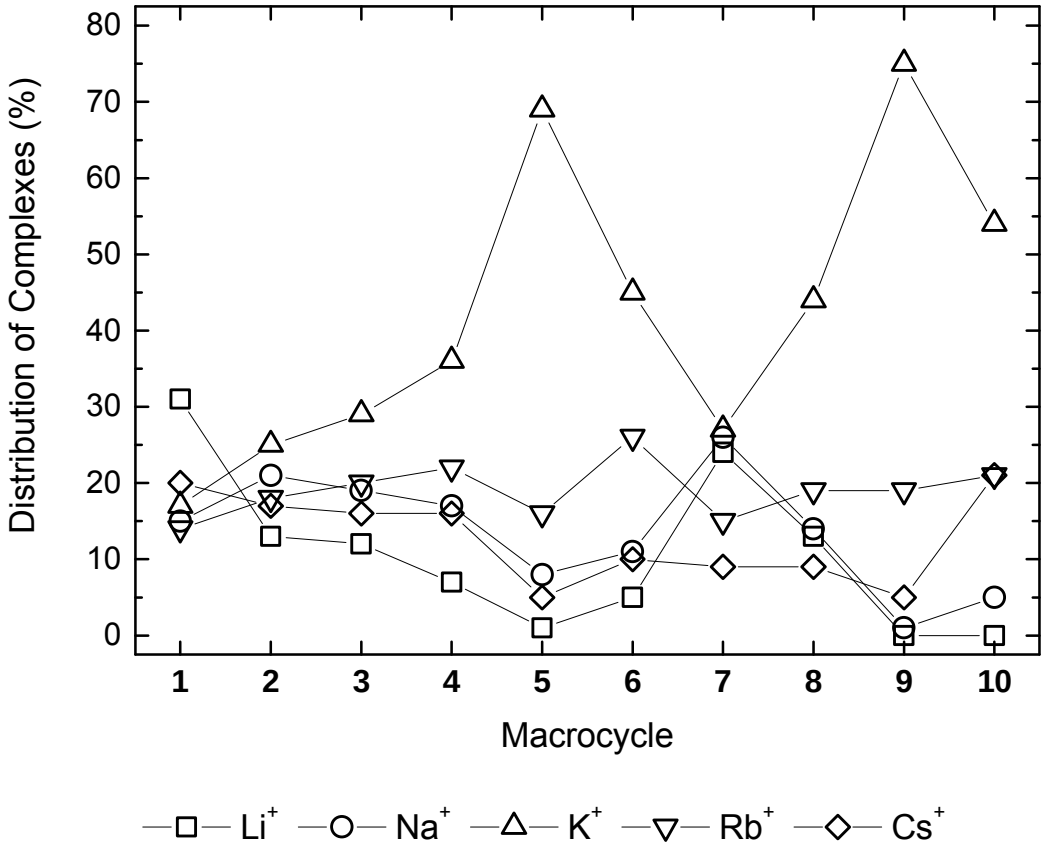

6.3.2 Selectivities of Macrocycles for Silver and Alkali Metals

To compare the selectivities of the nitrogen-containing macrocycles for Ag^+ versus other monopositive metals, namely the alkali metals, solutions containing one macrocycle with equimolar silver nitrate and the alkali metal perchlorates of lithium, sodium, potassium, and rubidium were analyzed. Figure 6.4 compares spectra for these solutions for three of the macrocycles. Nearly exclusive Ag^+ complexation was observed for **3** and **8** relative to **9**, demonstrating that nitrogen-containing macrocycles show significant selectivity towards silver versus alkali metals. In fact, virtually no alkali metal complexes were detected for **3** or **8** in the presence of Ag^+. In contrast, 18-crown-6, with a similar cavity diameter as **8**, but no nitrogen atoms, binds Na^+, K^+, and Rb^+ ions preferentially to Ag^+. Results for macrocycles **1** – **10** are summarized in Table 6.3 as the percentage of total signal area of alkali metal and Ag^+ complexes in each mass spectrum. For macrocycles **2** – **5** and **7** (diaza-18-crown-6), no signals for alkali metal complexes were observed, showing exclusive or near exclusive selectivity for Ag^+ complexation. For macrocycle **1**, small amounts of lithium and sodium complexes were observed in the presence of Ag^+. Macrocycle **1** has the smallest cavity diameter of the ten

Figure 6.4 Complexation of macrocycles with Ag^+, Li^+, Na^+, K^+, and Rb^+ in methanol for (A) macrocycle **3**, (B) **8**, and (C) **9**. The macrocycle:metal ratio is 1:3:3:3:3:3.

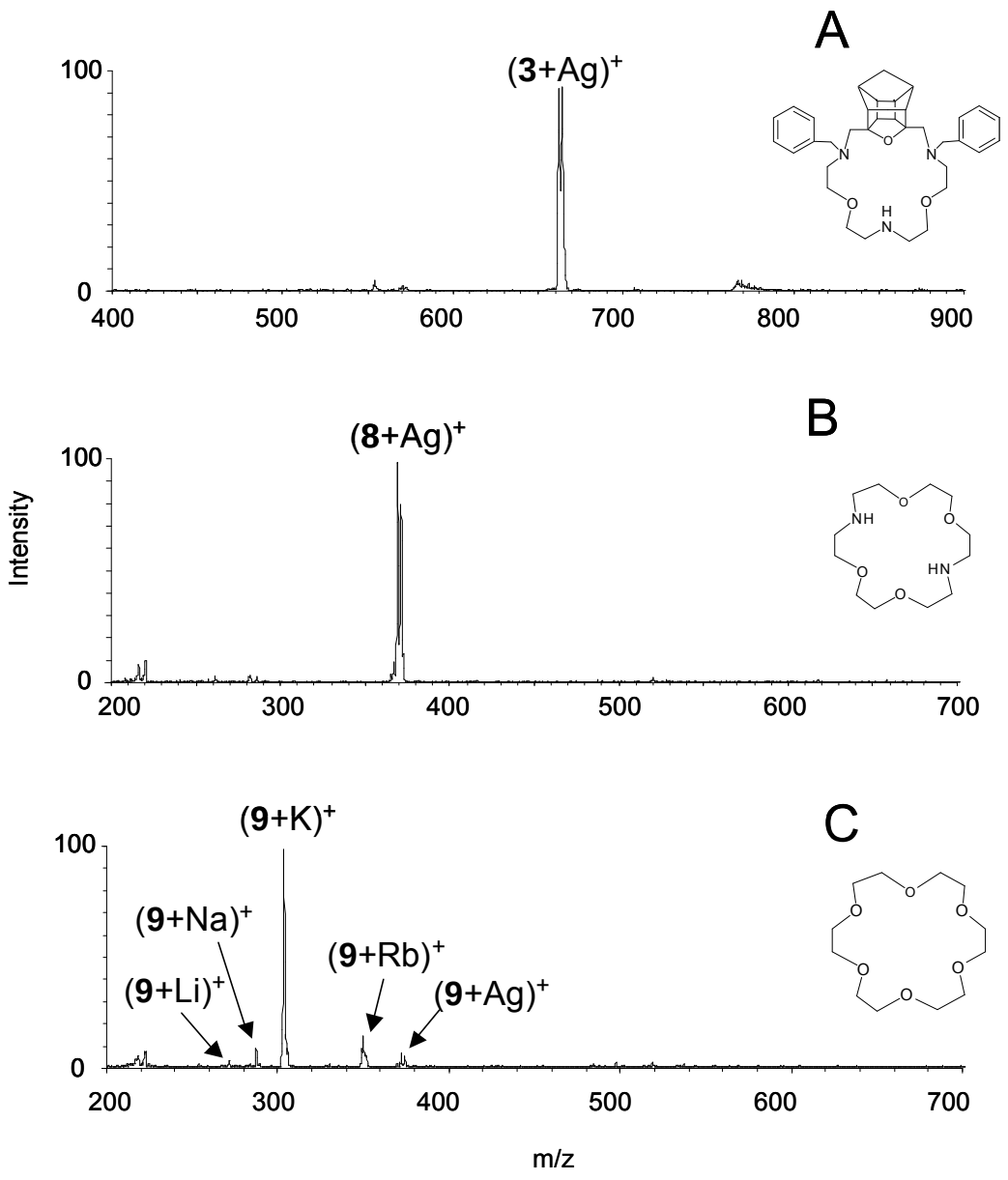

Table 6.3 Relative percentages[a] of alkali metal complexes detected compared to silver ion complexes.

Macrocycle	Metal Ion				
	Li^+	Na^+	K^+	Rb^+	Ag^+
1	4	6	0	0	90
2	0	0	0	0	100
3	0	0	0	0	100
4	0	0	0	0	100
5	0	0	0	0	100
6	0	0	1	0	99
7	0	0	0	0	100
8	0	1	0	0	99
9	1	4	81	12	2
10	2	11	59	15	13

[a] Error is $\pm$ 20% RSD.

macrocycles, and this reduces its Ag^+ affinity. For macrocycles **9** and **10**, which do not contain nitrogen heteroatoms, complexation of alkali metals, predominantly K^+ is observed over Ag^+ complexation. From these results, it is apparent that both a cavity size which can most effectively accommodate the silver ion and the presence of at least one nitrogen heteroatom are necessary for optimum silver selectivity.

6.3.3 Selectivities of Macrocycles towards Transition Metals

For evaluation of the silver selectivities of the macrocycles in the presence of other transition metals, solutions containing one macrocycle and Ag^+, Mn^{2+}, Cu^{2+}, Zn^{2+}, Co^{2+} and Au^{3+}, or one macrocycle and Ag^+, Fe^{3+}, Ni^{2+}, and Pb^{2+} were analyzed by ESI-MS. Figure 6.5 compares ESI-mass spectra for solutions containing Ag^+, Cu^{2+}, Au^{3+}, Mn^{2+}, Co^{2+}, and Zn^{2+} nitrates with either macrocycle **3**, **8**, **9**, or **10**, and Figure 6.6 compares the ESI-mass spectra for solutions of **3, 8** and **10** with Ag^+, Ni^{2+}, Fe^{3+}, and Pb^{2+} nitrates. The ESI-mass spectra typically show complexes involving a macrocycle and a singly-charged metal ion or singly charged tertiary complexes consisting of a macrocycle, a metal dication, and a single counter-ion. Because of the basic nitrogens on all the aza-crown ether macrocycles, there is also a tendency for the azacrown ethers to protonate. No complexes containing Au^{3+} were ever observed, and ones containing Cu^{2+} were never or only weakly observed. The absence of these latter metal complexes may be due to the high solvation energies relative to the complexation energies for Au^{3+}

Figure 6.5 Complexation of macrocycles with Ag^{+}, Mn^{2+}, Cu^{2+}, Zn^{2+}, and Au^{3+} in methanol for (A) macrocycle **3**, (B) **8**, (C) **9**, and (D) **10**. The macrocycle:metal ratio is 1:3:3:3:3:3.

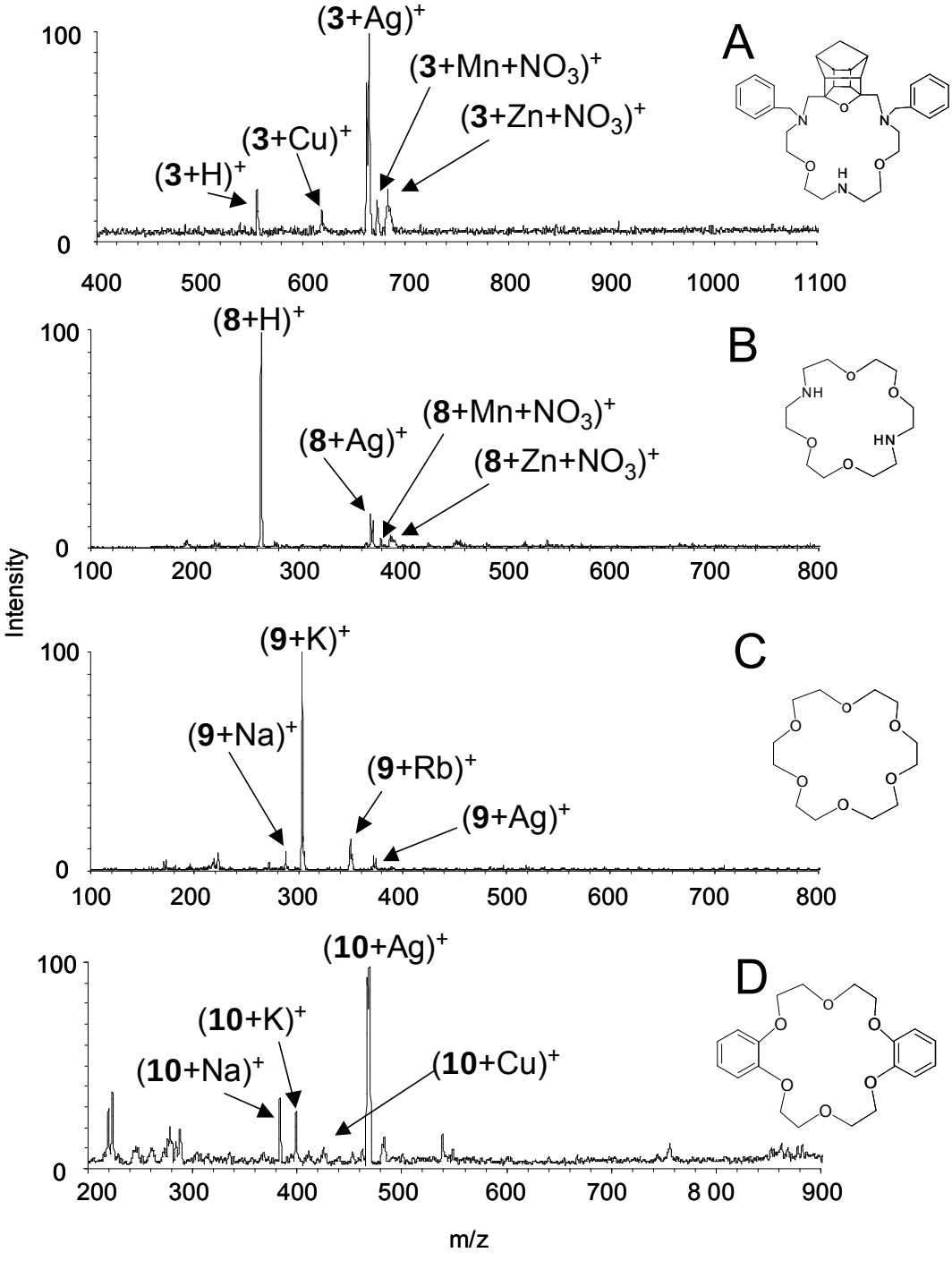

Figure 6.6 Complexation of macrocycles with Ag^{+}, Fe^{3+}, Ni^{2+}, and Pb^{2+}, in methanol for (A) macrocycle **3**, (B) **8**, and (C) **10**. The macrocycle:metal ratio is 1:3:3:3:3:3.

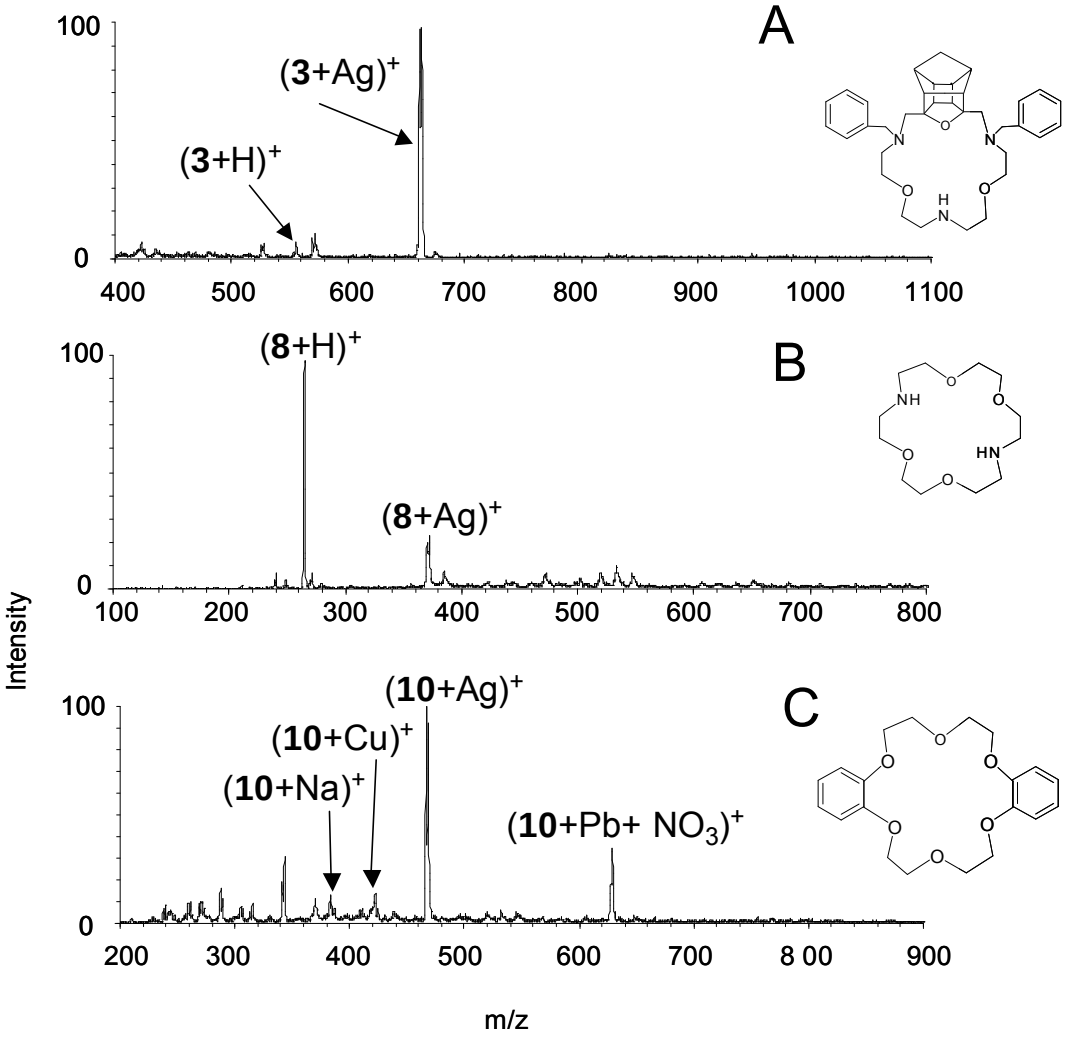

and Cu^{2+}. The relative signal intensities for the transition metal complexes in the mass spectra for **1** to **10** are shown in Table 6.4, all processed with the appropriate ESI spray efficiency correction factors.

All of the caged aza-crown ethers, with the exception of **1**, do, in fact, show a high degree of selectivity for Ag^{+}. However, there is a notable amount of complexation of other metals for some of the macrocycles. For example, macrocycle **1** also has a moderate affinity for Pb^{2+} and Ni^{2+}. Although macrocycles **2** through **6** all favor Ag^{+}, macrocycles **2** and **3** also show some affinity for Zn^{2+}. For reference macrocycle **9**, the intensity of the Ag^{+} complex represents less than 50% of the total distribution of complexes observed, and thus this ligand is not selective for Ag^{+}.

Based on the signal intensities of the Ag^{+} complexes relative to the other metal complexes for each ligand, macrocycles **4, 5**, and **6** are the most Ag^{+} selective. The order of decreasing Ag^{+} selectivities of the macrocycles is **4** ≈ **5** ≈ **6** ≈ **10** > **3** > **2** > **1** ≈ **8** ≈ **7** > **9**. Although the ionic radius of Ag^{+} is closer to that of Na^{+} than K^{+}, the electronic arrangement of the silver orbitals prefers the larger cavity sizes of macrocycles **4**, **5**, and **6**, rather than **2**, **3**, or **7**, all which have the largest relative avidities towards Na^{+} versus the other alkali metals. The higher Ag^{+} selectivities of macrocycles **2** – **6** relative to that of **9** confirm the impact of the nitrogen atoms. The influence of the aromatic substituents on the Ag^{+} selectivity

Table 6.4 Relative percentages of transition metal complexes detected compared to silver ion complexes.[a]

[a] Error is ± 20% RSD. All percentages are corrected for ESI efficiencies.

Macrocycle	Cu^{2+}	Mn^{2+}	Zn^{2+}	Ni^{2+}	Pb^{2+}	**Ag^{+}**
1	0	1	1	15	24	**58**
2	0	2	13	7	0	**78**
3	2	2	10	2	0	**85**
4	0	1	2	4	1	**93**
5	0	1	1	0	5	**93**
6	0	1	2	4	2	**92**
7	11	4	33	0	0	**52**
8	1	2	18	25	0	**54**
9	5	0	0	48	21	**26**
10	3	0	0	0	7	**90**

of the caged azacrown ethers is substantiated based on comparison of the silver selectivities of macrocycles **4** and **5** versus crown ether **8**: macrocycles **4** and **5** are more Ag^+ selective than **8**. Likewise, the aromatic groups of **10** increase its Ag^+ selectivity significantly over that of **9**. The enhancement in selectivity due to the aromatic substituents may be due to interactions of the d-orbitals of Ag^+ with the aromatic groups of **4, 5**, and **10**, because aromatic groups have been shown to display weak bonding interactions with metal ions through pi bond electron donation [63-65].

Density functional theory (DFT) calculations were conducted with B3LYP methods to produce calculated geometries for complexes of Ag^+ with **2, 3** and **4**, shown in Figure 6.7, and also with Na^+, Cu^+, and Au^+ with **2** in Figure 6.8. The oxygens incorporated into the cage group are referred to as "cage-oxygens" and the other oxygens in the macrocyclic ring are "ring-oxygens". The two nitrogens nearest the cage-oxygen are referred to as "γ-nitrogens". Metal-heteroatom distances are reported as averages for metal binding to two or more ring-oxygens or γ-nitrogens. In all cases, the distance between the metal ion and the cage-oxygen is the shortest of the metal-heteroatom distances.

In Figure 6.7, it can be seen that silver ion rises above the plane of the oxygen heteroatoms in **2**, but the nitrogen atoms maintain a linear coordination with Ag^+. The ionic diameter of Ag^+ is slightly larger than the cavity diameter of **2**

Figure 6.7 Models of macrocycle **2**, **3** and **4** with Ag^+ determined by density functional theory calculations. Gray = carbon, black = oxygen, light gray = nitrogen. Horizontally adjacent models are rotated 90° about their vertical axis with respect to each other.

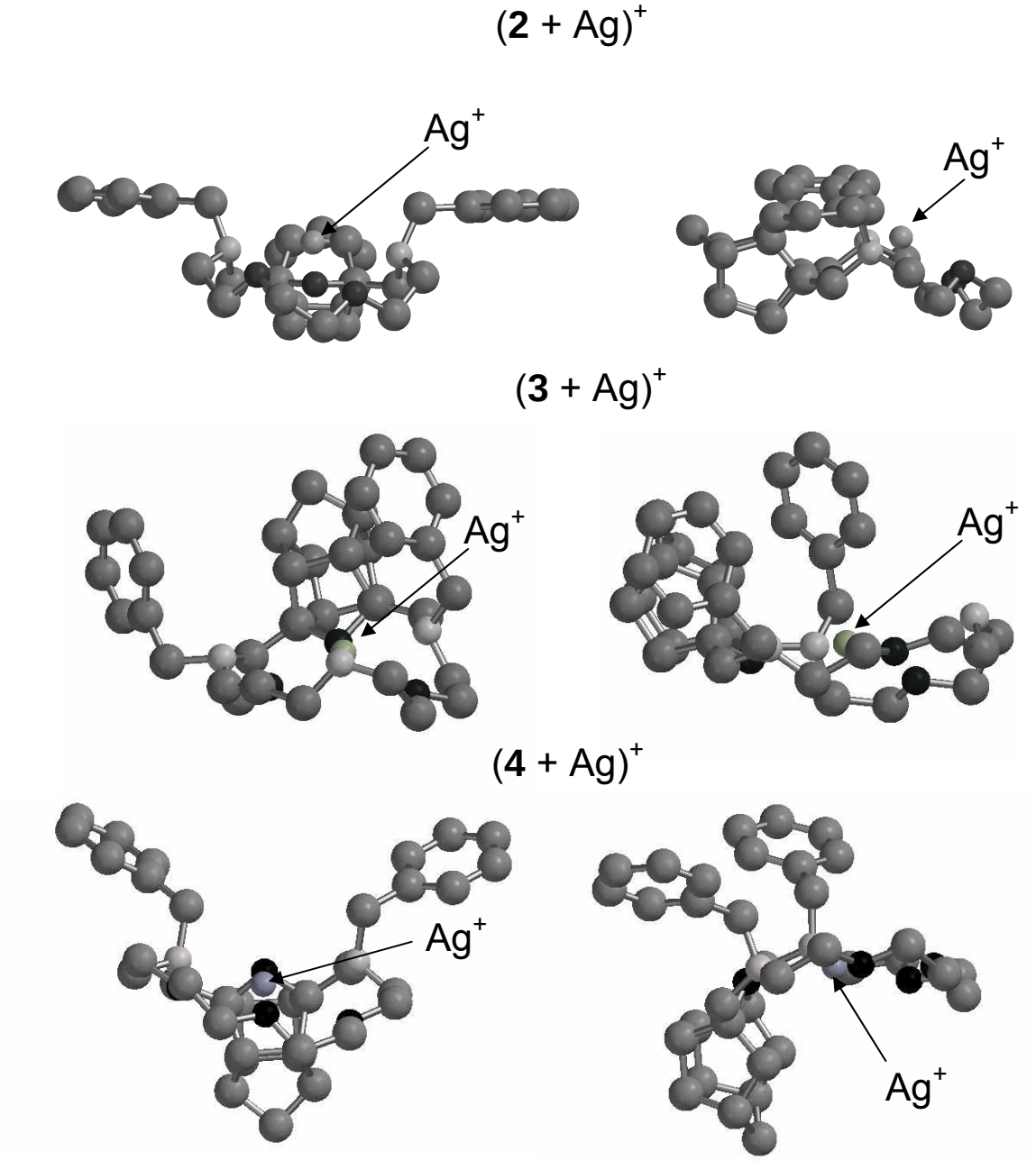

Figure 6.8 Models of macrocycle **2** with Au^+, Cu^+, and Na^+ determined by density functional theory calculations. Gray = carbon, black = oxygen, light gray = nitrogen. Horizontally adjacent models are rotated 90° about their vertical axis with respect to each other.

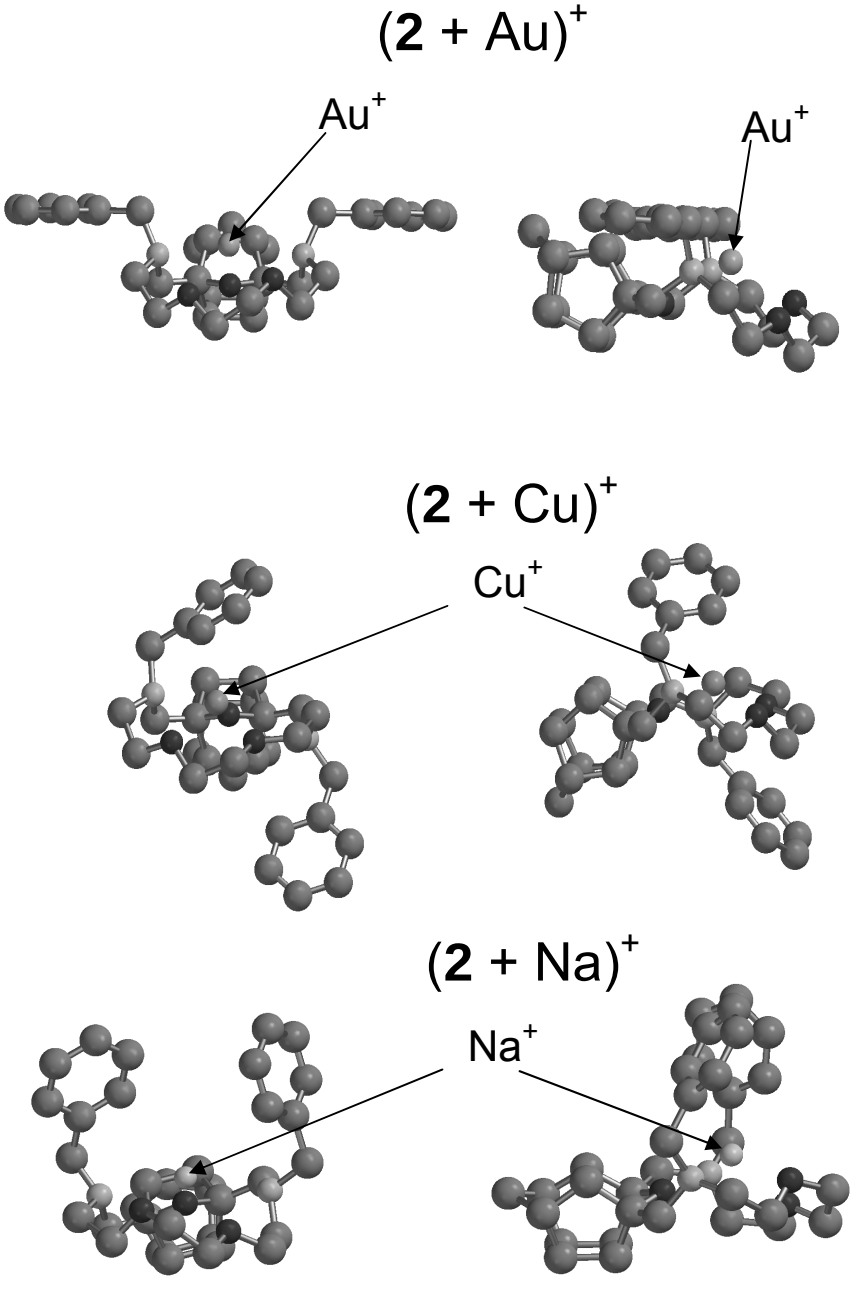

which results in it "perching" slightly above the plane of the crown ether ring. For the complex of Ag^+ with **3** or **4**, the Ag^+ ion is "nested" into the plane of the larger cavities. The larger ring cavity sizes appear to allow enough flexibility so that the phenyl rings can bend around to partially interact with the metal ions. When Ag^+ is perched above the cavity in the complex with **2**, the two phenyl groups are co-planar with the plane of the ring cavity.

Among the three macrocyclic complexes shown in Figure 6.7, the distance between the Ag^+ and γ-nitrogens is shortest relative to the distance between the Ag^+ and ring-oxygens for (**4** + Ag^+), which allows for a preferred linear coordination with Ag^+ [66-68]. For (**4** + Ag)$^+$, the metal ion nests in the plane of the cavity and the metal–γ-nitrogen and metal-ring-oxygen distances are 284.7 pm and 279.5 pm, respectively. The Ag^+ is pulled slightly away from a linear bond between the nitrogens due to the electrostatic attraction by the three ring-oxygen atoms, but this complex still has the most ideal linear N-Ag^+-N geometry of the three. For (**2** + Ag)$^+$, the metal ion is too large to fit in the cavity, and metal–ring-oxygen and metal-γ-nitrogen distances are 251.3 pm and 266.6 pm, respectively. For (**3** + Ag)$^+$, the silver ion fits into the cavity somewhat better, though still above the cavity plane, but the third nitrogen atom located on the opposite side of the ring relative to the cage-oxygen pulls Ag^+ toward it away from the other γ-nitrogens. The metal-ring-oxygen distance is 255.6 pm, and the metal-γ-nitrogen distance is 314.6 pm. Although shorter average distances are achieved by less ideal interactions between

Ag^+ and five or six heteroatoms, the greatest selectivity for Ag^+ among the structurally similar series of **2**, **3**, and **4** is achieved via interactions which optimize the Ag^+ d-orbital interactions and soft ion character with nitrogens and their lone pairs.

Geometries of complexes containing Cu^+, Au^+, and Na^+ with **2**, the smallest of the series of dibenzyl-crown ether analogs, were also calculated to rationalize why this smaller macrocycle is still Ag^+ selective. The resulting models are shown in Figure 6.8. For $(\mathbf{2} + Na)^+$, Na^+, a hard ion, prefers binding to the hard oxygen atoms rather than the softer nitrogens (237.6 pm for metal-ring-oxygen distance and 273.6 pm for the metal–nitrogen distance). For copper as well, binding to the oxygen atoms is preferred, and the model shows that the Cu^+ ion attempts to adopt a tetrahedral coordination geometry with the three oxygens of **2** and the pi electrons of one of the aromatic rings. This results in the other benzyl group being bent away from the ring such that the nitrogen it is attached to is pulled 336.7 pm away from the Cu^+ ion. The complex involving Au^+ ion adopts a geometry almost identical to that of the $(\mathbf{2} + Ag^+)$ complex. This is demonstrative of how the softer coinage metal ions, silver and gold, form preferred linear $N\text{-}M^+\text{-}N$ complexes despite creating interactions that are otherwise very unfavorable.

6.3.4 Extractions

Extraction experiments were undertaken to further evaluate the ability of the macrocycles to extract silver ion selectively from aqueous solutions. For this part of the study, three of the macrocycles were chosen. Macrocycle **3** was chosen due to its greatest resistance to protonation in the screening studies conducted in methanol discussed in the previous sections. Macrocycle **4** was chosen due to its highest Ag^+ selectivity in the presence of other transition metals and the alkali metals. Macrocycle **8** (diaza-18-crown-6) was chosen as a reference ligand that does not contain either the cage group nor aromatic groups and possesses a lower Ag^+ selectivity relative to that of macrocycles **3** and **4** based on the previous ESI-MS experiments. Experiments were carried out by extracting metal ions from an aqueous phase into an organic (chloroform) phase by complexation with a macrocycle present in the organic phase. The organic phase was then separated from the aqueous phase and analyzed by ESI-MS. Initial extraction experiments with Ag^+ alone in the aqueous phase at a 25-fold greater concentration than **3**, **4**, or **8** in the organic chloroform phase resulted in mass spectra with the (**3** + Ag^+) complex at a signal-to-noise ratio (SNR) greater than 500, the (**4** + Ag^+) complex with a SNR of about 30, and no observable signal for the (**8** + Ag^+) complex (data not shown).

In the ESI-mass spectra obtained upon analysis of the chloroform phase after extractions of Ag^+, Cu^{2+}, Zn^{2+}, and Mn^{2+} in the aqueous phase by either **3** or **4**,

(**3** + Ag^+) is detected with a SNR of greater than 500 (Figure 6.9A), and (**4** + Ag^+) is detected with a SNR of about 30. Also, complexes with other transition metals were not observed for either **3** or **4**. Analogous results (i.e. detection of (macrocycle + Ag^+) but not other metal complexes) were observed for extractions of Ag^+, Fe^{3+}, Ni^{2+}, and Pb^{2+} in the aqueous phase by complexation with either **3** or **4** in the organic chloroform phase. When ESI spray efficiencies are factored into the experimental measurements, it is clear that **3** is a more successful extraction agent than **4**.

A final experiment involved extractions of Ag^+, Cu^{2+}, Zn^{2+}, Mn^{2+}, Fe^{3+}, Ni^{2+}, Pb^{2+} , Na^+, K^+, Mg^{2+}, and Ca^{2+} as nitrates in the aqueous phase with a five-fold greater concentration of the transition metals and a 25-fold greater concentration of the alkali and alkaline earth metals relative to that of **3** in the organic chloroform phase (**3** at 2 x 10^{-4} M in chloroform). The large excess of metal ions results in a more acidic environment than the previous extraction experiments, resulting in some observation of protonated **3** in the ESI-mass spectra, along with the (**3** + Ag^+) complexes with a SNR of 12. Complexes of **3** with alkali, alkaline earth, or transition metals other than Pb^{2+} were not observed. By adding a relatively low amount of a base, potassium hydroxide, to the aqueous phase (4 x 10^{-3} M, pH 5.4), the extraction avidity of **3** is restored (see Figure 6.9B) because the addition of potassium hydroxide controls the extent of protonation of the macrocycle, a process that directly competes with Ag^+ complexation.

Figure 6.9 ESI-MS of chloroform phase containing **3** after extraction of an aqueous phase containing metals. (A) **3** with Ag^{+}, Mn^{2+}, Cu^{2+} and Zn^{2+} in the aqueous phase (1:5:5:5:5). (B). **3** with Na^{+}, K^{+}, Mg^{2+}, Ca^{2+}, at 25-fold greater concentrations than **3** and Ag^{+}, Mn^{2+}, Cu^{2+}, Zn^{2+}, Fe^{3+}, Ni^{2+}, and Pb^{2+} at five-fold greater concentrations than **3** in the aqueous phase and 4 x 10^{-3} M KOH in the aqueous phase.

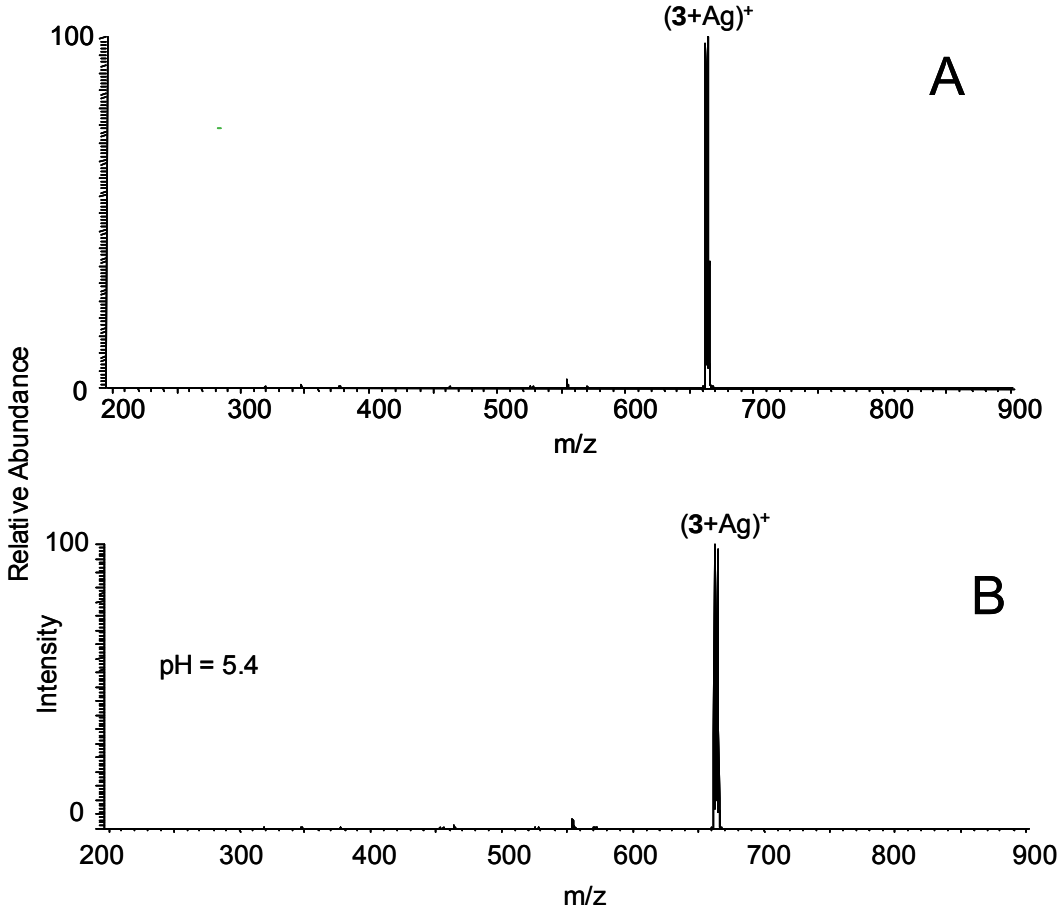

These results demonstrate that the silver selective macrocycle **3** is capable of nearly exclusively selective extraction of Ag^+ in the presence of other transition metal ions and the most common alkali and alkaline earth metal ions. The major factor limiting extraction efficiency appears to be a decrease in the extraction capacity of the macrocycle with increasing acidity of the system.

6.4 Conclusions

Electrospray ionization-mass spectrometry allowed efficient evaluation of several new silver-selective macrocycles, both in homogeneous methanolic solutions and based on extractions of metals from aqueous solutions into macrocycle-containing organic solutions. Five of the caged nitrogen-containing macrocycles are selective for Ag^+ over a variety of other transition metals and alkali metal ions. Silver selectivity was found to increase with larger cavity diameters, with cavities 20 to 40 pm larger than the known ionic diameter of Ag^+, likely due to the orientation of the d-orbitals in the cavity. Appropriate cavity size, nitrogen heteroatoms, and the presence of both aromatic groups and structurally stabilizing groups on a macrocycle are able to enhance Ag^+ selectivity. The Ag^+ avidity and selectivity enhancements observed with the presence of aromatic groups on macrocycle **10** versus **9** and with macrocycles **4, 5**, and **6** may involve interactions between the metal ion and the aromatic groups via cation-pi interactions. Macrocycles **4**, **5**, and **6** were observed to have the greatest Ag^+

selectivities, while **3** was observed to have the lowest tendency to protonate, making these good future candidates as selective silver extraction agents. The resistance towards protonation of **3** was observed to be of greater importance for Ag^+ extraction performance than the Ag^+ selectivity in methanol, although high Ag^+ selectivity is still essential. Nearly exclusively selective extraction of Ag^+ from aqueous solutions was observed for **3**, even with equimolar concentrations of other transition metals and five-fold greater concentration of several alkali and alkaline earth metals, relative to Ag^+, present in the aqueous phase. The extraction capacity of the macrocycle in the organic phase was found to decrease with increasing acidity of the aqueous phase due to competition from protonation of the macrocycle.

6.5 Acknowledgements

Support from the Robert A. Welch Foundation (F-1155 to J.S.B and B-0963 to A.P.M.), the Texas Advanced Technology Program (Grant 003659-0206-1999), and the U.S. Department of energy (Grant DE-FG07-98ER14936 to A.P.M.) is gratefully acknowledged.

6.6 References

1. Gokel, G.W., Ed., *Comprehensive Supramolecular Chemistry: Molecular Recognition: Receptors for Cationic Guests, Vol. 1*, Elsevier Science, New York, **1996**.

2. Martell, A.E.; Hancock, R.D. *Metal Complexes in Aqueous Solution*, Plenum Press, New York, **1996**.

3. Izatt, R. M.; Pawlak, K.; Bradshaw, J. S. "Thermodynamic and kinetic data for macrocycle interactions with cations and anions." *Chem. Rev.*, **1991**, *91*, 1721-2085.

4. Koryta, J.; Stulik, K. *Ion Selective Electrodes, 2nd Ed.*, Cambridge: Cambridge University Press, **1983**.

5. Yamashita, K.; Kurita, K.; Ohara, K.; Tamura, K.; Nango, M.; Tsuda, K. "Syntheses of thiacrown ethers polymers and their application for heavy metal ion adsorbents." *React. Funct. Polym.*, **1996**, *31*, 47-55.

6. Wu, G.; Jiang, W.; Lamb, J. D.; Bradshaw, J. S.; Izatt, R. M. "High-specificity thiacrown ether reagents for silver(I) over bivalent mercury and lead. Thermodynamic and carbon-13 NMR relaxation time studies." *J. Am. Chem. Soc.*, **1991**, 113, 6538-6541.

7. Zong, Z.; Dong, S.; Hu, Y.; Xu, Y.; Liu, W. "Synthesis and complexation properties of polystyrene supported polymeric thiacrown ether." *Eur. Polym. J.*, **1998**, *34*, 761-766.

8. Baumann, T. F.; Reynolds, J. G. "Polymer pendant crown thioethers: synthesis and Hg(II) extraction studies of a novel thiacrown polymer." *Chem. Commun. (Cambridge)*, **1998**, *16*, 1637-1638.

9. Nelson, A. J.; Reynolds, J. G.; Baumann, T. F.; Fox, G. A. "X-ray photoemission investigation of binding sites in polymer-bound thiacrowns used for environmental remediation of Hg in aqueous solutions." *Appl. Surf. Sci.*, **2000**, *167*, 205-215.

10. Baumann, T. F.; Reynolds, J. G.; Fox, G. A. "Polymer pendant crown thioethers: synthesis, characterization and Hg2+ extraction studies of polymer-supported thiacrowns ([14]aneS4 and [17]aneS5)." *React. Funct. Polym.*, **2000**, *44*, 111-120.

11. Saad, B.; Sultan, S. M. "Extraction spectrophotometric determination of mercury(II) using thiacrown ethers and Bromocresol Green." *Talanta*, **1995**, *42*, 1349-1354.

12. Yordanov, A. T.; Roundhill, D. M. "Chemically modified calix[4]arenes as selective complexants for heavy metal ions: comparison with crowns and thiacrowns." *New J. Chem.*, **1996**, *20*, 447-451.

13. Merrill, D. T.; Van Maltby, C.; Kahmark, K.; Gerhardt, M.; Melcer, H. "Evaluating treatment processes to reduce metals concentrations in pulp and paper mill wastewaters to extremely low values." *Tappi J.*, **2001**, *84*, 63.

14. de Sousa, M. ; Bertazzoli, R. « Preconcentration and Voltammetric Determination of Mercury(II) at a Chemically Modified Glassy Carbon Electrode. " *Anal. Chem.*, **1996**, *68*, 1258-1261.

15. Bartsch, R.A.; Hayashits, T. *Metal Ion Separations with Lariat Ether Ion-Exchange Resins. ACS Symposium Series*, **1999**, *716*, 183-193.

16. Alexandros, S.D.; Crick, D.W. "Polymer-Supported Reagents: Application to Separation Science." *Int. Eng. Chem. Res.*, **1996**, *35*, 635-644.

17. Grzejdziak, A.; Olejniczak, B.; Seliger, P. "Complexing Equilibria of Ag(I) Ion in the Presence of Heterocyclic Amines in DMSO. Comparison with Other Solvents." *J. Mol. Liq.*, **2002**, *100*, 81-90.

18. Vela, J.; Sharma, P.; Cabrera, A.; Alverez, C.; Rosas, N.; Hernandez, S.; Toscano, A. "Tertiary Stibines Containg Aromatic Heterocycles and Their Silver Complexes: Synthesis and X-ray Structures." *J. Organomet. Chem.*, **2001**, *634*, 5-11.

19. Adams, H.; Bailey, N.A.; Collinson, S.R.; Fenton, D.E.; Fukuhara, C.; Hellier, P.C.; Hempstead, P.D.; Leeson, Philip B. *Disilver(I) Complexes of Pendant-Arm Macrocycles. Special Publication – Royal Society of Chemistry*, **1993**, *131*, 113-116.

20. Blake, A.J.; Gould, R.O; Radek, C.; Reid, G.; Taylor, A.; Schroeder, M. *Structural Mis-Matches in Silver and Gold Complexes of Thioether Macrocycles. Special Publication – Royal Society of Chemistry*, **1993**, *131*, 95-101.

21. Kim, J.S.; Rim, J.A.; Shon, O.J.; Noh, K.H., Kim, E.-H., Cheong, C.; Vicens, J. "Cation Recognition by Picolyl-Armed Calix[4]Crown-5-Azacrown-5s." *J. Incl. Phenom. Macrocyclic Chem.*, **2002**, *43*, 51-54.

22. Kim, J.S.; Yu, S.H.; Cho, M.H.; Shon, O.J.; Rim, J.A.; Yang, S.H.; Lee, J.K.; Lee, S.J. "Calix[4]Azacrown Ethers in Polymeric CTA Membrane." *Bull. Korean Chem. Soc.*, **2001**, *22*, 519-522.

23. Inokuma, S.; Kimura, K.; Funaki, T.; Nishimura, J. "Synthesis of chrownophane possessing pyridine moieties on the aromatic nuclei (pyridine-lariat crownophane): a crownophane exhibiting perfect selectivity towards Ag^{+}." *Heterocycles*, **2001**, *55*, 447-451.

24. Dondoni, A.; Ghiglione, C.; Marra, A.; Scoponi, M. "Synthesis and Characterization of Bisphenol-A Copolyethers and Copolyesters Carrying Calix[4]arene Units in the Main Chains and Their Binding Properties towards Silver Cations." *Macromol. Chem. Phys.*, **1999**, *200*, 77-86.

25. Howard-Lock, H.E. "Structures of Gold(I) and Silver(I) Thiolate Complexes of Medicinal Interest: A Review of Recent Results." *Met.-Based Drugs*, **1999**, *6*, 201-209.

26. Lee, K.J.; Jho, J.Y.; Joo, S.H.; Kang, Y.S. "Complexation of Silver Ion with Carbonyl Oxygen Poly(n-Butyl Methacrylate) and Facilitated Transport." *Polym. Prepr. (Am. Chem. Soc., Div. Polym. Chem.)*, **2002**, *43*, 1399-1400.

27. Paiva, A.P. "Sulphur-Nitrogen Ligands in the Solvent Extraction of Silver from Chloride Solutions." *Solvent Extraction for the 21st Century, Proceedings of ISEC '99, Barcelona, Spain, July 11-16, 1999*, **2001**, 399-404.

28. Herrin, R.T.; Andren, A.W.; Shafer, M.M.; Armstrong, D.E. "Determination of Silver Speciation in Natural Waters. 2. Binding Strength of Silver Ligands in Surface Freshwaters." *Environ. Sci. Technol.*, **2001**, *35*, 1959-1966.

29. Nabeshima, T.; Tsukada, N.; Nishijima, K.; Ohshiro, H.; Yano, Y. "Remarkably Selective Ag^{+} Extraction and Transport by Thiolariat Ethers." *J. Org. Chem.*, **1996**, *61*, 4342-4350.

30. Guevremont, R.; Siu, K. W. M.; Le Blanc, J. C. Y.; Berman, S. S. “Are the electrospray mass spectra of proteins related to their aqueous solution chemistry?” *J. Am. Soc. Mass Spectrom.*, **1992**, *3*, 216-224.

31. Wang, G.; Cole, R. B. “Disparity between solution-phase equilibria and charge state distributions in positive-ion electrospray mass spectrometry.” *Org. Mass Spectrom.*, **1994**, *29*, 419-427.

32. Chapeaurouge, A.; Bigler, L.; Shafer, A.; Bienz, S. “Correlation of Stereoselectivity and Ion Response in Electrospray Mass-Spectrometry. Electrospray Ionization-Mass Spectrometry as a Tool to Predict Chemical Behavior?” *J. Am. Soc. Mass Spectrom.*, **1995**, *6*, 207-211.

33. Gokel, G. W.; Wang, K. “Correlation of Solution and Gas Phase Complexation Assessed by Electrospray Ionization Mass Spectrometry: Application to One-, Two-, and Three-Ring Macrocycles.” *J. Org. Chem.*, **1996**, *61*, 4693-4697.

34. Leize, E.; Jaffrezic, A.; Van Dorsselaer, A. « Correlation Between Solvation Energies and Electrospray Mass Spectrometric Response Factors. Study by Electrospray Mass Spectrometry of Supramolecular Complexes in Thermodynamic Equilibrium in Solution. » *J. Mass. Spectrom.*, **1996**, *31*, 537-544.

35. Young, D-S.; Hung, H-Y. Liu, L. K. “Estimation of Selectivities and Relative Cationization Efficiencies of Different [Crown+M]+ by Electrospray Mass Spectrometry.” *J. Mass. Spectrom.*, **1997**, *32*, 432-437.

36. Young, D-S.; Hung, H-Y. Liu, L. K. “An Easy and Rapid Method for Determination of Stability Constants by Electrospray Ionization Mass Spectrometry.” *Rapid Commun. Mass Spectrom.*, **1997**, *11*, 769-773.

37. Blair, S.M.; Kempen, E.C.; Brodbelt, J.S. “Determination of Binding Selectivities by ESI/Quadrupole Ion Trap Mass Spectrometry.” *J. Am. Soc. Mass Spectrom.*, **1998**, *9*, 1049-1059.

38. Kempen, E.C.; Brodbelt, J.S.; Bartsch, R.A.; Jang, Y.;Kim, J.S. “Investigation of Alkali Metal Cation Selectivities of Lariat Ethers by Electrospray Ionization Mass Spectrometry.” A*nal..Chem.*, **1999**, *71*, 5493-5500.

39. Blair, S.M.; Brodbelt, J.S.; Marchand, A.P.; Kumar, K.A.; Chong, H-S. “Evaluation of Binding Selectivities of Caged Crown Ligands towards

Heavy Metals by Electrospray Ionization/Quadrupole Ion Trap Mass Spectrometry." *Anal. Chem.*, **2000**, *72*, 2433-2445.

40. Goolsby, B.; Hall, B.J.; Brodbelt, J.S.; Adou, E.; Blanda, M. "Determination of Alkali Metal Ion Binding Selectivities of Calixerenes by MALDI and ESI in a Quadrupole Ion Trap." *Int. J. Mass Spectrom.*, **1999**, *193*, 197-204.

41. Blanda, M.T.; Farmer, D.B.; Brodbelt, J.S.; Goolsby, B. "Synthesis and Alkali Metal Ion Binding Properties of Two Rigid Stereochemical Isomers of Calix[6]arene-Bis-Crown-4." *J. Am. Chem. Soc.* **2000**, *122*, 1486-1491.

42. Reyzer, M.L., Brodbelt, J. S., Marchand, A.P., Chen, Z., Huang, Z., Namboothiri, I.N. N. "Determination of alkali metal binding selectivities of caged crown ligands by electrospray ionization quadrupole ion trap mass spectrometry." *Int. J. Mass Spectrom.*, **2001**, *204*, 133-142.

43. Blair, S., Brodbelt, J., Marchand, A., Chong, H.-S., Alidhodzic, S. "Evaluation of Alakli Metal Binding Selectivities of Caged Aza-Crown Ligands by Electrospray Ionization Quadrupole Ion Trap Mass Spectrometry." *J. Am. Soc. Mass Spectrom.*, **2000**, *11*, 884-891.

44. Williams, S.; Blair, S. M.; Brodbelt, J. S.; Huang, X.; Bartsch, R. A. "Determination of Alkali Metal Cation Selectivities of Dibenzo-16-Crown-5 Lariat Ethers with Ether Pendant Groups using Electrospray Ionization Quadrupole Ion Trap Mass Spectrometry." *Int. J. Mass Spectrom.*, **2001**, *212*, 389-401.

45. Williams, S. M.; Brodbelt, J. S.; Marchand, A. P.; Cal, D.; Mlinaric-Majerski, K. "Metal Complexation of Thiacrown Ether Macrocycles by Electrospray Ionization Mass Spectrometry." *Anal. Chem.*, **2002**, *74*, 4423-4433.

46. Kempen, E., Brodbelt, J. "A Novel Method for the Determination of Binding Constants by Electrospray Ionization Mass Spectrometry." *Anal. Chem.*, **2000**, *72*, 5411-5416.

47. Brady, Paul A.; Sanders, Jeremy K. M. "Electrospray mass spectrometry and supramolecular complexes: quantifying the metal ion binding properties of cholic acid derivatives." *New J. Chem.*, **1998**, *22*, 411-418.

48. Lim, H.-K.; Hsieh, Y.L.; Ganem, B.; Henion, J. "Recognition of cell-wall peptide ligands by vancomycin group antibiotics: studies using ion spray mass spectrometry." *J. Mass Spectrom.*, **1995**, *30*, 708-714.

49. Loo, J.A.; Hu, P.; McConnell, P.; Mueller, W.T.; Sawyer, T.K.; Thanabal, V. "A study of Src SH2 domain protein-phosphopeptide binding interactions by electrospray ionization mass spectrometry." *J. Am. Soc. Mass Spectrom.*, **1997**, *8*, 234-243.

50. Young, D.-S.; Hung, H.-Y.; Liu, L.K. "An Easy and Rapid Method for Determination of Stability Constants by Electrospray Ionization Mass Spectrometry." *Rapid Commun. Mass Spectrom.*, **1997**, *11*, 769-773.

51. Jorgensen, T.J.D.; Roepstorff, P.; Heck, A.J.R. "Direct Determination of Solution Binding Constants for Noncovalent Complexes between Bacterial Cell Wall Peptide Analogs and Vancomycin Group Antibiotics by Electrospray Ionization Mass Spectrometry." A*nal. Chem.*, **1998**, *70*, 4427-4432.

52. Griffey, R.H.; Hofstadler, S.A.; Sannes-Lowery, K.A.; Ecker, D.J.; Crooke, S.T. "Determinants of aminoglycoside-binding specificity for rRNA by using mass spectrometry." *Proc. Natl. Acad. Sci. USA*, **1999**, *96*, 10129-10133.

53. Siegel, M. M.; Tabei, K.; Bebernitz, G. A.; Baum, E. Z. "Rapid methods for screening low molecular mass compounds non-covalently bound to proteins using size exclusion and mass spectrometry applied to inhibitors of human cytomegalovirus protease." *J. Mass Spectrom.*, **1998**, *33*, 264-273.

54. Zhao, Y.-Z.; van Breemen, R. B.; Nikolic, D.; Huang, C.-R.; Woodbury, C. P.; Schilling, A.; Venton, D. L. "Screening Solution-Phase Combinatorial Libraries Using Pulsed Ultrafiltration/Electrospray Mass Spectrometry." *J. Med. Chem.*, **1997**, *40*, 4006-4012.

55. Gao J.; Cheng X.; Chen R.; Sigal G. B.; Bruce J. E.; Schwartz B. L.; Hofstadler S. A.; Anderson G. A.; Smith R. D.; Whitesides G. M. "Screening derivatized peptide libraries for tight binding inhibitors to carbonic anhydrase II by electrospray ionization-mass spectrometry." *J. Med. Chem.*, **1996**, *39*, 1949-55.

56. Wieboldt, R.; Zweigenbaum, J.; Henion, J. "Immunoaffinity Ultrafiltration with Ion Spray HPLC/MS for Screening Small-Molecule Libraries." *Anal. Chem.*, **1997**, **69**, 1683-1691.

57. Kelebek, S., Wells, P.F., Fekete, S.O., Burrows, M.J., Suarez, D.F., "Froth flotation process for separation of sulfide minerals assoiated with pyrrhotite ores", Can. Pat. App., (1996) Canadian Patent: 2151316AA, US patent 5795466A, 46 pp.

58. Marchand, A. P.; Huang, Z.; Lai, H.; Brodbelt, J. S.; Williams, S. "Synthesis and Electrospray Ionization Mass Spectrometric Evaluation of the Metal Cation Complexation Behavior of Cage-annulated Azacrown Ethers" *Heterocycles*, manuscript submitted electronically 5/19/03.

59. Khlobystov, A. N.; Blake, A. J.; Champness, N. R.; Lemenovskii, D. A.; Majouga, A. G.; Zyk, N. V.; Schroder, M. "Supramolecular design of one-dimensional coordination polymers based on silver(I) complexes of aromatic nitrogen-donor ligands." *Coord. Chem. Rev.*, **2001**, *222*, 155-192.

60. G. Wilkinson (Ed.), *Comprehensive Coordination Chemistry*, **1987**, *Vol. 5*, p. 786.

61. Kebarle, P., Ho, Y., Chapter 1 in *Fundamental Aspects of Electrospray Ionization*, "On the Mechanism of Electrospray Mass Spectrometry", R.B. Cole, Ed., John Wiley and Sons, Inc., New York, **1997**.

62. Emsley, J. Ed. *The Elements (2nd Edn.)*, Clarendon Press, Oxford, **1991**.

63. Dougherty, D.A. "Cation-Pi Interactions in Chemistry and Biology: A New View of Benzene, Phe, Tyr, and Trp." *Science*, **1996**, 271, 163-168.

64. Ma, J.C.; Dougherty, D.A. "The Cation-Pi Interaction. *Chem. Rev*., **1997**, 97, 1303-1324.

65. Gallivan, J.P.; Dougherty, D.A. Cation-Pi Interactions in Structural Biology." *Proc. Natl. Acad. Sci. USA*, **1999**, 96, 9459-9464.

66. Ma, N.L. "How Strong Is the Ag^+-ligand bond?" *Chem. Phys. Lett*., 1998, 297, 230-238.

67. Koizumi, H.; Larsen, M.; Armentrout, P.B.; Feller, D. "Collision-Induced Dissociation and Theoretical Studies of $Ag^+(methanol)_n$, n=1-4," *J. Phys. Chem. A*, **2003**, *107*, 2829-2838.

68. El Aribi, H.; Rodriquez, C.F.; Shoeib, T.; Ling, Y.; Hopkinson, A.C.; Siu, K.W.M. "Threshold Collision-Induced Dissociation Determination and Molecular Orbital Calculations of the Binding Energies of Sodium and

Silver Ions to Small Nitrogen-Containing Ligands," *J. Phys. Chem. A*, **2002**, *106*, 8798-8805.

CHAPTER 7

Fragmentation of Cyclic Peptides Complexed with Various Alkali, Alkaline Earth, and Transition Metal Ions

7.1 Introduction

Cyclic peptides are an important class of antibiotics that have been isolated from organisms such as bacteria, fungi, and plants or prepared by synthetic methods [1-6]. In addition, new cyclic peptide antibiotics are being synthesized and discovered on a regular basis and have been found to have numerous pharmaceutical applications including enzyme inhibitors, antifungal and antibacterial agents, and immunosuppresion and anti-cancer drugs [1-30].

The recent development of fast peptide and protein sequencing methods using mass spectrometry has been most beneficial for structural identification of linear peptides and proteins. CAD analyses of cyclic peptides are complicated, compared to linear peptides, by their circular nature. Losses of amino acid residues for sequencing must involve cleavage of two bonds of the peptide backbone, as opposed to only one cleavage for linear peptides. Moreover, the cleavage can occur at several backbone positions simultaneously, meaning that all the fragment ions are not references to a single 'terminal' position. One approach to expedite analysis

of the sequence from the mass spectrometric data is to use fragmentation libraries or sophisticated algorithms to suggest possible sequence matches. Another approach is to increase the dimensionality of the mass spectrometry experiments by isolating and dissociating ions from the initial MS^2 spectrum of the cyclic peptide ion, and repeating this with subsequent MS^n experiments until the identity of the peptide or its sequence is satisfactorily determined. Recent studies have reported MS^n collision activated dissociation (CAD) of protonated synthetic cyclic peptides with polypeptide rings of five to six residues [31] polymyxins [32], and microcystins [33] using electrospray ionization mass spectrometry (ESI-MS). One study investigated CAD of seven residue cyclopeptides and tentoxin and destruxin depsipeptides using fast atom bombardment (FAB) and ESI sources [34]. MS^n experiments may be time-consuming and restricted due to signal-to-noise limitations. Another approach is to use other methods to ionize the cyclic peptides, in addition to or as an alternative to conventional protonation, to improve the quality and/or quantity of diagnostic MS^n data. CAD studies have been undertaken for cyclic peptides and depsipeptides. Depsipeptides have combinations of peptide bonds and ester bonds along their backbones.[1] These studies include investigations of (i) cyclic petapeptides complexed with lithium and sodium ions [35], (ii) cyclic hexapeptides with four or five residue rings with sodium ion [36], (iii) the octapeptide surfactin complexed with sodium ion using Cs^+ ion bombardment (LSIMS) [37], (iv) valinomycin with lithium ion [38], (v) the six

residue depsipeptides beuveracin, didemning B, and enniatin B1 with sodium ion [39], and (vi) the cyclic hexapeptide, ferrichrome, with Fe(III) ion [40]. Several other studies have examined the dissociation patterns of metal-cationized peptides [41-62], especially with high energy CAD methods such as post-source decay and in sector instruments [41,43-52,60]. To our knowledge, no studies have previously reported the comparison of low energy CAD of alkali, alkaline earth, and transition metal ion complexes with cyclic peptides with protonated cyclic peptides.

The present work focuses on the use of CAD and MS^n experiments of protonated and metal-cationized cyclic peptides in a quadrupole ion trap mass spectrometer. The cyclic peptides studied ranged in size from five to twelve residues and included cyclosporin A (Figure 1), the two depsipeptides, valinomycin and enniantin A_1 (Figure 2), the lipopeptides iturin A and surfactin (Figure 3), and the two synthetic peptides cyclo(RGDFV) and cyclo(RGDSPAG) (Figure 4). Cyclosporin A is a cyclic peptide antibiotic commonly used in topical antibiotics to prevent wound infections and promote faster healing and is also a potent immunosuppressant widely used to prevent rejection of transplanted organs [63]. Iturin A and surfactin are lipopeptides, biosurfactants and antibiotics. They are powerful antifungal agent produced naturally by *Bacillus subtilis*, and as such are used as easily biodegradable pesticides against certain pathogens of stone fruit, tomato, table grape, and other agricultural product pathogens [15-19]. Cyclo(RGDFV) and Cyclo(RGDSPAG) are antagonists of RGD peptides'

Figure 7.1. Chemical structure of cyclosporin A.

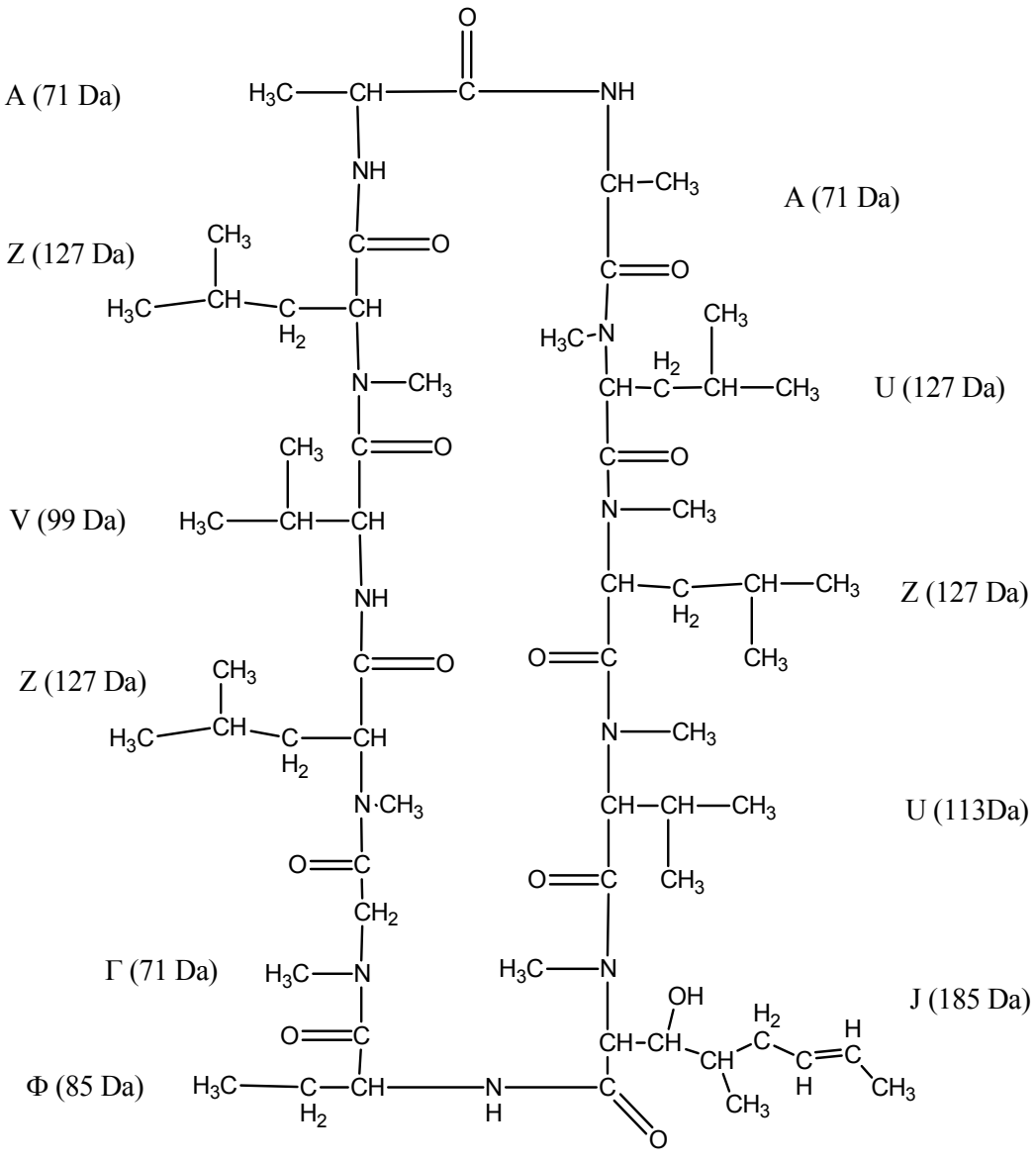

Z = N-methyl leucine
Γ = N-methyl glycine (sarcosine)
Φ = 3-amino butanoic acid
J = (4R)-4-[(E)-2-butenyl]-4-methyl-L-threonine

Figure 7.2. Chemical structure of depsipeptides A) valinomycin and B) enniatin A_1.

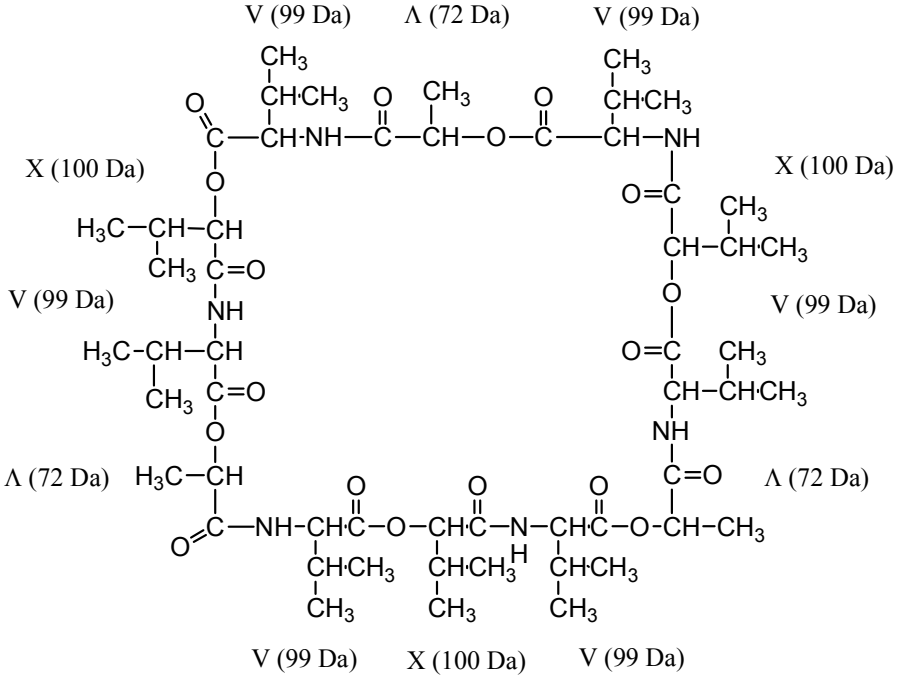

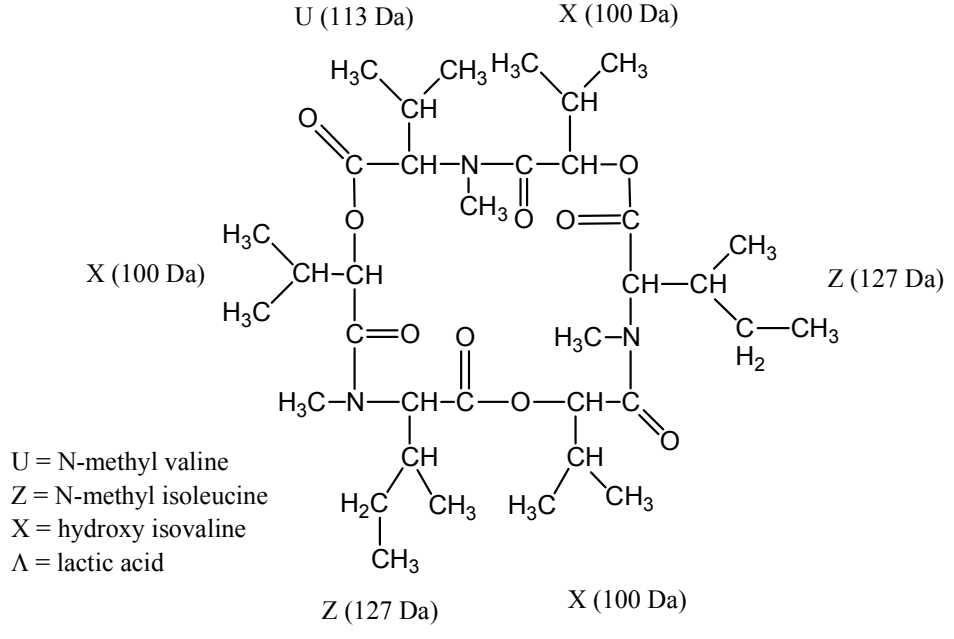

Figure 7.3. Chemical structures of lipopeptides A) iturin A and B) surfactin.

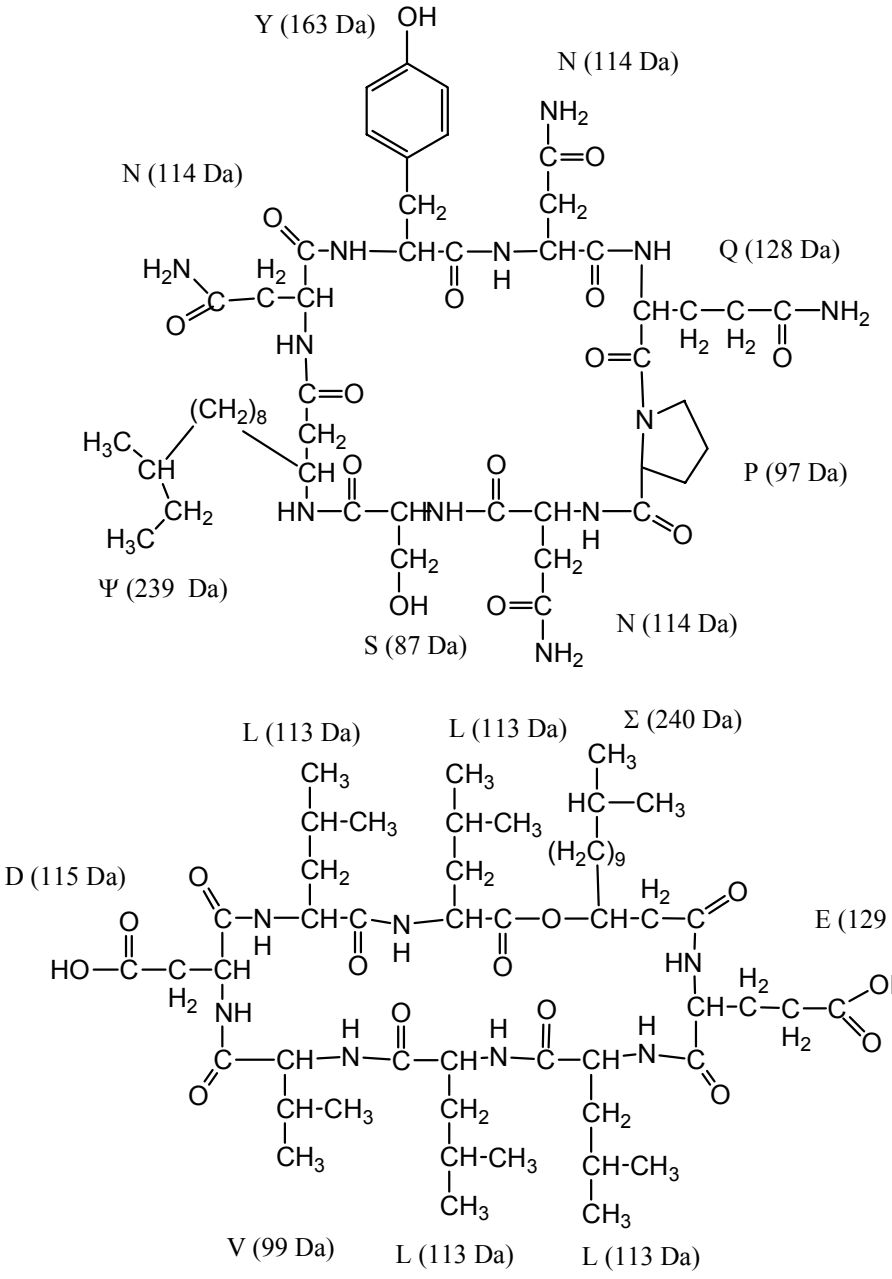

Ψ = 3-amino-12-methyl tetradecanoic acid

Σ = 3-hydroxy-13-methyl tetradecanoic acid

Figure 7.4. RGD peptide antagonists A) cyclo (RGDFV) and B) cyclo (RGDSPAG)

.

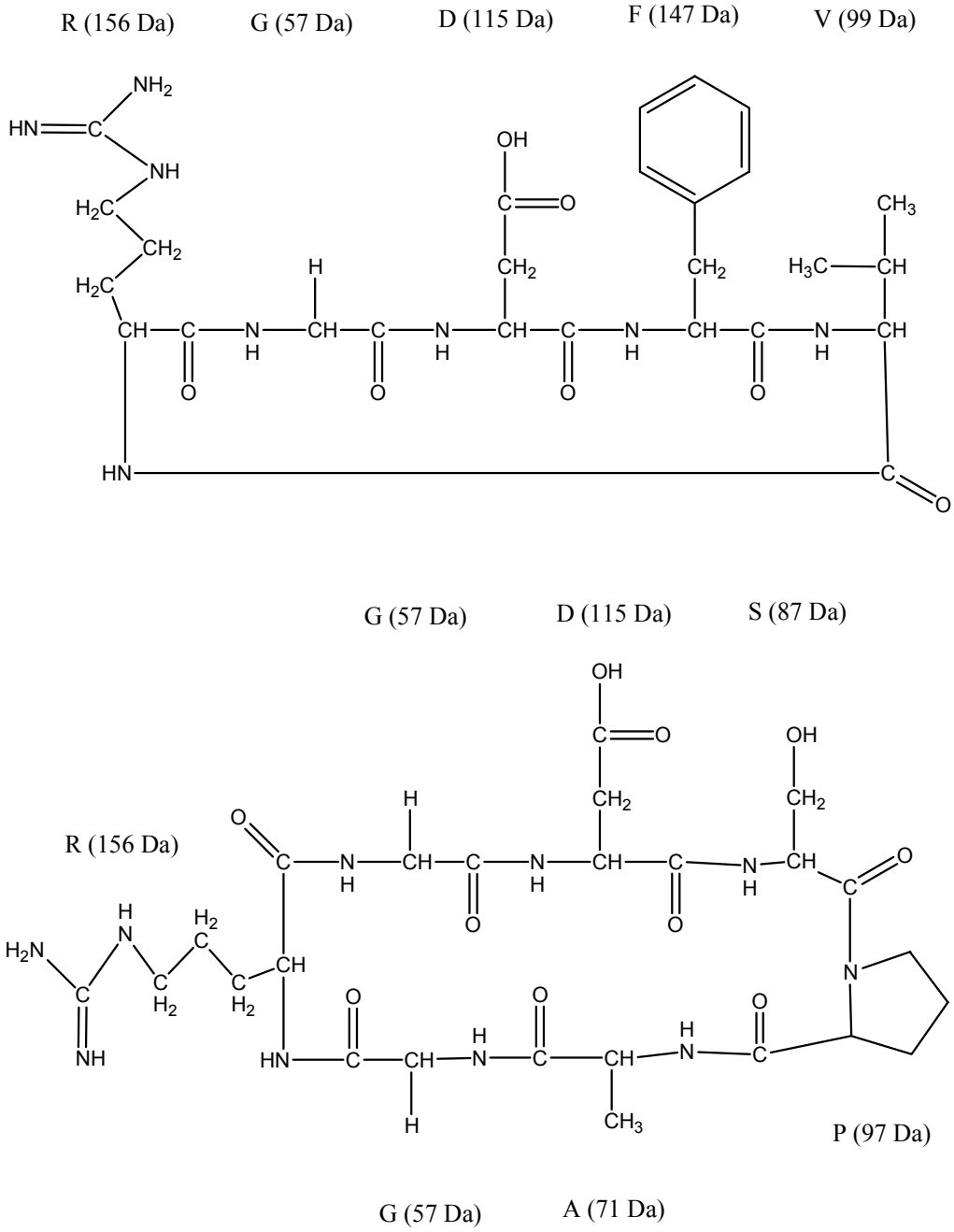

interaction with the RGD binding domains in mammalian psysiological. RGD peptide antagonists have been found to have many medicinal applications, including potent tumor cell adhesion and thrombonin induced blood platelet aggregation inhibition [20-30]. Valinomycin and enniatins such as enniantin A_1 are, like cyclosporin A, common potent antiobiotics and are also depsipetides. In addition, the enniatins are a class of cyclic peptides with alternating D,L residues which are currently of great interest for the development of new antibiotics and other pharmaceuticals [11-13, 64,65]. In this study, the CAD patterns of the protonated and metal-cationized peptides (Ag^+, Mn^{2+}, Ni^{2+}, Pb^{2+}, Co^{2+}, K^+, Na^+, Li^+, Sr^{2+}, and Ca^{2+}) were compared.

Of all the metal ions tested, those which provided the most useful complementary structural information to that of the protonated cyclic peptides were Na^+ and Pb^{2+} ions with the depsipeptides, and Ni^{2+}, Sr^{2+}, Ag^+ and Li^+ with the other cyclic peptides.

7.2 Experimental Methods

All mass spectrometry experiments were performed on a ThermoQuest LCQ quadrupole ion trap mass spectrometer (ThermoFinnigan, San Jose, CA) operated in the ESI mode with a needle voltage of 5.0 kV, a heated-capillary temperature of 125 ^oC, and sheath flow nitrogen gas set at 20 arbitrary units. The Harvard syringe pump system (Harvard Apparatus Inc., Holliston, MA) was

operated at a flow rate of 4 μl/min for all experiments. Lens voltages were set for all experiments by auto-tuning the LCQ on the ion of interest. Solution containing 2.5 to 10 μM of the macrocycle in a solution of 2% glacial acetic acid in methanol for studies of protonated macrocycle or a 20-fold excess of a metal ion in methanol were used for studies of metal ion complexes with the macrocycles. The ion trap was operated at a nominal pressure of 1 x 10^{-5} torr with He. Spectra used for this report are an average of 1000 scans. All metals salts used for these experiments were purchased from Aldrich Chemical Co. (Milwaukee, Wisconsin) and used without further purification. Cyclosporin A was obtained from Calbiochem (La Jolla, California), Surfactin, Iturin A, Valinomycin, and Enniatin A_1 were obtained from Sigma (Milwaukee, Wisconsin). The cyclo(RGDFV) and cyclo(GRGDSPA) peptides were obtained from BACHEM Bioscience Inc. (King of Prussia, Pennsylvania). The methanol was Certified A.C.S. Spectranalyzed® grade from Fisher Scientific (Pittsburg, Pennsylvania).

7.2.1 Nomenclature For Labeling the Fragment Ions

Fragment ions are labeled according to a slight variation of the descriptor system developed by Ngoka and Gross [66]. An ion is labeled as $x_m{}^n{}_{J/Z}$, where x is the designation for the ion (b or y, lower case). Thus, a b ion is an acylium ion, which may lose a carbon monoxide to form an a ion [35]. The term m is the number of amino acid residues in the ion, n is the ion's charge, and J and Z are the

single letter (upper case) codes for the two amino acid residues connecting the backbone amide bond J-Z that was broken to form the decomposing linear acylium ion or isomeric equivalent. Some possible CAD reaction pathways are shown in Scheme 1. The backslash is added for consistency for occasional occurrences when the same two adjacent residues occur more than once in a cyclic peptide amongst unidentical surrounding residues. In such cases, the residue sequence subscript (i.e. J/Z) is extended to include one unidentical residue so that the subscript refers to one unique location in the peptide sequence (e.g. $x_m{}^n{}_{J/ZU}$). Since in the MS^n data presented herein the cation is always attached to the peptide, for simplicity, the metal ion or proton is omitted from the labels, whether a proton or metal ion is bound to the peptide. Although the nomenclature is derived on the assumption of a reaction mechanism for fragmentation, the purpose is to designate product ions and not to specify their origins or exact nature [35]. An appendix is included at the end of this publication which gives abbreviations for all residues relevant to this work.

Also, as indicated in Scheme 1, the designated site of ring cleavage is the site of ring cleavage from which b and y ion designations are derived.

7.3 Results and Discussion

For each of the seven cyclic peptides in this study, solutions were prepared containing one of the metal ions and one of the cyclic peptides at a 25-fold lower concentration. After electrospray ionization (ESI) of the solution and accumulation

Scheme 7.1. Formation of $b^{+}_{J/Z}$ and $y^{+}_{J/Z}$ ions and peptide fragment ion label designations

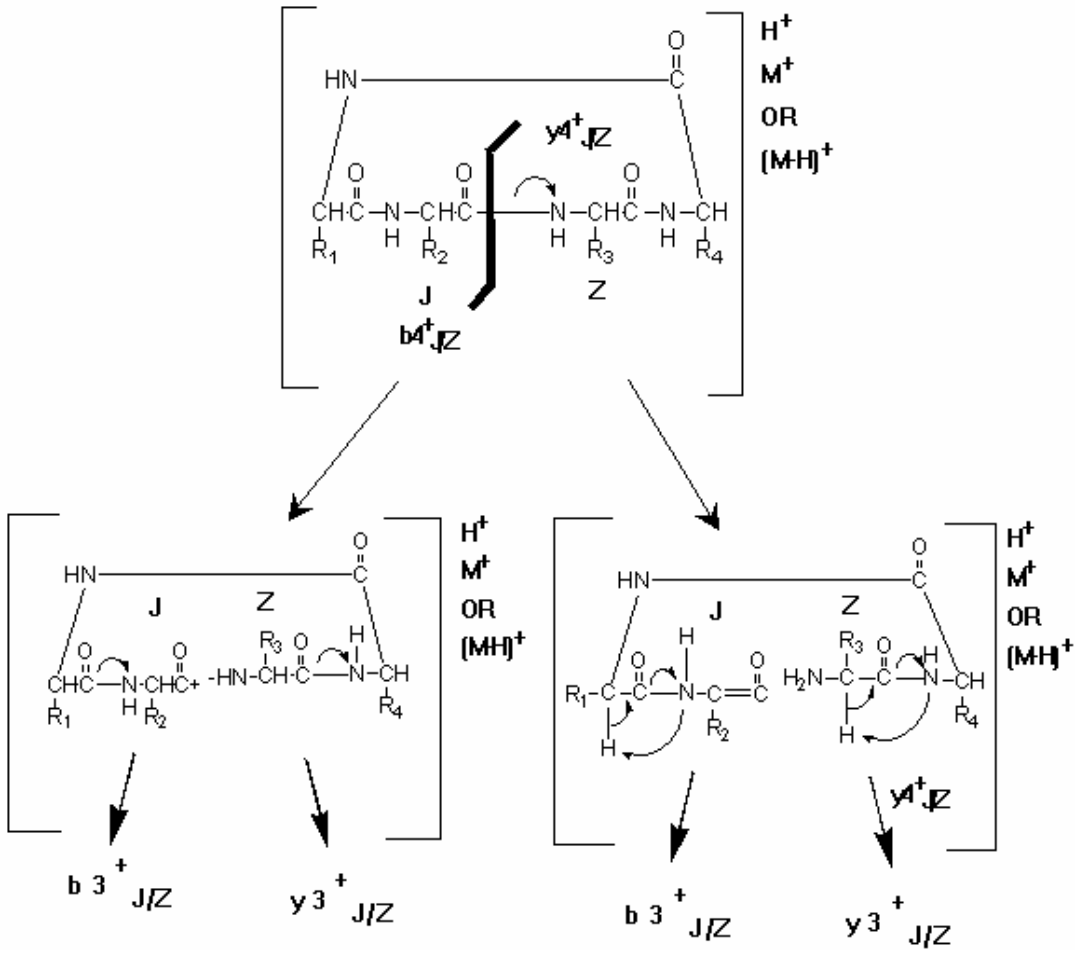

of ions into the quadrople ion trap, singly charged [host + metal(I)]$^{+}$ or [host + metal(II)-H]$^{+}$ complexes and, if observed, the doubly charged [host + 2 metal(I)]$^{2+}$ or [host + metal(II)]$^{2+}$ complex ions were isolated (in separate experiments) and subjected to MS^n analysis. The CAD experiments were conducted so that one to five percent of the precursor ion remained in the product spectra. This work focuses on those metal ions that have the most potential for providing complementary information for peptide structure characterization compared to that obtained for the protonated peptide ions. The signal intensities for singly charged metal complexes and doubly charged divalent metal complexes varied from a 2 to 100% relative abundance, as shown in Table 1. Complexes with two monovalent ions were often not present, but could be as intense as 80% relative abundance, as seen for dilithiated iturin A. For divalent metal ion complexes with the peptides, (host + metal(II) + NO_3)$^{+}$ signals were often observed along with (host + metal(II) –H)$^{+}$ signals. CAD of the former always resulted in conversion of at least 90% of the signal intensity to the latter or an identical product ion spectrum as the latter.

Metal complexed cyclic peptides appear to usually undergo ‘charge remote’ fragmentation in which successive MS^n cleavages do not continuously move the position of the metal ion [35]. Conversely, protonated peptides often undergo ‘charge driven’ fragmentation where the proton is on the terminal charged residue and moves to the adjacent rediue upon loss of the terminal residue. It has been proposed that charge remote fragmentation product ion spectra of protonated

Table 7.1. Relative intensities of metal complexed and doubly protonated cyclic peptides compared to singly protonated peptide.

Cyclic Peptide [a]	Percent relative abundance of complex in spectrum with given cation (with H^+ in same spectrum)									
	H^+	K^+	Na^+	Li^+	Ag^+	Sr^{2+}	Ca^{2+}	Co^{2+}	Ni^{2+}	Pb^{2+}
Singly charged complexes										
CSA	20 (100)	100 (5)	100 (0.2)	100 (0.5)	100 (0.5)	40 (4)	80 (1)	90 (0.2)	35 (25)	40 (7)
VM	40 (100)	100 (∞)	80 (0.2)	100 (2)	100 (0.2)	30 (25)	50 (5)	60 (1)	20 (25)	50 (25)
EA	40 (100)	60 (∞)	50 (∞)	40 (∞)	100 (0.2)	40 (15)	40 (25)	40 (5)	30 (40)	30 (40)
IA	100 (100)	100 (1)	100 (0.5)	100 (1)	100 (100)	25 (5)	10 (5)	100 (2)	70 (100)	25 (0.5)
SF	80 (100)	100 (5)	80 (5)	70 (5)	85 (3)	85 (2400)	80 (2)	80 (10)	85 (2)	60 (40)
RG1	100 (100)	10 (100)	100 (90)	85 (100)	100 (100)	5 (100)	10 (100)	10 (100)	20 (100)	15 (100)
RG2	100 (100)	10 (100)	100 (70)	100 (75)	15 (100)	2 (10)	2 (10)	30 (100)	20 (100)	15 (85)
Doubly charged complexes										
CSA	5 (60)	N/A	40 (0.2)	40 (0.5)	60 (0.2)	100 (4)	100 (1)	100 (0.2)	100 (50)	100 (7)
VM	N/A	N/A	N/A	0.5 (0.5)	0.5 (0.2)	30 (25)	100 (5)	40 (15)	35 (25)	40 (20)
EA	N/A	N/A	N/A	N/A	N/A	3 (15)	7 (25)	N/A	10 (40)	N/A
IA	N/A	N/A	N/A	80 (∞)	35 (100)	100 (0.5)	100 (5)	25 (2)	30 (100)	100 (0.5)
SF	1 (100)	N/A	N/A	N/A	N/A	85 (3)	40 (20)	10 (8)	25 (35)	35 (25)
RG1	N/A	N/A	0.5 (90)	3 (100)	N/A	20 (100)	15 (100)	15 (100)	2 (100)	10 (100)
RG2	N/A	N/A	2 (70)	10 (70)	N/A	2 (10)	2 (10)	20 (100)	20 (100)	10 (85)

[a] CSA = cyclosporin A, VM = valinomycin, EA = enniatin A_1, IA = iturin A, SF = surfactin, RG1 = cyclo(RGFV), RG2 = cyclo(RGSPAG).

peptides are easiler to interpret than charge driven fragmentation product ion spectra [67]. It is also probable that some metal ions would be more mobile than others depending on the metal and peptide.

7.3.1 Cyclosporin A

The fragment ions observed in the MS^2 and MS^3 spectra of protonated cyclosporin A (abbreviated CSA) are shown in Table 2. Both the singly and doubly protonated complexes are included. In Tables 3-10 are listed the fragment ions observed for CSA complexed with the various metal ions tested. Both singly and doubly charged precursor ions that were observed are included. In addition, MS^2 – MS^5 spectra for the $(CSA+Ni)^{2+}$ precursor ion are shown in Figure 5. Diagnostic product ion formation for protonated and sodium and lithium ion complexed cyclosporin A is depicted in Scheme 2A. As can been seen in Table 2, singly protonated cyclosporin A gives little sequence information. Only MS^2 and MS^3 spectra could be obtained for $(CSA+H)^+$ because of loss of signal, even though the intensity of the initially isolated $(CSA+H)^+$ ions was optimized as rigorously as the $(CSA+Ni)^{2+}$ signal. The ion signals observed in Table 2 for the $(CSA+H)^+$ precursor ion show very few simple b or y ions without additional gains or losses. MS^n of the $(CSA+2H)^{2+}$ ion produces the $(b_{10}+H)^{2+}_{U/J}/(y_{10}+H)^{2+}$, which is isomeric with the loss of the J sidechain (-112 Th), $(a_9+H)^{2+}_{U/J}$, $(b_9+H)^{2+}_{U/J}$, $(c_9+H)^{2+}_{U/J}$, $(b_8+H)^{2+}_{U/J}$, $(b_6+H)^{2+}_{U/J}$, $(b_5+H)^{2+}_{U/J}$, $(b_8+H)^{+}_{U/J}$, $(b_6+H)^{+}_{U/J}$, $(b_5+H)^{+}_{U/J}$, $(y_9-2H)^{+}_{Z/U}$,

Table 7.2. MS^n results for cyclosporin A complexes with H^+.[a] CSA = cyclosporin A

$(CSA+H)^+$					
MS^n	Precursor ion	Product ions			
		single residue losses	a, b, & c ions	x,y & z ions	small ions
MS^{2} [b]	$(CSA+H)^+$	$(CSA-U)^+$	$(b_{6Z/V}-H)^+$		
MS^{3} [c]	$(CSA-U)^+$	$(CSA-U-mNH_2)^+$	$a_9^+{}_{U/J}$, $b_6^+{}_{U/J}$		
$(CSA+2H)^{2+}$					
MS^n	Precursor ion	Singly charged product ions			
		single residue losses	a, b, & c ions	x, y, & z ions	small ions
MS^{2} [b]	$(CSA+2H)^{2+}$	$(CSA+2H-U+H)^{2+}$, $(CSA+2H-112)^+$	$(b_9+H)^{2+}{}_{U/J}$, $(a_9+H)^{2+}{}_{U/J}$, $(a_9+H)^+{}_{U/J}$, $(c_9+H)^+{}_{U/J}$,	$(y_9-2H)^+{}_{Z/U}$, $y_5^+{}_{Z/U}$	$(Z+\Phi)^+$, $(ZAA+H)^+$
MS^{3} [c]	$(CSA+2H-U+H)^{2+}$		$(b_9+H)^{2+}{}_{U/J}$, $(a_9+H)^{2+}{}_{U/J}$	$(y_7-CO)^+{}_{Z/U}$, $(y_8-2H)^+{}_{Z/U}$, $(y_7+H)^+{}_{Z/U}$	$(Z+\Phi)^+$, $(ZAA+H)^+$
MS^{4} [c]	$(b_9+H)^{2+}{}_{U/J}$		$(b_8+H)^{2+}{}_{U/J}$, $(b_6+H)^{2+}{}_{U/J}$, $(b_8+H)^+{}_{U/J}$, $(b_6+H)^+{}_{U/J}$, $(b_5+H)^+{}_{U/J}$		$(Z+\Phi)^+$, $(ZAA+H)^+$
MS^{3} [c]	$a_9^{2+}{}_{U/J}$				$(Z+\Phi)^+$, $(ZAA+H)^+$

[a] U = N-methyl valine; mL = N-methyl leucine; J = 4(R)-4[(E)-2-butenyl]-4-methyl-L-threonine; Φ = 2-amino-butanoic acid; 112 = side chain of J: $C_7H_{12}O$.H = hydrogen; C = carbon; O = oxygen . Signal intensity cutoffs (relative abundance): [b] 5%, [c] 10%.

Table 7.3. MS^n results for cyclosporin A complex with K^+.[a] CSA = cyclosporin A.

$(CSA+K)^+$					
MS^n	Precursor ion	Product ions			
		single residue losses	a, b, & c ions	x, y, & z ions	small ions
MS^{2} [b]	$(CSA+K)^+$	$(CSA+K-U+H)^+$, $(CSA+K-112)^+$ $(CSA+K-U-CO)^+$			
MS^{3} [b]	$(CSA+K-U)^+$	$(CSA+K-U-CO+H)^+$	$(b_9+CO+H)^+_{U/J}$		
MS^{4}[c]	$(CSA+K-U-CO)^+$		$(b_9+CO+H)^+_{U/J}$, $(b_8+CO+H)^+_{U/J}$, $(b_7+CO+H)^+_{U/J}$, $(b_7+H)^+_{U/J}$, $(b_5+H)^+_{U/J}$, $(a_5+H)^+_{U/J}$		
MS^{5} [d]	$(b_9+CO)^+_{U/J}$		$(b_8+CO+H)^+_{U/J}$, $(b_7+CO+H)^+_{U/J}$		
MS^{6} [e]	$(b_8+CO)^+_{U/J}$		$(b_5+CO+A+H)^+_{U/J}$		

[a] U = N-methyl valine; mL = N-methyl leucine; J = 4(R)-4[(E)-2-butenyl]-4-methyl-L-threonine; Φ = 2-amino-butanoic acid; 112 = side chain of J: $C_7H_{12}O$.H = hydrogen; C = carbon; O = oxygen . Signal intensity cutoffs (relative abundance): [b] 2%, [c] 5%, [d] 10%, [e] 20%.

Table 7.4. MS^n results for cyclosporin A complex with Na^+.[a] CSA = cyclosporin A.

MS^n	Precursor ion	Product ions			
		single residue losses	a, b, & c ions	x, y, & z ions	small ions
MS^{2} [b]	$(CSA+Na)^+$	$(CSA+Na-112)^+$, $(CSA+Na-112-CO)^+$, $CSA+Na-U+H)^+$, $(CSA+Na-U+H-CO)^+$			
MS^{3} [b]	$(CSA+2Na-112)^{2+}$		$(b_9+H)^+_{U/J}$, $(b_9+H+CO)^+_{U/J}$, $(b_8+H+CO)^+_{U/J}$, $(b_7+H)^+_{U/J}$,		
MS^{4} [c]	$(b_9+H+CO)^+_{U/J}$		$(b_9+H)^+_{U/J}$, $(b_7+H)^+_{U/J}$, $(b_7+H+CO)^+_{U/J}$, $(a_7+H)^+_{U/J}$,		

[a] U = N-methyl valine; mL = N-methyl leucine; J = 4(R)-4[(E)-2-butenyl]-4-methyl-L-threonine; Φ = 2-amino-butanoic acid; 112 = side chain of J: $C_7H_{12}O$.H = hydrogen; C = carbon; O = oxygen . Signal intensity cutoffs (relative abundance): [b] 2%, [c] 20%.

Table 7.5. MS^n results for cyclosporin A complex with Li^+.[a] CSA = cyclosporin A.[a]

$(CSA+Li)^+$					
MS^n	Precursor ion	Product ions			
		single residue losses	a, b, & c ions	x, y, & z ions	small ions
$MS^{2\,b}$	$(CSA+Li)^+$	$(CSA+ Li –U+H)^+$, $(CSA+ Li –U+H-CO)^+$			
$MS^{3\,b}$	$(CSA+ Li -U)^+$		$(b_9+CO+H)^+_{U/J}$, $(b_9+H)^+_{U/J}$		
$MS^{4\,c}$	$CSA+ Li -U-CO)^+$		$(a_9+H)^+_{U/J}$,$(b_8+CO)^+_{U/J}$, $b_7^+{}_{U/J}$, $(b_7+CO)^+_{U/J}$, $b_5^+{}_{U/J}$, $a_5^+{}_{U/J}$, $b_4^+{}_{U/J}$, $(b_4+CO)^+_{U/J}$, $(b_3+CO)^+_{U/J}$,		
$(CSA+2Li)^{2+}$					
MS^n	Precursor ion	Product ions			
		single residue losses	a, b, & c ions	x, y, & z ions	small ions
$MS^{2\,b}$	$(CSA+2Li)^{2+}$	$(CSA+ 2Li -U)^{2+**}$, $(CSA+ 2Li -U-CO)^{2+**}$			
$MS^{3\,b}$	$(CSA+ 2Li -U)^{2+}$		$(b_9+CO)^{2+**}_{U/J}$, $b9^{2+}_{U/J}$		
$MS^{4\,d}$	$(b_9+CO)^{2+}_{U/J}$		$(b_8+CO)^{2+**}_{U/J}$, $(b_7+CO)^{2+**}_{U/J}$, $a_7^{2+**}{}_{U/J}$, $a_7^{+**}{}_{U/J}$, $a_7^+{}_{U/J}$		

[a] U = N-methyl valine; mL = N-methyl leucine; J = 4(R)-4[(E)-2-butenyl]-4-methyl-L-threonine; Φ = 2-amino-butanoic acid; 112 = side chain of J: $C_7H_{12}O$.H = hydrogen; C = carbon; O = oxygen; a double asterisk superscipt (**) identifies complexes with two lithium ions complexed with a single cyclosporin A fragment. Signal intensity cutoffs (relative abundance): [b] 2%, [c] 4%, [d] 10%

Table 7.6. MS^n results for cyclosporin A complexes with with Sr^{2+} and Ca^{2+}.[a] CSA = cyclosporin A.

$(CSA+Sr-H)^+$					
Initial loss of 112, then a very complicated spectrum with many small intervals.					
$(CSA+Sr)^{2+}$					
MS^n	Precursor ion	Product ions			
		single residue losses	a, b, & c ions	x, y, & z ions	small ions
$MS^{2\,a}$	$(CSA+Sr)^{2+}$	$(CSA+Sr-U+H)^{2+}$, $(CSA+Sr-U+H-CO)^{2+}$, $(CSA+Sr-112)^{2+}$, $(CSA+Sr-112-CO)^{2+}$			
$MS^{3\,b}$	$(CSA+Sr-U+H)^{2+}$	$(CSA+Sr-112-\Phi)^{2+}$	$(b_9+H)^{2+}{}_{U/J}$, $(b_8+H+CO)^{2+}{}_{U/J}$, $(b_7+H+CO)^{2+}{}_{U/J}$	$(y_9+mNH_2)^{2+}{}_{U/J}$, $(y_9+CO+mNH_2)^{2+}{}_{U/J}$	
$(CSA+Ca-H)^+$					
Initial loss of 112, then a very complicated spectrum with many small intervals.					
$(CSA+Ca)^{2+}$					
MS^n	Precursor ion	Product ions			
		single residue losses	a, b, & c ions	x, y, & z ions	small ions
$MS^{2\,b}$	$(CSA+Ca)^{2+}$	$(CSA+Ca-U+H)^{2+}$, $(CSA+Ca-U+H-CO)^{2+}$			
$MS^{3\,c}$	$(CSA+Ca-U+H)^{2+}$		$(b_9+H)^{2+}{}_{U/J}$, $(b_8+H+CO)^{2+}{}_{U/J}$, $(b_7+H+CO)^{2+}{}_{U/J}$	$(y_9+mNH_2)^{2+}{}_{U/J}$, $(y_9+CO+mNH_2)^{2+}{}_{U/J}$	
$MS^{4\,d}$	$(b_9+H)^{2+}{}_{U/J}$		$(b_8+H+CO)^{2+}{}_{U/J}$, $(b_7+H+CO)^{2+}{}_{U/J}$		

[a] U = N-methyl valine; mL = N-methyl leucine; J = 4(R)-4[(E)-2-butenyl]-4-methyl-L-threonine; Φ = 2-amino-butanoic acid; 112 = side chain of J: $C_7H_{12}O$.H = hydrogen; C = carbon; O = oxygen . Signal intensity cutoffs (relative abunance): [b] 2%, [c] 5%, [d] 20%.

Table 7.7. MS^n results for cyclosporin A complexes with Ag^+.[a] CSA = cyclosporin A.

$(CSA+Ag)^+$					
MS^n	Precursor ion	Product ions			
		single residue losses	a, b, & c ions	x, y, & z ions	small ions
$MS^{2\,b}$	$(CSA+Ag)^+$	$(CSA+Ag-U+H)^+$, $(CSA+Ag-U+H-CO)^+$, $(CSA+Ag-112)^+$, $CSA+Ag-112-CO)^+$		$(y_9+H)^+_{Z/U}$, $(y_9+H-CO)^+_{Z/U}$	
$MS^{3\,b}$	$(CSA+Ag-U+H)^+$/ $(CSA+Ag-112)^+$	$(CSA+Ag-J+2H)^+$, $(CSA+Ag-J+2H-CO)^+$	$(b_9+H+CO)^+_{Z/U}$	$(y_7+H+J\Phi)^+_{Z/Z}$, $(x_6+H+J\Phi)^+_{Z/Z}$, $(x_6{+}{+}COH+J\Phi)^+_{Z/Z}$, $(y_6+H+J\Phi)^+_{Z/Z}$, $(x_5+H+J\Phi)^+_{Z/Z}$, $(x_5+J\Phi)^+_{Z/Z}$, $(y_5+CO+J\Phi)^+_{Z/Z}$, $(x_8+2H-CO)^+_{U/J}$, $(x_7+2H)^+_{U/J}$, $(x_7+CO+2H)^+_{U/J}$, $(y_7+2H)^+_{U/J}$, $(x_6+2H)^+_{U/J}$, $x6^+_{U/J}$, $(x_5+H)^+_{U/J}$, $(y5+H)^+_{U/J}$, $(x_5+CO+H)^+_{U/J}$, $(x_4+H)^+_{U/J}$, $(y4+H)^+_{U/J}$	

$(CSA+2Ag)^+$					
MS^n	Precursor ion	Product ions			
		single residue losses	a, b, & c ions	x, y, & z ions	small ions
$MS^{2\,b}$	$(CSA+2Ag)^+$	$(CSA+2Ag-U+H)^{2+}$, $(CSA+2Ag-U+H-CO)^{2+}$, $(CSA+2Ag-112)^{2+}$, $CSA+2Ag-112-CO)^{2+}$	$a_9{}^{2+}_{U/J}$	$(y_9+2H)^{2+}_{U/J}$, $(y_9+2H-U)^{2+}_{U/J}$	
$MS^{3\,b}$	$(CSA+2Ag-U+H)^+$/ $(CSA+2Ag-112)^+$	$(CSA+2Ag-J+2H)^{2+}$, $(CSA+Ag-J-mNH)^+$		$(y_9+2H)^{2+}_{U/J}$, $(y_9+2H-U)^{2+}_{U/J}$, $(x_9+2H-U)^{2+}_{U/J}$	$(y_9+2H)^{2+}_{U/J}$, $(y_9+2H-U)^{2+}_{U/J}$, $(x9+2H-U)^{2+}_{U/J}$

[a] U = N-methyl valine; mL = N-methyl leucine; J = 4(R)-4[(E)-2-butenyl]-4-methyl-L-threonine; Φ = 2-amino-butanoic acid; 112 = side chain of J: $C_7H_{12}O$.H = hydrogen; C = carbon; O = oxygen . Signal intensity cutoffs (relative abundance): [b] 5%.

Table 7.8. MS^n results for cyclosporin A complex with Co^{2+}. [a] CSA = cyclosporin A.[c]

$(CSA+Co-H)^+$					
MS^n	Precursor ion	Product ions			
		single residue losses	a, b, & c ions	x, y, & z ions	small ions
MS^{2} [b]	$(CSA+Co-H)^+$	$(CSA+Co-U)^+$, $(CSA+Co-H-U)^+$	$(b_9+H)^+_{U/J}$, $b9^+_{U/J}$,		
MS^{3} [c]	$(CSA+Co-U)^+$		$(b_9+H+CO)^+_{U/J}$, $(b_9+CO)^+_{U/J}$	$(y_9+H)^+_{Z/U}$, $(y_8+H-H_2O)^+_{Z/U}$, $(y_7+H-H_2O)^+_{Z/U}$	
MS^{4} [d]	$(b_9+H+CO)^+_{U/J}$		$(b_8+H+CO)^+_{U/J}$, $(b_8+H+CO-mNH_2)^+_{U/J}$, $(b_8+H+mNH_2)^+_{U/J}$, $(b_8-Z+H+CO)^+_{U/J}$, $(b_8-Z+H+CO-mNH_2)^+_{U/J}$, $(b_8-Z+H+mNH_2)^+_{U/J}$		
$(CSA+Co)^{2+}$					
MS^n	Precursor ion	Product ions			
		single residue losses	a, b, & c ions	x, y, & z ions	small ions
MS^{2} [b]	$(CSA+Co)^{2+}$	$(CSA+Co-U+H)^{2+}$, $(CSA+Co-U+H-CO)^{2+}$	$b_9^{2+}{}_{U/J}$, $(a_9-H)^{2+}_{U/J}$		
MS^{3} [c]	$(CSA+Co-U+H)^{2+}$		$(b_9+H)^{2+}_{U/J}$, $(a_9-H)^{2+}_{U/J}$, $(a_8-H)^{2+}_{U/J}$, $(b_8+H)^+_{U/J}$, $(b_6+H)^+_{U/J}$, $(b_5+H)^+_{U/J}$	$(y_9+mNH_2)^{2+}_{U/J}$, $(y_9+CO+mNH_2)^{2+}_{U/J}$	$(VZ-2H)^+$
MS^{4} [e]	$(b_9+H)^{2+}_{U/J}$		$(b_8+H)^{2+}_{U/J}$, $(b_8+H)^+_{U/J}$		

[a] U = N-methyl valine; mL = N-methyl leucine; J = 4(R)-4[(E)-2-butenyl]-4-methyl-L-threonine; Φ = 2-amino-butanoic acid; 112 = side chain of J: $C_7H_{12}O$.H = hydrogen; C = carbon; O = oxygen . Signal intensity cutoffs (relative abundance): [b] 2%, [c] 5%, [d] 10%, [e] 20%

Table 7.9. MS^n results for cyclosporin A complexes with Ni^{2+}.[a] CSA = cyclosporin A.

$(CSA+Ni-H)^+$					
MS^n	Precursor ion	Product ions			
		single residue losses	a, b, & c ions	x, y, & z ions	small ions
MS^{2} [b]	$(CSA+Ni-H)^+$	$(CSA+Ni-U)^+$			
MS^{3} [c]	$(CSA+Ni-U)^+$		$(b_9+H)^+_{U/J}$, $a9^+_{U/J}$,		
MS^{4} [d]	$(b_9+H)^+_{U/J}$		$(b_8+H-mNH_2)^+_{U/J}$, $(b_8+H+mNH_2)^+_{U/J}$, $(b_8-Z+H+CO)^+_{U/J}$, $(b_8-Z+H+CO-mNH_2)^+_{U/J}$, $(b_8-Z+H+mNH_2)^+_{U/J}$	$(y_9+2H)^+_{Z/U}$, $(y_8+2H-H_2O)^+_{Z/U}$, $(y_7+H-H_2O)^+_{Z/U}$, $(y_7+H-CO-H_2O)^+_{Z/U}$	
$(CSA+Ni)^{2+}$					
		Product ions			
MS^n	Precursor ion	single residue losses	a, b, & c ions	x, y, & z ions	small ions
MS^{2} [b]	$(CSA+Ni)^{2+}$	$(CSA+Ni-H_2O)^{2+}$, $(CSA+Ni-CO)^{2+}$, $(CSA+Ni-U)^{2+}$,	$(CSA+Ni-H_2O)^{2+}$, $(CSA+Ni-CO)^{2+}$, $b_{10}{}^{2+}_{U/J}$, $b_9{}^{2+}_{U/J}$, $a_9{}^{2+}_{U/J}$		
MS^{3} [b]	$(CSA+Ni-U)^{2+}$		$a_{10}{}^{2+}_{U/J}$, $b_9{}^{2+}_{U/J}$, $a_9{}^{2+}_{U/J}$, $b_8{}^{2+}_{U/J}$, $(b_8+mNH_2)^+_{U/J}$, $b_8{}^{+}_{U/J}$, $b_6{}^{+}_{U/J}$		
MS^{4} [c]	$b_9{}^{2+}_{U/J}$,		$b_8{}^{2+}_{U/J}$, $b_8{}^{+}_{U/J}$, $(b_8+CO)^+_{U/J}$		
MS^{5} [e]	$b_8{}^{2+}_{U/J}$		$a_8{}^{2+}_{U/J}$, $b_7{}^{2+}_{U/J}$, $b_6{}^{2+}_{U/J}$		

[a] U = N-methyl valine; mL = N-methyl leucine; J = 4(R)-4[(E)-2-butenyl]-4-methyl-L-threonine; Φ = 2-amino-butanoic acid; 112 = side chain of J: $C_7H_{12}O$.H = hydrogen; C = carbon; O = oxygen . Signal intensity cutoffs (relative abundance):[b] 2%, [c] 5%, [d] 10%, [e] 20%

Table 7.10. MS^n results for cyclosporin A complexes of Pb^{2+}.[a] CSA = cyclosporin A.

MS^n	Precursor ion	Product ions			
		single residue losses	a, b, & c ions	x, y, & z ions	small ions
MS^{2} [b]	$(CSA+Pb-H)^+$	$(CSA+Pb-H-U)^+$			
MS^{3} [b]	$(CSA+Pb-H-U)^+$		$b_9^+{}_{U/J}$, $b_8^+{}_{U/J}$, $a_8^+{}_{U/J}$		
MS^{4} [c]	$b_9^+{}_{U/J}$		$(a_7+H)^+{}_{U/J}$, $(b_9-b_1+H)^+{}_{U/J}$, $(b_8-b_1+H)^+{}_{U/J}$		
$(CSA+Pb)^{2+}$					
MS^n	Precursor ion	Product ions			
		single residue losses	a, b, & c ions	x, y, & z ions	small ions
MS^{2} [b]	$(CSA+Pb)^{2+}$	$(CSA+Pb-U)^{2+}$	$(a_9+H)^+{}_{U/J}$		
MS^{3} [b]	$(CSA+Pb-U)^{2+}$, $(CSA+Pb-H-U)^+$,	$b_9^+{}_{U/J}$, $(a_9+H)^+{}_{U/J}$, $c_9^+{}_{U/J}$, $c_8^+{}_{U/J}$,			$(ZV+H)^+$

[a] U = N-methyl valine; mL = N-methyl leucine; J = 4(R)-4[(E)-2-butenyl]-4-methyl-L-threonine; Φ = 2-amino-butanoic acid; 112 = side chain of J: $C_7H_{12}O$.H = hydrogen; C = carbon; O = oxygen . Signal intensity cutoffs (relative abundance):[b] 2%, [c] 5%

Figure 7.5. Mass spectra for complexes of (cyclosporin A +Ni)$^{2+}$: A) MS^2, B) MS^3, C) MS^4, D) MS^5. CSA = cyclosporin A, U = N-methyl valine, Z = N-methyl leucine, J = 4(R)-4[(E)-2-butenyl]-4-methyl-L-threonine, and mNH_2 = methyl amine

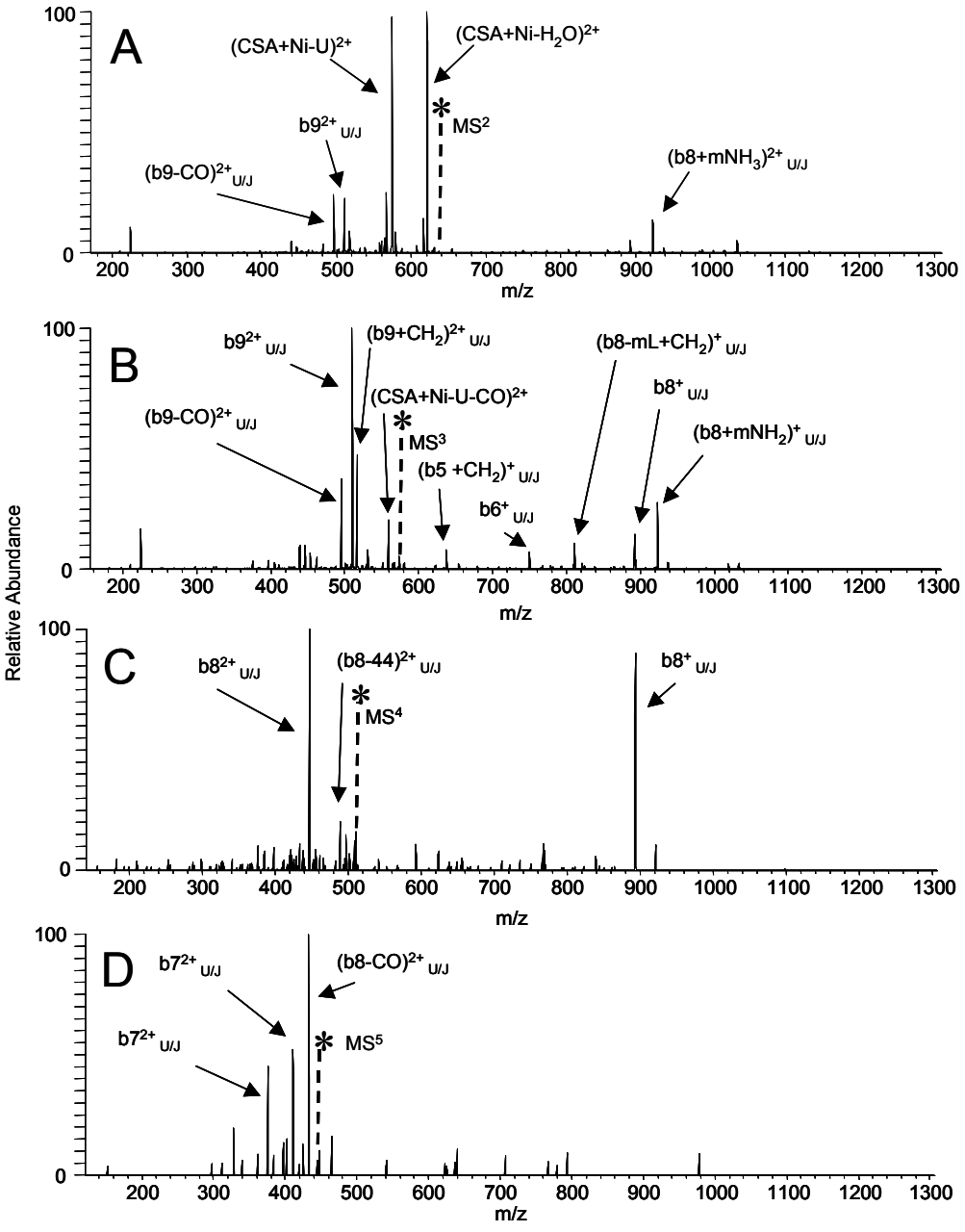

Scheme 7.2. A) Product ions formed by MS^n of protonated and lithium and nickel complexed cyclosporin A. Lines between letters represent cleavages and an asterisk (*) indicates site of ring cleavage. B) Depiction of preferred location of metal binding and region of proton mobility.

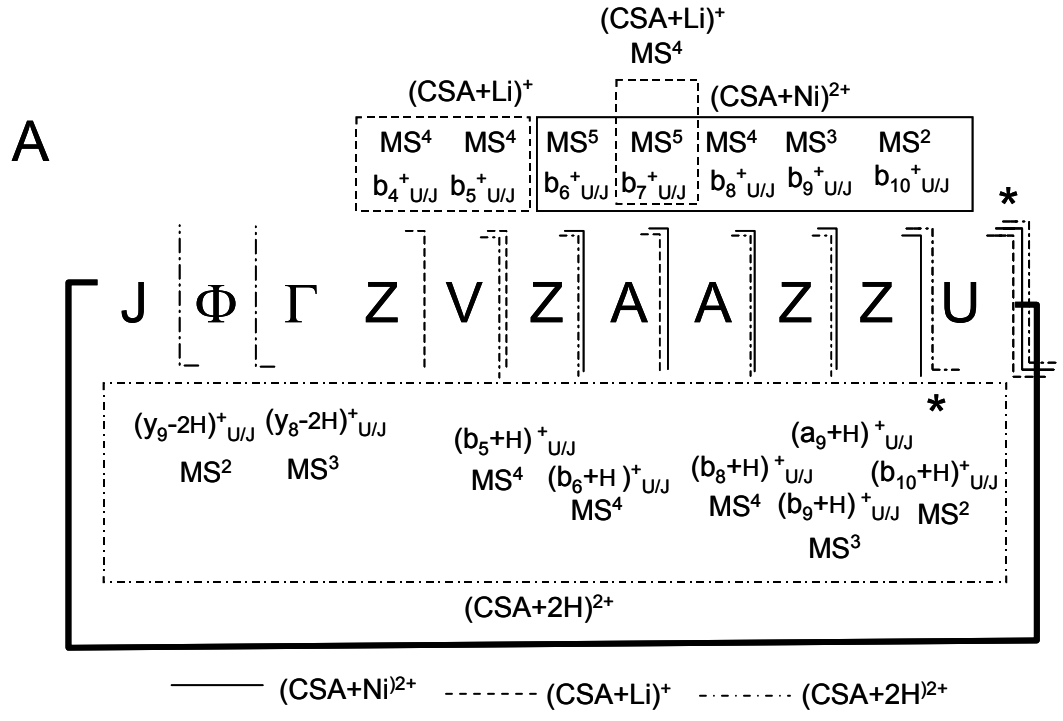

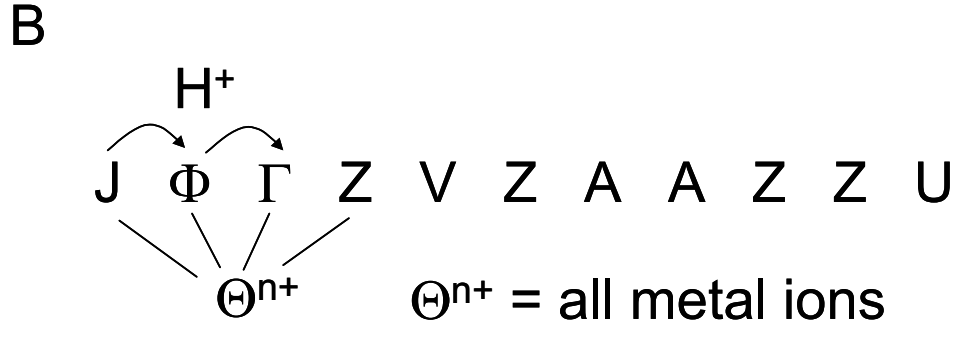

$(y_8\text{-}2H)^{+}_{Z/U}$, and $y_5{}^{+}_{Z/U}$ ions. Most of these are not convensional a-c or x-z ions, but most of them show increments in fragment mass relative to the (precursor - 112)$^{2+}$ ion that correspond to the correct sequence and residue masses. The 1.0 Th shift could be problematic and could use complimentary confirming data. In addition, most of the ions observed in the MS^n experiment do not correspond to these simple b or y ions. In contrast, for (CSA+Ni)$^{2+}$, with MS^n results shown in Table 9, the percentage of simple b or y ions in the spectra increase with increasing cycles of MS^n experiments. Also, as can be seen in the spectra in Figure 5, besides the small losses such as H_2O and CO from the precursor ion, one or two b ions are the major signals in each spectrum in each round of MS^n. For MS^2 to MS^4 product ion spectra (Figures 5A to 5C), disregarding loss of H_2O from the precursor ion, the most abundant signal is due to a b ion, resulting from the loss of a single residue. In the MS^5 spectrum (Figure 5D), two peaks corresponding to the $b_6{}^{2+}_{U/J}$ and $b_7{}^{2+}_{U/J}$ ions are nearly identical in intensity and have significantly greater intensities than surrounding ions signal, except for the loss of CO from the precursor ion. Along with the $b_8{}^{+}_{U/J}$ and $b_6{}^{+}_{U/J}$ ions in the MS^3 and MS^4 spectra, the doubly charged b ions, five sequentially arranged residues are easily identified in order from (CSA-U)$^{2+}$ (which can be designated as $b_{10}{}^{2+}_{U/J}$ and $y_{10}{}^{2+}_{U/J}$, $b_9{}^{2+}_{U/J}$, $b_8{}^{2+}_{U/J}$, $b_7{}^{2+}_{U/J}$, and $b_6{}^{2+}_{U/J}$ ions. Together the MS^n data for protonated cyclosporin A and (CSA+Ni)$^{2+}$ can be used to identify eight of the eleven residues in order, ZAAZZUJΦ, whereas the singly and doubly protonated CSA data together only identifies five, ZZUJΦ.

However, the identification of Φ is not wholly acceptable, as with the loss of 112 Da, because an increment of 183 Th, rather than 185 Th, corresponding to the true molecular weight of Φ. For MS^n of $(CSA+Li)^+$ (Table 5), although simple $b_{10}{}^+{}_{U/J}$, $b_9{}^+{}_{U/J}$, $b_8{}^+{}_{U/J}$, and $b_6{}^+{}_{U/J}$ ions are not observed in the MS^n spectra, $b_5{}^+{}_{U/J}$, $a_5{}^+{}_{U/J}$, and $b_4{}^+{}_{U/J}$ ions are present. Combining the protonated and nickel and lithium complexed CSA data, nine of the eleven CSA residues could be identified in order: VZAAZZUJΦ, with Φ identification still less than ideal.

For the cyclosporin A complexes with other metal ions, there is either a loss of 112 Da from the $(CSA+2H)^{2+}$ precursor in the MS^2 spectrum, which creates ambiguity between V and the side chain of J, or fewer diagnostic ions are observed than for $(CSA+2H)^{2+}$ and $(CSA+Ni)^{2+}$ and they do not contribute much to further the sequence analysis of CSA. Also, unlike with $(CSA+2H)^{2+}$, along with the 112 Da loss from the original precursor ion, many of the other a-c and x-z ions are shifted to 1.0 Th higher from what would be expected if the 112 Da loss corresponded to V, suggesting the loss in these cases is indeed from the side chain of J.

The ring cleavage at the U/J bond is nearly universal for all cation complexes and product ions with three-to-five residues lost without loss of the metal ion are common. These results make it likely that the preferred location of binding for the metal ions tested is in the region of the JΦΓZ sequence, where Γ = N-methyl glycine (aka sarcosine). This scenario is depicted in Scheme 2. Most

likely, the metal ions are mainly coordinated with the heteroatoms (N and O) of J and Φ. The proton is probably mobile, allowing formation of y-ions in this region.

7.3.2 Depsipeptides: Valinomycin and Enniatin A_1

7.3.2.1 Valinomycin

Figure 6 indicates the results for MS^2, MS^3, and MS^4 experiments on the $(valinomycin + H + H_2O)^+$ ions (protonated valinomycin without a water adduct was not observed) and the MS^2 experiment on the $(valinomycin + Na)^+$ ion. Data for further rounds of MS^n experiments from n = 3 to 10 for the $(valinomycin + Na)^+$ ion are shown in Table 11. The dominant protonated peak in the MS^1 precursor ion spectrum for the solution of valinomycin (abbreviated VM) in methanol with 2% glacial acetic acid had a water adduct, $(VM+H+H_2O)^+$. Thus, greater than 90% of the signal intensity in the MS^2 was due to the $(VM+H)^+$ from loss of the water adduct, so the spectra for this reaction is not explicitly shown, but the loss of water is indicated in Figure 6A along with the MS^3 data. In the MS^3 spectrum, 90% of the signal intensity resulting from CAD of the $(VM+H)^+$ ion is due to the $(VM+H-CO)^+$ ion. CAD of this $(VM+H-CO)^+$ ion in the MS^4 experiment results in ions with no less than two residue losses from the precursor ion at 1083 Th. Most of the other peaks in the MS^4 spectrum are due to losses of various possible and often isobaric sequences of two to eight residues. Because of the complexity of the spectrum, the

Figure 7.6. Mass spectra for A) MS^2 and MS^3 of (valinomycin + H)$^+$, B) MS^4 of (valinomycin + H)$^+$, C) MS^2 of (valinomycin + H)$^+$. VM = valinomycin, X = hydroxy valine, and Λ = lactic acid. An asterisk (*) identifies the precursor ion.

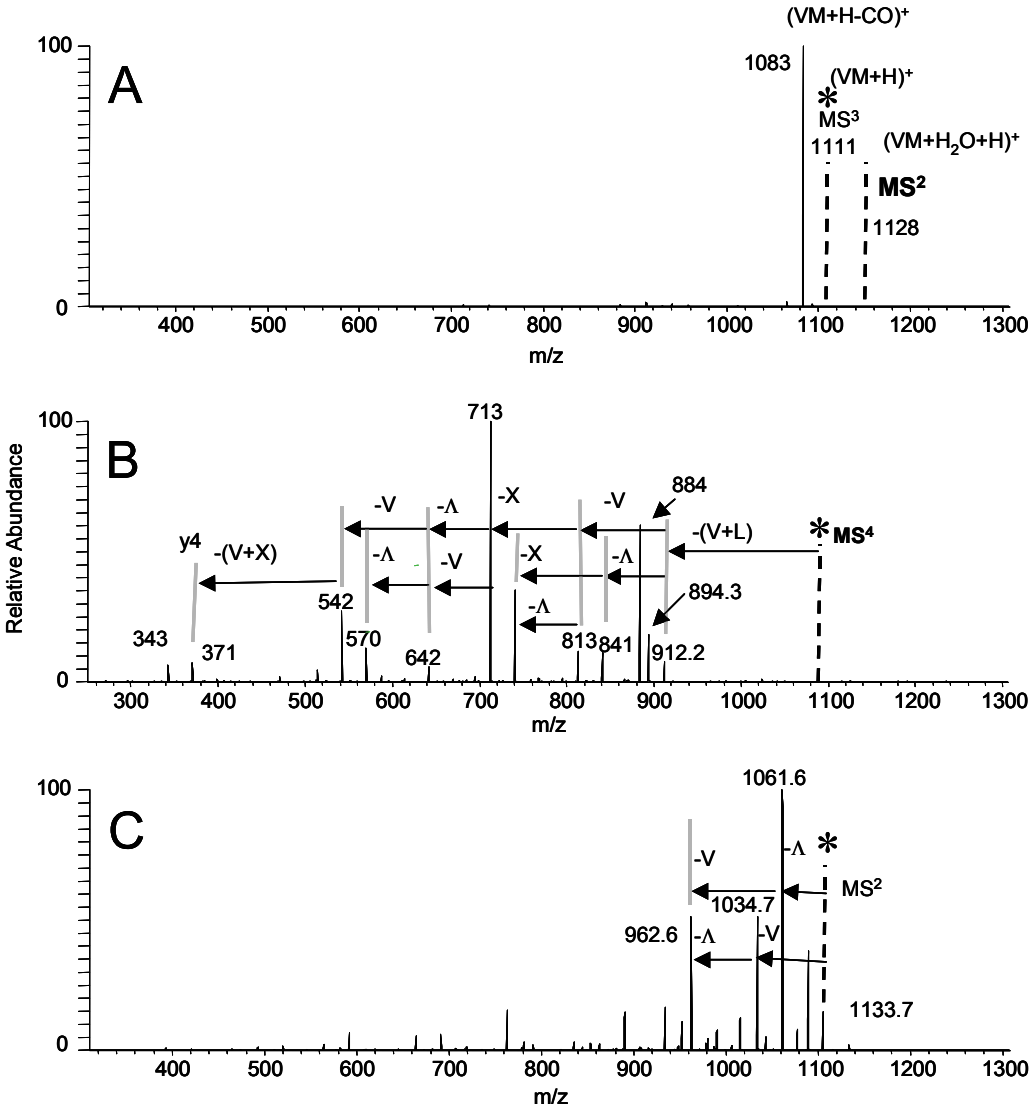

Table 7.11. MS^n results for valinomycin complexes with Na^+ and Pb^{2+} for peaks over 10% relative abundance (singly charged precursors only).[a]

$(VM+Na)^+$		
MS^n	Precursor ion [a]	Remaining fragment ions[a]
MS^3	$(VM+Na-V)^+$	$b_{10}{}^+{}_{V/\Lambda}$, $b_9{}^+{}_{V/\Lambda}$, $(VM+Na-V-CO)^+$
MS^4	$b_{10}{}^+{}_{V/\Lambda}$	$b_9{}^+{}_{V/\Lambda}$, $b_8{}^+{}_{V/\Lambda}$, $(VM+Na-VXV\Lambda+H_2O)^+$
MS^5	$b_9{}^+{}_{V/\Lambda}$	$b_8{}^+{}_{V/\Lambda}$
MS^6	$b_8{}^+{}_{V/\Lambda}$	$b_7{}^+{}_{V/\Lambda}$, $b_6{}^+{}_{V/\Lambda}$
MS^7	$b_7{}^+{}_{V/\Lambda}$	$b_6{}^+{}_{V/\Lambda}$
MS^8	$b_6{}^+{}_{V/\Lambda}$	$b_5{}^+{}_{V/\Lambda}$
MS^9	$b_5{}^+{}_{V/\Lambda}$	$b_4{}^+{}_{V/\Lambda}$
MS^{10}	$b_4{}^+{}_{V/\Lambda}$	$b_3{}^+{}_{V/\Lambda}$
$(VM+Pb-H)^+$		
MS^n	Precursor ion [a]	Remaining fragment ions[a]
MS^2	$(VM+Pb-H)^+$	$(b_{10}-H)^+{}_{V/X}$, $(b_{10}-H)^+{}_{V/\Lambda}$, $(b_{10}+OH)^+{}_{V/X}$, $(b_{10}+OH)^+{}_{V/L}$, $(b_8-H)^+{}_{V/X}$, $(b_8-H)^+{}_{V/\Lambda}$, $(b_8+OH)^+{}_{V/X}$, $(b_8+OH)^+{}_{V/\Lambda}$
MS^3	$(b10+OH)^+{}_{V/\Lambda}$	$(b_8+OH)^+{}_{V/L}$, $(b_6+OH)^+{}_{V/\Lambda}$, $(b_4+OH)^+{}_{V/\Lambda}$
MS^4	$(b_6+OH)^+{}_{V/\Lambda}$	$(V\Lambda+PbOH)^+$, $(VX+Pb+OH)^+$, $(V+Pb+OH)^+$
MS^5	$(V+Pb+OH)^+$	$(V+Pb-H)^+$

[a] VM = Valinomycin = cyclo[$(VXVL)_3$]; X = Hydroxy isovaline; Λ = Lactic acid; V = Valine; H = hydrogen; C = carbon; O = oxygen.

lowering of the average peak intensity of the spectrum, the lack of a peptide due to a single residue loss, and the low relative intensity of the peptide fragment ion with the most residues, further rounds of MS^n were not feasible.

The sodiated valinomycin complex signal showed no solvent adducts and was the dominant peak in the spectrum. For first round of MS^n on this ion (MS^2), it is observed that the dominant signal is due to loss of a single lactic acid residue from the precursor ion. The next three most dominant peaks are due to fragments with losses of one to two residues. In additional rounds of MS^n from n = 3 to 10, the spectra quickly become even more simplified and for n =4 to 10, only one or two ions are present with one always due to the loss of an additional residue in the correct sequence. Whether the fragments are b-type or y-type ions can be determined from the surrounding peaks due to NH_3, H_2O, and CO gains or losses relative to residue losses. Although the MS^n information provided in Table 10 refer mostly to b ions, it is important to note that according to similar data not shown, similar MS^n spectra with y ions could also be obtained. This data is similar to that obtained by Gross and co-workers for $(VM+Li)^+$ complex [38].

Since there are twelve residues in the peptide and only nine consecutive CAD experiments can be carried out, only nine residues in sequence could be determined, leaving three remaining. For valinomycin, complexation with lithium ion was observed to produce nearly identical results. Analysis with divalent alkaline earth metal ions and transitional metal ions such as nickel(II), cobalt(II),

and lead(II) predominantly effect residue losses from the precursor ion in increments of two residue units. Thus, as shown in the data in Table 11 for MS^2 through MS^5 for $(VM+Pb-H)^+$ ion, residues are lost in larger increments than for the monovalent metal or protonated complexes, and produce fragments that are fewer but valuable. By comparison of the MS^n data for lead and sodium complexes, missing residues from the sodium experiments can be identified. Unfortunately, when only the last two or three residues of a peptide remain, the residue loss often does not continue in the same order, removing residues from the opposite end of the peptide fragment. Thus, it was determined that for depsipeptides such as valinomycin, as well as for ennianatin A_1, as will be discussed below, the identity, but not the complete sequence can be determined with a high degree of certainty. Another caveat with the analysis of the MS^n spectra of VM with divalent metal ions is that the cleavages are either c or x ions, with cleavage only at the ester bonds. This also creates an ambiguity that does not allow us to determine whether the ions are c or x ions. When the high tendency for lead ion to complex with hydroxide is considered, it is also feasible that the terminal hydroxy group of the c or x ion is transferred to the lead ion forming b or y ions with $PbOH^+$ as the cation. MS^2 spectra for $(VM+Ag)^+$ were similar to the alkali monovalent ions, but dozens of ions present with signal intensities of 5-10% relative abundance, and not corresponding to a-c or x-z ions, obscured the spectrum.

7.3.2.2 Enniatin A_1

Tables 12 compares the results for MS^n experiments performed on protonated enniatin A_1, which was observed only with a water adduct, and sodium and lead complexes of enniatin A_1 of the form $(EA+Na)^+$ and $(EA+Pb-H)^+$. The results are similar to those obtained with valinomycin. The initial protonated complex had a water adduct and the loss of the water was the only significant reaction in the MS^2 experiment. For analysis of the solution of enniatin A_1 in 2% glacial acetic acid, sodium and potassium complexes dominated the MS^1 spectrum, as they did for valinomycin. For the peptide solution with added sodium ion, sodiated complex signal dominated the MS^1 spectrum. In addition, for the sodiated complex, the increasing simplification of fragment data with increasing rounds of MS^n again proceeds to signals that are fewer, but are the most useful for sequence determination. Since there are only six residues in enniatin A_1, sequential rounds of MS^n can be conducted for each individual residue losses from the precursor ion. By this method, the sequence of the first four residues can be correctly determined, but when only two residues remain, the sodium ion can be lost, and the last remaining residue ion is out of sequence order, although the identities of the last two residues can be narrowed down and speculated on from the final data when small molecule losses such as CO are considered, the unit residue mass of the last two separate residues is not directly obtainable from the spectral data.

Table 7.12. MS^n results for enniatin A_1 complexes with H^+ and Na^+ for peaks over 5% relative abundance.[a]

$(EA+H+H_2O)^+$		
MS^n	Precursor ion	Remaining fragment ions
MS^2	$(EA+H+H_2O)^+$	$(EA-H_2O)^+$
MS^3	$(EA-H_2O)^+$	$(XZXUX+H)^+$, $(XUXZX+H)^+$, $(XZXZX+H)^+$, $(XZXU+H)^+$, $(XUXZ+H)^+$, $(XZXZ+H)$, $(XZXZ-H_2O+H)$
MS^4	$(XZXZX+H)^+$	$(XZXZX-CO+H)^+$, $(XZX+X+H)^+$, $(XZXZ+H)^+$, $(XZX+H)^+$, $(ZX+H)^+$, $(ZX-H_2O+H)^+$
MS^5	$(ZX-H_2O+H)^+$	$(Z-CO+H)^+$
(Enniatin A_1+Na)$^+$		
MS^n	Precursor ion[b]	
MS^2	(Enniatin A_1+Na)$^+$	$(XZXZX+Na)^+$, $(XZXUX+Na)^+$, $(XUXZX+Na)^+$, $(XZXZ+Na)^+$, $(XZXU+Na)^+$, $(XUXZ+Na)^+$, $(XZX+Na)^+$, $(XUX+Na)^+$
MS^3	$(XZXUX+Na)^+$, $(XUXZX+Na)^+$	$(XZXU+Na)^+$, $(XUXZ+Na)^+$, $(XZX+Na)^+$, $(XUX+Na)^+$
MS^4	$(XZXU+Na)^+$, $(XUXZ+Na)^+$	$(XZX+Na)^+$
MS^5	$(XZX+Na)^+$	$(XZ+Na)^+$, $(XZ+Na-H_2O)^+$, $(XZ+H-H_2O)^+$, $(XZ+H-H_2O-CO)^+$
MS^6	$(XZ+Na-H_2O)^+$	$(XZ+Na-H_2O-CO)^+$
MS^7	$(XZ+Na-H_2O-CO)^+$	$(Z+H-CO)^+$
(Enniatin A_1+Pb-H)$^+$		
MS^2	(Enniatin A_1+Pb-H)$^+$	$(XZXZ+Pb+OH)^+$, $(XZXU+Pb+OH)^+$, $(XUXZ+Pb+OH)^+$, $(XZX+Pb+OH)^+$, $(XUX+Pb+OH)^+$, $(XZ+Pb+OH)^+$, $(XU+Pb+OH)^+$, $(Z+Pb+OH+H_2O)^+$, $(U+Pb+OH+H_2O)^+$
MS^3	$(XZXZ+Pb+OH)^+$	$(XZX+Pb+OH)^+$, $(XZ+Pb+OH)^+$, $(Z+Pb+OH+H_2O)^+$
MS^4	$(XZX+Pb+OH)^+$	$(XZ+Pb+OH)^+$, $(Z+Pb+OH+H_2O)^+$, $(X+Pb+OH)^+$, $(XZ+H)^+$
MS^5	$(XZ+Pb+OH)^+$	$(Z+Pb+OH+H_2O)^+$
MS^3	$(XZXU+Pb+OH)^+$, $(XUXZ+Pb+OH)^+$	$(XZX+Pb+OH)^+$, $(XUX+Pb+OH)^+$, $(XZ+Pb+OH)^+$, $(XU+Pb+OH)^+$, $(Z+Pb+OH)^+$, $(U+Pb+OH)^+$
MS^4	$(XZX+Pb+OH)^+$	$(XZ+Pb+OH)^+$, $(XZ+Pb+OH-CO)^+$, $(Z+Pb+OH+H_2O)^+$, $(X+Pb+OH)^+$, $(XZ+H)^+$
MS^4	$(XUX+Pb+OH)^+$	$(XU+Pb+OH)^+$, $(XU+Pb+OH-CO)^+$, $(U+Pb+OH+H_2O)^+$, $(X+Pb+OH)^+$, $(XU+H)^+$

[a] Enniatin A_1 = EA = cyclo(XZXZXU); X = Hydroxy isovaline; U = N-methyl valine; Z = N-methyl isoleucine; H = hydrogen; C = carbon; O = oxygen.

MS^n analysis with the lithium ion complex of enniatin A_1 was similar to the analysis with sodium ion, but the higher charge density of the lithium versus sodium ion caused water adducts to form during ion trapping of isolated precursor ions and several subsequent product ions, especially after three residues where lost from the original $(EA + Li)^+$ ion. For larger alkali ions such as potassium and rubidium, much poorer signal intensities for product ions were obtained compared to the precursor ion because of simple ejection of the metal ion during CAD leaving the peptide portion of the precursor ion intact and neutral in charge. This observation was common to valinomycin with larger alkali metals as well as other cyclic peptides studied.

Lead again showed preferential loss of two residues from the precursor ion $(EA+Pb-H)^+$, leaving the c/x ions $(XZXZ+Pb+OH)^+$, and the isobaric $(XUXZ+Pb+OH)^+$ and $(XZXU+Pb+OH)^+$. Beyond this double residue loss, increasing mass losses were in one-residue increments down to $(XZ+Pb+OH)^+$ and $(XU+Pb+OH)^+$. CAD of these last ions produced $(Z+Pb+OH+H_2O)^+$ and $(U+Pb+OH+H_2O)^+$, with an adventitious water molecule from the trap environment adsorbed. Further CAD resulted in loss of the water quickly followed by the ion adsorbing another adventitious water, such that CAD resulting in the appearance of only the precursor ion in the product ion spectrum. CAD of $(XZX+Pb+OH)^+$ or $(XUX+Pb+OH)^+$ produced the $(XZ+Pb+OH)^+$ or $(XU+Pb+OH)^+$ ions, respectively and, additionally, the $(X+Pb+OH)^+$ ion and the $(XZ+H)^+$ or $(XU+H)^+$ ions.

Therefore, CAD of the $(XZX+Pb+OH)^+$ or $(XUX+Pb+OH)^+$ ions produced $PbOH^+$ complexes with loss increments corresponding to the correct sequential order (-X as well as –XZ and -XU), while CAD of the $(XZ+Pb+OH)^+$ or $(XU+Pb+OH)^+$ ions resulted in loss of X, which deviates from the sequence order. Compared to the enniatin A_1 complexes with lead, complexes with metal ions with higher charge densities such as calcium, strontium, nickel(II), and cobalt(II) showed greater problems with water adducts, which began forming after loss of the first two residues, XL or XU. Complexes of enniatin A_1 with silver showed problems similar to those with $(VM+Ag)^+$.

7.3.3 Lipopeptides: Iturin A and Surfactin

7.3.3.1 Iturin A

Tables 13-15 show results of MS^n experiments for Iturin A (abbreviated IA) complexes $(IA + H)^+$, $(IA + Ag)^+$, and $(IA + Sr - H)^+$, respectively. Scheme 3 is a depiction of these results. The Greek letter 'Ψ' is used to represent the '3-amino-12-methyl tetradecanoic acid' fatty acid residue of iturin A. Figure 7 compares MS^2 spectra for CAD of these three ions. From the MS^2 spectra shown in Figure 7, it is clear that several of the product ion signals that result from the loss of one residue from the precursor ion have greater relative abundances in the MS^2 spectra for $(IA + Ag)^+$ and $(IA + Sr - H)^+$ compared to $(IA + H)^+$ (the absolute intensities of the

Table 7.13. MS^n results for analysis of $(iturin\ A+H)^+$ complex. IA = iturin A.

MS^n	Precursor ion	Product ions			
		single residue losses	a, b, & c	x, y, & z	small ions
$MS^{2\,b}$	$(IA+H)^+$	$(IA-P)^+$, $(IA-N)^+$, $(IA-Q)^+$	$b_6^+{}_{N/S}$, $b_5^+{}_{N/S}$, $b_6^+{}_{Q/P}$, $b_5^+{}_{Q/P}$, $c_6^+{}_{N/Q}$	$y_6^+{}_{Q/P}$, $y_5^+{}_{Q/P}$	
$MS^{3\,b}$	$b_5^+{}_{Q/P}$		$(b_5\text{-}b_1)^+{}_{Q/P}$, $(b_4\text{-}b_1)^+{}_{Q/P}$, $(b_4\text{-}b_2)^+{}_{Q/P}$, $(a_4\text{-}b_2)^+{}_{Q/P}$,		$(\Psi+H)^+$
$MS^{3\,c}$	$b_7^+{}_{N/S}$ / $b_7^+{}_{Q/P}$		$b_6^+{}_{Q/P}$	$y_6^+{}_{N/Q}$	
$MS^{3\,c}$	$b_6^+{}_{N/S}$		$b_6^+{}_{N/S}$, $b_5^+{}_{N/S}$, $b_4^+{}_{N/S}$, $b_3^+{}_{N/S}$, $b_2^+{}_{N/S}$		

[a] Ψ = 3-amino-12-methyl tetradecanoic acid; Signal intensity cutoffs (relative abundance):[b] 1%,
[c] 10%.

Table 7.14. MS^n results for analysis of $(iturin\ A+Ag)^+$ complex. IA = iturin A.

MS^n	Precursor ion	Product ions			
		single residue losses	a, b, & c ions	x, y, & z ions	small ions
$MS^{2\,b}$	$(IA+Ag)^+$	$(IA+Ag\ -Q)^+$, $(IA+Ag\ -S)^+$, $(IA+Ag\ -Q+NH_3)^+$, $(IA+Ag\ -Y)^+$	$b_6^+{}_{Q/P}$, $a_6^+{}_{Q/P}$, $b_5^+{}_{Q/P}$, $b_5^+{}_{N/S}$, $(IA+Ag\ -NP/PN)^+$, $(b_6\text{-}b_1)^+{}_{Q/P}$,	$y_6^+{}_{N/Y}$, $y_5^+{}_{N/Y}$, $y_5^+{}_{N/Q}$, $y_4^+{}_{N/Q}$, $y_5^+{}_{Q/N}$	
$MS^{3\,c}$	$(IA-Q)^+$		$(IA+Ag\ -Q\text{-}NH_3)^+$, $(IA+Ag\ -Q\text{-}CO)^+$, $(IA+Ag\ -Q\text{-}CO\text{-}NH_3)^+$, $b_6^+{}_{Q/P}$, $a_6^+{}_{Q/P}$, $(b_6\text{-}NH_3)^+{}_{Q/P}$, $b_5^+{}_{Q/P}$,	$y_6^+{}_{N/Q}$, $y_5^+{}_{N/Q}$	
$MS^{4\,d}$	$b_6^+{}_{Q/P}$		$(b_6\text{-}NH_3)^+{}_{Q/P}$, $a_6^+{}_{Q/P}$, $b_5^+{}_{Q/P}$		
$MS^{4\,d}$	$b_5^+{}_{Q/P}$		$(b_5\text{-}NH_3)^+{}_{Q/P}$, $a_5^+{}_{Q/P}$, $(a_5\text{-}NH_3)^+{}_{Q/P}$, $b_4^+{}_{Q/P}$, $a_4^+{}_{Q/P}$, $(b_4\text{-}b_1)^+{}_{Q/P}$, $b_2^+{}_{Q/P}$		

[a] Ψ = 3-amino-12-methyl tetradecanoic acid; Signal intensity cutoffs (relative abundance):[b] 5%, [c] 10%,. [d] 20%.

Table 7.15. MS^n results for analysis of $(iturin\ A+Sr-H)^+$ complex. IA = iturin A.

MS^n	Precursor ion	Product ions	
		single residue losses	x, y, & z ions
$MS^{2\ b}$	$(IA+Sr-H)^+$	$(IA+Sr-H-P)^+$, $(IA+Sr-H-S-NH_3)^+$, $(IA+Sr-2H-N)^+$, $(IA+Sr-H-S-NH_3)^+$	${y_6}^+_{P/N}$, ${y_5}^+_{P/N}$, $(z_5-Y)^+_{P/N}$,
$MS^{3\ c}$	$(IA+Sr-2H-N)^+$	$(IA+Sr-2H-N-NH_3)^+$	${b_6}^+_{N/Y}$, ${y_6}^+_{P/N}$, ${y_5}^+_{P/N}$, $(y_4+NH_3)^+_{P/N}$, ${y_3}^+_{P/N}$
$MS^{4\ c}$	${y_5}^+_{P/N}$		${z_5}^+_{P/N}$, ${y_4}^+_{P/N}$, ${y_3}^+_{P/N}$
$MS^{5\ c}$	${y_3}^+_{P/N}$		${z_3}^+_{P/N}$, ${y_2}^+_{P/N}$, $(y_2+NH_3)^+_{P/N}$
$MS^{3\ c}$	$(IA+Sr-H-S-NH_3)^+$		${z_6}^+_{N/S}$, ${z_4}^+_{N/S}$
$MS^{4\ c}$	${z_6}^+_{N/S}$		${y_5}^+_{N/S}$, ${z_4}^+_{N/S}$, ${y_3}^+_{N/S}$
$MS^{5\ c}$	${z_4}^+_{N/S}$		$(y_3+CO-2H)^+$, ${y_3}^+_{N/S}$, $(y_3-y_1)^+_{N/S}$

[a] Ψ = 3-amino-12-methyl tetradecanoic acid; Signal intensity cutoffs (relative abundance): [b] 5%, [c] 10%.

Scheme 7.3. A) Product ions formed by MS^n of A) protonated and B) silver and C) strontium complexed iturin A. Lines between letters represent cleavages and an asterisk (*) indicates site of ring cleavage.

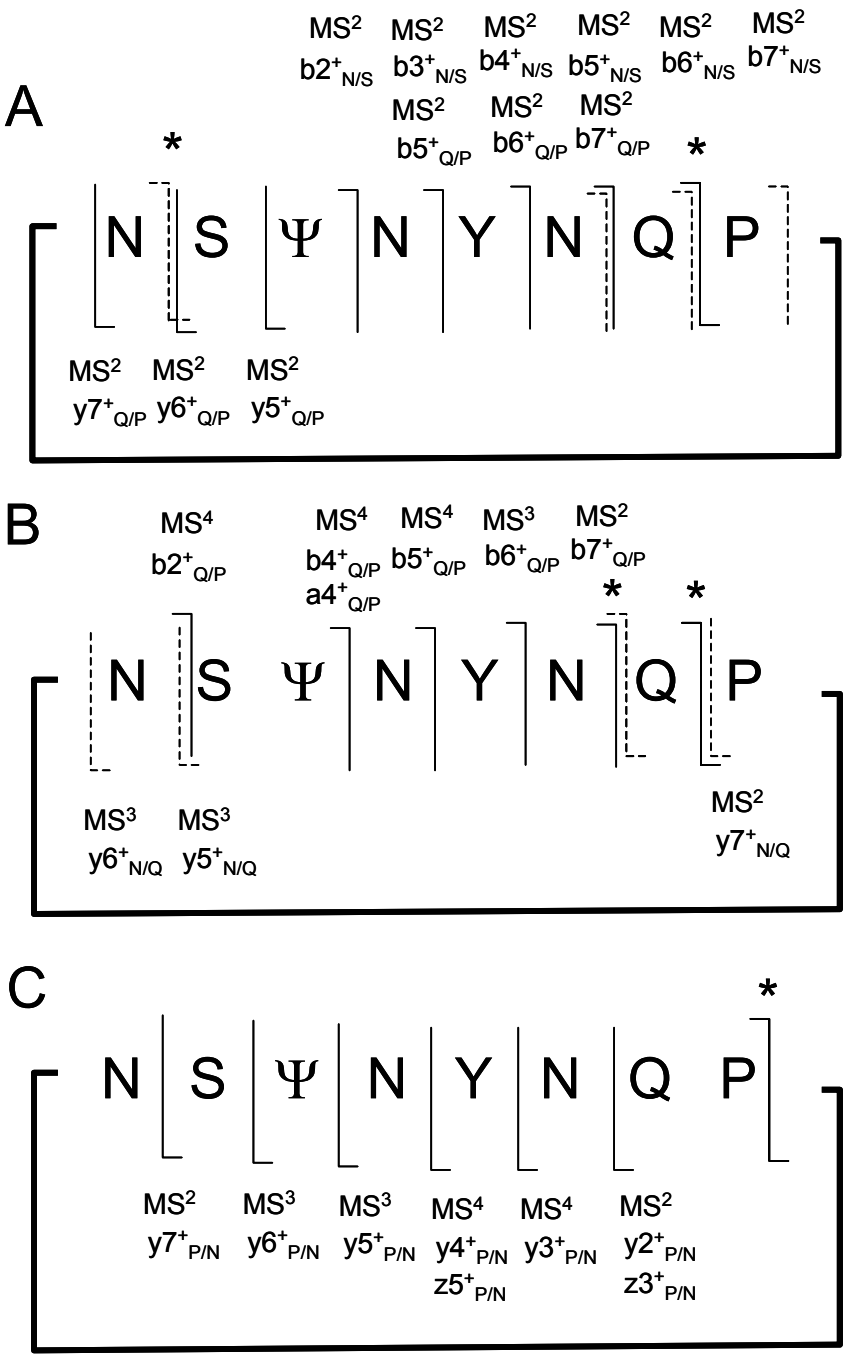

Figure 7.7. MS^2 spectra for complexes of A) $(\text{iturin A} + H)^+$, B) $(\text{iturin A} + Ag)^+$, C) $(\text{iturin A} + \text{Sr-H})^+$. IA = iturin A. An asterisk (*) identifies the precursor ion.

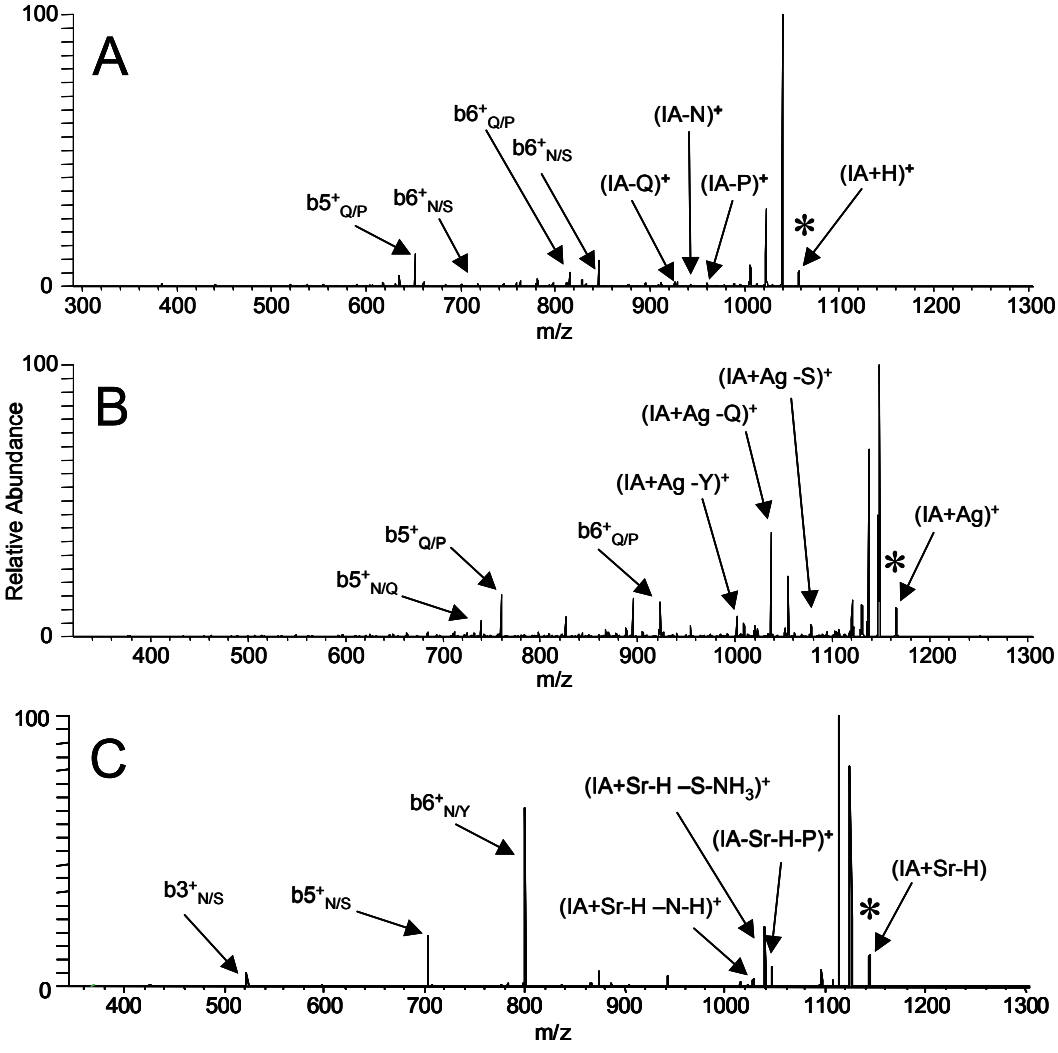

MS^2 spectra are similar: 2.2 x 10^5, 1.57 x 10^5, and 2.84 x 10^5 arbitrary units for Figures 7A, 7B, and 7C, respectively). The absolute intensities of the isolated precursor ions are also within 15% of each other. From Table 13 and Scheme 3, MS^n of $(IA + H)^+$ provides $b_7^+{}_{Q/P}$ to $b_5^+{}_{Q/P}$, $b_7^+{}_{N/S}$ to $b_2^+{}_{N/S}$ and $y_7^+{}_{Q/P}$ to $y_5^+{}_{Q/P}$ ions, along with $(b_5 - b_1)^+$, $(b_4 - b_1)^+$, and $(b_4 - b_2)^+$ ions. As seen in Table 14 and Scheme 3, MS^n experiments with $(IA + Ag)^+$ provide b_7^+ to b_4^+ ions, along with $(b_4 - b_1)^+$ and b_2^+ ions, and y_7^+ to y_4^+ ions. The MS^4 and MS^5 spectra for $(IA + Ag)^+$ are also quite simple. MS^n of $(IA + Sr - H)^+$ provides the most complete and accurate y ion sequence information of the protonated and silver and strontium complex experiments. As shown in Table 15, the MS^n experiments for $(IA + Sr - H)^+$ gave simple MS^3 to MS^5 spectra, with y_7^+ to y_2^+ ions, along with a $(y_3 - y_1)^+$ ion. In addition, the MS^n experiments with strontium are the only ones to directly provide the mass of the lipid residue of 239 Da as one of the peptide cleavage mass increments. Combining the MS^n data from any two of these three experiments can provide one with complete sequence coverage with generous overlap, simple b and y ions, and greater certainty because of the more intense diagnostic ions from the metal complexes. Combining all three provides even greater sequence confirmation.

The lead complex MS^2 spectrum showed an enhanced $(IA+Pb-H-P)^+$ ion at a ten-fold greater absolute and percent relative abundance than protonated iturin A, but MS^3 of the lead complex was not very informative. The other major diagnostic

ion in the MS^2 spectrum for lead complex, a $b_6^+{}_{P/N}$ ion, was similar in intensity to the analogous signal in the MS^2 spectrum of protonated iturin A. MS^3 of the $b_6^+{}_{P/N}$ ion provided $b_5^+{}_{P/N}$ and $b_4^+{}_{P/N}$ ions. The MS^n experiments for $(IA+Pb)^{2+}$ precursor were less diagnostically useful than MS^n of $(IA+Pb-H)^+$. Other divalent metal ion complexes with iturin A produced MS^n product ions similar to those for lead or strontium complexes, but diagnostic product ions were not over 10% relative abundance. Monovalent ion complexes provide $z_7^+{}_{Q/P}$ and $b_6^+{}_{N/Q}$ product ions in the MS^2 spectra with relative abundances for K^+ of 10% and 1%, respectively, and for Li^+ and Na^+ of 20% and 5%, respectively. MS^3 of the $z_7^+{}_{Q/P}$ ion provided sequence information that was out of order, indicating the residue order QNPS, rather than the correct QPNS order. P and N differ by 17 Da, indicating the increasing residue losses from the precursor were in the correct order but $(QP+NH_3)$ and QPN were lost rather than (Q+N) and (QPN).

Analysis of fragmentation patterns allows one to determine the sites of ring cleavage from the largest fragments in the MS^2 spectrum and the most stable site of gas phase cation binding. The cation binding site is identified from the smallest fragments in the MS^n spectra still complexed with the cation. The MS^n spectra for iturin A provided information about both of these characteristics. In Scheme 4, the results of this investigation are presented. The bracket ($\prod$) shows the first residue likely to be lost, and locations of stable cation binding are indicated by a straight line drawn between the cation and the residue. Arrows pointing to a hydrogen from

Scheme 7.4. Probable cation binding, proton loss and ring cleavage sites for iturin A. Cation binding is indicated by a straight solid line, dahed lines indicate a site of second cation binding, ring cleavage is indicated by in intermitant dashed line, and proton loss from a doubly charged complex to form a singly charged complex is indicated by an arrow.

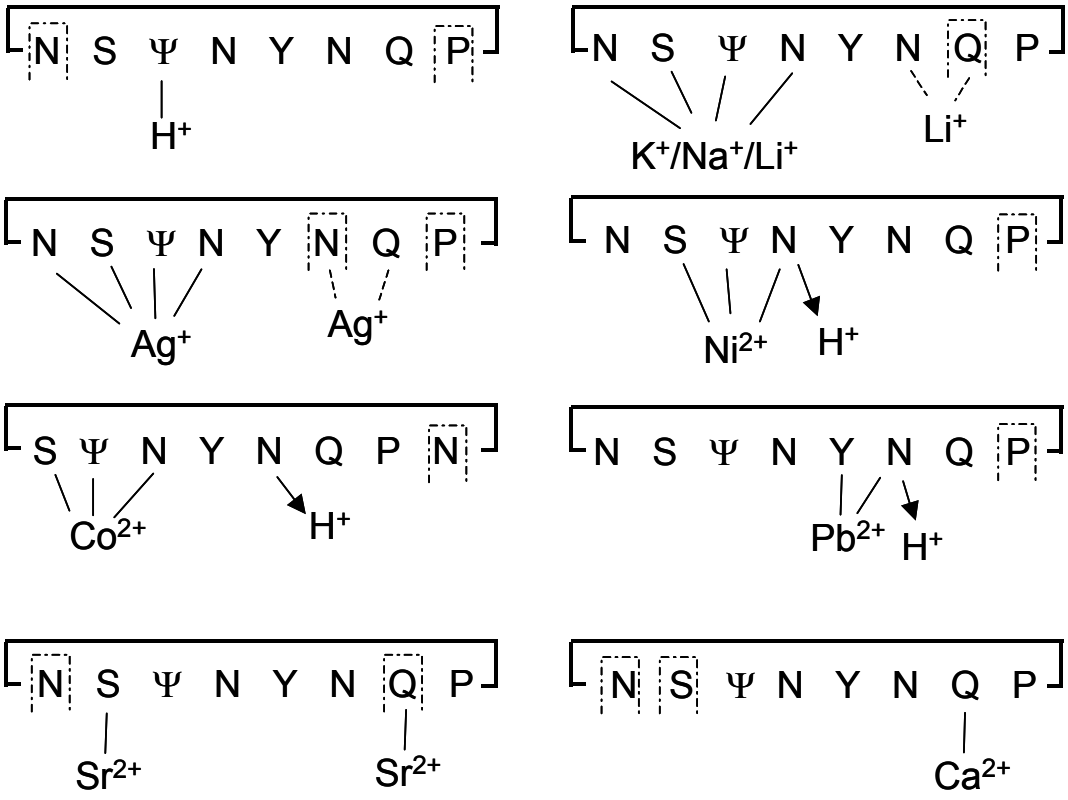

a residue indicate that doubly charge precursor ion complexes with divalent metals lose a proton and become singly charged when this residue is lost.

For protonated complex, it appears that cleavage occurs between P and the adjacent N. The lack of observation of a loss increment equivalent to Ψ indicates the proton may prefer this site in the gas phase. However, the proton may also be mobile in a charge driven mechanism. All the monovalent metals appear to coordinate cooperatively with the NSΨN sequence, as no signals are observed for loss of any of these residues from the peptide complexes with monovalent metal ions.

Nickel ion requires binding to the SΨN sequence for the $(IA+Ni-H)^+$ complex, this is a sequence of residues with one N less than the NSΨN sequence monovalent ions preferentially bind to. This could indicate that nickel ion is more strongly bound to a single N, while the monovalent ions are more weakly coordinated to two, and the CAD energy effects loss of the cation along with the loss of the N adjacent to the S. The MS^2 fragment with one residue loss has lost the P residue. For the $(IA+Ni)^{2+}$ complex, the MS^2 fragment with a single residue loss is due to loss of Q residue. Along with Q, a proton is lost creating a singly charged complex, which suggests that in the $(IA+Ni-H)^+$ complex, the nickel binds to the deprotonated Q residue. The cobalt ion shows the same interactions as nickel for the singly charged complex, except that a series of b ions can begin with loss of P or the N adjacent to it. For the $(IA+Co)^{2+}$ complex, the Q or N in the QPN sequence

can be the only MS^2 residue lost. The loss of the N in the QPN sequence results in loss of a proton and conversion to a singly charged complex. Thus, a different deprotonated N may be involved in metal coordination in the $(IA+Co-H)^+$ versus the $(IA+Ni-H)^+$ complex. The $(IA+Pb-H)^+$ complex shows a ring cleavage at P along with loss of this residue. The fragmentation pattern indicates preferred binding at the YN sequence. For the $(IA+Pb)^{2+}$ complex, ring cleavage at, and initial single residue loss of, Y or P occur. Either the Y or N can serve as a sole Pb^{2+} anchor. Loss of N from the YN sequence results in deprotonation to the singly charged complex. For the alkaline earth metal ions strontium and calcium, complexes with iturin A show interesting differences, in contrast to the similar characteristics of the alkali metal complexes. While both show a preference for Q binding, strontium shares its preference with the S residue. Also, while Q and N in the QPNS sequence can be sites of ring cleavage and loss of the first single residue, for intact strontium complex, no intact complexes with Q loss are observed for calcium complex. For the strontium complex it appears that Q can be lost with complex retention, but not with loss of S, suggesting a preference of S binding for strontium and Q binding for calcium.

7.3.3.2 Surfactin

In the discussion of surfactin (abbreviated SF) complexes, which follows, three letters are used to designate the region of the site of ring cleavage and the

backslash indicates the ring cleavage site itself. This method of designation is followed here for surfactin, because there are two locations with two adjacent leucines which must be differentiated. The Greek letter 'Σ' is used to represent the '3-hydroxy-13-methyl tetradecanoic acid' fatty acid residue in surfactin and the other amino acids are assigned their standard letter.

For surfactin, an eight-residue peptide, fragmentation of the protonated cyclic peptide, as shown in Table 16, provided very good data from b_7^+ to b_4^+ and y_7^+ to y_3^+ ions along with a series of b_7^+ to b_5^+ ions with water loss. This covers the entire sequence of the cyclic peptide. However, only the y_7^+/b_7^+, $(y_6\text{-}2H)^+$ and b_4^+ ions were above 5% relative abundance (see Figure 8). MS^n of $(SF+Ag)^+$, $(SF+Ni)^{2+}$, and $(SF+Pb)^{2+}$ provide product spectra with much greater relative abundances of several of these important product ions (Tables 17-19). MS^6 data can be obtained for $(SF+Ag)^+$, where silver ion complexed to a single L residue is observed (Table 17). MS^n of $(SF+Ag)^+$ also provides a series of strong y_7^+ to y_3^+ and b_7^+ to b_4^+ ions with larger intensities than for protonated surfactin. In this sense it is superior to the protonated peptide analysis. The MS^2 spectrum for $(SF+Ni)^{2+}$ shows y_7^+ to y_4^+ ions, all with intensities above 60% relative abundance. The MS^n data available for $(SF+Pb)^{2+}$ is roughly equivalent to that for protonated surfactin, with greater product ion signals. There are about five fragments in the spectra not due to losses of unit residues or unit residues with some combination of water, CO, or NH_3, but because of the low intensity of ions in the protonated peptide spectra,

Table 7.16. MS^n results for analysis of $(surfactin+H)^+$. SF = surfactin.

MS^n	Precursor ion	Product ions			
		single residue losses	a, b, & c ions	x, y, & z ions	small ions
$MS^{2\,b}$	$(SF+H)^+$	$(SF+H-L)^+$, $(SF+H-L-H_2O)^+$	$b_6^+{}_{L/L\Sigma}$, $b_5^+{}_{L/L\Sigma}$, $b_4^+{}_{L/L\Sigma}$, $b_3^+{}_{L/L\Sigma}$, $(b_6-H_2O)^+{}_{L/L\Sigma}$, $(b_5-H_2O)^+{}_{L/L\Sigma}$, $(a_4-H_2O)^+{}_{L/L\Sigma}$, $(a_3-H_2O)^+{}_{L/L\Sigma}$	$(y_6-2H)^+{}_{L/L\Sigma}$, $y_5^+{}_{L/L\Sigma}$	
$MS^{3\,c}$	$(y_6-2H)^+{}_{L/LQ}$			$y_5^+{}_{L/L\Sigma}$, $y_4^+{}_{L/L\Sigma}$	
$MS^{4\,c}$	$y_4^+{}_{L/LQ}$			$y_3^+{}_{L/L\Sigma}$	$(y_4-D)^+{}_{L/L\Sigma}$, $(y_4-V)^+{}_{L/L\Sigma}$, $(L+L+H)^+$
$MS^{5\,c}$	$(L+L+H)^+$				$(L+L+H-CO)^+$
$MS^{6\,c}$	$(L+L+H-CO)^+$				$(L+H-CO)^+$

[a] Σ = 3-hydroxy-13-methyl tetradecanoic acid; Signal intensity cutoffs (relative abundance): [b] 1%, [c] 5%.

Figure 7.8. MS^2 spectra for complexes of A) $(surfactin+H)^+$, B) $(surfactin+Ag)^+$, C) $(surfactin+Ni)^{2+}$, D) $(surfactin+Pb)^{2+}$. SF=surfactin, Σ = 3-hydroxy-13-methyl-tetradecanoic acid . An asterisk (*) identifies the precursor ion.

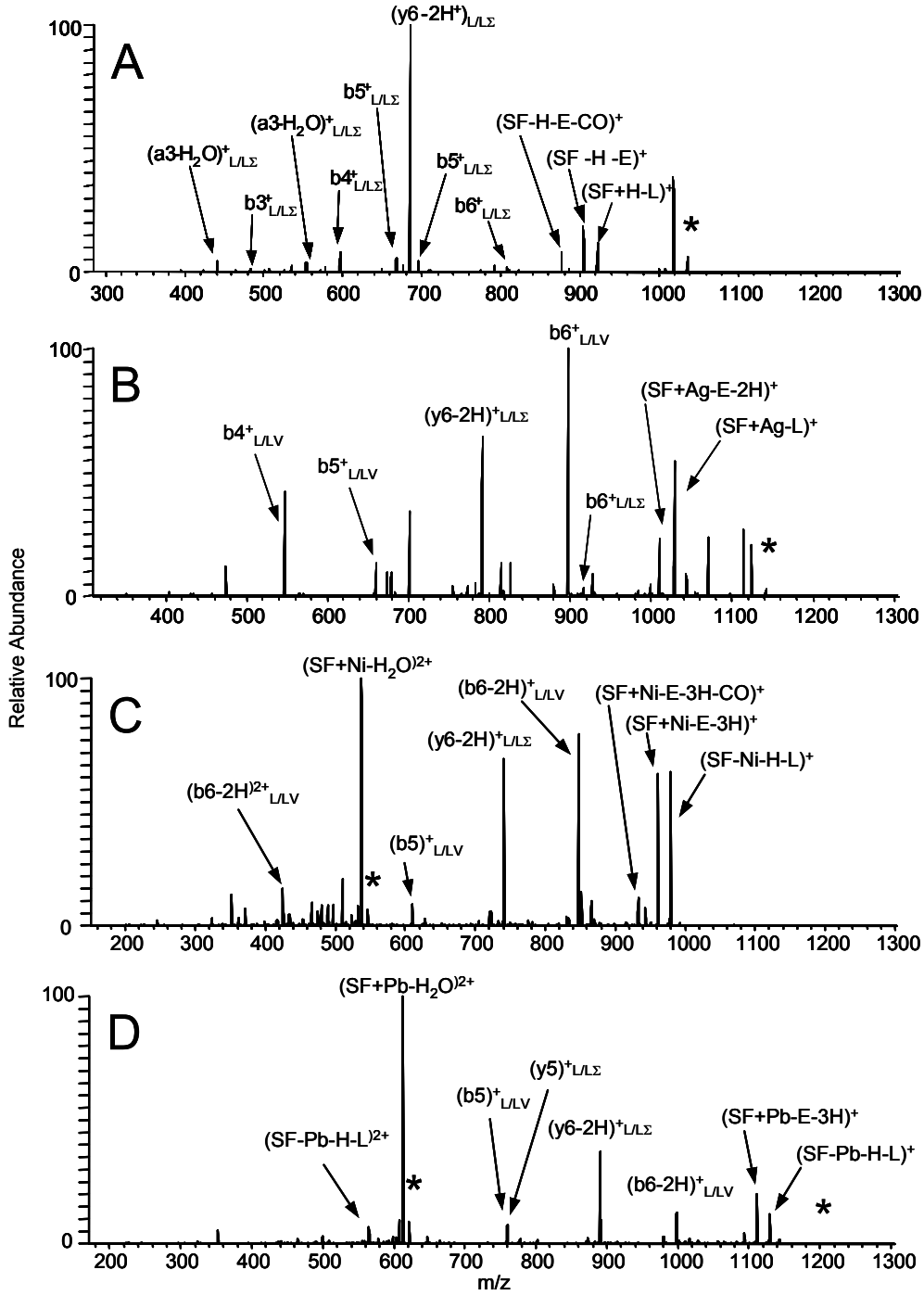

Table 7.17. MS^n results for analysis of $(surfactin+Ag)^+$. SF = surfactin.

MS^n	Precursor ion	Product ions			
		single residue losses	a, b, & c ions	x, y, & z ions	small ions
$MS^{2\,b}$	$(SF+Ag)^+$	$(SF+Ag-L)^+$	$(b_6\text{-}2H)^+_{E/LL}$, $b_5^+_{E/LL}$, $b_4^+_{E/LL}$,	$(y_6+2H)^+_{L/L\Sigma}$, $y_5^+_{L/L\Sigma}$, $y_4^+_{L/L\Sigma}$	
$MS^{3\,b}$	$(SF+Ag-L)^+$		$(b_6\text{-}2H)^+_{E/LL}$,	$y_6^+_{D/LL}$, $(y_5+2H)^+_{D/LL}$, $y_4^+_{D/LL}$, $y_3^+_{D/LL}$	
$MS^{4\,c}$	$y_4^+_{D/LL}$			$(y_4\text{-}72)^+_{D/LL}$	
$MS^{5\,c}$	$(y_4\text{-}72)^+_{D/LL}$			$(y_4\text{-}y1)^+_{D/LL}$	$(L+L+Ag)^+$
$MS^{6\,c}$	$(L+L+Ag)^+$				$(L+Ag+NH_3+CO)^+$

[a] Σ = 3-hydroxy-13-methyl tetradecanoic acid; Signal intensity cutoffs (relative abundance): [b] 1%, [c] 5%.

Table 7.18. MS^n results for analysis of $(surfactin+Ni)^{2+}$. SF = surfactin.

MS^n	Precursor ion	Product ions			
		single residue losses	a, b, & c ions	x, y, & z ions	small ions
$MS^{2\,b}$	$(SF+Ni)^{2+}$	$(SF+Ni\text{-}L)^+$, $(SF+Ni\text{-}2L)^+$,	$(b_6\text{-}2H)^+_{L/L\Sigma}$, $b_5^+_{L/L\Sigma}$	$(y_6+2H)^+_{L/L\Sigma}$, $y_5^+_{L/L\Sigma}$	
$MS^{3\,b}$	$(y_6+2H)^+_{L/L\Sigma}$			$y_5^+_{L/L\Sigma}$, $y_4^+_{L/L\Sigma}$	

[a] Σ = 3-hydroxy-13-methyl tetradecanoic acid; Signal intensity cutoffs (relative abundance): [b] 1%.

Table 7.19. MS^n results for analysis of $(surfactin+Pb)^{2+}$. SF = surfactin.

MS^n	Precursor ion	Product ions			
		single residue losses	a, b, & c ions	x, y, & z ions	small ions
$MS^{2\,b}$	$(SF+Pb)^{2+}$	$(SF+Pb\text{-}L)^{2+}$, $(SF+Pb\text{-}L)^+$, $(SF+Pb\text{-}2L)^{2+}$	$(b_6\text{-}2H)^+_{L/L\Sigma}$, $(b_6\text{-}2H)^{2+}_{L/L\Sigma}$, $b_5^+_{L/L\Sigma}$, $b_4^+_{L/L\Sigma}$	$(y_6+2H)^+_{L/L\Sigma}$, $y_5^+_{L/L\Sigma}$, $y_4^+_{L/L\Sigma}$	
$MS^{3\,b}$	$(y_6+2H)^+_{L/L\Sigma}$			$y_5^+_{L/L\Sigma}$, $y_4^+_{L/L\Sigma}$	
$MS^{3\,b}$	$b_5^+_{L/L\Sigma}$/ $y_5^+_{L/L\Sigma}$		$b_4^+_{L/L\Sigma}$, $b_3^+_{L/L\Sigma}$	$y_4^+_{L/L\Sigma}$	

[a] Σ = 3-hydroxy-13-methyl tetradecanoic acid; Signal intensity cutoffs (relative abundance): [b] 1%.

the problem is even worse for protonated peptide. For silver ion complex, the final residue attached to the ion appears to be the same as for proton, a L residue. The doubly charged alkaline earth metal ion complexes, $(SF+Sr)^{2+}$ and $(SF+Ca)^{2+}$, and the singly charged alkali metal complexes, $(SF+K)^{+}$, $(SF+Na)^{+}$ and $(SF+Li)^{+}$, all provided MS^n results which gave complete sequence coverage of surfactin, but the product ion signals were less intense than those for the silver, nickel, and lead ion complexes discussed. The MS^n data for the other metal ions only allowed sequence information for four or less residues, also with product ion signals less intense than those for the silver, nickel, and lead ion complexes.

While the divalent metal ion complexes yielded b ions beginning with an L/LV cleavage, the complexes with proton and silver yielded b ions, beginning with a L/LΣ cleavage. This pattern suggests preferences for different carboxylate containing residues (E vs. D) for the two valencies. $(SF+Sr-H)^{+}$ and $(SF+Sr)^{2+}$ complexes provided provided some unique fragments where the ring was not cleaved between two leucines. Instead LL/Σ and D/LL ring cleavages are observed amongst the more common ring cleavages. The b ions for $(SF+H)^{+}$ begin with an DL/L cleavage, whereas the $(SF+Pb)^{2+}$ ions begin with a EL/L cleavage. The MS^n of $(SF+Pb)^{2+}$ provided very informative spectra as well, enabling the determination of the final two residues attached to the Pb ion (V and D). There is some ambiguity as to whether the final residue bound to Pb ion is a $(V + CO_2)$ or a (D + CO), but

(D + CO) seems more likely. All the peaks used in this determination are above 10% relative abundance, and also serve as good complementary information.

7.3.4 RGD Binding Domain Peptide Antagonists: Cyclo(RGDFV) and Cyclo(RGDSPAG)

7.3.4.1 Cyclo(RGDFV)

Regarding sequence information obtained from the MS^n spectra for cyclo(RGDFV), the protonated peptide experiments resulted in $y_4^+{}_{F/V}$ to $y_2^+{}_{F/V}$ ions and a $y_2^+{}_{V/R}$ ion, along with $b_4^+{}_{D/F}$ to $b_3^+{}_{V/R}$, $b_1^+{}_{V/R}$, $b_4^+{}_{R/G}$, and $b_3^+{}_{R/G}$ ions. On the other hand, MS^n with nickel complex resulted mainly in only b ions, with $b_4^+{}_{F/V}$ to $b_1^+{}_{F/V}$, $b_4^+{}_{D/F}$, $b_3^+{}_{D/F}$, $a_3^+{}_{D/F}$ and $a_2^+{}_{F/V}$ ions, but complete sequence coverage. Thus, MS^n of protonated and nickel complexed cyclo(RGDFV) provide complementary information. This is important because MS^n of the protonated complex provided both y and b ions, while with nickel complex, a complete series of ions from $b_4^+{}_{F/V}$ to $b_1^+{}_{F/V}$ ions, along with a $a_2^+{}_{F/V}$ ion, were obtained.

For cyclo(RGDFV), the MS^n data for complexes with proton and nickel ion is shown in Tables 20 and 21, respectively. For all three species, MS^n experiments could be used to determine the final residue of substrate ion attachment (see Scheme 5). For proton, the final residue was an intact R residue, determined with the $b_1^+{}_{V/R}$ ion. For this complex, ring cleavage occurs at all peptide bonds and any

Table 7.20. MS^{n}[6] results for (cyclo[RGDFV]+ H)$^+$ complex. RG1 = cyclo[RGDFV].

MS^n	Precursor ion[f]	Product ions[f]			
		single residue losses	a, b, & c ions	x, y, & z ions	small ions
$MS^{2\,a}$	$(RG1+H)^+$	$(RG1-V)^+$, $(RG1-D)^+$, $(RG1-V-NH_3)^+$, $(RG1-R)^+$, $(RG1-F-72)^+$, $(RG1-R-CO)^+$	$b_3{}^+_{D/F}$, $(b_3-NH_3)^+_{D/F}$, $(b_3-NH_3)^+_{V/R}$	$y_3{}^+_{F/V}$, $y_2{}^+_{F/V}$, $y_2{}^+_{D/F}$	
$MS^{3\,b}$	$(RG1-R)^+$	$(RG1-R-CO)^+$	$b_3{}^+_{R/G}$	$y_2{}^+_{V/R}$	
$MS^{4\,b}$	$b_3{}^+_{R/G}$		$a_3{}^+_{R/G}$		$(F-CO+H)^+$
$MS^{3\,b}$	$(RG1-V)^+$	$(RG1-V-NH_3)^+$, $(RG1-V-CO)^+$	$b_3{}^+_{V/R}$, $(b_3-NH_3)^+_{V/R}$		
$MS^{4\,c}$	$b_3{}^+_{V/R}$		$(b_3-NH_3)^+_{V/R}$, $(b_3-90)^+_{V/R}$, $c2^+_{V/R}$, $(b_2-H)^+_{V/R}$, $(b_2-NH_3)^+_{V/R}$, $b1^+_{V/R}$		
$MS^{5\,d}$	$(b_2-H)^+_{V/R}$		$(b_2-NH_3)^+_{V/R}$, $(b_2-44)^+_{V/R}$		
$MS^{6\,e}$	$(b_2-44)^+_{V/R}$		$(a_2-CO-44)^+_{V/R}$		

Signal intensity cutoffs (relative intensity): [a] 2%, [b] 3%, [c] 5%, [d] 10%, [e] 40%; [f] 72 = $C(NH_2)_2NH$, 90 = $CH_2NHCN_2H_3$, 44 = $NHCHNH_2$.

Table 7.21. MS^n results for (cyclo[RGDFV]+Ni-H)$^+$ complex. RG1 = cyclo[RGDFV].

MS^n	Precursor ion	Product ions		
		single residue losses	a, b, & c ions	x, y, & z ions
$MS^{2\,a}$	$(RG1+Ni-H)^+$	$(RG1+Ni-H-V)^+$, $(RG1+Ni-H-V-CO)^+$, $(RG1+Ni-H-F)^+$, $(RG1+Ni-H-R)^+$	$b_3{}^+_{D/F}$, $a_3{}^+_{D/F}$	
$MS^{3\,a}$	$(RG1+Ni-H-F)^+$	$(Par+Ni-H-F-NH_3)^+$, $(Par+Ni-H-F-CO)^+$	$(b_3+43)^+_{F/V}$, $b_3{}^+_{F/V}$, $b_2{}^+_{F/V}$, $a_2{}^+_{F/V}$	$(y_3+NH_3)^+_{D/F}$
$MS^{4\,c}$	$(b_3+43)^+_{F/V}$		$b_3{}^+_{F/V}$, $b_2{}^+_{F/V}$, $a_2{}^+_{F/V}$	
$MS^{5\,c}$	$a_2{}^+_{F/V}$		$b_1{}^+_{F/V} = (V+Ni-H)^+$	

Signal intensity cutoffs (relative abundance): [a] 2%, [b] 5%.

Scheme 7.5. Probable cation binding, proton loss and ring cleavage sites for cyclo(RGDFV). Cation binding is indicated by a straight solid line, dahed lines indicate a site of second cation binding, ring cleavage is indicated by in intermitant dashed line, and proton loss from a doubly charged complex to form a singly charged complex is indicated by an arrow.

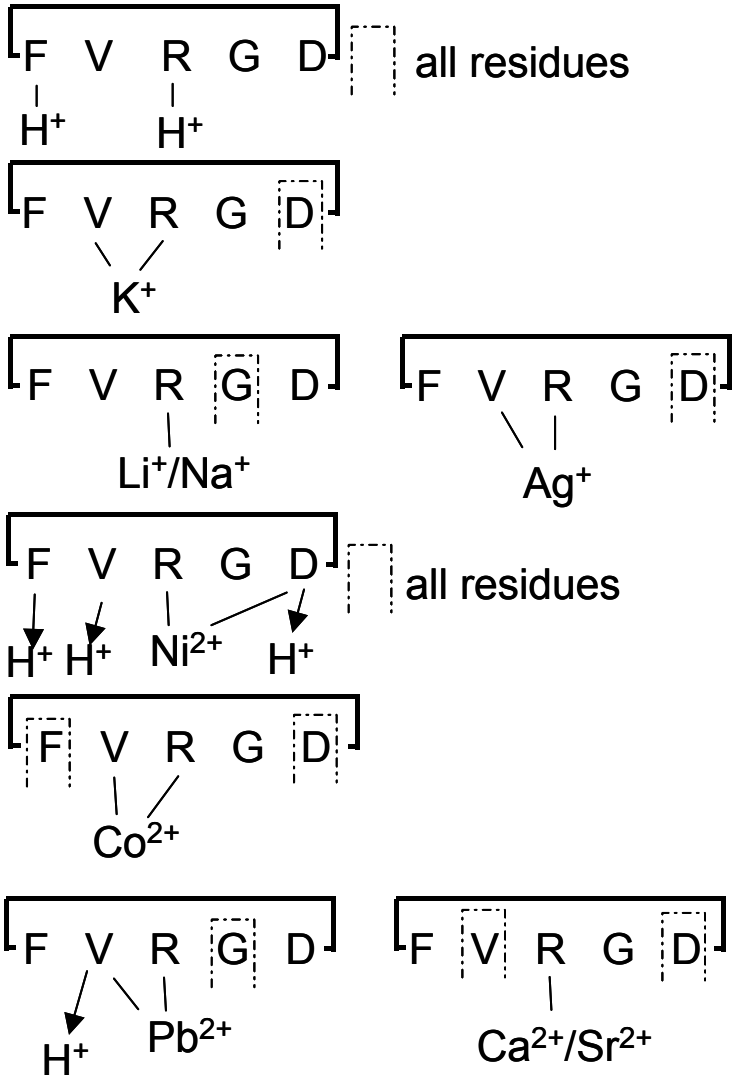

of the residues can be the initial single residue loss. The final residue complexed with lithium and sodium is also an R, but with most of the side chain lost, from the smallest metalated complexes observed, i.e. $(R+Li-C(NH_2)_2NH+NH_3)^+$ and $(R+Li-C(NH_2)_2NH)^+$ ions. It appears that three amine groups and possibly the carboxyl group are necessary for lithium and sodium attachment. Initial single residue loss occurs for G, which is adjacent to R. The binding and ring cleavage sites for silver ion complex appear to be the same as for potassium ion, perhaps due to similar charge densities versus the smaller alkali metal ions.

For nickel ion complex, the final residue is a deprotonated V or R residue, in contrast to only the expected R complexation. For this complex, like the protonated complex, any of the residues can be the initial single residue loss. For conversion from the doubly to singly charged nickel complex via deprotonation, according to the spectral information, the residue that is deprotonated could be the D, F, or V, suggesting backbone amide interaction. For cobalt complex, the preferred metal-residue interactions are the same as for nickel complex, R and V, however first single residue loss is limited to D or F, suggesting ring cleavage between these two residues.

Lead and strontium ion also appear to prefer interaction with R. However, in the case of lead complex, the side chain of R can be lost with the lead remaining bound to the FV sequence. For lead, initial single residue loss occurs at the G and for strontium it can occur at either the V or D residue. For the doubly charged lead

complex, as with nickel complex, loss of V can result in deprotonation, forming the singly charged lead complex, suggesting that the peptide backbone amide nitrogen can serve as a formally negative interaction site for a metal ion in preference to the amide group on the side chain of D, where deprotonation was observed for nickel complex. Due to water adduction, good information for characteristics of the calcium ion was not obtained.

7.3.4.2 Cyclo(RGDSPAG)

For cyclo(RGDSPAG) (abbreviated RG2), just as for cyclo(RGDFV), sequencing of the RDG sequence is a challenge. Primarily, difficulty arises in trying to lose R from the linearized peptide fragment after loss of G (see Table 23). The preference for metal ion and proton binding again appears to be at R, just as for cyclo(RGDFV). For cyclo(RGDSPAG), however, ring cleavage at multiple sites is not observed. The site of ring cleavage is universally at the DS peptide bond for all metal and proton complexes. Loss of serine from the $(RG2+H)^+$ forms a $y6^+_{D/S}$ product ion, which does not appear for CAD of any of the metal complexes. MS^n spectra for neither $(RG2+H)^+$ nor $(RG2+2H)^{2+}$ show loss of R or the RGD sequence. Loss of the D and G seem facile, often with an initial loss from the precursor ion of the backbone carbonyl of D and a CO_2 from its side chain, for a loss of 72 Da. This is isobaric with the $C(NH_2)_2NH$ loss from the side-chain of R, observed for CAD of cyclo(RGDFV) complexes, but with cyclo(RGDSPAG),

Table 7.22. MS^2 to MS^6 results for analysis of $(cyclo[RGDSPAG]+H)^+$ complex. RG2 = cyclo[RGDSPAG].

$(cyclo[RGDSPAG]+H)^+$					
MS^n	Precursor ion[e]	Product ions[e]			
		single residue losses	a, b, & c ions	x, y, & z ions	small ions
$MS^{2\,a}$	$(RG2+H)^+$	$(RG2+H-72)^+$, $(RG2+H-S)^+$	$b_5^+{}_{D/S}$		
$MS^{3\,b}$	$(RG2+H-72)^+$	$(RG2+H-D)^+$	$b_5^+{}_{D/S}$		
$MS^{4\,c}$	$b_5^+{}_{D/S}$		$(b_5-42)^+{}_{D/S}$		
$(cyclo[RGDSPAG]+Li)^+$					
MS^n	Precursor ion[e]	Product ions[e]			
		single residue losses	a, b, & c ions	x, y, & z ions	small ions
$MS^{2\,a}$	$(RG2+Li)^+$		$b_5^+{}_{D/S}$		
$MS^{3\,b}$	$b_5^+{}_{D/S}$		$(b_4+2H)^+{}_{D/S}$		
$(cyclo[RGDSPAG]+Ag)^+$					
MS^n	Precursor ion[e]	Product ions[e]			
		single residue losses	a, b, & c ions	x, y, & z ions	small ions
$MS^{2\,a}$	$(RG2+Ag)^+$	$(RG2+Ag-72)^+$	$b_5^+{}_{D/S}$, $(b_5-42)^+{}_{D/S}$, $a_4^+{}_{D/S}$		
$MS^{3\,d}$	$(RG2+Ag-72)^+$	$(RG2+Ag-D)^+$, $(RG2+Ag-72-P)^+$	$b_5^+{}_{D/S}$, $(b_5-42)^+{}_{D/S}$, $(b_5-72)^+{}_{D/S}$, $b_4^+{}_{D/S}$		
$MS^{3\,b}$	$(b_5-42)^+{}_{D/S}$		$(b_5-b_1-42)^+{}_{D/S}$, $b_4^+{}_{D/S}$, $a_4^+{}_{D/S}$, $(b_4-b_1)^+{}_{D/S}$		
$(cyclo[RGDSPAG]+K)^+$					
MS^n	Precursor ion[e]	Product ions[e]			
		single residue losses	a, b, & c ions	x, y, & z ions	small ions
$MS^{2\,a}$	$(RG2+H)^+$	$(RG2+Ag-D)^+$	$b_5^+{}_{D/S}$, $(b_5-42)^+{}_{D/S}$		
$MS^{3\,a}$	$(RG2+K-D)^+$		$(b_5-H_2O)^+{}_{D/S}$, $(b_5-b1)^+{}_{D/S}$, $b_4^+{}_{D/S}$		

Signal intensity cutoffs (relative intensity): [a] 2%, [b] 3%, [c] 40%, [d] 20%; [e] 72 $=(CO_2+CO)$, 42 $= C(NH)_2$.

CAD of the (precursor-72)$^+$ ion in the MS^2 spectra results in a $b_6^+{}_{D/S}$ ion. MS^n experiments on almost all protonated and metal ion complexed cyclo(RGDSPAG) ions tested produced $b6^+{}_{D/S}$ and $b5^+{}_{D/S}$ ions. However, only MS^n experiments with $(RG2+Ag)^+$ and $(RG2+K)^+$ produced b4 ions, specifically $b4^+{}_{D/S}$ ions, due to loss of RGD. MS^3 of $(RG2+Li)^+$ produced a $(b_4+2H)^+{}_{D/S}$ ion. MS^n of silver complex produced the most information for the complexes tested. Along with $b_6^+{}_{D/S}$, $b_5^+{}_{D/S}$ and $b_4^+{}_{D/S}$ ions, identifying the RGD sequence, a $(b_4\text{-}_b1)^+{}_{D/S}$ ion was observed, which is a $(b_4\text{-}S)^+{}_{D/S}$ ion. In the case of silver complex, it would seem that it is able to coordinate strongly enough with residues adjacent to R (in this case the G residues of GRG), while binding to R, such that when R is lost during CAD, in a significant number of reactions the silver ion is not dislodged from the remaining peptide fragment. One can rationalize the same explanation for similar observations with lithium and potassium ion complexes. However, these observations only occurred for the monovalent metal ions, K^+, Li^+, and Ag^+. The MS^n spectra were similar for Na^+ complex as well, but a lower relative abundance of the $b_5^+{}_{D/S}$ ion in the MS^2 product ion spectrum resulted in visible but questionable ion signals below 1% relative abundance for $b_5^+{}_{D/S}$, $(b_4\text{-}b_1)^+{}_{D/S}$, $(b_4\text{-}b_1\text{-}A)^+{}_{D/S}$, and $(b_5\text{-}72\text{-}b_1)^+{}_{D/S}$ ions. Apparently, the lower charge density of the monovalent ions compared to the divalent ions and proton may allow the ion to bind less strongly to R and not be dislodged upon loss of R, continuing to coordinate to another residue.

Since greater sequence information that can be obtained by combining the MS^n data from protonated and monovalent metal ion complexed cyclo(RGDSPAG) versus the protonated cyclopeptide alone, monovalent metal ions, and especially silver ion, may be good candidates for further testing with RDG cyclopeptides. If similar enhancements in identification of the RGD sequence information are observed, an fast, easy method for detecting RGD cyclopeptides in media may be possible.

7.4 Conclusions

For cyclosporin A, nickel and lithium complexation provided improved sequence coverage in the MS^n spectra and simpler, more easily interpretable data than did protonation. In the cases of valinomycin and enniatin A_1, sodium ion and lead ion provided superior sequence analysis potential versus protonation. For the lipopeptides iturin A and surfactin, silver showed improvement in sequence coverage and/or increased relative abundance of important versus less important diagnostic product ion signals for cyclopeptide sequence determination. For the two RGD sequence containing peptides, nickel or silver ion complexation improved the sequence coverage for thr peptides, while lithium, potassium and silver ions were found to also be advantageous for analysis of the larger cyclo(RGDSPAG) peptide. Overall, the MS^n data obtained from complexes of cyclic peptides with metal ions

provided valuable complementary and often superior information for identity and sequence determination of cyclic peptides.

7.5 Acknowledgements

Support from the Robert A. Welch Foundation (F-1155) and the National Science Foundation (CHE-0315337) is gratefully acknowledged.

7.6 Appendix: Residue Abbreviation Key

7.6.1 Standard Residues

A = alanine
C=cysteine
D=aspartate
E=glutamate
F=phenylalaine
G=glycine
H=histidine
I=isoleucine
K=lysine
L=leucine
M=methionine
N=asparagines
P=proline
Q=glutamine
R=arginine
S=serine
T=threonine
V=valine
W=tryptophan
Y=tyrosine

7.6.2 Other residues

U = N-methyl valine;
Z = N-methyl leucine (Z = methyl isoleucine for enniatin A_1);
X = hydroxy isovaline;
J = 4(R)-4[(E)-2-butenyl]-4-methyl-L-threonine;
Φ = 2-amino-butanoic acid;
Γ = N-methyl glycine (aka sarcosine)
Ψ = 3-amino-12-methyltetradecanoic acid, the fatty acid residue on iturin A;.
Σ = 3-hydroxy-13-methyl-tetradecanoic acid, the fatty acid residue on surfactin;

7.7 References

1. Davies, John S. Cyclic peptides. *Cyclic Polymers (2nd Edition)*, Semlyen, J. Anthony, Ed., Kluwer Academic Publishers, Dordrecht, Netherlands, **2000**, pp 85-124.

2. Michael, J.P.; Pattenden, G. Marine Metabolites and the Complexation of Metal Ions: Facts and Hypotheses. *Angew. Chem.*, **1993**, *105*, 1-24. Angew. Chem., Int. Ed. Engl., 1993, 32, 1-23.

3. Faulkner, D.J. Marine Natural Products. *Nat. Prod. Rep.*, **1988**, *5*, 613-663.

4. Lewis, J.R. Muscarine, Oxazole, and Peptide Alkaloids and Other Miscellaneous Alkaloids. *Natural Products Report*, **1989**, *6*, 503.

5. H.C. Krebs, Recent Developments in the Field of Marine Natural Products with Emphasis on Biologically Active Compounds. *Fortschr. Chem. Org. Naturst.*, **1986**, *49*, 151-163.

6. Rosen, M.K.; Schreiber, S.L. Natural Products as Probes in the Study of Cellular Functions: Investigation of Immunophilins. *Angew. Chem.*, **1992,** 104, 413-430. *Angew. Chem., Int. Ed. Engl.*, **1992**, *31*, 384-400.

7. Evans, D.A.; Ellman, J.A. The Total Syntheses of the Isodityrosine-Derived Cyclic Tripeptides OF4949-III and K-13. Determination Of The Absolute Configuration of K-13. *J. Am. Chem. Soc.*, **1989**, *111*, 1063-72.

8. Fusetani, N.; Sugawara, T.; Matsunaga, S.; Hirota, H. Orbiculamide A: A Novel Cytotoxic Cyclic Peptide from a Marine Sponge Theonella Sp. *J. Am. Chem.Soc.*, **1991**, *113*, 7811-12.

9. Fairlie, D.P.; Abbenante, G.; March, D.R.. Macrocyclic Peptidomimetics - Forcing Peptides into Bioactive Conformations. *Curr. Med. Chem.*, **1995**, *2*, 654-86.

10. Breithaupt, H. The New Antibiotics, *Nature Biotech.*, **1999**, *17*, 1165-1169.

11. Fernandez-Lopez, S.; Kim, H.-S.; Choi, E.C.; Delgado, M.; Granja, J.R.; Khasanov, A.; Kraehenbuehl, K.; Long, G.; Weinberger, D.A.; Wilcoxen, K.M.; Ghadiri, M.R. Antibacterial Agents Based on the Cyclic D-L-Alpha-Peptide Architecture, *Nature*, **2001**, *412*, 452-455.

12. Ghadiri, M.R.; Granja, J.R.; Buehler, L.K. Artificial Transmembrane Ion Channels from Self-Assembling Peptide Nanotubes. *Nature*, **1994**, *369*, 301-304.

13. Kim, H.S.; Hartgerink, J.D.; Ghadiri, M.R. Oriented Self-Assembly of Cyclic Peptide Nanotubes in Lipid Membranes. *J. Am. Chem. Soc.*, **1998**, *120*, 4417-4424.

14. Kohil, R.M.; Walsh, C.T.; Burkart, M.D. Biomimetic Synthesis and Optimization of Cyclic Peptide Antibiotics, *Nature*, **2002**, *418*, 658-661.

15. Georgou, G.; Lin, S.C.; Sharma, M.M. Surface-Active Compounds from Microorganisms. *Bio/Technology*, **1992**, *10*, 60-65.

16. Muller-Hurtig, R., Blaszczyk, R.; Wagner, F.; Kosaric, N. Biosurfactants for Environmental Control. *Biosurfactants*, Kosaric, N., Ed., Marcel Dekker, Inc, New York, New York, **1993**, p. 447-69.

17. Van Dyke, M.I.; Lee, H.; Trevors, J.T. Applications of Microbial Surfactants. *Biotechnol. Adv.*, **1991**, *9*, 241-252.

18. Pusey, P.L.; Wilson, C.L.; Postharvest Biological Control of Stone Fruit Brown Rot by Bacillus Subtillus. *Plant Disease*, **1984**, *68*, 753-756.

19. Asaka, O.; Shoda, M. Biocontrol of Rhizoctonia Solani Damping-Off of Tomato with Bacillus Subtillus RB14. *Appl. Environ. Microbiol.*, **1996**, *62*, 4081-4085.

20. Hammes, H.-P.; Brownlee, M.; Jonczyk, A.; Sutter, A.; Preissner, K.T. Subcutaneous Injection of a Cyclic Peptide Antagonist of Vitronectin Receptor-Type Integrins Inhibits Retinal Neovascularization. *Nature Medicine*, **1996**, *2*, 529-533.

21. Noiri, E.; Gailit, J.; Sheth, D.; Magazine, H.; Gurrath, M.; Muller, G.; Kessler, H.; Goligorsky, M.S. Cyclic RGD Peptides Ameliorate Ischemic Acute Renal Failure in Rats. *Kidney Int.*, **1994**, *46*, 1050-8.

22. Gurrath, M.; Mueller, G.; Kessler, H.; Aumailley, M.; Timpl, R. Conformation/Activity Studies of Rationally Designed Potent Anti-Adhesive RGD Peptides. *Eur. J. Biochem.*, **1992**, *210*, 911-21.

23. Mueller, G.; Gurrath, M.; Kessler, H.; Timpl, R. Dynamic Forcing: An Aid for the Determination of the Activity and Selectivity of RGD (Arg-Gly-Asp) Peptides. *Angew. Chem.*, **1992**, *1043*, 341-3. *Angew. Chem., Int. Ed. Engl.*, **1992**, *31*, 358.

24. Mohri, H.; Ohkubo, T. Effect of Cyclic Arg-Gly-Asp-Containing Peptide on Fibronectin Binding to Activated Platelets: Role of Fibronectin on Platelet Aggregation. *Peptides*, **1993**, *14*, 861-5.

25. Mohri, H.; Ohkubo, T. The Role of the RGD Peptides and the γ Chain Peptide of Fibrinogen on Fibrinogen Binding to Activated Platelets. *Peptides*, **1993**, *14*, 353-7.

26. Kerr, J.S.; Wexler, R.S.; Mousa, S.A.; Robinson, C.S.; Wexler, E.J.; Mohamed, S.; Voss, M.E.; Devenny, J.J.; Czerniak, P.M.; Gudzelak, A., Jr.; Slee, A.M. Novel Small Molecule αV Integrin Antagonists: Comparative Anti-Cancer Efficacy with Known Angiogenesis Inhibitors. *Anticancer Res.*, **1999**, *19*, 959-968.

27. Srivatsa, S.S.; Fitzpatrick, L.A.; Tsao, P.W.; Reilly, T.M.; Holmes, D.R., Jr; Schwartz, R.S.; Mousa, S.A. Selective Alpha V Beta 3 Integrin Blockade Potently Limits Neointimal Hyperplasia and Lumen Stenosis Following Deep Coronary Arterial Stent Injury: Evidence for the Functional Importance of Integrin Alpha V Beta 3 and Osteopontin Expression During Neointima Formation. *Cardiovasc.Res.*, **1997**, *363*, 408-28.

28. Luna, J.; Tobe, T.; Mousa, S.A.; Reilly, T.M.; Campochiaro, P.A. Antagonists Of Integrin αVβ3 Inhibit Retinal Neovascularization in a Murine Model. *Lab. Invest.*, **1996**, *75*, 563-573.

29. Kerr, Janet S.; Slee, Andrew M.; Mousa, Shaker A. Small Molecule αV Integrin Antagonists: Novel Anticancer Agents. *Expert Opin. Invest. Drugs*, **2000**, *9*, 1271-1279.

30. Kerr, Janet S.; Slee, Andrew M.; Mousa, Shaker A. The αV Integrin Antagonists as Novel Anticancer Agents: An Update. *Expert Opin. Invest. Drugs*, **2002**, *11*, 1765-1773.

31. Ngoka, L.C.; Gross, M.L Multistep Tandem Mass Spectrometry for Sequencing Cyclic Peptides in an Ion-Trap Mass Spectrometer. *J. Am. Soc. Mass Spectrom.*, **1999**, *10*, 732-746.

32. Govaerts, C.; Rozenski, J.; Orqa, J.; Roets, E.; Van Schepdael, A.; Hoogmartens, J. Mass Spectrometric Fragmentation of Cyclic Peptides Belonging to the Polymyxin and Colistin Antibiotics Studied by Ion Trap and Quadrupole/Orthogonal-Acceleration Time-of-Flight Technology. *Rapid Commun. Mass Spectrom.*, **2002**, *16*, 823-833.

33. Zweigenbaum, J.A.; Henion, J.D., Beattie, K.A.; Codd, G.A.; Poon, G.K. Direct Analysis of Microcystins by Microbore Liquid Chromatography Electrospray Ionization Ion-Trap Tandem Mass Spectrometry. J. Pharm. Biomed. Anal., 2000, 23, 723-733.

34. Cavelier, F.; Enjalbal, J.M.; Roque, M.; Sanchez, P.; Aubagnac, J.-L. Comparison of Collisionally Dissociation Mass Spectra for the Identification of Cyclopeptides and Cyclodepsipeptides. *Rapid Commun. Mass Spectrom.*, **1999**, *13*, 880-885.

35. Ngoka, L.C.M.; Gross, M.L. Location of Alkali Metal Binding Sites in Endothelin A Selective Antagonists, Cyclo(D-Trp-D-Asp-Pro-D-Val-Leu) and Cyclo(D-Trp-D-Asp-Pro-D-Ile-Leu), from Multistep Collisionally Activated Decompositions. *J. Mass Spectrom.*, **2000**, *35*, 265-276.

36. Lin, S.; Liehr, S.; Cooperman, B.S.; Cotter, R.J. Sequencing Cyclic Peptide Inhibitors of Mammalian Ribonuclease Reductase by Electrospray Ionization Mass Spectrometry. *J. Mass Spectrom.*, **2001**, *36*, 658-663.

37. Hue, N.; Serani, L.; Laprevote, O. Structural Investigation of Cyclic Petolipids from Bacillus Subtillis by High-Energy Tandem Mass Spectrometry. *Rapid Commun. Mass Spectrom.*, **2001**, *15*, 203-209.

38. Ngoka, L.C.M., Gross, M.L. Multistep Collisionally Activated Decomposition in an Ion Trap for the Determination of the Amino-Acid Sequence and Gas Phase Ion Chemistry of Lithium-Coordinated Valinomycin. *Int. J. Mass Spectrom.*, **2000**, *194*, 247-259.

39. Lambert, C.M.N.; Gross, M.L.; Toogood, P.L. Sodium-Directed Selective Cleavage of Lactones: A Method for Structure Determination of Cyclodepsipeptides. *Int. J. Mass Spectrom.*, **1999**, *182/183*, 289-298.

40. Kaltashov, Igor A.; Cotter, Robert J.; Feinstone, W. Harry; Ketner, Gary W.; Woods, Amina S. Ferrichrome: Surprising Stability of a Cyclic Peptide-Fe(III) Complex Revealed by Mass Spectrometry. *J. Am. Soc. Mass Spectrom.*, **1997**, *8*, 1070-1077.

41. Jayawargene, D.; Dass, C. Fragmentation Characterstics of Peptide-Metal Ion Adducts under Matrix-Assisted Laser Desorption/Ionization Post-Source Decay Time-of-Flight Mass Spectrometric Conditions, *J. Mass. Spectrom.*, **2002**, *37*, 389-394.

42. Rodriquez, C.F.; Fournier, R.; Chu, I.K.; Hopkinson, A.C.; Siu, K.W.M. A Possible Origin of $[M - nH + mX](m-n)^+$ Ions (X = Alkali Metal Ions) in Electrospray Mass Spectrometry of Peptides. *Int. J. Mass. Spectrom.*, **1999**, *192*, 303-317.

43. Kenny, P.T.M.; Nomoto, K.; Orlando, R. Fragmentation Studies of Gas-Phase Complexes between Alkali Metal Ions and a Biologically Active Peptide, Achatin-1, *Rapid Commun. Mass. Spectrom.*, **1997**, *11*, 224-227.

44. Tomlinson, M.J.; Scott, J.R.; Wilkins, C.L.; Wright, J.B.; White, W.E. Fragmentation of an Alkali Metal-Attached Peptide Probed by Collision-Induced Dissociation Fourier Transform Mass Spectrometry and Computational Methodology, *J. Mass Spectrom.*, **1999**, *34*, 958-968.

45. Kuckelmann, U.; Muller, D.; Weber, C. Systematic Studies of the Mass Spectrometric Properties of Alkaline Earth Metal Cationized Amino Acids and Peptides, *J. Molec. Strctr.*, **1997**, *412*, 135-139.

46. Nemirovskiy, O.V.; Gross, M.L. Gas Phase Studies of the Interactions of Fe^{2+} with Cysteine-Containing Peptides, *J. Am. Soc. Mass. Spectrom.*, **1998**, *9*, 1285-1292.

47. Brewer, D.; Lajolie, G. Evaluation of the Metal Binding Properties of the Histidine-Rich Antimicrobial Peptides Histatin 3 and 5 by Electrospray Ionization Mass Spectrometry. *Rapid Commun. Mass Spectrom.*, **2000**, *14*, 1736-1745.

48. Shields, S.J.; Bluhm, B.K.; Russel, D.H. Fragmentation Chemistry of $[M+Cu]^+$ Peptide Ions Containing an N-terminal Arginine. *J. Am. Soc. Mass Spectrom.*, **2000**, *11*, 626-638.

49. Hu, Peifeng; Loo, Joseph A. Gas-Phase Coordination Properties of Zn^{2+}, Cu^{2+}, Ni^{2+}, and Co^{2+} with Histidine-Containing Peptides. *J. Am. Chem. Soc.*, **1995**, *117*, 11314-19.

50. Loo, Joseph A.; Hu, Peifeng; Smith, Richard D. Interaction of Angiotensin Peptides and Zinc Metal Ions Probed by Electrospray Ionization Mass Spectrometry. *J. Am. Soc. Mass Spectrom.*, **1994**, *5*, 959-65.

51. Hu, P.; Gross, M.L. Gas-Phase Interactions of Transition-Metal Ions and Di- and Tripeptides: A Comparison with Alkaline-Earth-Metal-Ion Interactions. *J. Am. Chem. Soc.*, **1993**, *115*, 8821-8828.

52. Lee, V. W.-M.; Li, H.; Lau, T.-C.; Siu, K.W.M. Structure of b and a Product Ions from the Fragmentation of Argentinated Peptides, *J.Am.Chem.Soc.*, **1998**, *120*, 7309.

53. Afonso, C.; Hathout, Y.; Fenselau, C.. Qualitative Characterization of Biomolecular Zinc Complexes by Collisionally Induced Dissociation. *J. Mass Spectrom.*, **2002**, *37*, 755-759.

54. Vaisar, T.; Gatlin, C.L.; Rao, R.D.; Seymour, J.L.; Turecek, F. Sequence Information, Distinction and Quantitation of C-Terminal Leucine and Isoleucine in Ternary Complexes of Tripeptides with Cu(II) and 2,2'-Bipyridine. *J. Mass Spectrom.*, **2001**, *36*, 306-316.

55. Chu, I.K.; Shoeib, Guo, X.; Rodriquez, C.F.; Lau, T.-C., Hopkinson, A.C.; Siu, K.W.M. Characterization of the Product Ions from the Collision Induced Dissociation of Argentinated Peptides, *J. Am. Soc. Mass Spectrom.*, **2001**, *12*, 163-175.

56. Wee, S.; O'Hair, R. A. J.; McFadyen, W.D. Side-Chain Radical Losses from Radical Cations allows Distinction of Leucine and Isoleucine Residues in the Isomeric Peptides Gly-Xxx-Arg. *Rapid Commun. Mass Spectrom.*, **2002**, *16*, 884-890.

57. Zirah, S.; Rebuffat, S.; Kozin, S. A.; Debey, P.; Fournier, Francoise; Lesage, D.; Tabet, J.-C. Zinc Binding Properties of the Amyloid Fragment Aβ(1-16) Studied by Electrospray-Ionization Mass Spectrometry. *Int. J. Mass Spectrom.*, **2003**, *228*, 999-1016.

58. Chu, I.K.; Cox, D.M.; Guo, X.; Kireeva, I.; Lau, T.-C.; McDermott, J.C.; Siu, K.W.M. Sequencing of Argentinated Peptides by Means of Matrix-Assisted Laser Desorption/Ionization Tandem Mass Spectrometry. *Anal. Chem.*, **2002**, *74*, 2072-2082.

59. Chu, I.K.; Guo, X.; Lau, T.-C; Siu, K.W.M. Sequencing of Argentinated Peptides by Means of Electrospray Tandem Mass Spectrometry. *Anal. Chem.*, **1999**, *71*, 2364-2372.

60. Cerda, D.A.; Cornett, L.; Wesdemiotis, C. Probing the Interaction of Alkali and Transition Metal Ions with Bradykinin and Its Des-arginine Derivatives via Matrix-assisted Laser Desorption/ Ionization and Postsource Decay Mass Spectrometry, *Int. J. Mass Spectrom.*, **1999**, *193*, 205-226.

61. Barr, J.M.; Van Stipdonk, M.J. Multi-stage Tandem Mass Spectrometry of Metal Cationized Leucine Enkephalin and Leucine Enkephalin Amide, *Rapid. Commun. Mass Spectrom.*, **2002**, *16*, 566-578.

62. Kish, M.K.; Wesdemiotis, C. Selective Cleavage at Internal Lysine Residues in Protonated vs. Metalated Peptides. *Int. J. Mass Spectrom.*, **2003**, *227*,191-203.

63. Wenger, R.M. Cyclosporine and Analogs: Isolation and Synthesis. Mechanism of Action and Structural Requirements for Pharmacological Activity., *Progr. Chem. Org. Nat. Prod.*, **1986**, *50*, 123-68.

64. Ovchinnikov, Y.A. Second FEBS-Ferdinand Springer Lecture: Membrane Active Complexones. Chemistry and Biological Function. *FEBS Lett.*, **1974**, *44*, 1-21.

65. Visconti, A.; Blais, L.A.; ApSimon, J.W.; Greenhalgh, R.; Miller, J. D. Production of Enniatins by Fusarium Acuminatum and Fusarium Compactum in Liquid Culture: Isolation and Characterization of Three New Enniatins, B2, B3, and B4. *J. Agricul. Food Chem.*, **1992**, *40,* 1076-82.

66. Ngoka, L.C.M.; Gross, M.L.A. A Nomenclature System for Labelling Cyclic Peptide Fragments. *J. Am. Soc. Mass Spectrom.*, **1999**, *10*, 360-363.

67. Cheng, C.; Gross, M.L. Applications and Mechanisms of Charge-Remote Fragmentation. *Mass Spectrom. Rev.*, **2000**, *19*, 398-420.

CHAPTER 8

Conclusions

Host-guest chemistry is a field of research with numerous current and future applications, and the need for efficient, versatile analytical methods for evaluating the binding properties of new hosts has motivated the present work. The studies discussed in Chapters 3-6 on selectivity determinations of crown compounds were initiated in order to develop methods which could increase the rate at which the relative selectivities of host compounds for several metal ions could be determined. This methodology allowed candidates with the greatest potential for applications involving selective detection of metals or sequesteration agents to be rapidly determined and further tested. These studies also demonstrated the breadth of the mass spectrometry method used and determined directions for further studies to improve the method's flexibility.

The many positive aspects of electrospray ionization combined with quadrupole ion trap mass spectrometry have been an integral part of this research, in large part because of the sensitivity, dynamic range, and sample flexibility of ESI-QIT-MS. These characteristics of ESI-MS show great promise for the development of rapid screening, identification and characterization methods in host-guest chemistry.

The studies performed with lariat ethers and lariat ether amides in Chapters 3 and 4 supported the development of more selective chelating agents for several alkali and alkaline earth metal ions. Insight was obtained into several subtle influences on metal binding selectivity. One example is the steric factors enhancing ion selectivity, such as the geminal propyl group increasing Na^+/K^+ selectivity. Another example is the influence of solution acidity on ionizable lariat ether selectivity. One advantage of using mass spectrometry for such studies is that the mass of the species are continuously monitored and changes in selectivity due to side reactions of the host would be detected – a source of systematic error that could not be as easily determined by several other conventional selectivity determination methods other than mass spectrometry. The information gained from these studies can potentially be applied not only to simple crown ether species with pendant arms, but also to recent exciting advances in more complicated selective metal binding agents such as calixarenes and in biomolecules with functions that are modulated by metal binding.

The studies of the mercury and silver selectivities of cage annulated crown ethers in homogenous solutions and extractions from a two-phase condensed phase system in Chapters 5 and 6 demonstrated the applicability of ESI-MS for rapid screening of candidates in the development of metal sequestering agents. The ESI screening methods were quick and effective in distinguishing the best extraction agents for mercury and silver ions, determining their effectiveness in

environmentally anticipated conditions such as in the presence of high alkali and alkaline earth ion concentrations and increases in media acidity. These methods were also able to differentiate the important contributions of both innate ion selectivity and tendency towards protonation of the host in the effective sequestering of silver ion by the cage annulated aza-crown ethers. Overall, these studies have produced several potential means of improving ion exchange systems for precious metal purification and wastewater remediation.

The work that involved complexes of metal ions with cyclic peptides in Chapter 7 demonstrated the potential of metal complexation for improved detection and characterization of agriculturally and medically important cyclic peptides. The continuing search for cyclic peptides with advantageous properties, either by isolation from life forms such as plants and micro-organisms or synthesis, would benefit greatly from methods which can increase the speed of identification and characterization of current and future cyclic peptides. Mass spectrometry fragmentation methods using CAD for peptide identification and sequence characterization have become extremely important techniques in protein and peptide identification. However, although these mass spectrometric methods have made a very valuable contribution to the field of proteomics and peptide analysis, resolving current issues with the sequence ambiguity and information complexity of the methods would increase the power and breadth of applicability. The metal complexation of several cyclic peptides discussed in Chapter 7 demonstrated the

potential of using alkali, nickel and silver ions to enhance the abundances of important fragment ions in mass spectrometric peptide fragmentation methods. This study also demonstrated the improved sequence determination capabilities of Na^+ and Pb^{2+} complexation for analysis of large depsipeptides.

Electrospray ionization quadrupole ion trap mass spectrometry has been a valuable tool for progress in the field of host-guest chemistry and its many applications. Despite the proven efficacy of this instrumentation and prosperousness of this field of study, further advances could follow from a deepened understanding of the fundamental mechanism of the solution-to-gas-phase analyte transfer process of ESI-MS and the myriad aspects of chemistry still to be discovered in host-guest selectivity. Current studies to understand the influence of species partitioning between the surface and interior of ESI droplets and a more complete characterization of other factors which effect electrospray efficiencies allow more quantitative measurements. Improved selectivity screening methods could be applied to a greater range of hosts such as modified calixerenes, other heterocycles, and biomolecules. Such studies would support the development of ion selective sensors, and lead to more profitable and/or environmentally beneficial metal sequesteration agents.

VITA

Sheldon Myles Williams was born in Hibbing, Minnesota, on August 31, 1969, the son of James LeRoy Willams and Judy Elena Williams. After completing his work at Bemidji High School, Bemidji, Minnesota, in 1987, he entered Bemidji State University in Bemidji, Minnesota. He received the degree of Bachelor of Science from Bemidji State University in May of 1992. He then began graduate studies at the Graduate School at Purdue University in West Lafayette, Indiana, in September of 1992. While attending graduate school, he also worked as a technician at Purdue University. He received the degree of Master of Science from Purdue University in August of 1998. In August of 1998, he entered the Graduate School of The University of Texas at Austin in Austin, Texas.

Permanent Address: 3413 Adelia Drive Southeast, Bemidji, Minnesota 56601

This dissertation was typed by the author.